

ABSTRACT

Title of Document: SILENCING BACTERIA WITH SMALL
MOLECULES.

Min Guo, Doctor of Philosophy, 2015

Directed By: Professor Herman O. Sintim,
Department of Chemistry and Biochemistry

Quorum sensing (QS) is a phenomenon in bacteria where the accumulation of extracellular signaling molecules (autoinducers, AIs), which enable bacterial cells to sense neighboring cells (population density), reaches certain threshold and triggers group behaviors of bacteria including virulence production and biofilm formation. The inhibition of QS and hence toxin production or biofilm formation by pathogenic bacteria has been suggested as an alternative strategy to deal with the problem of bacterial resistance to traditional antibiotics. Inhibiting QS will not kill bacteria, however the expectation is that resistance to a QS antagonist will not be as widespread as it is for traditional cytotoxic antibiotics.

In Chapters 2 and 3 of this dissertation, we report the syntheses and biological evaluations of various analogs (C1 substituted, ester protected and 3,3-dihalogenated) of a universal QS signaling molecule, AI-2, which is found in both Gram-positive and Gram-negative bacteria. We report that modifications to the native AI-2 molecule affords analogs that can potently inhibit QS processes in *E. coli* and *Salmonella*.

In Chapter 4, we explore the development of small molecule modulators of species-specific acylhomoserine lactone autoinducers, called AI-1. In the past three

decades, intensive efforts have been dedicated to the development of modulators of AI-1-based QS signaling. The majority of modulators, reported to date, have kept the lactone head group and modified the acyl tail. These synthetic modulators, although effective, are not drug-like because lactones are susceptible to chemical and enzymatic hydrolysis. We demonstrate that 3-aminooxazolidinone based AI-1 analogs, which are hydrolytically more stable than homoserine lactone-based compounds, can also modulate AI-1-based QS.

SILENCING BACTERIA WITH SMALL MOLECULES

By

Min Guo

Dissertation submitted to the Faculty of the Graduate School of the
University of Maryland, College Park, in partial fulfillment
of the requirements for the degree of
Doctor of Philosophy
2015

Advisory Committee:

Professor Herman O. Sintim, Chair

Professor Philip DeShong

Professor Andrei N. Vedernikov

Professor Daniel Falvey

Professor William E. Bentley

© Copyright by
Min Guo
2015

Dedication

Dedicated to my father and mother for selflessly raising me up and supporting me all the way and Yifan Wang who accompanied me in my hardest time.

Acknowledgements

I would like to thank my dissertation advisor Dr. Herman O. Sintim, who has given me precious advice and ideas in the past five years. I will like to thank my committee member Dr. William Bentley (and the Bentley lab) for the collaboration over the years. Special thanks to his student, Jessica L. Terrell for conducting the cytometry FACS experiments shown in Chapter 3. I also want to thank my other committee members Dr. Philip DeShong, Dr. Andrei N. Vedernikov and Dr. Daniel Farvelly for their valuable advice during my graduate training.

I will like to thank Dr. Yiu-Fai Lam and Dr. Yinde Wang for training me in the use of the NMR instrument. I thank Dr. Yue Li for the helpful discussions on mass spectrometry.

I will like to thank Dr. Jingxin Wang, former member of the Sintim group, for providing synthesis and Gaussian calculation trainings. I also thank former Sintim group members, Dr. Jacqueline A. I. Smith and Sonja Gamby for teaching me how to synthesize AI-2, as well as providing training in various biological assays. I thank former post-doc in our group Dr. Shizuka Nakayama, who helped me with β -galactosidase assay in Chapter 2, as well as training me on a variety of biological assays and experiments. Special thanks goes to Yue Zheng, a member of the Sintim group, who helped me with so many quorum sensing assays in Chapter 3 and 4, such as β -galactosidase assay, bioluminescence assay, stability assay and *C. violaceum* CV026 AHL reporter assay. I also thank Clement Opoku-Temeng, a member of the Sintim group, for his help in β -galactosidase assay in Chapter 3. Finally I thank all members of the Sintim group for memorable five years.

Table of Contents

Dedication.....	ii
Acknowledgements.....	iii
Table of Contents.....	iv
List of Tables	vi
List of Figures	vii
List of Schemes.....	xii
List of Abbreviations	xiii
Chapter 1: Introduction	1
1.1 A bacterial battle and a post-antibiotic era	1
1.2 Quorum sensing inhibition—a new strategy to fight bacteria.....	9
1.3 AI-2 signaling in other bacteria and inhibitors of AI-2 signaling.....	16
1.4 AI-1 mediated quorum sensing.....	27
Chapter 2: AI-2 analogs selectively modulate QS in bacteria	33
2.1 Improvement in AI-2 synthesis	33
2.2 A pro-drug approach for selective modulation of AI-2 mediated bacterial cell-cell communication	36
2.2.1 Introduction.....	36
2.2.2 Results and discussion	37
2.2.3 Conclusion	43
2.2.4 Experimental section.....	44
Chapter 3: Geminal dihalogen isosteric replacement in hydrated AI-2 affords analogs that potently modulate quorum sensing.....	63
3.1 Introduction	63
3.2 Results and discussion.....	67
3.3 Conclusion.....	76

3.4 Detailed experimental procedures and characterizations	76
Chapter 4: 3-Aminooxazolidinone head group-based AHL analogs that function as quorum sensing agonists in Gram-negative bacteria	93
4.1 Introduction	93
4.2 Results and discussion.....	95
4.3 Conclusion.....	102
4.4 Detailed experimental procedures and characterizations	103
Chapter 5: Conclusions	111
5.1 AI-2 mediated quorum sensing inhibitors	111
5.2 AI-1 mediated quorum sensing inhibitors	113
Appendix: NMR spectra.....	114
References.....	149

List of Tables

Table 1-1. Successive generations of representative antibiotic classes and their primary targets. Core scaffolds are highlighted in blue while peripheral chemical modifications (R groups) are in black. Most antibiotics on the market inhibit five major targets in bacteria (also see Figure 1-2).....	4
Table 1-2. Some bacterial phenotypes, which are regulated by AI-2/LuxS. Note: ^a Transporter, ^b Transcriptional regulator, ^c Kinase, ^d AI-2 degradative enzyme, ^e Chemoreceptor.....	17
Table 1-3. Representative AHL structures and their corresponding organism, synthases/receptors and QS phenotypes.....	30
Table 1-4. Significant AHL analogs and their activities.....	31
Table 2-1. Bacterial strains used in this study.....	47
Table 3-1. Comparison of properties of AI-2 and analogs.....	74

List of Figures

Figure 1-1.	Timeline showing the deployment of representative antibiotics and resistance observed (summarized from the literature ¹⁻³).	3
Figure 1-2.	Major targets for antibacterial action. a) Inhibition of cell wall synthesis. b) Inhibition of protein synthesis. c) Inhibition of DNA or RNA synthesis. d) Inhibition of folate synthesis. e) Disruption of membrane. Modified from the literature. ^{3,14}	7
Figure 1-3.	a) Increased concentration of autoinducers in bacterial biofilms promotes the synthesis of biofilm matrices, such as adhesion proteins and polysaccharides, which are required for the maintenance of the biofilm structure; b) Autoinducers repress the production of virulence factors as well as the synthesis of the components of the bacterial secretory system, such as T3SS, in some bacteria (for example, AI-1, AI-2 and CAI-1 represses T3SS gene expression in <i>V. harveyi</i> ²⁶).	10
Figure 1-4.	Structures of Autoinducer molecules. AI-2 is a term used to described DPD (4,5-dihydroxy-2,3-pentanedione, 1-25a) and isomers in equilibrium.	12
Figure 1-5.	<i>V. harveyi</i> quorum sensing system. Arrows denote the phosphorelay at low cell density.	14
Figure 1-6.	Quorum sensing model in <i>S. typhimurium</i> and <i>E. coli</i>	15
Figure 1-7.	Possible AI-2-based “druggable” targets. (1) LuxS; (2) AI-2 transporter (such as LsrB); (3) efflux pump for AI-2; (4) extracellular receptor for AI-2 (such as LuxP); (5) intracellular receptor for AI-2; (6) AI-2-regulated transcription factor or repressor (such as LsrR) (7) small regulatory RNA (sRNA) mediated QS circuit.	20
Figure 1-8.	A) Crystal structure of LuxP from <i>V. harveyi</i> in complex with AI-2 (PDB code: 1JX6); B) AI-2 binding site of LuxP, showing protein residues that are within 3 Å of AI-2.	21
Figure 1-9.	A) Crystal structure of LsrB from <i>S. typhimurium</i> , in complex with AI-2	

	(PDB code: 1TJY). B) AI-2 binding site of LsrB, showing protein residues that are within 3 Å of AI-2.....	22
Figure 1-10.	A) Crystal structure of LsrB from <i>Sinorhizobium meliloti</i> (PDB code: 3EJW). B) AI-2 binding site of LsrB, showing protein residues that are within 3 Å of AI-2.....	22
Figure 1-11.	A) Crystal structure of LsrB from <i>Y. pestis</i> (PDB code: 3T95). B) AI-2 binding site of LsrB, showing protein residues that are within 3 Å of AI-2.....	23
Figure 1-12.	A) Crystal structure of LsrR from <i>E. coli</i> (PDB code: 4L4Z). B) AI-2 binding site of LsrR, showing protein residues that are within 3 Å of AI-2.....	23
Figure 1-13.	A) Crystal structure of LsrF from <i>E. coli</i> (PDB code: 4P2V) B) AI-2 binding site of LsrF, showing protein residues that are within 3 Å of AI-2.....	24
Figure 1-14.	Probing specificity of LuxP binding site with AI-2-like molecules.....	25
Figure 1-15.	C1-Modified AI-2 molecules synthesized by Janda and Sintim ^{83,84b}	25
Figure 1-16.	Acetate- and ester-protected AI-2 and analogs developed by Sintim and Doutheau ^{85,86}	26
Figure 1-17.	C5 Analogs of AI-2 developed by Ventura and co-workers (1-53 to 1-60), which contain stereochemical diversity at the C4 and C5 positions ⁸⁷	26
Figure 1-18.	Nomenclature of AI-1.....	27
Figure 1-19.	AI-1 signaling in <i>V. fischeri</i> ^{19a,21}	28
Figure 2-1.	First generation of C1 substituted AI-2 analogs synthesized and evaluated by Sintim and co-workers. ^{99,103,104}	35
Figure 2-2.	Structure of AI-2 dimer ¹⁰⁸	37
Figure 2-3.	Compounds evaluated as bis-ester protected AI-2 analogs.....	39
Figure 2-4.	Black bars: AI-2 or analogs-mediated expression of β -galactosidase in <i>S. typhimurium</i> (MET715: LuxS ⁻). Red bars: AI-2 or analogs-mediated expression of β -galactosidase in <i>E. coli</i> LW7/LuxS ⁻ . AI-2 or bis-ester analogs of AI-2 (20 μ M) were added to the bacterial strains, which do	

	not produce their own AI-2. Compounds 2-57 to 2-60 represent ester-protected DPD analogs: 2-57 : DPD <i>bis</i> -methyl ester; 2-58 : DPD <i>bis</i> -propyl ester; 2-59 : DPD <i>bis</i> -butyl ester; 2-60 : DPD <i>bis</i> -pentyl ester. (Done by Dr. Shizuka Nakayama, a former postdoc in the Sintim group).....	40
Figure 2-5.	Inhibition of AI-2-mediated β -galactosidase expression in <i>S. typhimurium</i> (Black Bars) and <i>E. coli</i> (Red Bars) with various <i>bis</i> -ester analogs of isobutyl DPD. [AI-2] = 20 μ M, [analogs] = 20 μ M. Compounds 23-26 represent ester protected isobutyl DPD analogs; 23 : isobutyl DPD <i>bis</i> -methyl ester, 24 : isobutyl DPD <i>bis</i> -propyl ester, 25 : isobutyl DPD <i>bis</i> -butyl ester, 26 : isobutyl DPD <i>bis</i> -pentyl ester. (Done by Dr. Shizuka Nakayama, a former postdoc in the Sintim group).....	42
Figure 2-6.	Inhibition of AI-2-mediated β -galactosidase expression in <i>E. coli</i> with various <i>bis</i> -ester analogs of hexyl DPD. [DPD] = 20 μ M, [analogs] = 20 μ M. Compounds 2-65 to 2-68 represent ester protected hexyl DPD analogs; 2-65 : hexyl DPD <i>bis</i> -methyl ester; 2-66 : hexyl DPD <i>bis</i> -propyl ester; 2-67 : hexyl DPD <i>bis</i> -butyl ester; 2-68 : hexyl DPD <i>bis</i> -pentyl ester. (Done by Dr. Shizuka Nakayama, a former postdoc in the Sintim group).....	43
Figure 2-7.	Proposed model of action in enteric bacteria. Ester protected DPD analogs diffuse into the cell, where esterases hydrolyze the ester pro-DPD and analogs and the DPD or analogs are subsequently phosphorylated by LsrK.....	44
Figure 3-1.	Chemical structures of AI-2.....	65
Figure 3-2.	a) 3-Hydrated DPD (3-7) and 3,3-dihalogen analogs that were planned to synthesize for this study. b) Degradation of AI-2 via LsrG/LsrF. We expect that the geminal dihalogen analogs cannot form the 1,3-diketone intermediate (3-10) hence would not be degraded by LsrG/LsrF.....	65
Figure 3-3.	Phospho-AI-2 in its hydrated form at C3 when binding with LsrR (PDB code: 4L4Z).....	66

Figure 3-4.	Postulated binding mode of AI-2 and dihalogenated AI-2 with Asp-243. a) carboxylic acid as hydrogen donor to form hydrogen bond with one of the hydroxyl groups on P-AI-2. b) one of the hydroxyl groups on P-AI-2 as hydrogen donor to form hydrogen bond with carboxylate. Halogens partaking in hydrogen bonding c) and halogen bonding d) ..68
Figure 3-5.	OD ₆₀₀ value of <i>E. coli</i> LW7 (luxS ⁻) after 24 hrs growth at different conditions: <i>E. coli</i> LW7 (luxS ⁻) alone; and <i>E. coli</i> LW7 (luxS ⁻) in the presence of 100 μM of each analog, respectively.....70
Figure 3-6.	a) AI-2 dependent β-galactosidase production of <i>E. coli</i> LW7 (luxS ⁻) in response to 20 μM synthetic AI-2 or analogs. 100% native <i>E. coli</i> LW7 (luxS ⁻) + AI-2 response = 167 Miller units. b) Analogs (20 μM) inhibit native β-galactosidase production in <i>E. coli</i> LW7 (luxS ⁻) in the presense of 20 μM synthetic AI-2. 100% native <i>E. coli</i> LW7 (luxS ⁻) + AI-2 response = 486 Miller units. (With the help of Yue Zheng, a graduate student from the Sintim group).....72
Figure 3-7.	AI-2 dependent EGFP induction in <i>E. coli</i> W3110 pCT6(luxS ⁺) in response to difluoro-i-Bu-AI-2 (3-35), dichloro-i-Bu-AI-2 (3-37) and dibromo-i-Bu-AI-2 (3-39) (FACS analysis with microscopic image). (Done by Jessica L. Terell, from the Bentley laboratory).....74
Figure 3-8.	Structures of AI-2 and its halogenated analogs with varied shapes and sizes.....75
Figure 3-9.	Molecular surface electrostatic potential of AI-2 and analogs in simplified models. Color ranges from -9.5 kcal/mol (red) to 9.5 kcal/mol (blue). Important atoms and σ-hole were labeled.....76
Figure 4-1.	Structures of oxazolidin AHL analogs compared with natural AI-1....97
Figure 4-2.	Stability studies of 3-oxo-C12-HSL 4-1 and 3-oxo-C12-3-aminooxazolidinone 4-3 . (Done by Yue Zheng, a graduate student in the Sintim group).....99
Figure 4-3.	Stability studies of 3-oxo-C12-3-aminooxazolidinone 4-3 monitored by TLC (stained with KMnO4 solution).....99
Figure 4-4.	Surface charge potential on simplified models of AHL and oxazolidinone

	based mimic. $n \rightarrow \pi^*$ interactions from one lone pair (n) of the acyl carbonyl group oxygen to the empty π^* on the carbon of carbonyl group in the lactone ring and the distances are highlighted. Computational level: B3LYP/6-311+G(d,2p). ¹⁵⁷	100
Figure 4-5.	The binding domain (green) in crystal structure of LasR (PDB code: 2UV0) with native 3-oxo-C12-HSL 4-1 (cyan) and re-docked analog 4-3 (yellow).....	100
Figure 4-6.	Bioluminescence production induced by native 3-oxo-C12-HSL 4-1 (10 nM orange) and 3-oxo-C12-3-aminooxazolidinone 4-3 (10 nM, blue) in <i>E. coli</i> pSB1075 (With the help of Yue, a graduate student in the Sintim group).....	102
Figure 4-7.	<i>Chromobacterium violaceum</i> CV026 agar assay. a) and b) : cultured with different concentrations of C4-HSL 4-2 and analog 4-4 . c) and d) : cultured with different concentrations of 3-oxo-C12-HSL 4-1 and analog 4-3 in presence of C4-HSL 4-2 (Done by Yue Zheng, a graduate student in the Sintim group).....	103
Figure 4-8.	<i>Chromobacterium violaceum</i> CV026 liquid broth assay. (Done by Yue Zheng, a graduate student in the Sintim group).....	104
Figure 5-1.	Chemical modification sites on AI-2.....	113

List of Schemes

Scheme 2-1. Synthesis of DPD and analogs developed by Sintim and co-workers..	34
Scheme 2-2. Arndt-Eistert type reaction and degradation pathway.....	35
Scheme 2-3. Synthetic strategy for making bis-ester protected AI-2 analogs. Reagents and conditions: (a) diazomethane, 0 °C, (b) tert-butyl-siloxyacetaldehyde, DBU (1,8 diazabicycloundec-7-ene), CH ₃ CN, RT (c) TBAF/THF. DCM= dichloromethane; DMDO = dimethyldioxirane.....	38
Scheme 2-4. Synthesis of ester protected diazodiol.....	48
Scheme 2-5. Oxidation of diazo moiety into carbonyl.....	50
Scheme 2-6. Note: Both the diazoketones and diketones did not have good MS spectrum (presumably due to decomposition under the MS conditions. Therefore, further MS characterization was done by adding phenyl diamine to the diketones and stirred overnight to convert the diketones into quinoxalines, see Scheme above (this is a standard practice). MS data is therefore reported for the quinoxaline derivatives	52
Scheme 3-1. Initial attempt to make dichloro AI-2 3-17	69
Scheme 3-2. Synthesis of dihalogenated AI-2 analogs.....	69
Scheme 4-1. Degradation of AHL under basic condition.....	98
Scheme 4-2. Synthesis of oxazolidine analogs.....	105

List of Abbreviations

ACP= Acyl-carrier protein
AHL= Acyl homoserine lactone
AIP= Autoinducing peptide
AI-2= Autoinducer 2
ATP= Adenosine triphosphate
CAI-1= *Cholerae* Autoinducer-1
DABCO= 1,4-Diazabicyclo[2.2.2]octane
DBU= 1,8-Diazobicyclo[5.4.0]undec-7-ene
DCM= Dichloromethane
DMSO= Dimethyl sulfoxide
DMS= Dimethyl sulfide
DPD= 4,5-Dihydroxyl-2,3-pentadione
EtOH= Ethanol
GFP= Green fluorescent protein
HAI-1= *Harveyi* Autoinducer-1
HSL= Homoserine lactone
LDA= Lithium diisopropylamide
LM= Luria Marine
MeCN= Methyl acetonitrile
MeI= Methyl iodide
MeOH= Methanol
MRSA= Methicillin-resistant *Staphylococcus aureus*
MTA= Methylthioadenosine
MTAN= Methylthioadenosine nuclease
MTR= Methylthioribose
nBuLi= (Normal) butyl lithium
ONPG= *O*-nitrophenyl-galactoside
PQS= *Pseudomonas* quinolone signal
R-DHMF= R-dihydroxymethyl furanone

RLU= Relative light units

R-THMF= R-tetrahydroxymethyl furanone

SAH= S-adenosylhomocysteine

SAM= S-adenosylmethionine

S-DHMF= S-dihydroxymethyl furanone

SRH= S-ribosehomocysteine

S-THMF= S-tetrahydroxymethyl furanone

TBAF= Tetrabutylammoniafluoride

TBS= Tertbutyldimethylsilyl

THF= Tetrahydrofuran

VRE= Vancomycin-resistant *Enterococcus*

VRSA= Vancomycin-resistant *Staphylococcus aureus*

Chapter 1. Introduction

1.1 A bacteria battle and a post-antibiotic era.

The fight against pathogenic bacteria has been ongoing since the beginning of human existence. Until the 1950s, when many antibiotics were discovered or developed, death from bacterial infections was common and many epidemics or pandemics occurred. For example, in the fourteenth century, more than one third of the population in Europe was killed by the Black Death epidemic, caused by *Yersinia pestis*. In the pre-antibiotic era, about 30% of all deaths were related to bacterial infection in the United States. In the present day, bacterial infection is still a common problem and new treatments continue to be developed.

The first commercially available antibiotic was sulfamide protonsil. However, it was the discovery by Sir Alexander Fleming in 1928 that ushered in a new era of antibacterial therapeutics. Fleming discovered that a *Penicillium* fungus produced an antibacterial substance that could kill bacteria. Following the golden age of antibiotic discovery, between 1940 and 1960, it was then discovered that bacteria have sophisticated mechanisms to develop resistance to antibiotics (**Figure 1-1** summarizes the timeline of antibiotic discovery or development and emergence of resistant bacterial strain in the clinic¹). During the past few decades, scientists have continued to develop new classes of antibiotics, as well as introduce successive generations of the existing drug classes that could increase spectrum activity and improve pharmacokinetics in order to replace the old antibiotics, which continue to be rendered ineffective due to

bacterial resistance (**Table 1-1**). There is however no reason to believe that new antibacterial agents will not face the same resistance issues and it appears that mankind will always have a never ending battle with bacteria. Currently, methicillin- and vancomycin-resistant *Staphylococcus aureus* (MRSA and VRSA), vancomycin-resistant *Enterococcus* (VRE), penicillin-resistant *Streptococcus pneumonia* (PRSP), multi-drug resistant (MDR) *Clostridium difficile* put enormous stress on global healthcare. It has been estimated that 20% of the global population are persistent carriers of *S. aureus*;² and about nineteen thousand deaths in the US are due to MRSA³. The annual cost of treating MRSA infections in the US is about three billion dollars.³

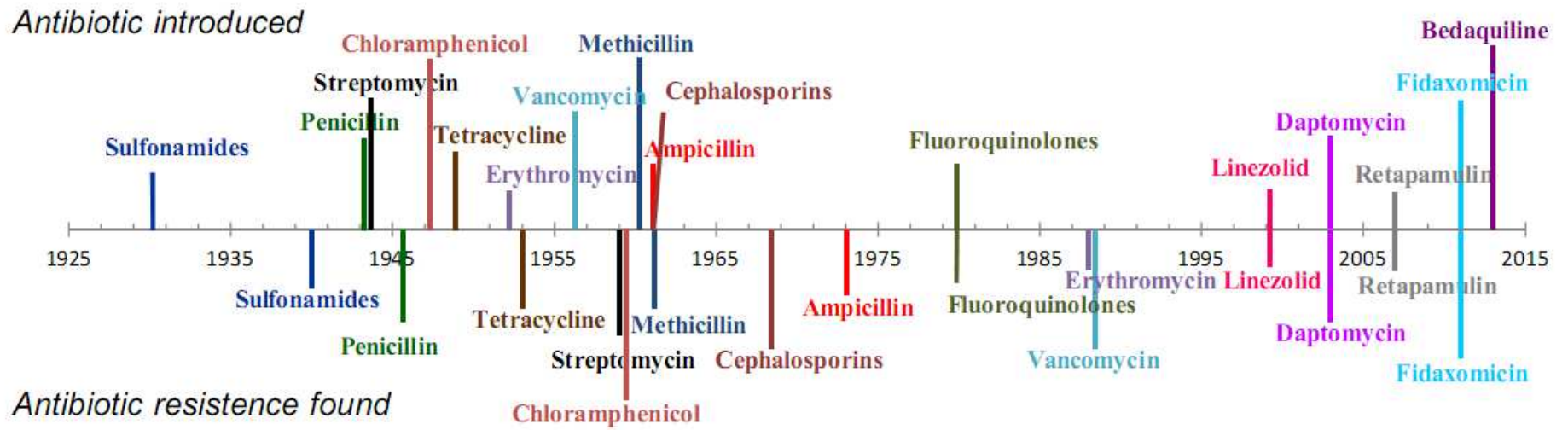
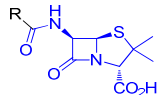
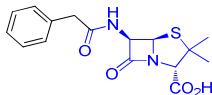
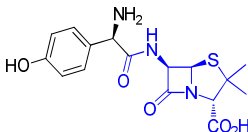
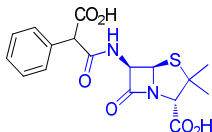
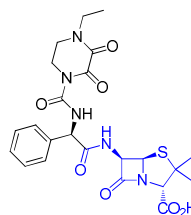
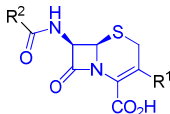
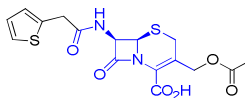
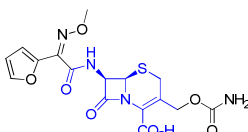
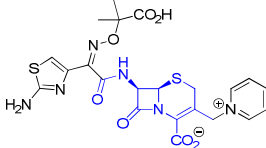
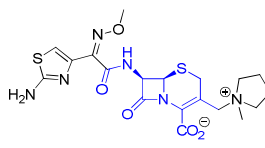
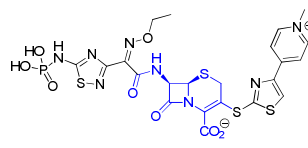
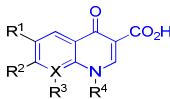
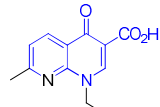
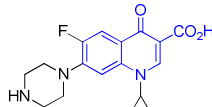
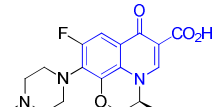

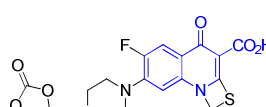


Figure 1-1. Timeline showing the deployment of representative antibiotics and resistance observed (summarized from literatures¹).

Antibiotic class	Generation 1	Generation 2	Generation 3	Generation 4	Generation 5	Primary target
 <p>Penicillin R=aklyls, aryls</p>	 <p>Penicillin G (1-1)</p>	 <p>Amoxicillin (1-2)</p>	 <p>Carbenicillin (1-3)</p>	 <p>Piperacillin (1-4)</p>	Penicillin binding proteins (PBPs), which is involved in the synthesis of peptidoglycan	
 <p>Cephalosporin R¹=aklyls, aryls R²=aklyls, aryls</p>	 <p>Cefalotin (1-5)</p>	 <p>Cefuroxime (1-6)</p>	 <p>Ceftazidime (1-7)</p>	 <p>Cefepime (1-8)</p>	 <p>Ceftaroline (1-9)</p>	Penicillin binding proteins (PBPs) that involved in the synthesis of peptidoglycan
 <p>Quinolone R¹=H,F; R²=alkyls, heterocyclics, X=C,N; R³=H, alkoxys, R⁴=alkyls</p>	 <p>Nalidixic acid (1-10)</p>	 <p>Ciprofloxacin (1-11)</p>	 <p>Levofloxacin (1-12)</p>	 <p>Moxifloxacin (1-13)</p>	 <p>Prulifloxacin (1-14)</p>	Topoisomerase II and IV in DNA unwinding

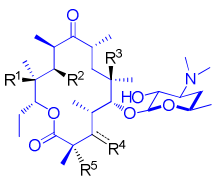
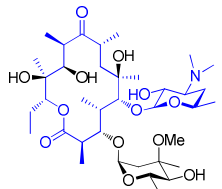
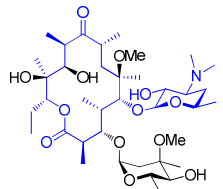
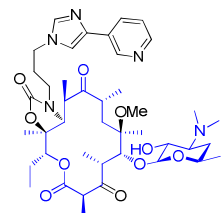
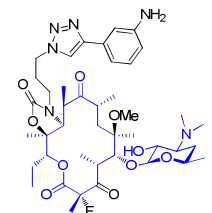
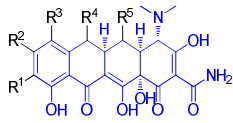
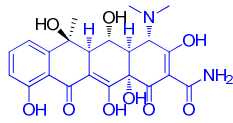
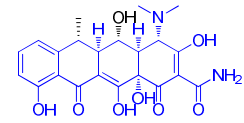
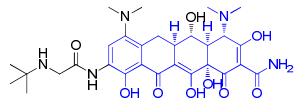
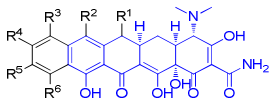
 <p>Macrolide</p> <p>R¹=OH, carbamates, R²=OH, carbomates, R³=OH, methoxy, H R⁴=O, alkoxys R⁵=H, F</p>	 <p>Erythromycin A (1-15)</p>	 <p>Clarithromycin (1-16)</p>	 <p>Telithromycin (1-17)</p>	 <p>Solithromycin (1-18)</p>	50S ribosomal subunit in peptide synthesis
 <p>Tetracycline</p> <p>R¹=H, amides, aryls R²=H, aryls, R³=H, amines, R⁴=H, alkyls, OH, R⁵=OH, H</p>	 <p>Oxytetracycline (1-19)</p>	 <p>Doxycycline (1-20)</p>	 <p>Tigecycline (1-21)</p>	 <p>Pentacycline (1-22)</p>	30S ribosomal subunit in peptide synthesis

Table 1-1. Successive generations of representative antibiotic classes and their primary targets. Core scaffolds are highlighted in blue while peripheral chemical modifications (R groups) are in black. Most antibiotics on the market inhibit five major targets in bacteria (also see **Figure 1-2**).

There are multiple factors that lead to the origin of bacterial resistance to antibiotics. Historically, more than 60% of existing antibiotics and their semi-synthetic derivatives are derived from or inspired by natural products,⁴ and many of them were discovered by systematic screening methods of soil bacteria *Streptomyces*. This method was introduced by Ukrainian-American microbiologist Selman Waksman in the 1940s. Antibiotic producing bacteria have co-existed with other bacteria for billions of years and so it is not surprising that resistance to these molecules evolved before they were discovered by man. Recently, Wright and colleagues identified diverse homologues of known antibiotic resistance genes from 30,000-year-old permafrost sediments, supporting the argument that these resistance genes evolved before man started using antibiotics on an industrial scale.⁵ Antibiotic resistance genes can be disseminated vertically and horizontally throughout microbial communities.⁶ As a result, it is not surprising that most soil-dwelling bacteria show some form of antibiotic resistance.⁷

Although antibiotic resistance genes and the spread of these genes occur naturally without man's intervention, modern activities have exacerbated the antibiotic resistance problem. It is believed that the widespread prescription of antibiotics to patients, excessive use of antibiotics in animal husbandry and non-therapeutic use of antibiotics, for example as prophylactics in household products, have put evolutionary pressure on bacteria to develop resistance.⁸

Bacteria use several pathways to render the antibiotics ineffective: 1. Overexpression of enzymes that can modify the antibiotics, rendering them inactive; 2.

Mutation of the bacterial target site, which blocks the binding of antibiotics to the target site; 3. Export of antibiotics to extracellular media or loss of porin channels, resulting in lower permeability of antibiotics.⁹

The rate of new antibiotic discovery is much slower than the rate of resistance development, and the additional decreased pharmaceutical investment is worrisome.¹⁰ Because developing new drugs against existing bacterial targets could lead to cross resistance, there is a need to find alternative targets or paradigms to contain bacterial infections.

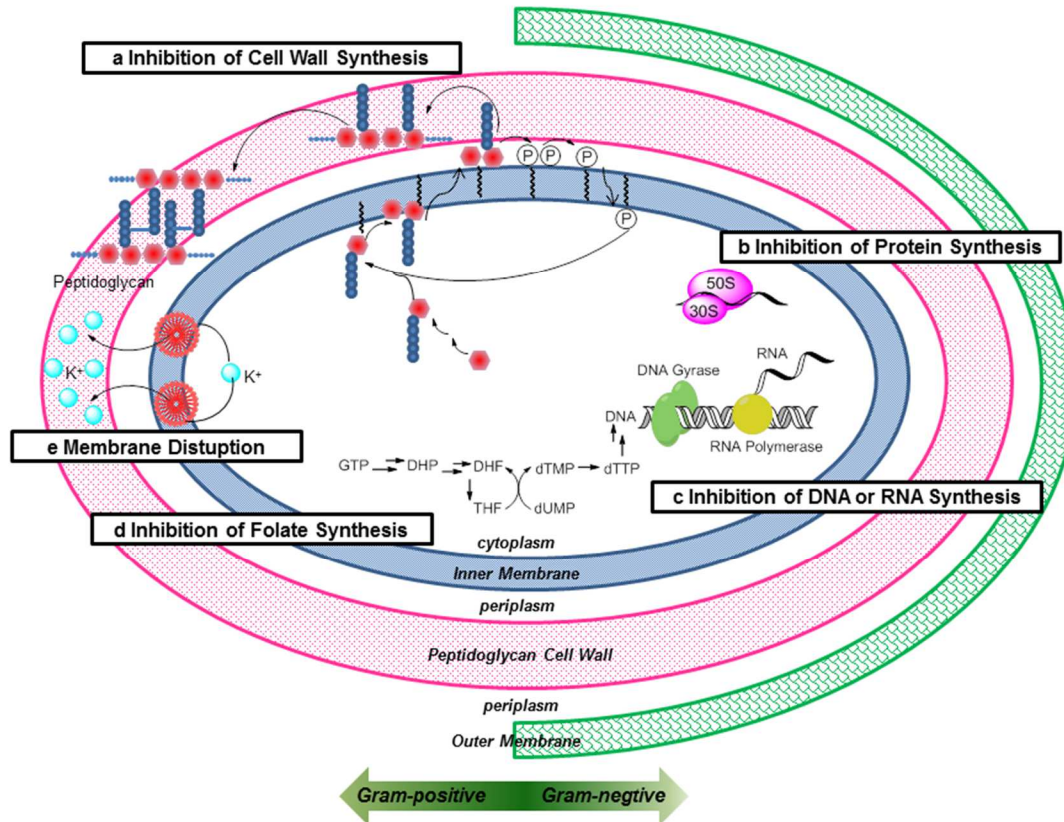


Figure 1-2. Major targets for antibacterial action. **a)** Inhibition of cell wall synthesis. **b)** Inhibition of protein synthesis. **c)** Inhibition of DNA or RNA synthesis. **d)** Inhibition of folate synthesis. **e)** Disruption of membrane. Modified from literature.^{1c, 11}

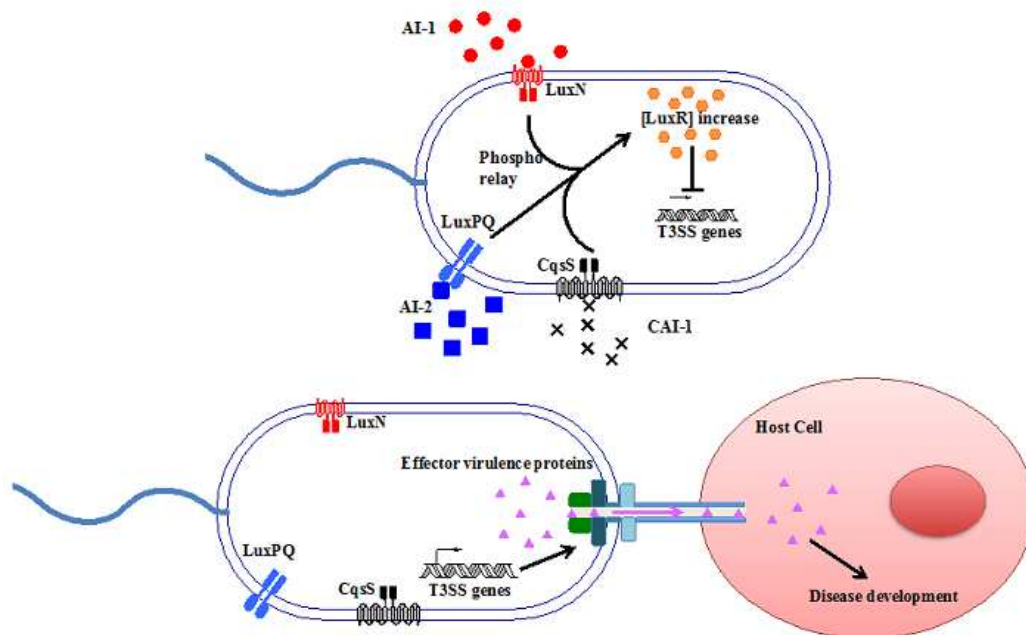
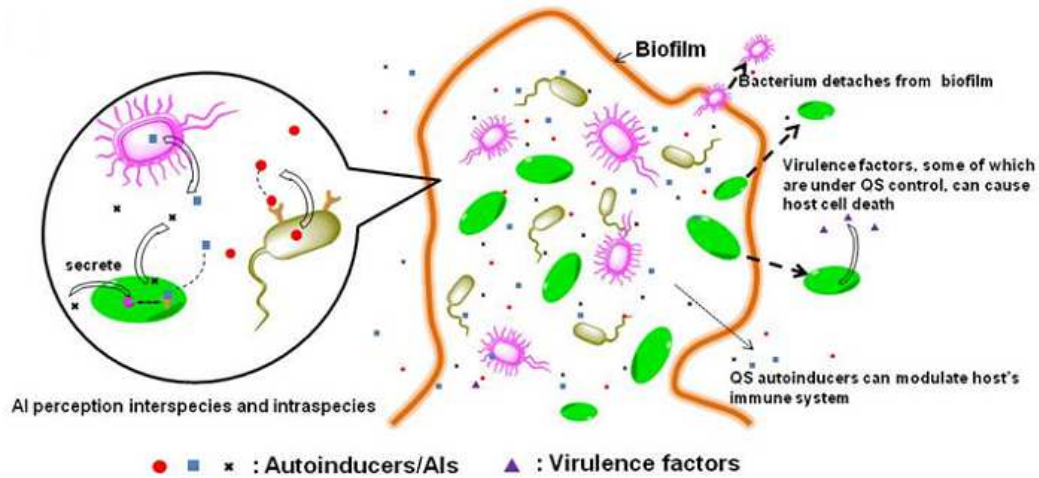
In 2010, the Infectious Diseases Society of America (IDSA) proposed the 10 x '20 Initiative, that calls for 10 new systematic antibiotics by 2020.¹² In 2011, the US government issued \$94 million of funding to support the search for chemically diverse novel antibiotic candidates. Policies and incentives have been made to favor antibiotic R&D, as well. This year, 2014, World Health Organization (WHO) published “Antimicrobial resistance: global report on surveillance 2014” to raise public awareness.¹³ Lastly, the academic society has also been advocating a paradigm shift in antibiotic discovery, by targeting processes in bacteria that cause disease rather than killing bacteria, which creates evolutionary pressures for resistance to emerge. Examples of processes to target in bacteria include toxin production and biofilm formation, both of which are partly regulated by bacterial cell-to-cell communication or quorum sensing (discussed in the next section).^{1b, 9}

1.2 Quorum sensing inhibition—a new strategy to fight bacteria

(Part of this section was published in reference ¹⁴.)

Since antibiotics ultimately put evolutionary pressure on pathogens to develop resistance, a new strategy to treat bacterial infections, which does not necessarily kill bacteria but rather curbs the virulence and biofilm formation (an aggregate of bacterial cells, extracellular DNA, proteins and polysaccharides, to some extent enhances bacterial tolerance to antibiotics¹⁵), has been proposed.^{1b, 9} It has been shown that quorum sensing (QS, **Figure 1-3**), a system bacteria use to communicate and respond as a collective to population density, but not critical to individual vitality, plays a critical role in regulating virulence and formation of biofilm.¹⁶ In 1965, a hormone-like cell product was discovered in *S. pneumonia*¹⁷ and was later identified as an autoinducing peptide.¹⁸ The term quorum sensing was first implicitly defined by Nealson and co-workers in 1970, to describe the production of light by *V. fischeri* at high cell densities (i.e., a population-dependent process).¹⁹ Nealson and co-workers then postulated that the bioluminescence from *V. fischeri* was regulated by molecules, called “autoinducers (AIs)”. Subsequently, several autoinducers (both intraspecies and interspecies) have been identified.

a)



b)

Figure 1-3. a) Increased concentration of autoinducers in bacterial biofilms promotes the synthesis of biofilm matrices, such as adhesion proteins and polysaccharides, which are required for the maintenance of the biofilm structure; **b)** Autoinducers repress the production of virulence factors as well as the synthesis of the components of the bacterial secretory system, such as T3SS, in some bacteria (for example, AI-1, AI-2 and CAI-1 represses T3SS gene expression in *V. harveyi*²⁰).

Because autoinducers (AIs) are the signaling molecules in QS, a useful strategy

to inhibit QS and hence reduce toxin production and biofilm formation in some bacteria is to use antagonists of autoinducers. It is however worth mentioning that bacterial toxin production and biofilm formation could also be regulated by pathways other than QS, so anti-QS agents should not be considered as the only method for reducing all toxin production and biofilm formation. There are three major classes of autoinducers (**Figure 1-4**): AI-1 (or N-Acyl homoserin lactones, AHLs, **1-23**),²¹ oligopeptides/AIP (autoinducing peptide, **1-24**)^{18, 22} and AI-2(**1-25**)²³. There are also other bacterial signaling molecules that do not fall under the above three classes, such as PQS (*P. pseudomonas* quinolone signal, **1-26**)²⁴, γ -butyrolactone(**1-27**)²⁵, CAI-1(**1-28**)²⁶, DSF (diffusible signal factor, **1-29**)²⁷, 2-AA (2-amino acetophenone, **1-30**)²⁸, DKP (diketopiperazine, **1-31**)²⁹, IQS (**1-32**)³⁰ and CSP (competence stimulating peptide, **1-33**)³¹. It is worth noting that AI-2 (**1-25**) exists as a collection of equilibrium mixtures. Starting with its linear form DPD (**1-25a**), the hydroxyl group at C5 position tends to attack the carbonyl group at C2 position and cyclize as a hydrofuranone, which goes through hydrolysis and tautomerization.

Due to the pivotal role played by quorum sensing in bacterial pathogenesis (virulence expression) and resistance (biofilm formation), quorum sensing receptors have emerged as potential targets for anti-infective therapy. In the last two decades, attempts have been made to find or develop inhibitors for different receptors, which are involved in the production and perception/response to autoinducers chiefly on AI-1 and AI-2. There are several established cell models and assays that aid the studies of

quorum sensing and herein a few representatives will be showcased.

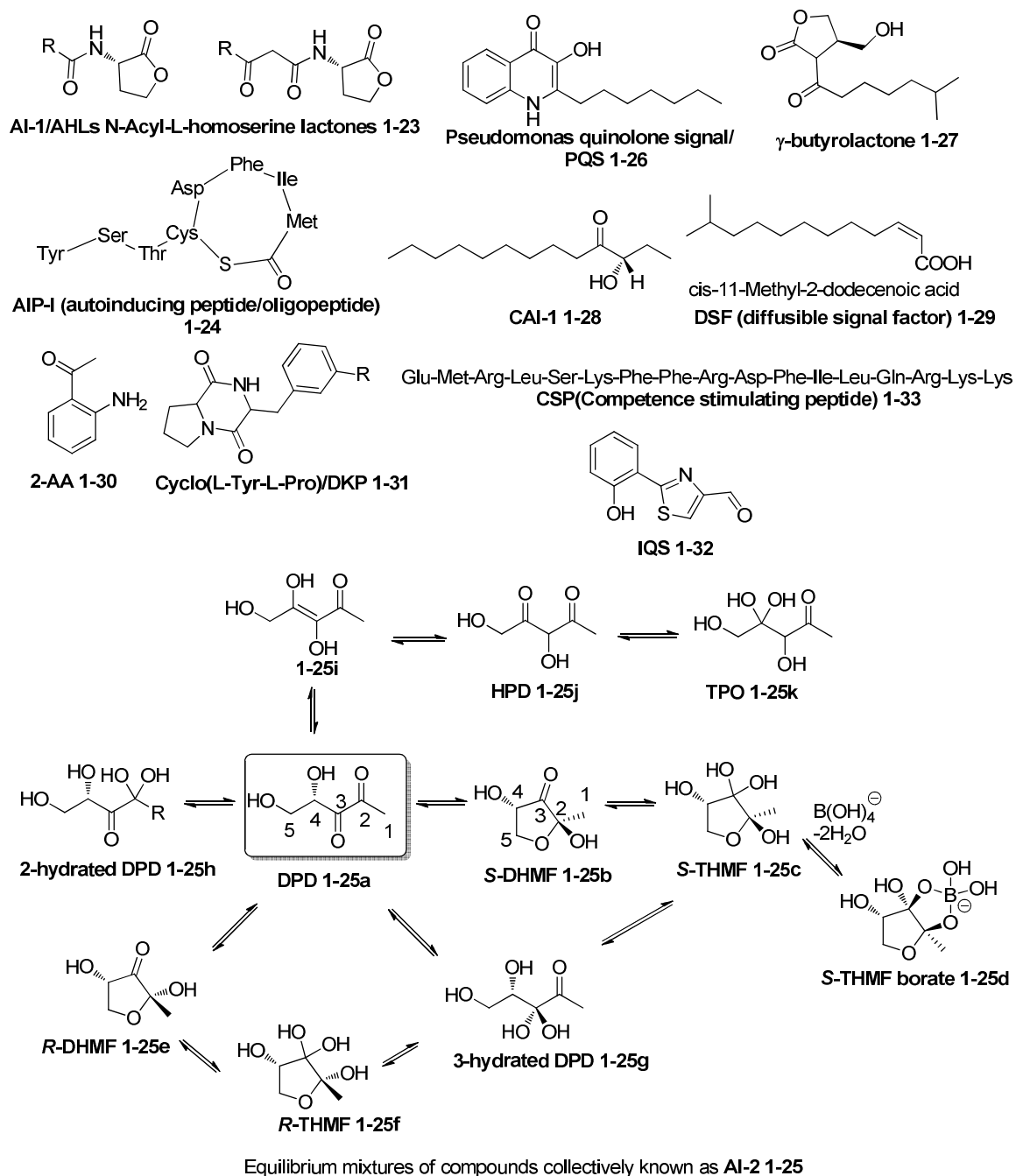


Figure 1-4. Structures of Autoinducer molecules. AI-2 is a term used to describe DPD (4,5-Dihydroxy-2,3-pentanedione, **1-25a**) and isomers in equilibrium.

The quorum sensing systems in *Vibrios* have been well studied.³² In *V. harveyi*, three QS systems mediated by three different autoinducers have been characterized

(Figure 1-5).³³ Whereas HAI-1 (1-26) is only found in *V. harveyi*,³⁴ CAI-1 (1-28) is found to be active in other *Vibrios*.³⁵ AI-2 is found in more than 70 bacterial species as a non-specific interspecies signaling molecule,³⁶ and the active form of AI-2 in *V. harveyi* is its borate form 1-25d. CAI-1, HAI-1 and AI-2 are sensed by CqsS, LuxN and LuxQ, respectively. LuxQ associates with LuxP, a periplasmic binding protein, to form LuxPQ and regulate phosphorylation signal transduction cascade.³⁷ At low cell density, as well as low AI concentration, these sensors act as kinases and transfer phosphate to LuxU, which then relays a phosphate group to LuxO. LuxO-phosphate (a transcriptional activator), along with sigma factor σ^{54} , activates the expression of regulatory small RNAs (sRNAs) Qrr1-5.³⁸ Qrr1-5, in conjunction with the chaperone Hfq, destabilizes the *luxR* mRNA so that LuxR synthesis is suppressed. Qrr1-5, in conjunction with the chaperone Hfq, destabilizes the *luxR* mRNA so that LuxR synthesis is suppressed. At high AI concentration, the sensors become phosphatases, which dephosphorylate LuxU, which in turn also dephosphorylates LuxO. Dephosphorylated LuxO is no longer active and therefore, the concentrations of Qrr1-5, which degrade the mRNA of LuxR, decrease. As the concentration of LuxR, which is a transcription factor, increases, the genes that are controlled by LuxR (some of which are virulence determinants) are expressed. In *V. cholerae*, sRNAs Qrr1-4 facilitate the degradation of *hapR* mRNA transcript and stabilize *aphA* mRNA transcript.³⁸

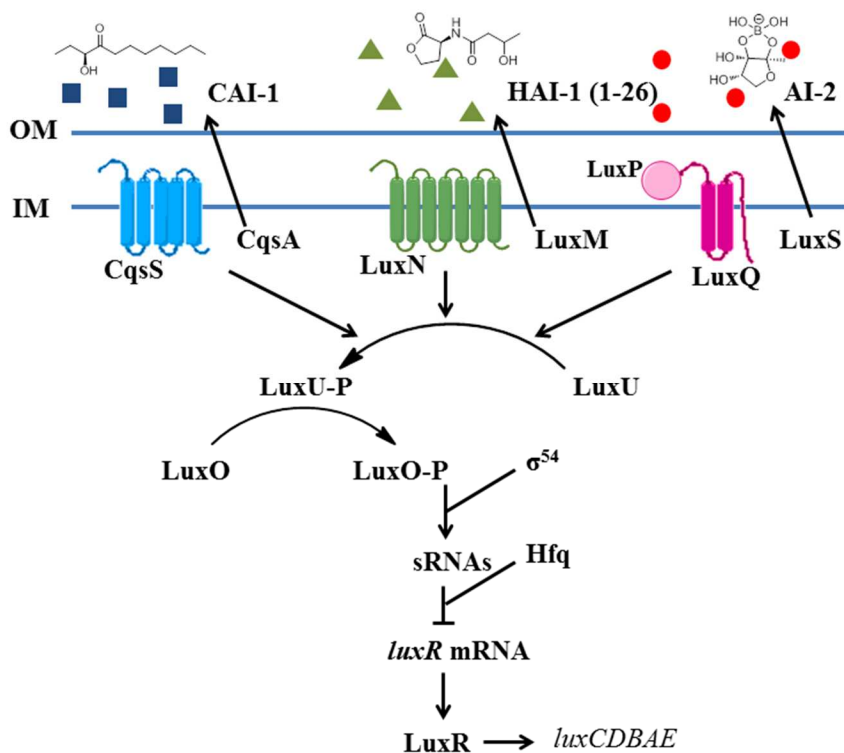


Figure 1-5. *V. harveyi* quorum sensing system. Arrows denote the phosphorelay at low cell density.

Apart from the characterized AI-2 system in *Vibrios*, AI-2 signaling in enteric bacteria has also been well characterized. *S. typhimurium* and *E. coli* share a similar QS system (**Figure 1-6**). In these bacteria, the cyclic form of AI-2, **R-THMF 1-25f**, is recognized by periplasmic binding protein LsrB.³⁹ Once AI-2 is internalized via LsrB, part of the Lsr transporter encoded by *lsrACDB* operon, it is phosphorylated by a kinase, LsrK, and the phospho-AI-2 then binds to the repressor LsrR to de-repress the *lsr* operon.⁴⁰ LsrF and LsrG can further process phospho-AI-2 and yield dihydroxyacetonephosphate (DHPA, **1-27**) and acetyl-CoA, two key metabolites.⁴¹ When AI-2 concentration is low and hence, the concentration of phospho-AI-2 is also low, LsrR binds the *lsr* promoter to inhibit the transcription of *lsr* genes whereas at high

AI-2 concentration, *lsr* genes are transcribed due to the de-repression of LsrR. Both LsrK and LsrR play key regulatory roles in the biofilm formation of *E. coli*.⁴² It has been shown that the deletion of *lsrR* affects the expression of 146 genes whereas deleting *lsrK* affected 149 genes.^{42a} Interestingly, *S. typhimurium* and *E. coli* do not produce AHLs, but they can detect AHLs synthesized by other Gram-negative bacteria via SdiA, a homologue of LuxR.⁴³ So far, little is known about the genes that SdiA regulate.⁴⁴

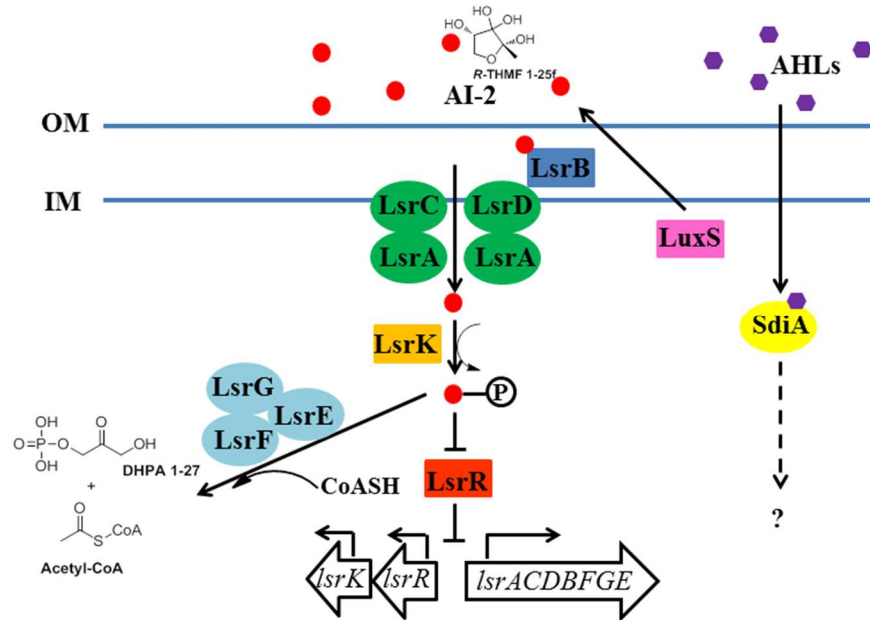


Figure 1-6. Quorum sensing model in *S. typhimurium* and *E. coli*.

1.3 AI-2 signaling in other bacteria and inhibitors of AI-2 signaling

As already stated, AI-2 is found in many bacteria and with the exception of enteric bacteria and *Vibrios*, remain poorly characterized in other bacterial species.

Table 1-2 lists the different bacteria that have been shown to respond to AI-2 and details some bacterial phenotypes that are regulated by the AI-2/LuxS QS system

In the last decade, attempts have been made to find or develop inhibitors for different receptors (**Figure 1-7**), which are involved in the production and perception/response to AI-2. There are a few crystal structures of receptor/AI-2 complexes that have been solved. These structures provide important insights for the medicinal chemist to develop anti-AI-2 small molecules. The structures could also be used for docking experiments to determine *in silico* which small molecules are viable candidates to develop into QS antagonists.

Strain	LuxS type synthase	AI-2 Receptor	Functions regulated by AI-2	Diseases	References
<i>Actinobacillus actinomycetemcomitans</i>	LuxS	RbsB, ^a LsrB ^a	Optimal growth under iron starvation and biofilm development	Associated with localized aggressive periodontitis	^{45, 46}
<i>Actinobacillus pleuropneumoniae</i>	LuxS	unknown	Pleiotropic effects on biofilm formation, adhesion ability, and iron metabolism. LuxS is essential for the survival in natural host	Respiratory pathogen found in pigs	⁴⁷
<i>Bacillus anthracis</i>	LuxS	unknown	Virulence gene expression, cell growth	Etiological agent of anthrax in livestock	⁴⁸
<i>Bacillus cereus</i>	LuxS	Lsr-like	Biofilm formation	Related to foodborne illness	⁴⁹
<i>Bacillus subtilis</i>	LuxS	unknown	Morphogenesis and social behavior	a normal gut commensal in humans	⁵⁰
<i>Borrelia burgdorferi</i>	LuxS	unknown	Increasing expression of the outer surface lipoprotein VlsE	causative agent of Lyme disease	⁵¹
<i>Campylobacter jejuni</i>	LuxS	unknown	motility, biofilm formation and expression of <i>flaA-B</i>	Causative agent of human gastroenteritis	⁵²
<i>Clostridium difficile</i>	LuxS	Unknown	Toxin synthesis	Causative agent of infectious diarrhea	⁵³
<i>E. coli</i> (EHEC)	LuxS	LsrB, ^a LsrR, ^b LsrK ^c	Chemotaxis towards AI-2, swimming motility, colonization	Causative agent of foodborne disease	⁵⁴
<i>E. coli</i> K12	LuxS	LsrB, ^a LsrR, ^b LsrF, ^d LsrK ^c	Motility, biofilm formation	model organism strains	^{41, 55}
<i>Enterococcus faecalis</i>	LuxS	unknown	Glyceraldehyde-3-phosphate dehydrogenase and malate dehydrogenase up-regulated by AI-2, biofilm formation	endocarditis and bacteremia, urinary tract infections, meningitis and other infections in human	⁵⁶
<i>Haemophilus influenzae</i>	LuxS	RbsB ^a	Biofilm formation	opportunistic pathogens that may cause bacteremia, pneumonia, epiglottitis and acute bacterial meningitis	⁵⁷
<i>Helicobacter pylori</i>	LuxS	TlpB ^e	Chemotaxis against AI-2	Associated with stomach inflammation, gastritis, and ulcer	⁵⁸

<i>Klebsiella pneumoniae</i>	LuxS	unknown	Early steps of biofilm formation, lipopolysaccharide synthesis	Causative agent of pneumonia, bloodstream infections, wound or surgical site infections, and meningitis	59
<i>Listeria monocytogenes</i>	LuxS	unknown	Biofilm formation	listeriosis	60
<i>Moraxella catarrhalis</i>	unknown	unknown	AI-2 promotes biofilm formation and antibiotic resistance	Causative agent of infections of the respiratory system, middle ear, eye, central nervous system, and joints of humans	61
<i>Mycobacterium avium</i>	Unknown	unknown	oxidative stress response up-regulated by AI-2	opportunistic pathogen that may cause fevers, diarrhea, malabsorption and anorexia	62
<i>Neisseria meningitidis</i>	LuxS	unknown	meningococcal virulence	Causative agent of meningitis	63
<i>Porphyromonas gingivalis</i>	LuxS		Modulates protease and haemagglutinin activities	pathogen in early onset periodontitis	64
<i>Pseudomonas aeruginosa</i>	Unknown	unknown	Virulence factor production	opportunistic pathogen that may cause infections of the pulmonary tract, urinary tract, burns,wounds,	65
<i>Salmonella enterica</i> serovar Typhimurium	LuxS	LsrB, ^a LsrR, ^b LsrK, ^c LsrF ^d	Pathogenicity island I gene expression And invasion into eukaryotic cells, biofilm formation, motility	salmonellosis	39, 66
<i>Sinorhizobium meliloti</i>	Unknown	SmlsrB ^a	interferes with AI-2-regulated behaviors of other species	nitrogen-fixing bacterium, forms a symbiotic relationship with plants	67
<i>Shewanella putrefaciens</i>	LuxS	unknown	AI-2 may involve in spoilage of fish and shrimp	a facultative anaerobe with the ability to reduce iron and manganese, associated with the odor of rotting fish	68
<i>Staphylococcus aureus</i>	LuxS	unknown	capsular polysaccharide synthesis	a common cause of skin infections, respiratory disease and food poisoning	69
<i>Staphylococcus epidermidis</i>	LuxS	unknown	Controls genes involved in phenol-soluble modulins peptides, acetoin dehydrogenase, gluconokinase, bacterial apoptosis protein LrgB,	Part of normal human flora but form biofilms on plastic devices placed within the body and cause infections	70

			nitrite extrusion protein and fructose PTS system subunit		
<i>Streptococcus anginosus</i>	LuxS	unknown	antibiotic susceptibility	part of the human bacteria flora, but can cause diseases including brain and liver abscesses	71
<i>Streptococcus intermedius</i>	LuxS	unknown	antibiotic susceptibility and biofilm formation	Associated with infective endocarditis and abscesses	72
<i>Streptococcus gordonii</i>	LuxS	unknown	carbohydrate metabolism and biofilm formation	can cause acute bacterial endocarditis and form biofilm on clean tooth surfaces	73
<i>Streptococcus mutans</i>	LuxS	unknown	Controls genes involved in biofilm formation, bacteriocin synthesis, competence, and acid tolerance	Associated with tooth decay	74
<i>Streptococcus pneumoniae</i>	LuxS	unknown	Biofilm formation and lysis	major cause of pneumonia, many types of pneumococcal infections and bacterial meningitis	75
<i>Vibrio cholerae</i>	LuxS	LuxP ^a	Biofilm formation, protease and virulence production, and competence	Cholera caused by infection of the intestine	26a, 76
<i>Vibrio harveyi</i>	LuxS	LuxP ^a	Bioluminescence, biofilm formation, colony morphology, siderophore production, type III secretion and metalloprotease production	a primary and opportunistic pathogen of marine animals	20, 33, 77
<i>Vibrio fischeri</i> (<i>Aliivibrio fischeri</i>)	LuxS	LuxP ^a	Bioluminescence, biofilm formation	Model strain	78
<i>Vibrio vulnificus</i>	LuxS	LuxP ^a	cytotoxicity	A causative agent of septicemia	79
<i>Yersinia pestis</i>	LuxS	LsrB ^a	regulates metabolic activities and oxidative stress genes	a causative agent of the systemic invasive infectious disease/plague	80

Table 1-2. Some bacterial phenotypes, which are regulated by AI-2/LuxS. Note: ^aTransporter, ^bTranscriptional regulator, ^cKinase, ^dAI-2 degradative enzyme, ^eChemoreceptor

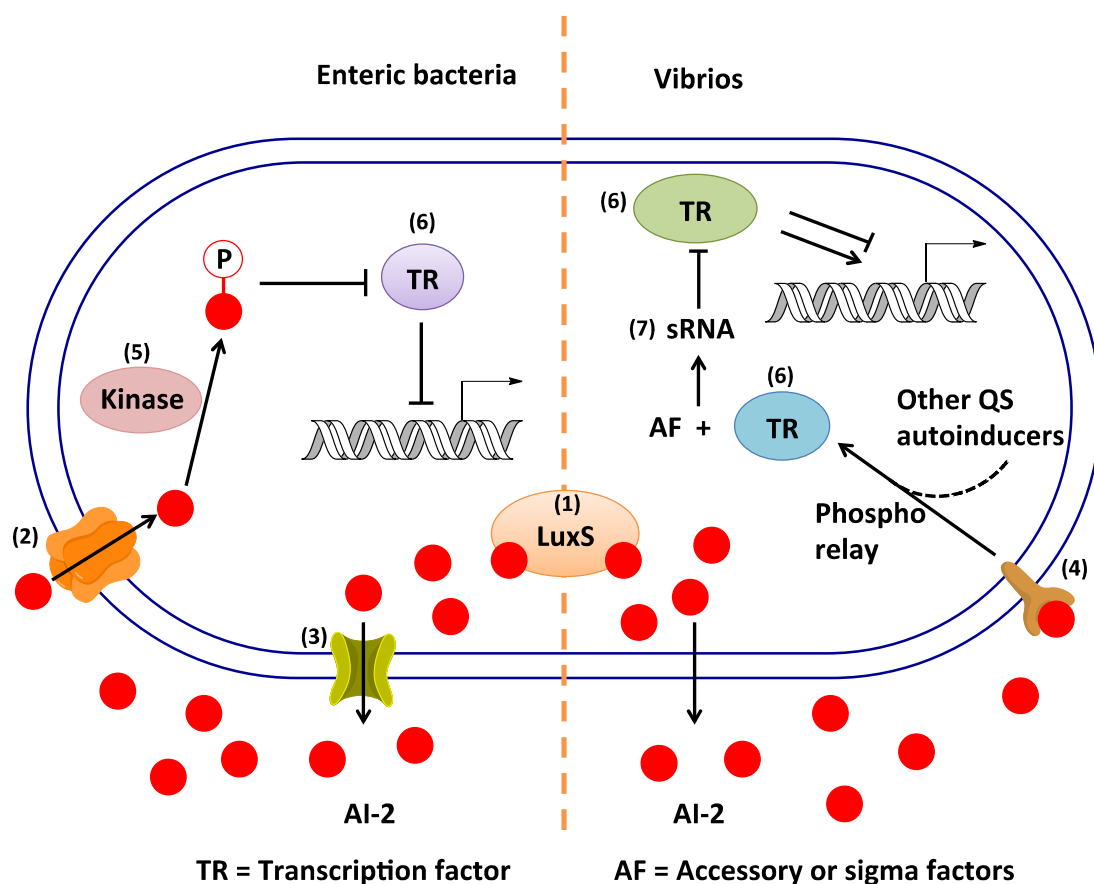


Figure 1-7. Possible AI-2-based “druggable” targets. (1) LuxS; (2) AI-2 transporter (such as LsrB); (3) efflux pump for AI-2; (4) extracellular receptor for AI-2 (such as LuxP); (5) intracellular receptor for AI-2; (6) AI-2-regulated transcription factor or repressor (such as LsrR) (7) small regulatory RNA (sRNA) mediated QS circuit.

The first AI-2 receptor that was structurally characterized was LuxP.³⁰ LuxP is a membrane bound, extra cytosolic receptor that binds to the furanosyl borate diester form of AI-2, **S-THMF borate 1-25d** (Figure 1-8).²³

Following the crystal structure of LuxP/AI-2 complex, the Bassler and Hughson laboratories solved the structure of a second AI-2 receptor, LsrB (from *S. typhimurium*) in complex with a cyclic and hydrated form of AI-2, **R-THMF 1-25f** (Figure 1-9).³⁹

21

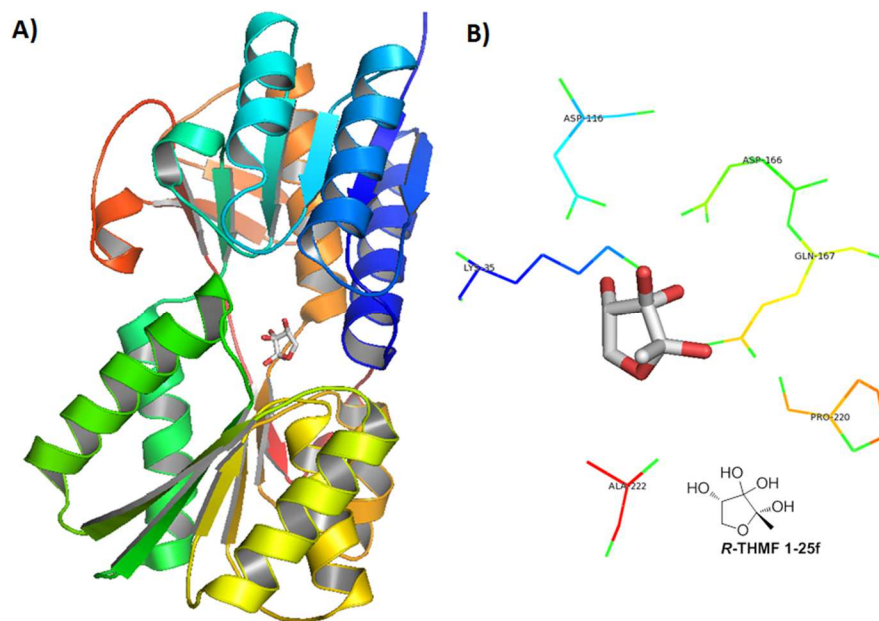


Figure 1-9. **A)** Crystal structure of LsrB from *S. typhimurium*, in complex with AI-2 (PDB code: 1TJY). **B)** AI-2 binding site of LsrB, showing protein residues that are within 3 Å of AI-2.

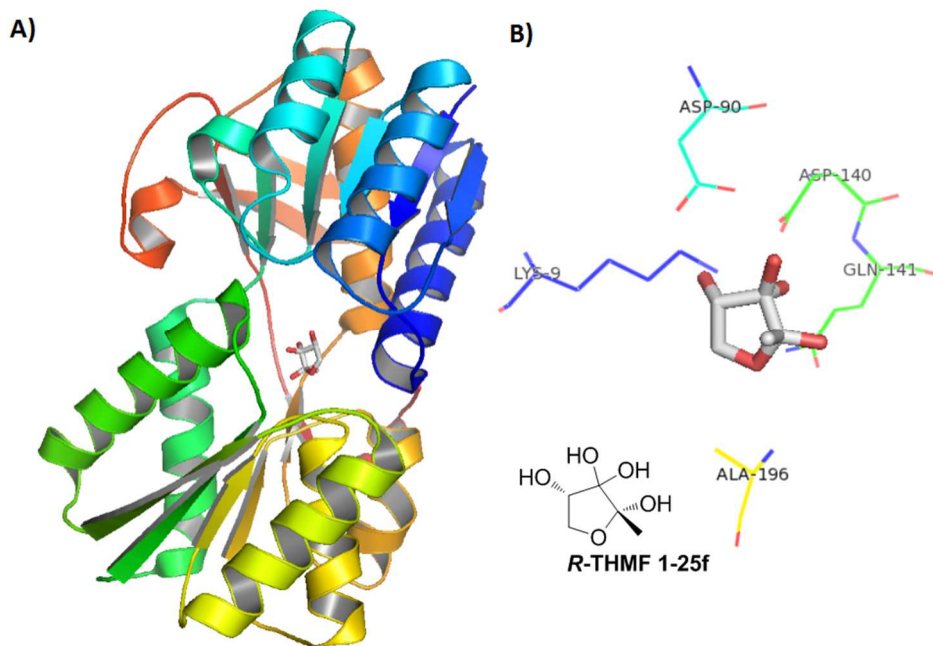


Figure 1-10. **A)** Crystal structure of LsrB from *Sinorhizobium meliloti* (PDB code: 3EJW). **B)** AI-2 binding site of LsrB, showing protein residues that are within 3 Å of AI-2.

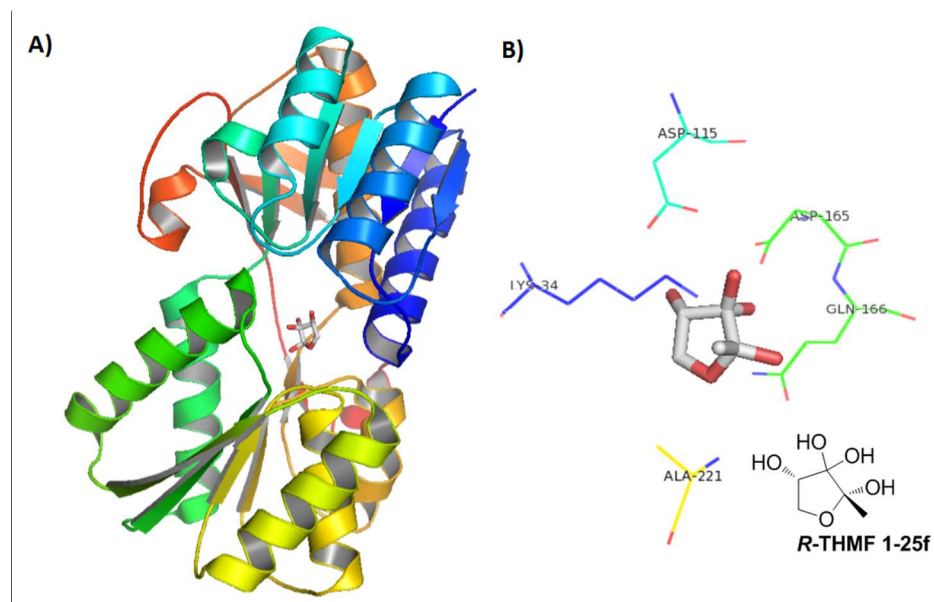


Figure 1-11. A) Crystal structure of LsrB from *Y. pestis* (PDB code: 3T95). B) AI-2 binding site of LsrB, showing protein residues that are within 3 Å of AI-2.

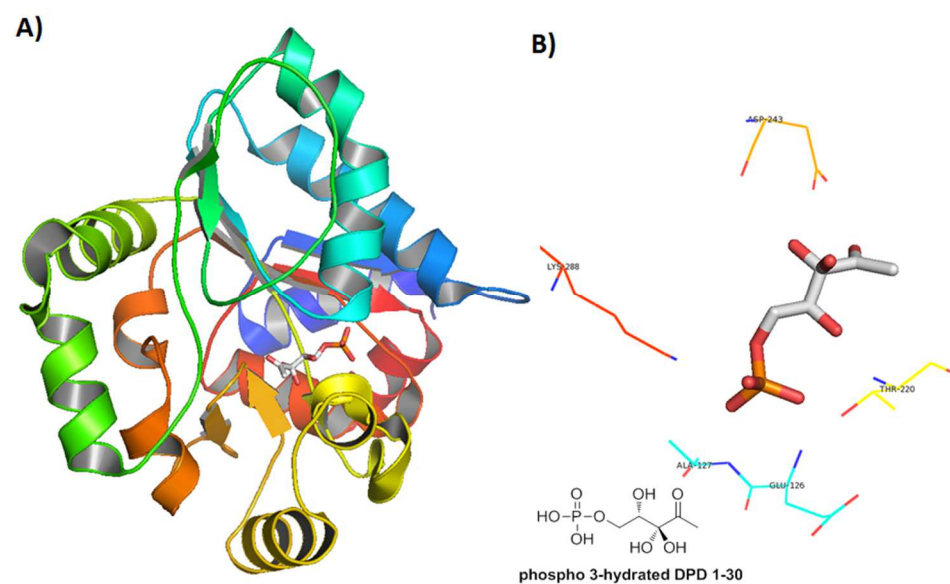


Figure 1-12. A) Crystal structure of LsrR from *E. coli* (PDB code: 4L4Z). B) AI-2 binding site of LsrR, showing protein residues that are within 3 Å of AI-2.

Recently, it has been reported that in *E. coli*, the key transcriptional regulator LsrR binds to AI-2 in its phospho 3-hydrated DPD form (1-30) as shown in **Figure 1-12**.⁸¹ This discovery has facilitated the design of new generation of AI-2 analogs, which

will be discussed in the next chapter.

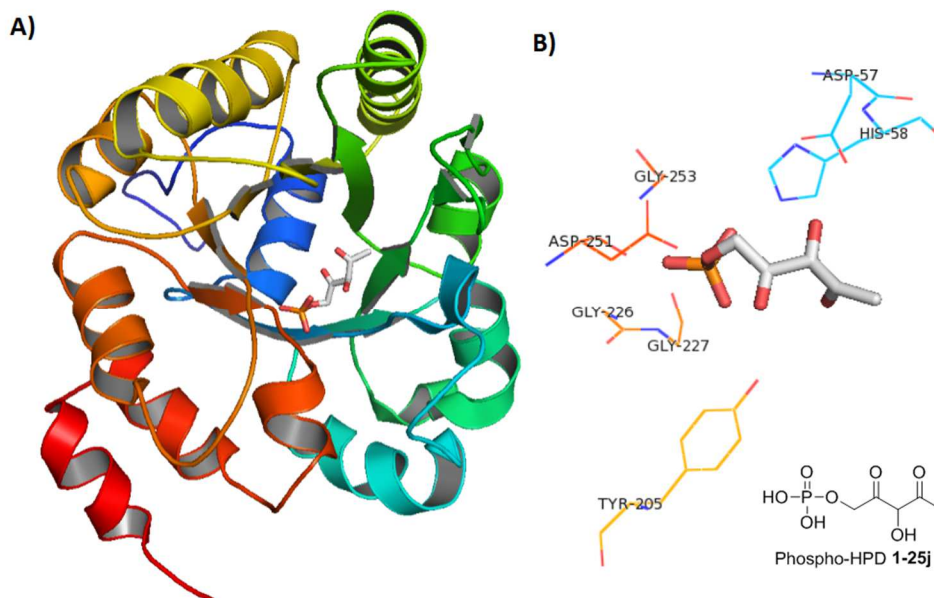


Figure 1-13. A) Crystal structure of LsrF from *E. coli* (PDB code: 4P2V) B) AI-2 binding site of LsrF, showing protein residues that are within 3 Å of AI-2.

During the course of writing this thesis, the crystal structure of LsrF, a co-enzyme A-dependent thiolase that catalyzes the terminal step of AI-2 metabolism, with the substrate phospho-HPD (**1-25j**) has been solved (**Figure 1-13**).⁴¹ This discovery has greatly expanded our understanding in AI-2 metabolism in bacterial cells.

A simple way of discovering antagonists of a natural ligand is to modify that ligand. Several groups have therefore modified AI-2, with the hope of arriving at analogs that could interfere with AI-2 signaling. Janda and co-workers prepared and tested a panel of AI-2-like molecules (**Figure 1-14**). Using bioluminescence assay of *V. harveyi*, they found that the oxidation states at C2, C3 and C4, as well as the chirality at C4, were important for the bioactivity in *V. harveyi*.⁸²

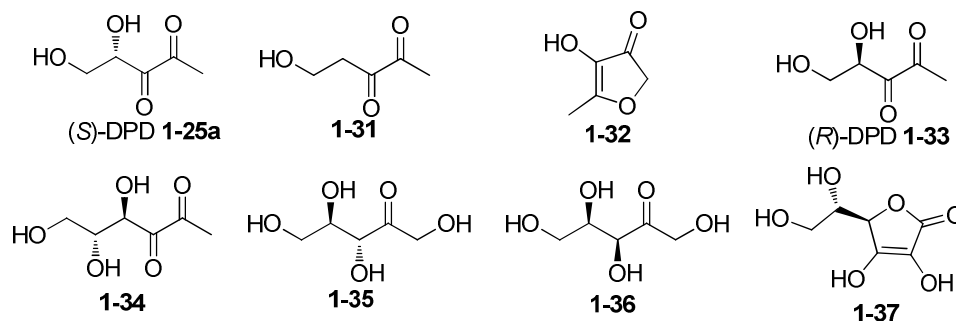


Figure 1-14. Probing specificity of LuxP binding site with AI-2-like molecules.⁸²

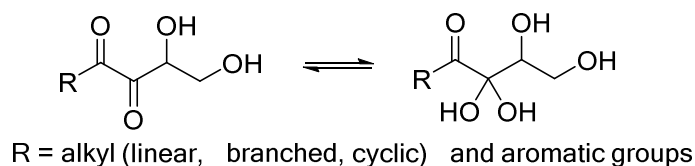


Figure 1-15. C1-modified AI-2 molecules synthesized by Janda and Sintim.^{83,84}

Janda and Sintim have also synthesized a panel of C1 AI-2 analogs (**Figure 1-15**) and tested for activities in *V. harveyi*,⁸³ *E. coli* and *Salmonella*.⁸⁴ In *V. harveyi*, C1-substituted AI-2 analogs act as synergistic agonists, in that they do not have any agonism on their own but enhance the agonism of AI-2.

AI-2 is a highly functionalized molecule and difficult to purify on column chromatography. In the presence of adventitious acid, AI-2 also decomposes. Doutheau and co-workers first demonstrated that acetate protected analogs of AI-2 were as effective as natural AI-2 in inducing bioluminescence in *V. harveyi* and β -galactosidase in *S. typhimurium*, but had the added advantage of being stable (**Figure 1-16**).⁸⁵ Later, Sintim extended this idea to make acetate protected C1 analogs of AI-2 and also showed that these could be deprotected *in vivo* by bacteria esterases and act as AI-2 antagonists (**Figure 1-16**).⁸⁶

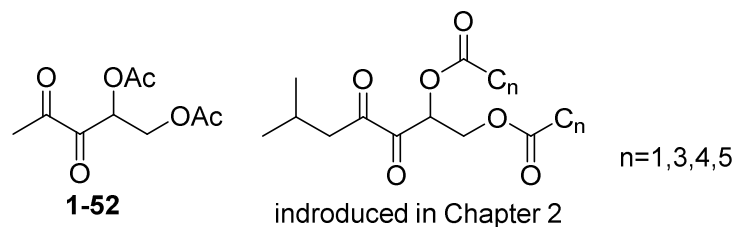


Figure 1-16. Acetate- and ester-protected AI-2 and analogs developed by Sintim and Doutheau.^{85,86}

Recently, Ventura and co-workers showed that C5-modified AI-2 analogs were synergistic agonists in *E. coli* and strong agonists in *V. harveyi* (**Figure 1-17**).⁸⁷

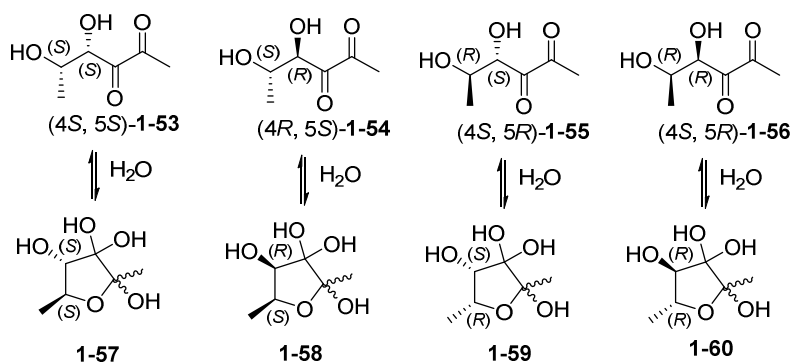


Figure 1-17. C5 analogs of AI-2 developed by Ventura and co-workers (**1-53** to **1-60**), which analogs contain stereochemical diversity at the C4 and C5 positions.⁸⁷

Other AI-2 inhibitors, targeting AI-2 synthase and receptors, that are not based on the AI-2 scaffold have also been reported. For excellent reviews, see those by Sintim,¹⁴ Spring⁸⁸ and Li.⁸⁹

1.4 AI-1 mediated quorum sensing

In the past decades, there have been extensive studies done on intraspecies quorum sensing molecules, AI-1, most commonly found in Gram-negative bacteria. Since chemists and microbiologists may call these molecules by different names, to clear the confusion, it is necessary to clarify the nomenclature (**Figure 1-18**). AI-1 usually refers to lactone-based QS autoinducers, one of the major classes of QS signaling molecules. AHL is a chemical structure featuring a *N*-acylhomoserine lactone scaffold whereas HSL is just the homoserine lactone moiety. Often times the side chain of AI-1 molecules has a 3-oxoacyl function group, so they are named 3-oxo-HSL for short.

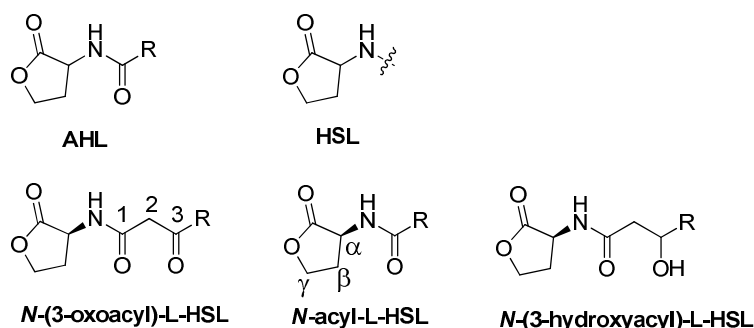


Figure 1-18. Nomenclature of AI-1.

Table 1-3 listed some representative natural AI-1 molecules and the corresponding bacteria that produce them, as well as QS phenotypes. Each bacterial species senses specific AI-1, which mainly differ by the length and functionality on the acyl chain. The first AI-1 mediated quorum sensing system was discovered in *V. fischeri*, which uses 3-oxo-C₆-HSL as the autoinducer.^{19a, 21} LuxI is the synthase while LuxR is the receptor of 3-oxo-C₆-HSL. The majority of later discovered quorum

sensing systems are LuxI/R type. AI-1 circuit in *V. fischeri* is shown below in **Figure 1-19**.

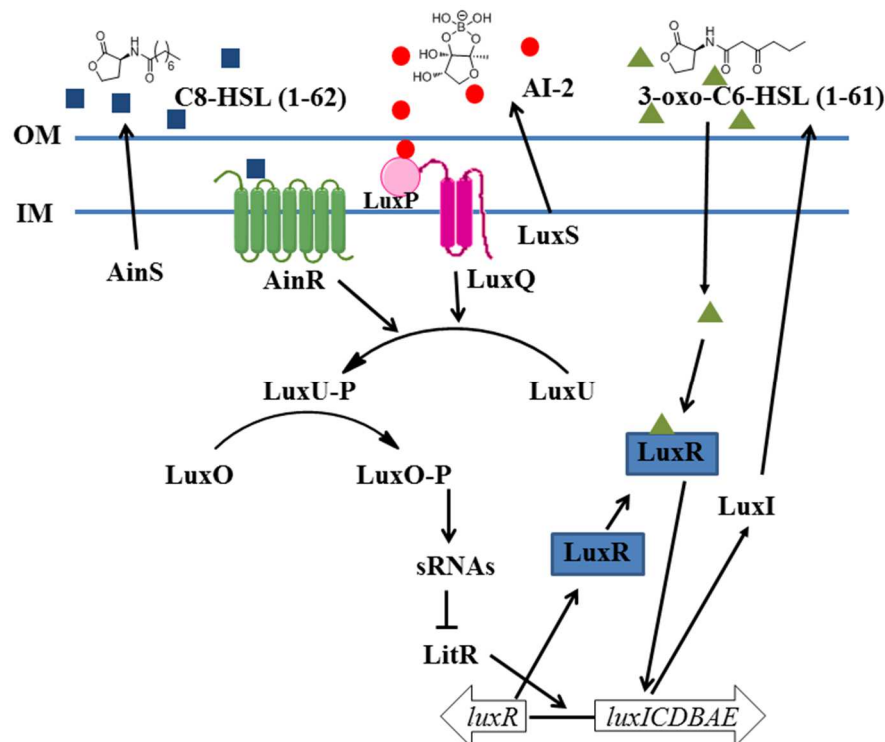


Figure 1-19. AI-1 signaling in *V. fischeri*.

In the past decades, the community has been heavily focused on chemical modifications on either the lactone head group or the acyl chain, or both of AI-1. **Table 1-4** highlights some biologically active AHL analogs that have been made.

In early years, studies were focused on changing the length of acyl chain and generally the chain lengths were important to the activities as even a small change in carbon number from the native AHLs could result in totally different outcome.⁹⁰ All the native AHLs are L-conformers because of their biosynthesis process.⁹¹ Synthetic D-AHLs have been investigated but were found to be significantly less active than the

L-AHLs, except very few examples.⁹² Later on, more modifications on lactone head group were explored however in many cases, these changes lead to less active compounds. Out of the lactone mimics, thiolactones were relatively popular not only because they somehow retain the electronic properties of the parent lactone ring but also they are more stable towards hydrolysis by lactonases. Some potent antagonists were found based on this head group.⁹³ On the chain side, the incorporation of aromatic rings often yields good antagonists and agonists.⁹³⁻⁹⁴

The goal of this thesis was to utilize synthetic chemistry tools to make analogs of AI-2 and AI-1 based on DPD and homoserine lactone structures, respectively. These medicinal chemistry modifications would be screened for their agonist or antagonist activities in quorum sensing of different bacteria. In turn, the results from the screening would further guide us to design the next generation of AI-like molecules. The studies in this thesis would be a valuable addition to the ultimate goal that one day, quorum sensing inhibition strategy could be a new therapy against bacterial infectious diseases.

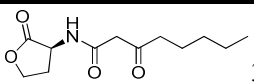
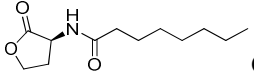
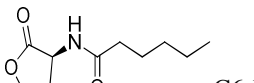
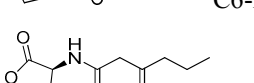
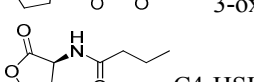
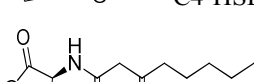
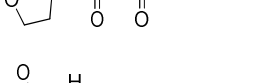
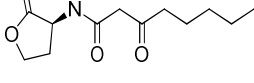
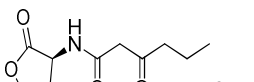
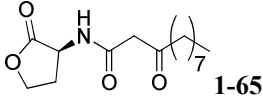
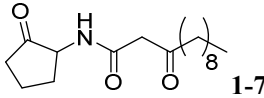
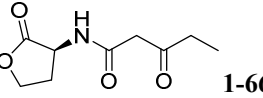
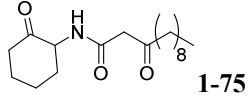
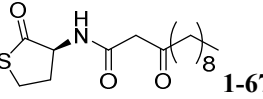
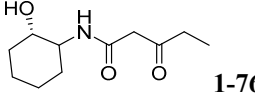
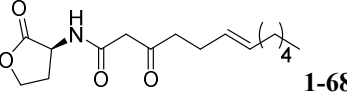
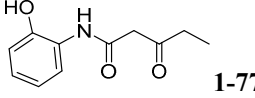
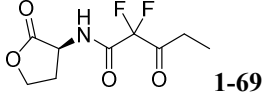
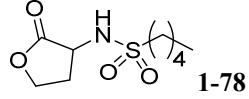
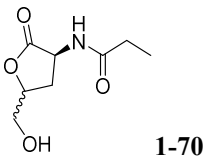
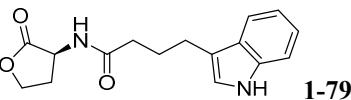
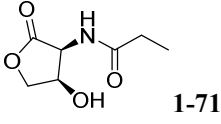
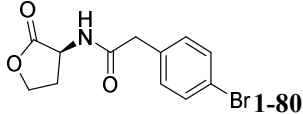
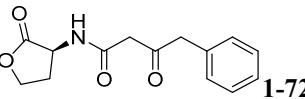
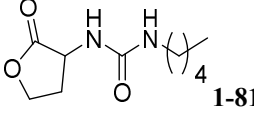
Organism	AI-1	LuxI/R homologs	QS phenotypes
<i>A. tumefaciens</i>	 3-oxo-C8-HSL 1-61	Tral/R	Plasmid conjugation
<i>B. cenocepacia</i>	 C8-HSL 1-62	CepI/R, CciI/R	Biofilm, swarming, motility, virulence
<i>C. violaceum</i>	 C6-HSL 1-63	CviI/R	Exoenzymes, cyanide, pigment
<i>E. carotovora</i>	 3-oxo-C6-HSL 1-64	ExpI/R, CarI/R	Carbapenem, exoenzymes, virulence
<i>P. aeruginosa</i>	 C4-HSL 1-65	RhII/R, LasI/R	Exoenzymes, secretion, pyocyanin, biofilm
	 3-oxo-C12-HSL 1-66		
<i>P. putida</i>	 3-oxo-C12-HSL 1-66	PpuI/R	Biofilm
<i>V. fischeri</i>	 3-oxo-C6-HSL 1-64	LuxI/R	Symbiosis
<i>V. harveyi</i>	 3-hydroxy-C4-HSL/HAI-1 1-26	LuxM/N	Bioluminescence, biofilm, TTS, protease

Table 1-3. Representative AHL structures and their corresponding organism, synthases/receptors and QS phenotypes.

Year	Structure	Activity	Year	Structure	Activity
------	-----------	----------	------	-----------	----------

1986		agonist in <i>V.fischeri</i> ^{90a}	2003		agonist in <i>P. aeruginosa</i> ⁹⁵
1996		both agonist in <i>V.fischeri</i> ^{90b}			antagonist in <i>P. aeruginosa</i> ⁹⁵
			2003		agonist in <i>P. aeruginosa</i> ⁹⁶
1996		agonist in <i>P. aeruginosa</i> ⁹⁷			antagonist in <i>P. aeruginosa</i> ⁹⁶
1999		agonist in <i>P. aeruginosa</i> ⁹⁸	2004		antagonist in <i>V.fischeri</i> ⁹⁹
2002		antagonist in <i>V.fischeri</i> ¹⁰⁰	2005		antagonist in <i>P. aeruginosa</i> and <i>A. tumefaciens</i> ^{94a}
2002		agonist in <i>V.fischeri</i> ¹⁰⁰	2005		antagonist in <i>P. aeruginosa</i> and <i>A. tumefaciens</i> ^{94a}
2002		antagonist in <i>V.fischeri</i> ^{94b}	2006		antagonist in <i>V.fischeri</i> ¹⁰¹

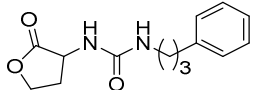
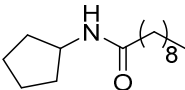
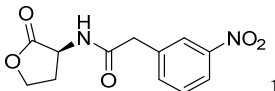
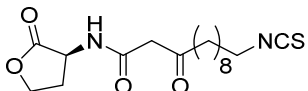
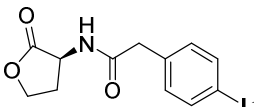
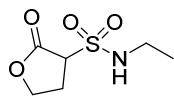
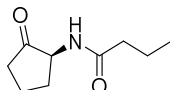
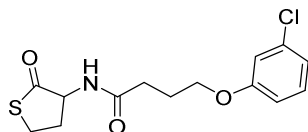
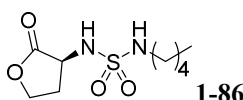
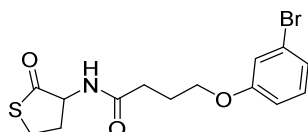
2002		antagonist in <i>V.fischeri</i> ^{94b}	2007		antagonist in <i>P. aeruginosa</i> ^{92a}
2007		agonist in <i>V.fischeri</i> ^{94c}	2009		antagonist in <i>P. aeruginosa</i> ¹⁰²
		antagonist in <i>V.fischeri</i> ^{94c}	2011		antagonist in <i>V.fischeri</i> ¹⁰³
2008		agonist in <i>P. aeruginosa</i> ¹⁰⁴	2013		both antagonist in <i>P. aeruginosa</i> ⁹³
2008		antagonist <i>V.fischeri</i> ¹⁰⁵			

Table 1-4. Significant AHL analogs and their activities.

Chapter 2. AI-2 analogs selectively modulate QS in bacteria

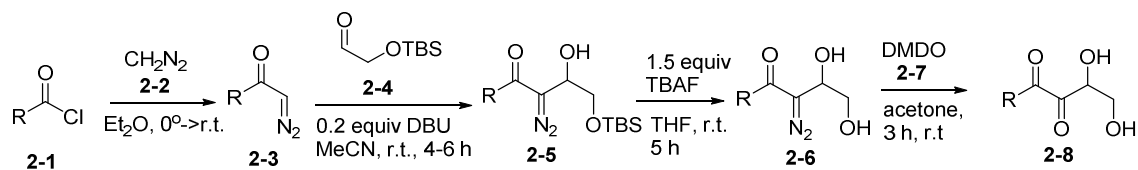
(The this section was modified from my publication⁸⁶)

The Sintim group has shown over the years that modification of AI-2 at the C1 position gives analogs that can antagonize the action of AI-2 in a variety of bacteria.^{83a, 84c, d, 86}

Chemists in the Sintim group have therefore been engaged in the development of methodologies to make modified analogs of AI-2, with the ultimate goal of modulating bacterial quorum sensing using these synthetic molecules.

2.1 Improvement in AI-2 synthesis.

A former member of the Sintim group, Dr Jacqueline Smith, developed a facile, two-flask synthesis of AI-2, which is amenable to the generation of a variety of C1 AI-2 analogs (**Scheme 2-1**).^{83a} The key step in this synthesis is the Aldol condensation between various diazocarbonyls **2-3** and a commercially available 2-(*tert*-butyldimethylsiloxy)acetaldehyde (**2-4**). The diazocarbonyls **2-3**, which are used in Sintim's synthesis, could be obtained from the requisite acyl chloride **2-1** and diazomethane (**2-2**). The resulting diazocarbonyls **2-3** were then condensed with 2-(*tert*-butyldimethylsiloxy)acetaldehyde (**2-4**) to afford diazo diol intermediates **2-6**, after deprotection of the silyl group with *tetra*-butyl ammonium fluoride. Column chromatography purification of the diazo diol followed by oxidation with dimethyl dioxirane (DMDO, **2-7**) resulted in pure DPD and analogs **2-8** in moderate to high yields.

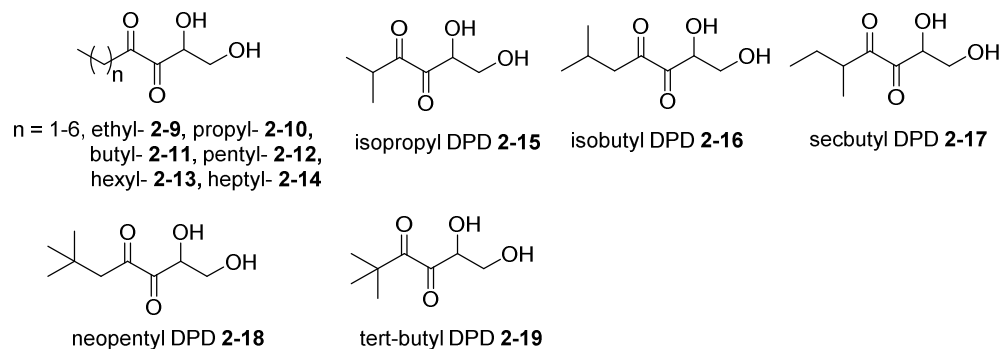


Scheme 2-1. Synthesis of DPD and analogs developed by Sintim and co-workers.

When I first joined the Sintim group, my first task was to re-synthesize a library of C1-substituted AI-2 analogs (with linear, branched, cyclic, and, aromatic C1 groups, **Figure 2-1**), which were first synthesized by Dr. Smith.^{84c, d} The goals of re-synthesizing Dr. Smith's compounds were to learn how to make AI-2 analogs, using the diazo carbonyl methodology and to provide more compounds for evaluation of biological activities. During the synthesis, I found that the first step, involving acyl chloride **2-1** and large excess (4-6 equiv) of diazomethane (**2-2**) was not efficient. This was because the HCl generated would degrade the desired diazocarbonyls **2-3** to an α -chloroketone and thus much more diazomethane (**2-2**) was needed to scavenge HCl (**Scheme 2-2**). Thus this step was low yielding with several byproducts, which purification difficult. Moreover, diazomethane (**2-2**) is toxic, volatile and shock sensitive, and therefore not ideal to prepare on large scale. In order to scavenge the generated HCl base was needed (note that Smith's procedure only used 0.2 equiv. DBU) and the choice of the base was critical because the base could also deprotonate the acidic α -hydrogen on the acyl chloride **2-1** and result in a ketene product **2-33** (**Scheme 2-2**). I discovered that adding 1.1 equiv of CaO to scavenge the generated HCl allowed for a reduction of the diazomethane that was used (from 4-6 equiv. in Smith's protocol

to 1,5 equiv. in my protocol), and also the yield of the reaction was improved to over 90%, with little byproduct.¹⁰⁶

a) Linear and branched C1-analogs



b) Cyclic and aromatic C1-analogs

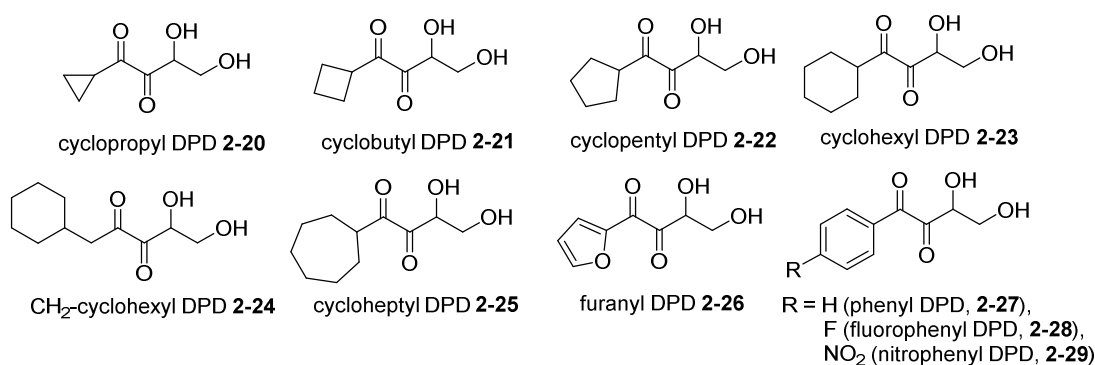
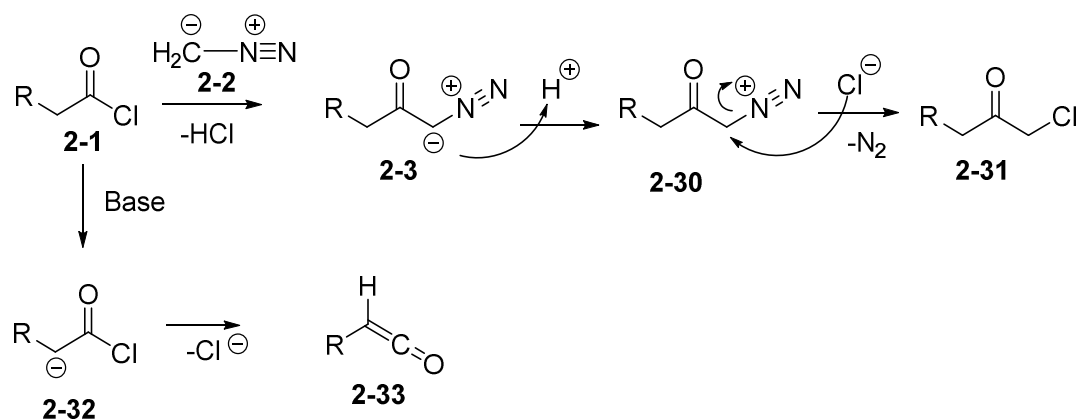


Figure 2-1. First generation of C1 substituted AI-2 analogs synthesized and evaluated for biological activities.^{83a, 84c, d}



Scheme 2-2. Arndt-Eistert type reaction and degradation pathway.

2.2 A pro-drug approach for selective modulation of AI-2 mediated bacterial cell-to-cell communication.

(Section 2.2 was published as Min Guo, Sonja Gamby, Shizuka Nakayama, Jacqueline Smith and Herman Sintim. *Sensors*, **2012**, 12, 3762-72)⁸⁶

2.2.1 Introduction

Several groups have been interested in the development of analogs of the universal quorum sensing molecule, AI-2.^{83b, 84a, 107} Analogs of AI-2 have been shown to either act as synergistic agonists in some *Vibrio* species⁸³ or antagonist^{84d} in enteric bacteria, such as *E. coli* and *S. typhimurium*. Interestingly, it has been demonstrated that the nature of the C1 acyl group in AI-2 analogs confers specificity in disrupting QS processes in a variety of bacteria.^{84d} For example, hexyl-DPD (**2-13**) inhibits AI-2-mediated *lsr* expression in *E. coli* whereas this same molecule is ineffective against AI-2-mediated *lsr* expression in the analogous enteric bacteria, *S. typhimurium*. On the other hand, isobutyl DPD (**2-16**) could inhibit AI-2-mediated *lsr* expression in *S. typhimurium*, implying that subtle differences in the C1 substituents of AI-2 could result in significant differences in biological response.^{84d}

One of the limitations of the use of AI-2 analogs in selectively modulating bacterial behavior is the instability of these analogs. At high concentrations, it has been shown that AI-2 form dimers (**2-34**, see **Figure 2-2**), which are not biologically active.¹⁰⁸ This makes the purification of AI-2 or analogs on silica gel problematic and most studies that use synthetic AI-2 use unpurified material. Others have attempted to

solve the instability issue associated with AI-2 by making ester derivatives that hydrolyze *in vivo* to release active autoinducers.⁸⁵ This strategy is promising in delivering purer and more stable AI-2 analogs that could be used in studying bacterial communication, with implications for disease control or synthetic biology applications. However, detailed study that correlates the nature of the ester group on AI-2 and biological activity has not been described. Additionally, as analogs of AI-2 are emerging as potent anti-QS molecules,^{84d} it is of interest to investigate if these QS signaling inhibitors could also be protected as ester “pro-drugs” and still retain their inhibitory activity. If different bacteria processed ester-protected AI-2 analogs differently, then one could selectively modulate the activity of specific bacteria in an ecosystem via the use of differently protected AI-2 analog.

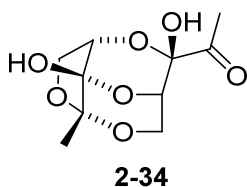
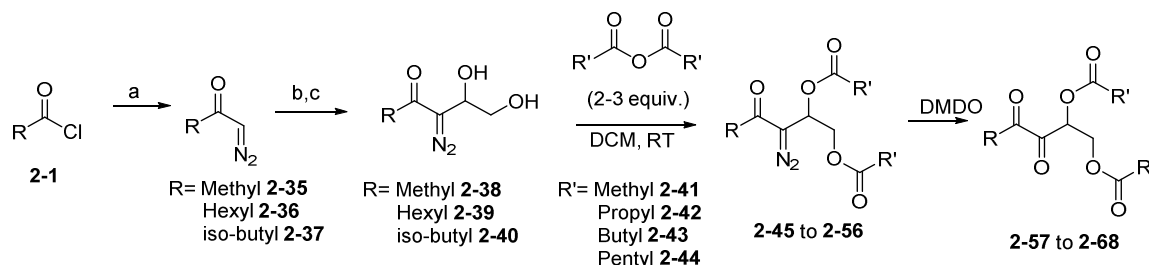


Figure 2-2. Structure of AI-2 dimer.

2.2.2 Results and discussion

The syntheses of bis-ester protected AI-2 and analogs 19–30 were achieved via the strategy shown in **Scheme 2-3**.^{83a, 84d} Briefly, an aldol reaction between diazocarbonyls **2-35** to **2-37** and 2-(tert-butyldimethylsilyloxy) acetaldehyde **2-4** afforded diazodiols **2-38** to **2-40**, after deprotection of the TBS group with TBAF. Oxidation of the diazo group in diazodiols **2-38** to **2-40** afforded AI-2 or analogs but

for the production of ester protected AI-2 and analogs, it was important to perform the esterification step first to give bis-ester **2-45** to **2-56** before the oxidation of the diazo bis-ester to give targeted compounds **2-57** to **2-68**.



Scheme 2-3. Synthetic strategy for making bis-ester protected AI-2 analogs. Reagents and conditions: (a) diazomethane, 0 °C, (b) *tert*-butyl-siloxyacetaldehyde, DBU (1,8 diazabicycloundec-7-ene), CH₃CN, RT (c) TBAF/THF. DCM= dichloromethane; DMSO = dimethyldioxirane.

With the various AI-2 or analog ester derivatives (methyl to pentyl esters, **Figure 2-3**) in hand, we proceeded to investigate the biological profiles of these esters. We have previously demonstrated that AI-2 analogs with longer C1-acyl chains permeate more readily into bacterial cells than shorter chains.¹⁰⁹ This is presumably due to the favorable interactions of the alkyl chain with the phospholipid of the bacterial membrane. Based on this earlier work, we hypothesized that the longer chain ester derivatives (such as butyl or pentyl) would permeate more readily into bacterial cells than the shorter chain analogs, such as the methyl ester series.¹⁰⁹ However, if the cellular esterases were sensitive to the size of the esters, then the longer chain analogs would be hydrolyzed slower than the shorter chain ones. Because biological activity of ester prodrugs is dependent on permeation and prodrug activation and both of these

processes would depend on the organism in question, it is not always easy to predict a priori which ester group is most suitable for derivatizing biologically active molecules.

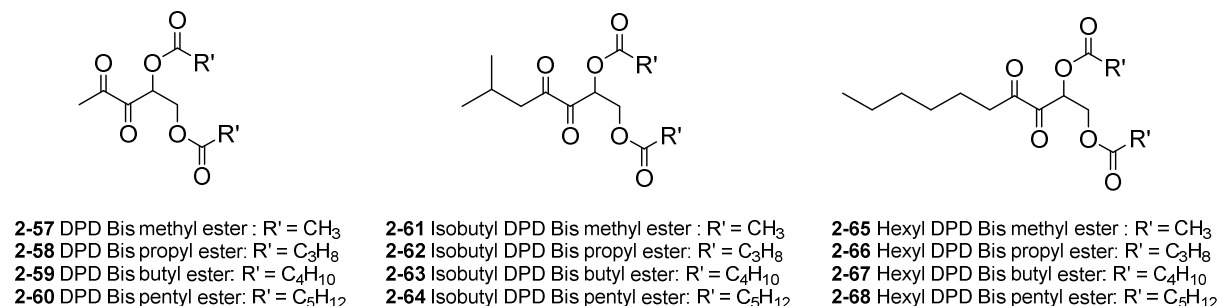


Figure 2-3. Compounds evaluated as bis-ester protected AI-2 analogs.

Bis-ester-protected AI-2 analogs (with different ester chains; methyl, propyl, butyl and pentyl) were all effective *lsr* expression inducers in *E. coli* (see **Figure 2-4**). For *S. typhimurium*, it appears that LsrR is not as good a repressor (compared to *E. coli*) and significant expression of the *lacZ* gene was observed even in the absence of added DPD (see control, **Figure 2-4**). Nonetheless, it is apparent that more LacZ protein was present in *S. typhimurium* in the presence of AI-2 than when AI-2 was not present [about 30% more LacZ present when AI-2 is added; see **Figure 2-4**, compare the histograms for “LuxS⁻ + AI-2” and “LuxS⁻ (no AI-2 added)”].

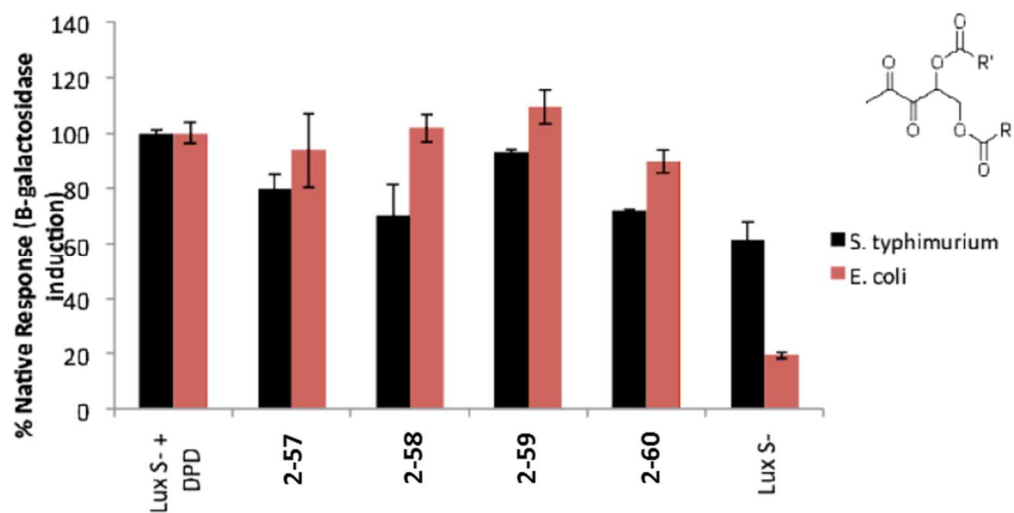


Figure 2-4. Black bars: AI-2 or analogs-mediated expression of β -galactosidase in *S. typhimurium* (MET715: LuxS⁻). Red bars: AI-2 or analogs-mediated expression of β -galactosidase in *E. coli* LW7/LuxS⁻. AI-2 or bis-ester analogs of AI-2 (20 μ M) were added to the bacterial strains, which do not produce their own AI-2. Compounds **2-57** to **2-60** represent ester-protected DPD analogs: **2-57**: DPD *bis*-methyl ester; **2-58**: DPD *bis*-propyl ester; **2-59**: DPD *bis*-butyl ester; **2-60**: DPD *bis*-pentyl ester. (Done by Dr. Shizuka Nakayama, a former postdoc in the Sintim group).

Therefore, even if *lacZ* expression is not solely controlled by AI-2, one can safely conclude that AI-2 plays some role in *lacZ* expression in the *S. typhimurium*.⁴⁰

The origin of “leaky” *lacZ* expression in the absence of LuxS, which makes AI-2, could be due to myriads of factors, such as a lower affinity of LsrR to the LsrR DNA binding region in *S. typhimurium* (compared to *E. coli*) or a higher concentration of other phosphorylated AI-2-like molecules (such as ribulose-5-phosphate) in *S. typhimurium* (compared to *E. coli*) or lower levels of LsrR in *S. typhimurium* (compared to *E. coli*) or even non-enzymatic production of AI-2 from ribulose-5-phosphate.¹¹⁰ Without experimental data to pinpoint the origin of the differential *lsr* expression in *S. typhimurium* (compared to *E. coli*), it is dangerous to make definitive statements about

the origin of this difference. Despite this high LacZ background in *S. typhimurium*, we can still conclude that the majority of the ester protected DPD analogs were not as good as DPD in inducing *lsr* expression in *S. typhimurium*, and only *bis*-butyl DPD appears to be as good as DPD (see **Figure 2-4**). It is important to note that DPD/AI-2 gets into *S. typhimurium* via a ribose transporter, such as LsrB, whereas the analogs would have to diffuse into the cells, probably via passive diffusion through the membrane. Hence the marginal differences in activity observed between *bis*-butyl DPD and the other ester-protected DPD could be due to differences in membrane transport. Next, we investigated the antagonistic profile of the *bis*-ester analogs of isobutyl DPD in both *E. coli* and *S. typhimurium*. Isobutyl DPD **2-16** is an antagonist of AI-2-mediated QS in both *E. coli* and *S. typhimurium* and stable versions of this analog have the potential to disrupt QS processes in these enteric bacteria, which sometimes cause food-borne diseases. For this assay, AI-2 was added to a LuxS-deficient strain of *E. coli* (LW7) or *S. typhimurium* (MET715) to induce *lsr* expression via the derepression of LsrR by phospho-AI-2.¹¹¹ In *E. coli*, *bis*-methyl and *bis*-propyl DPD analogs were as effective QS quenchers as the unprotected isobutyl DPD **2-16** (see **Figure 2-5**).

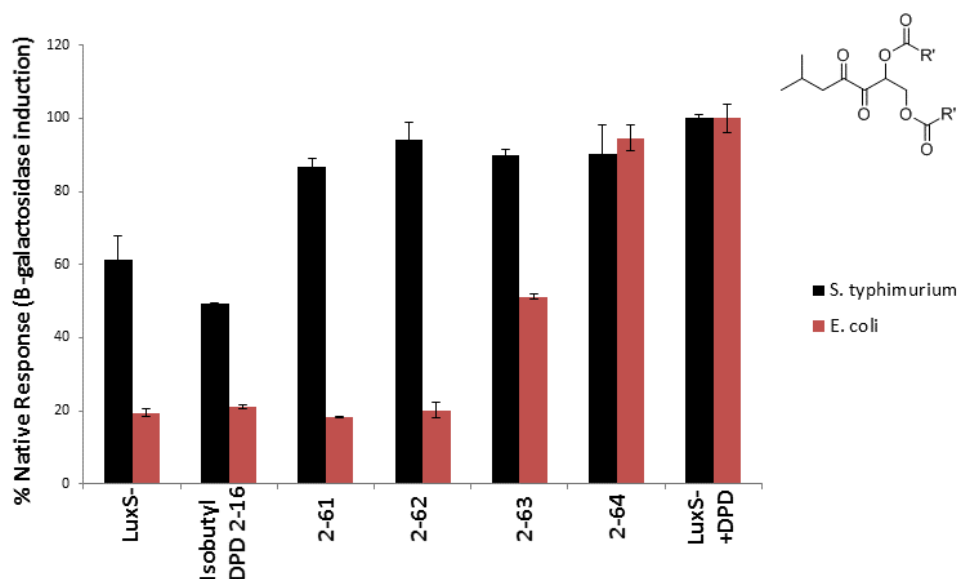


Figure 2-5. Inhibition of AI-2-mediated β -galactosidase expression in *S. typhimurium* (Black Bars) and *E. coli* (Red Bars) with various *bis*-ester analogs of isobutyl DPD. [AI-2] = 20 μ M, [analogs] = 20 μ M. Compounds **23-26** represent ester protected isobutyl DPD analogs; **23**: isobutyl DPD *bis*-methyl ester, **24**: isobutyl DPD *bis*-propyl ester, **25**: isobutyl DPD *bis*-butyl ester, **26**: isobutyl DPD *bis*-pentyl ester. (Done by Dr. Shizuka Nakayama, a former postdoc in the Sintim group).

Increasing the length of the ester chain to butyl or pentyl either reduced (butyl) or abrogated (pentyl) the inhibitory profile of the DPD analog. In *E. coli*, the same trend was also observed for the *bis*-ester derivatives of hexyl DPD (*bis*-methyl and *bis*-propyl analogs, but not butyl or pentyl derivatives, were QS inhibitors, **Figure 2-6**).

In *S. typhimurium*, however, none of the *bis*-ester protected isobutyl DPD analogs were able to antagonize the action of AI-2. Addition of isobutyl DPD to *S. typhimurium* however decreased *lacZ* expression by about 50% (compare black bar corresponding to “isobutyl DPD” to black bar corresponding to “LuxS- + DPD” in **Figure 2-5**). Thus, *S. typhimurium* and *E. coli* have similar QS systems, but differences

in the processing of ester analogs of isobutyl DPD allows for the selective modulation of QS processing in *E. coli*, but not in *S. typhimurium*.

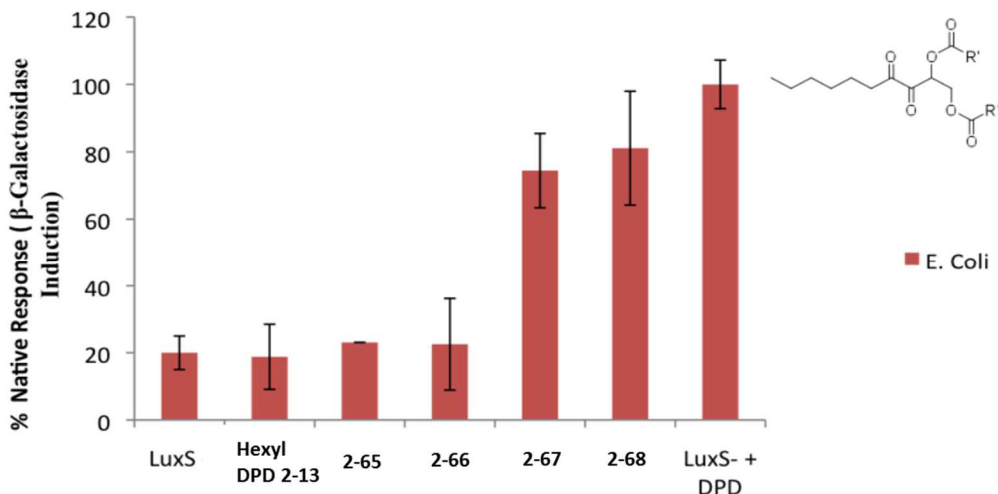


Figure 2-6. Inhibition of AI-2-mediated β -galactosidase expression in *E. coli* with various *bis*-ester analogs of hexyl DPD. [DPD] = 20 μ M, [analogs] = 20 μ M. Compounds **2-65** to **2-68** represent ester protected hexyl DPD analogs; **2-65**: hexyl DPD *bis*-methyl ester; **2-66**: hexyl DPD *bis*-propyl ester; **2-67**: hexyl DPD *bis*-butyl ester; **2-68**: hexyl DPD *bis*-pentyl ester. (Done by Dr. Shizuka Nakayama, a former postdoc in the Sintim group).

2.2.3 Conclusion

In conclusion, we have shown that ester derivatives of DPD analogs can be hydrolyzed inside bacterial cells to reveal the biologically active diol unit for quorum sensing disruption. We note that it is possible to achieve selectivity of QS modulation amongst closely related bacteria (in our case, between *E. coli* and *S. typhimurium*) via the use of ester protection of the diol unit of AI-2. The origin of this selectivity remains unknown at this moment, but it could be a number of several factors, including selective permeation of the analogs or different sensitivities of the esterases required for analog hydrolysis in the different bacteria (**Figure 2-7**). Future work will be aimed at obtaining

a more in depth molecular understanding of these interesting observations. This work adds to the growing list of different strategies that can be used to intercept AI-2 signaling in diverse bacteria.¹¹²

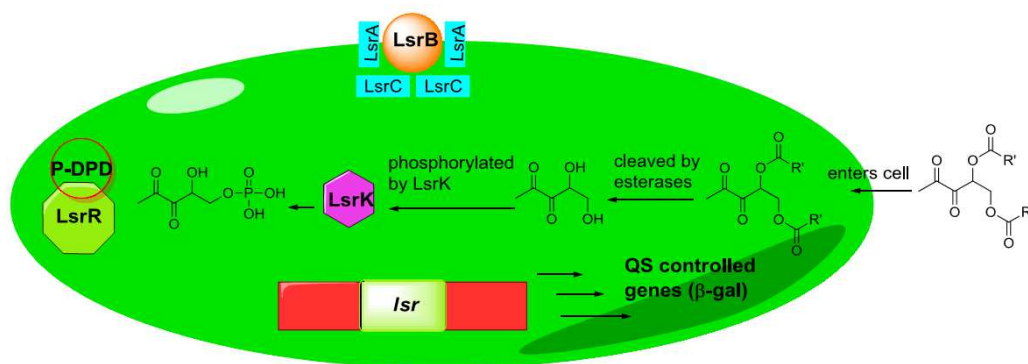


Figure 2-7. Proposed model of action in enteric bacteria. Ester protected DPD analogs diffuse into the cell, where esterases hydrolyze the ester pro-DPD and analogs and the DPD or analogs are subsequently phosphorylated by LsrK.

2.2.4 Experimental Section

Chemical Synthesis

a) Generation of Diazomethane

Diazomethane is toxic, volatile and shock sensitive. The synthesis was recommended to be at small scale with shield and reagent Diazald[®] (Sigma-Aldrich) as well as a diazomethane generator apparatus (Sigma-Aldrich), following the protocol provided by Sigma-Aldrich. Briefly, a solution of Diazald[®] (5 g) in diethyl ether (45 mL) was slowly added to a solution of KOH (5 g) in mixed solvent (water (8 mL) and ethanol (10 mL)) at 65 °C over 20 min. The generated diazomethane and the diethyl

ether solvent distilled and was trapped in a collecting vessel using a dry ice/isopropanol bath to give diazomethane as a solution in diethyl ether (ca. 0.4-0.5 M).

b) Addition of Diazomethane to Acyl Chlorides

To a solution of diazomethane (3 equiv.) in diethyl ether was added an acyl chloride (1 equiv.) dropwise at 0 °C. The resulting solution was allowed to stir for another 2 h and warmed up gradually to room temperature. The solvent was removed under vacuum and the diazocarbonyl residue (yellow liquid) was used for the next step without further purification.

c) Synthesis of Diazodiols

DBU (0.16–0.20 equiv.) and 2-(*tert*-butyldimethylsilyloxy) acetaldehyde (1–1.5 equiv.) were added to a solution of the diazocarbonyl (crude, 1 equiv.) in anhydrous acetonitrile (0.2 M). The reaction was stirred at room temperature under nitrogen for 4–8 h and monitored by TLC. Upon disappearance of starting material, the reaction was quenched with sodium bicarbonate. The organic layer was extracted with dichloromethane (3 × 20 mL) and dried with magnesium sulfate.

The solvent was evaporated under reduced pressure. To a solution of crude product in anhydrous tetrahydrofuran at 0 °C, TBAF was added (1–2 equiv.). The solution was allowed to warm to room temperature and stirred for 1–3 h under nitrogen. The solvent was evaporated, and the crude product was purified by column chromatography. The products eluted as yellow oils using 1:3 to 3:2 ethyl acetate/hexane as the mobile phase.

d) Synthesis of Ester Protected Diazo Compounds

To a stirring solution of diazodiol (1 equiv.) catalytic 4-dimethyl aminopyridine (DMAP) and suspended 4Å molecular sieves in dichloromethane (DCM) was added the requisite anhydride. The reaction was allowed to gently stir at room temperature for 2-4 h until complete disappearance of starting material was indicated by TLC. The crude reaction mixture was filtered washed with saturated NaHCO₃ aqueous solution and the organic phase was extracted with more DCM. The combined organic phases were dried with anhydrous MgSO₄ and the solvent was evaporated at reduced pressure. The crude product was purified by column chromatography. The products eluted as yellow oils using 1:3 to 1:2 ethyl acetate/hexane as the mobile phase ($R_f = 0.2$).

e) Synthesis of DPDs

Dimethyldioxirane in acetone (15–20 mL) was added dropwise to a solution of ester protected diazodiol (1 equiv.) in acetone (1–2 mL). The reaction was allowed to stir at room temperature (1–2 h) until complete disappearance of starting material was indicated by TLC (loss of UV activity). Solvent and excess reagents were evaporated under reduced pressure.

Bacterial Strains and Growth Conditions

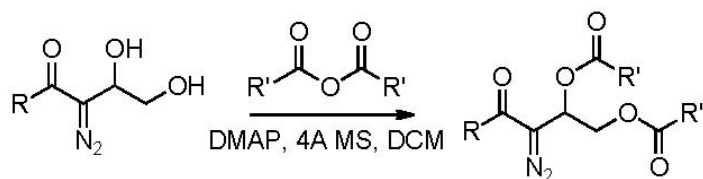
Table 2-1 lists the bacterial strains used in this study. *S. typhimurium* and *E. coli* strains were cultured in Luria–Bertani medium (LB, Sigma). These antibiotics were used for the following strains: (60 µg mL⁻¹) kanamycin for *S. typhimurium* (MET715) and (50 µg mL⁻¹) ampicillin for *E. coli* (LW7)

Strain	Relevant genotype and/or property
	<i>Escherichia coli</i>
LW7	W3110 Δ <i>lacU160-tna2</i> Δ <i>luxS</i> :: Kan (LuxS-deficient: does not produce AI-2)
	<i>Salmonella typhimurium</i>
MET715	<i>rpsL putRA</i> :: Kan- <i>lsr-lacZYA luxS</i> :: T-POP (LuxS-deficient: does not produce AI-2)

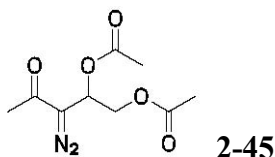
Table 2-1. Bacterial strains used in this study.

Measurement of the QS Response (lsr Expression)

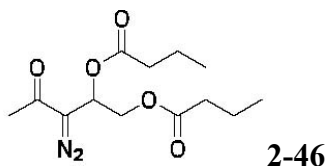
The QS response indicated by *lsr* gene expression was analyzed in pure culture studies by culturing *E. coli* LW7 pLW11 and *S. typhimurium* MET715 overnight at 30 °C in LB medium supplemented with appropriate antibiotics as stated previously. These cells were then diluted into fresh LB medium (with antibiotics) and grown to an OD₆₀₀ of 0.4–0.8 at 37 °C, 250 rpm. Cells were then collected by centrifugation at 10,000 × *g* for 10 min and resuspended in 10 mM phosphate buffer. AI-2 (20 μM) and the respective analog (20 μM) were added to the *E. coli* or *S. typhimurium* suspension for 2 h at 37 °C. AI-2 dependent β -galactosidase production was quantified by the Miller assay. (With the help of Shizuka Nakayama and Sonja Gamby)



Scheme 2-4. Synthesis of ester protected diazodiol.

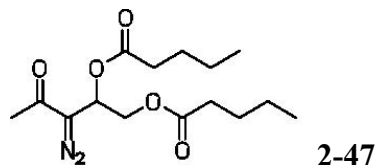


3-diazo-4-oxopentane-1,2-diyl diacetate (2-45): To a solution of methyl diazodiol **2-38**^{83a} (89 mg, 0.62 mmol), DAMP (15 mg, 0.2 equiv.) and suspended 4A molecular sieves (0.2 g) in anhydrous dichloromethane (DCM) was added acetic anhydride (0.12 mL, 2.0 equiv.). The reaction was gently stirred at room temperature overnight. The reaction was quenched with saturated aqueous NaHCO₃ solution. The organic and aqueous layers were separated and the organic layer was washed with brine and dried over anhydrous MgSO₄. The solvent was removed *in vacuo* and the residue was purified on silica gel, using 3:4 ethyl acetate/hexane as the mobile phase ($R_f = 0.2$). The product eluted as a yellow oil (yield = 90 mg, 64%).

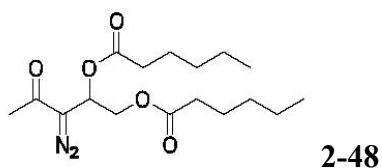


3-diazo-4-oxopentane-1,2-diyl dibutyrate (2-46): To a solution of methyl diazodiol **2-38** (23 mg, 0.16 mmol), DMAP (4 mg, 0.2 equiv.) and suspended 4A molecular sieves (0.1 g) in anhydrous dichloromethane (DCM) was added butyric anhydride (0.05 mL, 2 equiv.). The reaction was stirred at room temperature overnight. The reaction was quenched with saturated aqueous NaHCO₃ solution. The organic and aqueous

layers were separated and the organic layer was washed with brine and dried over anhydrous MgSO_4 . The solvent was removed *in vacuo* and the residue was purified on silica gel, using 1:5 ethyl acetate/hexane as the mobile phase ($R_f = 0.2$). The product eluted as a yellow oil (yield = 23 mg, 51%).

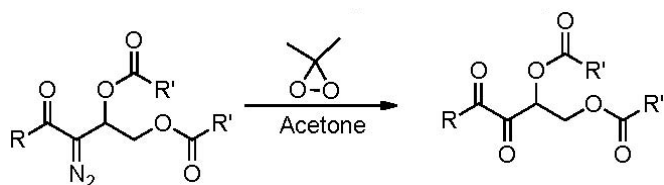


3-diazo-4-oxopentane-1,2-diyl dipentanoate (2-47): To a solution of methyl diazodiol **2-38** (23 mg, 0.16 mmol), DMAP (4 mg, 0.2 equiv.) and suspended 4A molecular sieves (0.1 g) in anhydrous dichloromethane (DCM) was added butyric anhydride (0.05 mL, 2 equiv.). The reaction was stirred at room temperature overnight. The reaction was quenched with saturated aqueous NaHCO_3 solution. The organic and aqueous layers were separated and the organic layer was washed with brine and dried over anhydrous MgSO_4 . The solvent was removed *in vacuo* and the residue was purified on silica gel, using 1:5 ethyl acetate/hexane as the mobile phase. The product eluted as a yellow oil (yield = 27 mg, 54%).

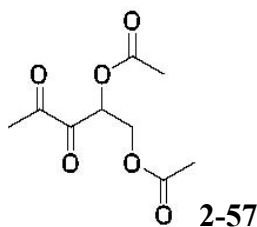


3-diazo-4-oxopentane-1,2-diyl dihexanoate (2-48): To a solution of methyl diazodiol **2-38** (23 mg, 0.16 mmol), DMAP (4 mg, 0.2 equiv.) and suspended 4A molecular

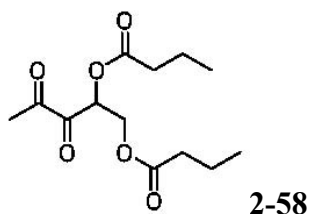
sieves (0.1 g) in anhydrous dichloromethane (DCM) was added butyric anhydride (0.05 mL, 2 equiv.). The reaction was stirred at room temperature overnight. The reaction was quenched with saturated aqueous NaHCO₃ solution. The organic and aqueous layers were separated and the organic layer was washed with brine and dried over anhydrous MgSO₄. The solvent was removed *in vacuo* and the residue was purified on silica gel, using 1:5 ethyl acetate/hexane as the mobile phase. The product eluted as a yellow oil (yield = 38 mg, 67%).



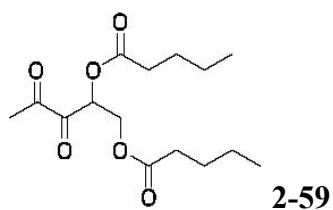
Scheme 2-5. Oxidation of diazo moiety into carbonyl.



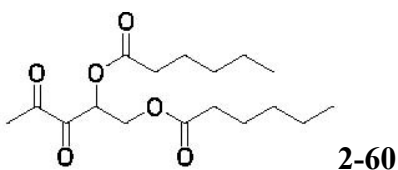
3,4-dioxopentane-1,2-diyl diacetate (2-57): To a solution of methyl diazo diacetate **2-45** (20 mg, 0.088 mmol) in acetone (1 mL) was added dimethyldioxirane acetone solution (2.5 mL, ca. 0.07–0.09 M). The resulting mixture was stirred for 1 h and solvent and excess reagents were removed under reduced pressure to obtain **2-57** as bright yellow oil (yield = 19 mg, quantitative).



3,4-dioxopentane-1,2-diyl dibutyrate (2-58): To a solution of methyl diazo dibutyrate **2-46** (23 mg, 0.081 mmol) in acetone (1 mL) was added dimethyldioxirane acetone solution (2.5 mL, ca. 0.07-0.09 M). The resulting mixture was stirred for 1 h and solvent and excess reagents were removed under reduced pressure to obtain **2-58** as bright yellow oil (yield = 22 mg, quantitative).

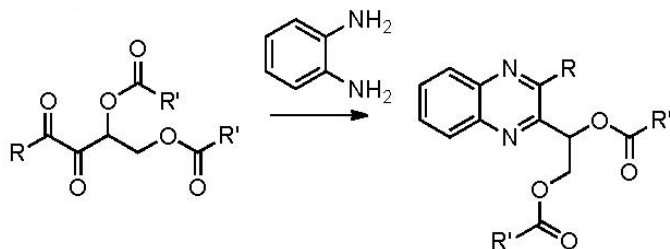


3,4-dioxopentane-1,2-diyl dipentanoate (2-59): To a solution of methyl diazo dipentanoate **2-47** (27 mg, 0.086 mmol) in acetone (1 mL) was added dimethyldioxirane acetone solution (2.5 mL, ca. 0.07–0.09 M). The resulting mixture was stirred for 1 h and solvent and excess reagents were removed under reduced pressure to obtain **2-59** as bright yellow oil (yield = 26 mg, quantitative).



3,4-dioxopentane-1,2-diyl dihexanoate (2-60): To a solution of methyl diazo

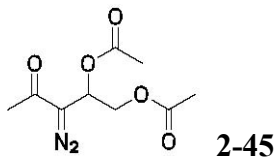
dihexanoate **2-48** (38 mg, 0.112 mmol) in acetone (1 mL) was added dimethyldioxirane acetone solution (2.5 mL, ca. 0.07–0.09 M). The resulting mixture was stirred for 1 h and solvent and excess reagents were removed under reduced pressure to obtain **2-60** as bright yellow oil (yield = 36.8 mg, quantitative).



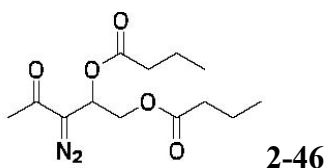
Scheme 2-6. Note: Both the diazoketones and diketones did not have good MS spectrum (presumably due to decomposition under the MS conditions. Therefore, further MS characterization was done by adding phenyl diamine to the diketones and stirred overnight to convert the diketones into quinoxalines, see Scheme above (this is a standard practice). **MS data is therefore reported for the quinoxaline derivatives.**

NMR and MS data: NMR spectra were measured on Bruker AV-400, Bruker DRX-400 (^1H at 400 MHz, ^{13}C at 100 MHz). Data for ^1H -NMR spectra are reported as follows: chemical shift (ppm, relative to residual solvent peaks or indicated external standards; s = singlet, t = triplets, m = multiplet), coupling constant (Hz), and integration. Data for ^{13}C -NMR are reported in terms of chemical shift (ppm) relative to residual solvent peak. Mass spectra (MS) were recorded by JEOL AccuTOF-CS (ESI positive, needle voltage 1800–2400 eV).

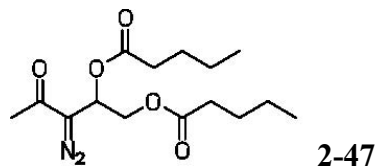
(Note, MS of diazo compounds could not be obtained due to decomposition of the diazo moiety under MS conditions).



3-diazo-4-oxopentane-1,2-diyl diacetate (2-45): ^1H NMR (CDCl_3 , 400 MHz) δ : 5.85–5.73 (m, 1H), 4.45–4.34 (m, 1H), 4.31–4.17 (m, 1H), 2.19 (s, 3H), 2.03 (s, 3H), 2.01 (s, 3H). ^{13}C NMR (CDCl_3 , 100 MHz) δ : 188.6, 170.1, 169.6, 68.5, 65.7, 63.5, 25.4, 20.7, 20.5. (carbon signal next to diazo group might not show up)

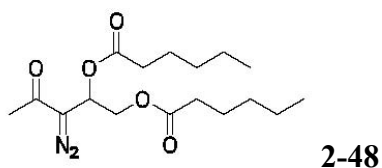


3-diazo-4-oxopentane-1,2-diyl dibutyrate (2-46): ^1H NMR (CDCl_3 , 400 MHz) δ : 5.93–5.83 (m, 1H), 4.55–4.43 (m, 1H), 4.38–4.27 (m, 1H), 2.38–2.28 (m, 4H), 2.26 (s, 3H), 1.73–1.59 (m, 4H), 1.01–0.89 (m, 6H). ^{13}C NMR (CDCl_3 , 100 MHz) δ : 173.3, 172.7, 65.9, 63.7, 37.0, 36.3, 36.2, 31.3, 25.9, 18.7, 14.0, 13.9. (carbon signal next to diazo group might not show up)

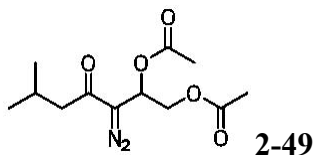


3-diazo-4-oxopentane-1,2-diyl dipentanoate (2-47): ^1H NMR (CDCl_3 , 400 MHz) δ :

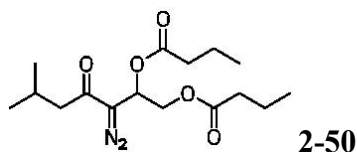
5.93–5.82 (m, 1H), 4.54–4.43 (m, 1H), 4.37–4.26 (m, 1H), 2.41–2.29 (m, 4H), 2.26 (s, 3H), 1.67–1.54 (m, 4H), 1.42–1.28 (m, 4H), 0.97–0.85 (m, 6H). ^{13}C NMR (CDCl_3 , 100 MHz) δ : 189.0, 173.4, 172.9, 67.0, 66.0, 63.7, 34.1, 34.0, 27.2, 25.9, 22.6, 22.5, 14.0.



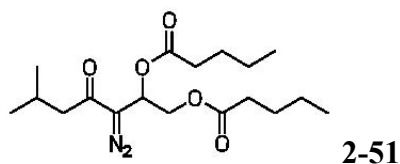
3-diazo-4-oxopentane-1,2-diyl dihexanoate (2-48): ^1H NMR (CDCl_3 , 400 MHz) δ : 5.92–5.82 (m, 1H), 4.55–4.42 (m, 1H), 4.37–4.26 (m, 1H), 2.40–2.28 (m, 4H), 2.26 (s, 3H), 1.68–1.56 (m, 4H), 1.38–1.25 (m, 8H), 0.96–0.83 (m, 6H). ^{13}C NMR (CDCl_3 , 100 MHz) δ : 173.4, 172.9, 66.0, 63.7, 34.4, 34.3, 31.6, 25.9, 24.9, 22.7, 14.3. (carbon signal next to diazo group might not show up)



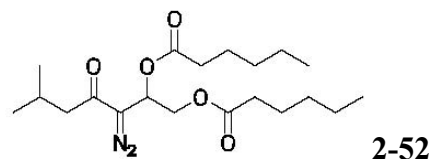
3-diazo-6-methyl-4-oxoheptane-1,2-diyl diacetate (2-49): ^1H NMR (CDCl_3 , 400 MHz) δ : 5.85–5.76 (m, 1H), 4.44–4.34 (m, 1H), 4.32–4.21 (m, 1H), 2.28 (d, J = 6.7 Hz, 2H), 2.15–2.07 (m, 1H), 2.03 (s, 3H), 2.01 (s, 3H), 0.89 (d, J = 8.0 Hz, 6H). ^{13}C NMR (CDCl_3 , 100 MHz) δ : 170.5, 169.9, 66.3, 63.8, 47.1, 26.0, 22.8, 22.7, 21.0, 20.8. (carbon signal next to diazo group might not show up)



3-diazo-6-methyl-4-oxoheptane-1,2-diyl dibutyrate (2-50): ^1H NMR (CDCl_3 , 400 MHz) δ : 5.92–5.81 (m, 1H), 4.50–4.39 (m, 1H), 4.34–4.22 (m, 1H), 2.37–2.21 (m, 6H), 2.18–2.04 (m, 1H), 1.69–1.54 (m, 4H), 0.96–0.85 (m, 12H). ^{13}C NMR (CDCl_3 , 100 MHz) δ : 173.2, 172.6, 66.1, 63.6, 47.2, 36.2, 36.1, 26.0, 22.8, 22.7, 18.7, 18.6, 13.9. (carbon signal next to diazo group might not show up)

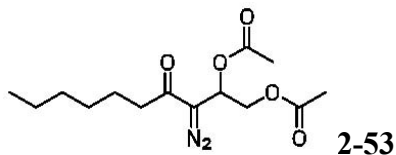


3-diazo-6-methyl-4-oxoheptane-1,2-diyl dipentanoate (2-51): ^1H NMR (CDCl_3 , 400 MHz) δ : 5.94–5.82 (m, 1H), 4.53–4.44 (m, 1H), 4.40–4.29 (m, 1H), 2.41–2.29 (m, 6H), 2.23–2.10 (m, 1H), 1.67–1.56 (m, 4H), 1.41–1.31 (m, 4H), 0.98–0.89 (m, 12H). ^{13}C NMR (CDCl_3 , 100 MHz) δ : 180.0, 173.5, 172.9, 66.2, 63.7, 47.3, 34.2, 34.1, 34.0, 27.3, 22.6, 22.5, 14.1, 14.0. (carbon signal next to diazo group might not show up)

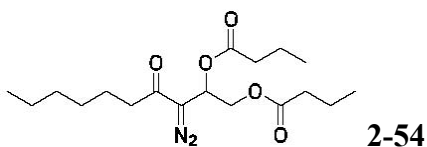


3-diazo-6-methyl-4-oxoheptane-1,2-diyl dihexanoate (2-52): ^1H NMR (CDCl_3 , 400 MHz) δ : 5.96–5.82 (m, 1H), 4.54–4.42 (m, 1H), 4.40–4.26 (m, 1H), 2.42–2.26 (m, 6H), 2.22–2.09 (m, 1H), 1.68–1.56 (m, 4H), 1.38–1.22 (m, 8H), 1.00–0.93 (m, 6H), 0.93–

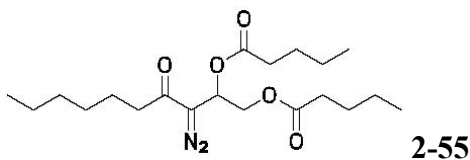
0.85 (m, 6H). ^{13}C NMR (CDCl_3 , 100 MHz) δ : 173.4, 172.8, 66.2, 63.7, 47.3, 34.3, 31.6, 24.9, 22.7, 14.3. (carbon signal next to diazo group might not show up)



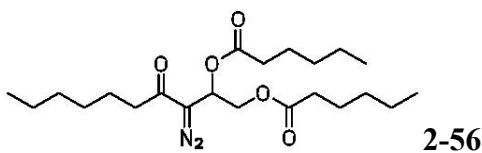
3-diazo-4-oxodecane-1,2-diyl diacetate (2-53): ^1H NMR (CDCl_3 , 400 MHz) δ : 5.95–5.85 (m, 1H), 4.54–4.43 (m, 1H), 4.41–4.29 (m, 1H), 2.49 (t, $J = 7.3$ Hz, 2H), 2.12 (s, 3H), 2.11 (s, 3H), 1.69–1.60 (m, 2H), 1.38–1.27 (m, 6H), 0.91 (t, $J = 6.9$ Hz, 3H). ^{13}C NMR (CDCl_3 , 100 MHz) δ : 170.7, 170.1, 66.4, 64.0, 38.6, 31.9, 29.2, 24.8, 22.9, 21.2, 21.0, 14.4. (carbon signal next to diazo group might not show up)



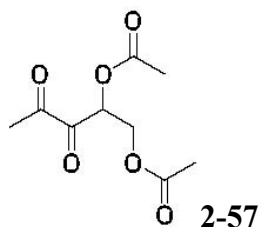
3-diazo-4-oxodecane-1,2-diyl dibutyrate (2-54): ^1H NMR (CDCl_3 , 400 MHz) δ : 5.96–5.85 (m, 1H), 4.56–4.46 (m, 1H), 4.40–4.28 (m, 1H), 2.53–2.43 (m, 2H), 2.38–2.29 (m, 4H), 1.72–1.61 (m, 6H), 1.37–1.25 (m, 6H), 1.02–0.94 (m, 6H), 0.94–0.87 (m, 3H). ^{13}C NMR (CDCl_3 , 100 MHz) δ : 173.3, 172.7, 66.2, 63.7, 36.3, 36.2, 31.9, 29.2, 24.9, 22.9, 18.7, 14.4, 14.0. (carbon signal next to diazo group might not show up)



3-diazo-4-oxodecane-1,2-diyl dipentanoate (2-55): ^1H NMR (CDCl_3 , 400 MHz) δ : 5.95–5.84 (m, 1H), 4.56–4.43 (m, 1H), 4.40–4.27 (m, 1H), 2.55–2.44 (m, 2H), 2.40–2.33 (m, 6H), 1.69–1.59 (m, 6H), 1.43–1.28 (m, 8H), 0.98–0.88 (m, 9H). ^{13}C NMR (CDCl_3 , 100 MHz) δ : 180.7, 173.5, 172.9, 66.2, 63.7, 34.2, 34.1, 31.9, 29.2, 27.3, 27.1, 24.9, 22.9, 22.6, 14.1, 14.1. (carbon signal next to diazo group might not show up)

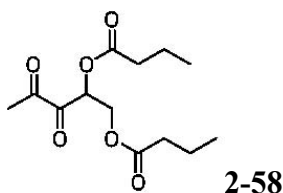


3-diazo-4-oxodecane-1,2-diyl dihexanoate (2-56): ^1H NMR (CDCl_3 , 400 MHz) δ : 5.97–5.83 (m, 1H), 4.56–4.42 (m, 1H), 4.40–4.27 (m, 1H), 2.57–2.2.43 (m, 2H), 2.43–2.28 (m, 6H), 1.73–1.57 (m, 6H), 1.40–1.26 (m, 12H), 0.97–0.86 (m, 9H). ^{13}C NMR (CDCl_3 , 100 MHz) δ : 180.2, 173.5, 172.9, 66.2, 63.7, 34.4, 31.6, 24.9, 24.8, 22.9, 22.7, 14.4, 14.3. (carbon signal next to diazo group might not show up)

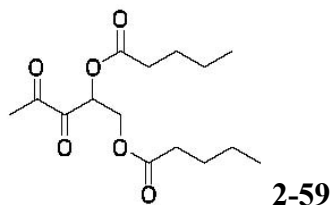


3,4-dioxopentane-1,2-diyl diacetate (2-57): ^1H NMR (CDCl_3 , 400 MHz) δ : 5.88–5.83 (m, 1H), 4.72–4.64 (m, 1H), 4.40–4.32 (m, 1H), 2.39 (s, 3H), 2.18 (s, 3H), 2.06 (s, 3H). ^{13}C NMR (CDCl_3 , 100 MHz) δ : 196.3, 190.4, 171.5, 170.5, 62.7, 24.1, 21.0, 20.7. Derivatization using 1,2-diaminobenzene MS (ESI): Calcd for $[\text{C}_{15}\text{H}_{16}\text{N}_2\text{O}_4 +$

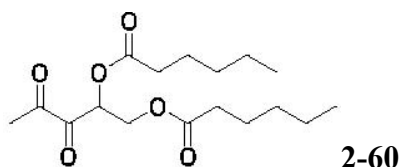
$\text{H}]^+$ 289.1188, found 289.1234.



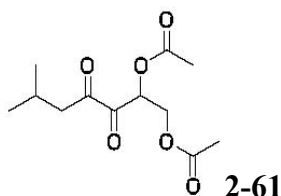
3,4-dioxopentane-1,2-diyl dibutyrate (2-58): ^1H NMR (CDCl_3 , 400 MHz) δ : 5.90–5.84 (m, 1H), 4.75–4.66 (m, 1H), 4.41–4.32 (m, 1H), 2.46–2.40 (m, 2H), 2.39 (s, 3H), 2.29 (t, $J = 7.4$ Hz, 2H), 1.73–1.66 (m, 2H), 1.66–1.58 (m, 2H), 0.99 (t, $J = 7.4$ Hz, 3H), 0.94 (t, $J = 7.4$ Hz, 3H). ^{13}C NMR (CDCl_3 , 100 MHz) δ : 196.3, 190.5, 174.1, 173.1, 62.5, 36.1, 35.8, 24.1, 18.7, 18.6, 13.9. Derivatization using 1,2-diaminobenzene MS (ESI): Calcd for $[\text{C}_{19}\text{H}_{24}\text{N}_2\text{O}_4 + \text{H}]^+$ 345.1814, found 345.1809.



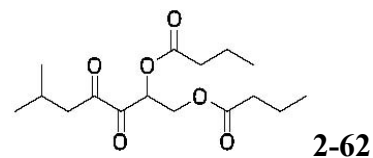
3,4-dioxopentane-1,2-diyl dipentanoate (2-59): ^1H NMR (CDCl_3 , 400 MHz) δ : 5.89–5.83 (m, 1H), 4.74–4.65 (m, 1H), 4.41–4.32 (m, 1H), 2.48–2.41 (m, 2H), 2.40 (s, 3H), 2.34–2.28 (m, 2H), 1.70–1.61 (m, 2H), 1.61–1.53 (m, 2H), 1.44–1.30 (m, 4H), 0.98–0.89 (m, 6H). ^{13}C NMR (CDCl_3 , 100 MHz) δ : 196.3, 190.5, 174.3, 173.3, 62.5, 34.0, 33.7, 27.2, 24.1, 22.5, 14.1, 14.0. Derivatization using 1,2-diaminobenzene MS (ESI): Calcd for $[\text{C}_{21}\text{H}_{28}\text{N}_2\text{O}_4 + \text{H}]^+$ 373.2127, found 373.2109.



3,4-dioxopentane-1,2-diyl dihexanoate (2-60): ^1H NMR (CDCl_3 , 400 MHz) δ : 5.91–5.82 (m, 1H), 4.75–4.64 (m, 1H), 4.42–4.30 (m, 1H), 2.47–2.40 (m, 2H), 2.39 (s, 3H), 2.33–2.25 (m, 3H), 1.72–1.62 (m, 2H), 1.62–1.53 (m, 2H), 1.40–1.21 (m, 8H), 0.97–0.83 (m, 6H). ^{13}C NMR (CDCl_3 , 100 MHz) δ : 196.3, 190.5, 174.2, 173.3, 72.9, 62.5, 34.2, 33.9, 31.5, 24.8, 24.1, 22.7, 22.6, 14.3. Derivatization using 1,2-diaminobenzene MS (ESI): Calcd for $[\text{C}_{23}\text{H}_{32}\text{N}_2\text{O}_4 + \text{H}]^+$ 401.2440, found 401.2479.



6-methyl-3,4-dioxoheptane-1,2-diyl diacetate (2-61): ^1H NMR (CDCl_3 , 400 MHz) δ : 5.89–5.83 (m, 1H), 4.70–4.61 (m, 1H), 4.45–4.36 (m, 1H), 2.78–2.58 (m, 2H), 2.23–2.19 (m, 1H), 2.19 (s, 3H), 2.06 (s, 3H), 0.98 (d, $J = 2.7$ Hz, 3H), 0.97 (d, $J = 2.7$ Hz, 3H). ^{13}C NMR (CDCl_3 , 100 MHz) δ : 198.2, 191.0, 171.2, 170.4, 73.2, 62.7, 45.0, 24.4, 22.9, 21.0, 20.7. Derivatization using 1,2-diaminobenzene MS (ESI): Calcd for $[\text{C}_{18}\text{H}_{22}\text{N}_2\text{O}_4 + \text{H}]^+$ 331.1658, found 331.1740.

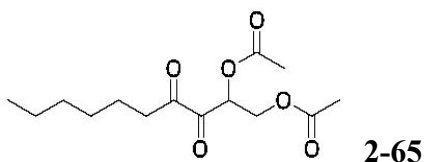


6-methyl-3,4-dioxoheptane-1,2-diyl dibutyrate (2-62): ^1H NMR (CDCl_3 , 400 MHz)

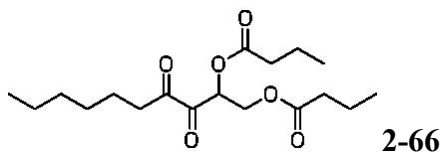
CCCC(=O)OCC(=O)C(C)C(=O)OCC(=O)CCCC 2-63CCCCC(=O)OCC(=O)C(=O)CC(C)C 2-64

60

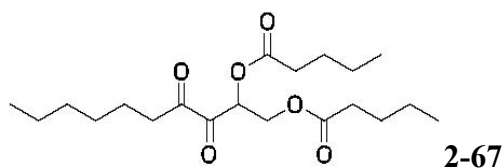
MS (ESI): Calcd for $[C_{26}H_{38}N_2O_4 + H]^+$ 443.2910, found 443.2855.



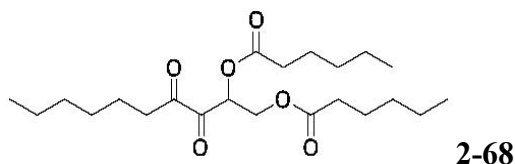
3,4-dioxodecane-1,2-diyl diacetate (2-65): 1H NMR ($CDCl_3$, 400 MHz) δ : 5.90–5.84 (m, 1H), 4.71–4.64 (m, 1H), 4.45–4.36 (m, 1H), 2.87–2.72 (m, 2H), 2.19 (s, 3H), 2.17 (s, 3H), 1.68–1.58 (m, 2H), 1.38–1.27 (m, 6H), 0.94–0.87 (m, 3H). ^{13}C NMR ($CDCl_3$, 100 MHz) δ : 198.7, 190.9, 171.2, 170.4, 73.2, 62.7, 36.5, 31.9, 29.1, 23.1, 22.9, 21.0, 20.8, 14.4. Derivatization using 1,2-diaminobenzene MS (ESI): Calcd for $[C_{20}H_{26}N_2O_4 + H]^+$ 359.1971, found 359.1963.



3,4-dioxodecane-1,2-diyl dibutyrate (2-66): 1H NMR ($CDCl_3$, 400 MHz) δ : 5.91–5.84 (m, 1H), 4.72–4.64 (m, 1H), 4.46–4.37 (m, 1H), 2.86–2.2.72 (m, 2H), 2.47–2.38 (m, 2H), 2.33–2.24 (m, 2H), 1.76–1.1.60 (m, 6H), 1.38–1.27 (m, 6H), 1.04–0.88 (m, 9H). ^{13}C NMR ($CDCl_3$, 100 MHz) δ : 198.7, 191.0, 173.9, 173.1, 73.1, 62.5, 36.5, 36.2, 35.9, 31.9, 29.1, 23.1, 22.9, 18.7, 14.4, 14.0. Derivatization using 1,2-diaminobenzene MS (ESI): Calcd for $[C_{24}H_{34}N_2O_4 + H]^+$ 415.2597, found 415.2528.



3,4-dioxodecane-1,2-diyl dipentanoate (2-67): ^1H NMR (CDCl_3 , 400 MHz) δ : 5.90–5.83 (m, 1H), 4.71–4.63 (m, 1H), 4.45–4.37 (m, 1H), 2.85–2.72 (m, 2H), 2.48–2.40 (m, 2H), 2.40–2.34 (m, 2H), 2.34–2.27 (m, 2H), 1.69–1.57 (m, 6H), 1.45–1.30 (m, 8H), 0.97–0.89 (m, 9H). ^{13}C NMR (CDCl_3 , 100 MHz) δ : 198.7, 191.0, 174.1, 173.3, 73.1, 62.5, 36.5, 34.0, 33.8, 31.9, 29.1, 27.2, 23.1, 22.9, 22.6, 22.5, 14.4, 14.1. Derivatization using 1,2-diaminobenzene MS (ESI): Calcd for $[\text{C}_{26}\text{H}_{38}\text{N}_2\text{O}_4 + \text{H}]^+$ 443.2910, found 443.2867.



3,4-dioxodecane-1,2-diyl dihexanoate (2-68): ^1H NMR (CDCl_3 , 400 MHz) δ : 5.90–5.83 (m, 1H), 4.72–4.62 (m, 1H), 4.45–4.36 (m, 1H), 2.86–2.71 (m, 2H), 2.48–2.40 (m, 2H), 2.40–2.33 (m, 2H), 2.33–2.25 (m, 2H), 1.71–1.58 (m, 6H), 1.39–1.27 (m, 12H), 0.96–0.87 (m, 9H). ^{13}C NMR (CDCl_3 , 100 MHz) δ : 198.7, 191.0, 174.1, 173.3, 73.1, 62.5, 36.5, 34.3, 34.0, 31.9, 31.6, 31.5, 29.1, 24.8, 23.1, 22.9, 22.7, 14.4, 14.3. Derivatization using 1,2-diaminobenzene MS (ESI): Calcd for $[\text{C}_{28}\text{H}_{42}\text{N}_2\text{O}_4 + \text{H}]^+$ 471.3223, found 471.3236.

Chapter 3. Geminal dihalogen isosteric replacement in hydrated AI-2 affords analogs that potently modulate quorum sensing

3.1 Introduction

AI-2 is probably the most complex and fascinating QS molecule described to date. It is produced by many bacterial strains and either the molecule itself or its synthase, LuxS, affect the physiology (including biofilm formation)^{42a, 113} of multitudes of bacteria, some of which are of clinical and bioterrorism relevance, such as *Vibrio cholera*,^{26a} *Yersinia pestis*¹¹⁴ and *Staphylococcus aureus*.⁷⁰ AI-2 production as well as degradation affects central metabolism and emerging data suggests that it could be used as an alternative carbon source to produce acetyl-CoA.^{41, 115} From a chemical perspective, AI-2 shows remarkable diversity as a signaling molecule (see **Figure 3-1** for the possible inter-converting isomers of AI-2) and depending on environmental conditions, AI-2 can exhibit selectivity in QS signaling. For example, in the presence of boric acid (such as in aquatic environment), AI-2 predominantly forms the boronate ester (**3-4**, **Figure 3-1**), which is a ligand for LuxP of *Vibrios*.²³ Enteric bacteria, such as *E. coli* and *Salmonella* use AI-2, only after it has been processed by LsrK kinase.¹¹¹ So far four different proteins have been characterized that bind to AI-2: LuxP, which binds to a boronated form (**3-4**);²³ LsrB (a transporter), which binds to the cyclic but non-boronated form (**3-6**);^{39, 80} LsrR, which binds to the phosphorylated linear form (and with the 3-position as the hydrate, **7**)⁸¹ and LsrF, which binds to the 1,3-diketo form of AI-2 (**3-10**).⁴¹

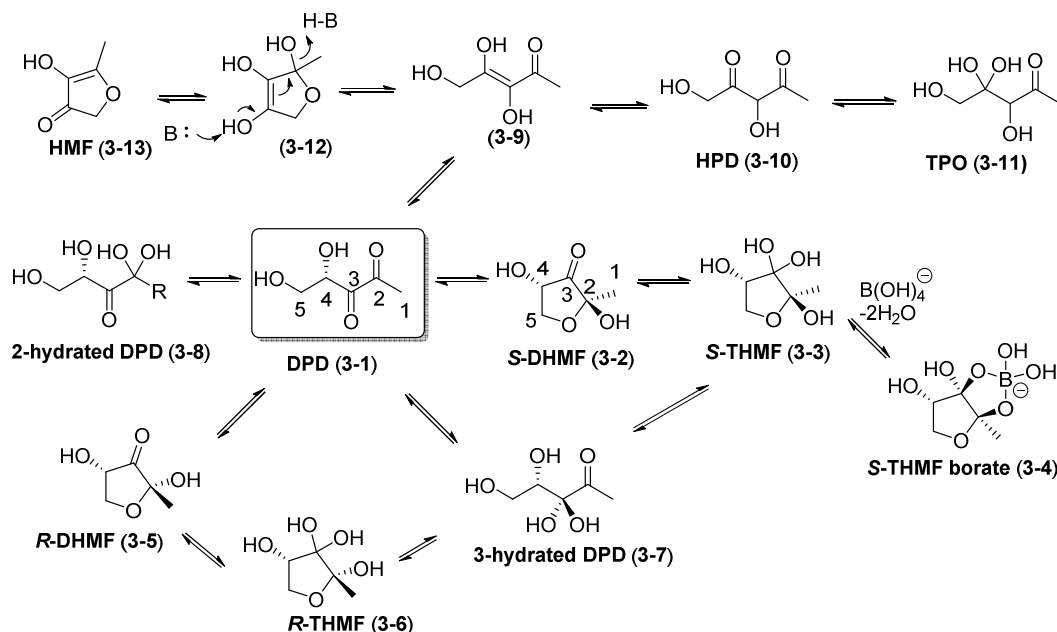


Figure 3-1. Chemical structures of AI-2.

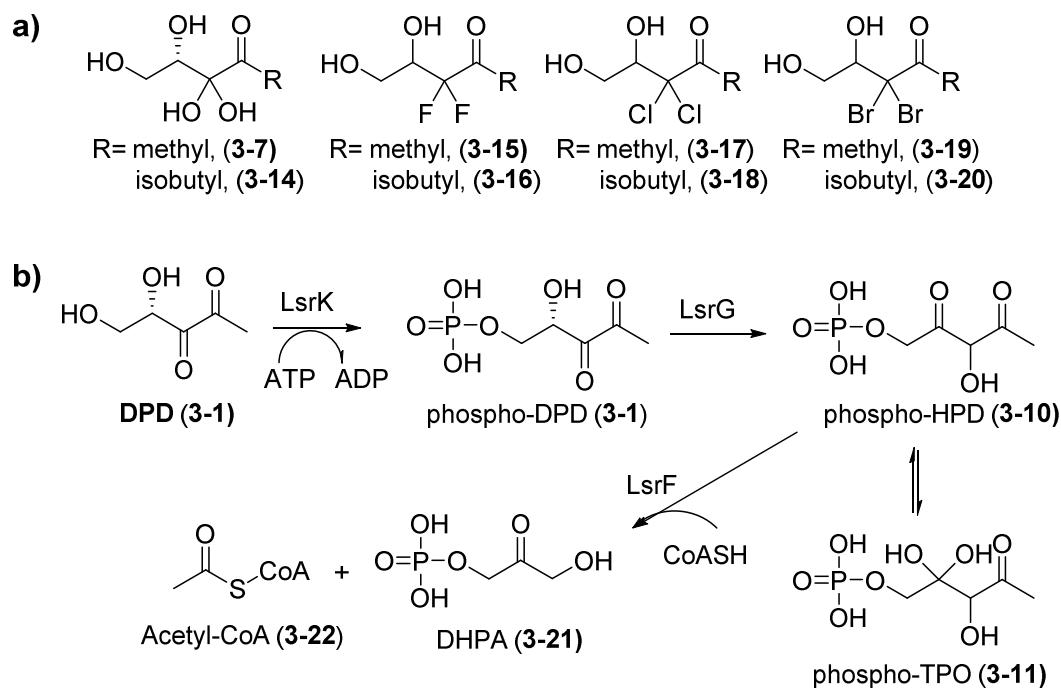


Figure 3-2. a) 3-hydrated DPD (3-7) and 3,3-dihaloanalogs that were planned to synthesize for this study. **b)** Degradation of AI-2 via LsrG/LsrF. We expect that the geminal dihalogen analogs cannot form the 1,3-diketone intermediate (3-10) hence would not be degraded by LsrG/LsrF.

Due to the ubiquity of AI-2 in bacterial QS signaling, there is interest in

developing small molecules that can modulate AI-2-based signaling. Such anti-AI-2 small molecules could be used in synergy with traditional antibiotics¹¹⁶ or as tools in synthetic biology to modulate systems that use AI-2-based circuits.^{84c} A fruitful approach to develop anti-AI-2 molecules have been the modification of AI-2 at the C1,^{83, 84c, d, 107a} C4^{107a, 117} or C5-positions⁸⁷ into analogs that have shown great promise as either antibiofilm or synergistic antibacterial agents.¹¹⁶ Recently, we disclosed that LsrR, the response regulator that binds to phosphorylated AI-2 to modulate many genes actually bound to the 3,3-hydrated form of AI-2 (**3-7**, **Figure 3-1**).⁸¹ We rationalized that isosteric replacement at the C3 position of AI-2 could prevent isomerization into the 1,3-diketo analog (**3-10**), which is a substrate for LsrF degradation (see **Figure 3-2b**).⁴¹

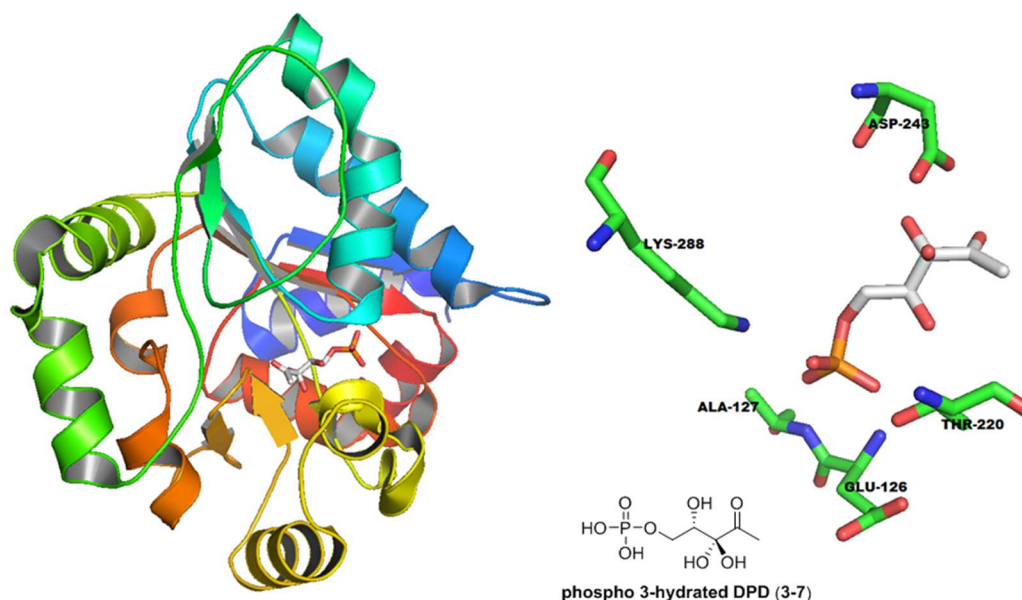


Figure 3-3. Phospho-AI-2 in its hydrated form at C3 when binding with LsrR (PDB code: 4L4Z).

Analysis of interactions between P-AI-2 (phospho-3-hydrated DPD) and active-

site residues in LsrR indicated that Asp243 was within 3Å of the geminal diol unit of AI-2 (see **Figure 3-3**), indicating that if Asp243 existed as the carboxylate form, then the hydrogens of the geminal diol could potentially form hydrogen-bonding interactions with this residue. A geminal bromide or chloride, but not fluoride, could recapitulate this interaction via the halogen bond (strength of halogen bond is as follows: $I > Br > Cl > F$).¹¹⁸ On the other hand, if the Asp243 is protonated in the active site, then it is conceivable that the carbonyl moiety could still partake in a halogen bond interaction with one of the geminal halogens whereas the carboxylic acid OH group would act as a hydrogen bond donor to the halogen.¹¹⁹ It is the ambivalence of higher halogens (presence of lone pairs for hydrogen bond formation and presence of a low lying σ^*_{C-X} bond for halogen bond formation, see **Figure 3-4**)¹²⁰ that makes them ideal for isosteric replacement for the geminal diol.

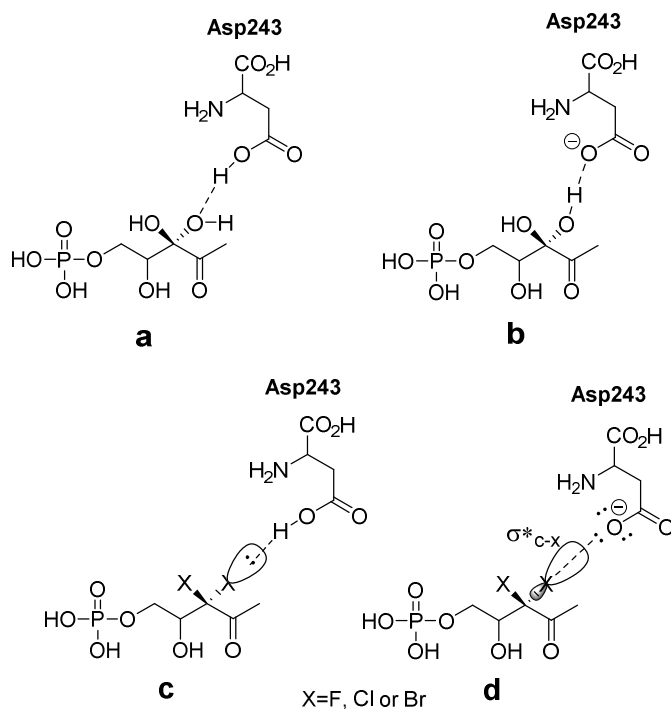
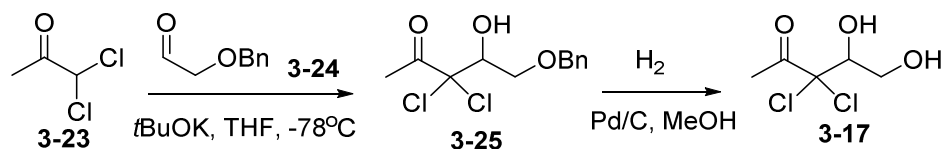


Figure 3-4. Postulated binding mode of AI-2 and dihalogenated AI-2 with Asp-243. **a)** carboxylic acid as hydrogen donor to form hydrogen bond with one of the hydroxyl groups on P-AI-2. **b)** one of the hydroxyl groups on P-AI-2 as hydrogen donor to form hydrogen bond with carboxylate. Halogens partaking in hydrogen bonding **c)** and halogen bonding **d)**.

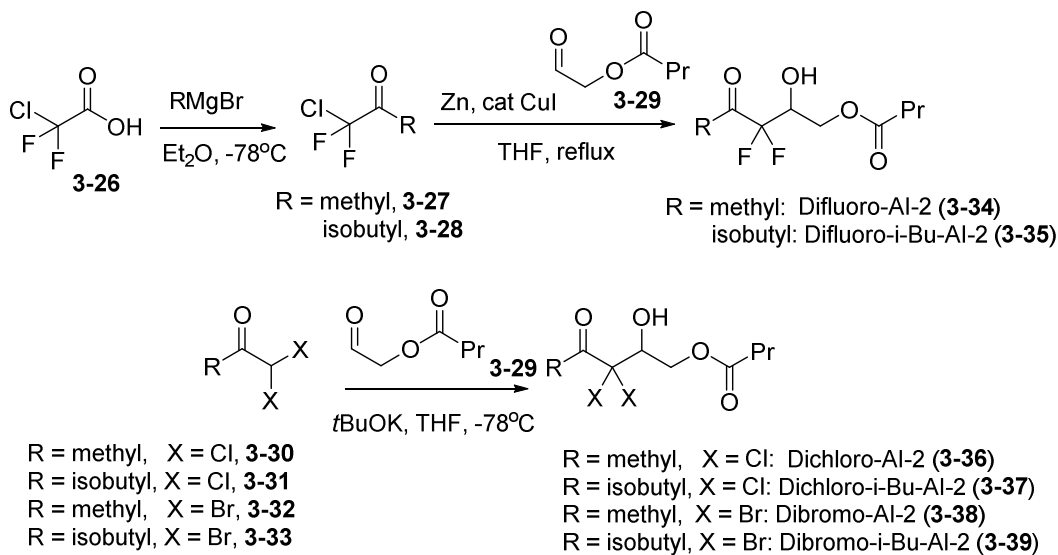
3.2 Results and discussion

Attempted synthesis of targeted dihalogen compounds **3-15** to **3-20** was fraught with difficulties because the final products were volatile (see **Scheme 3-1**). Others and us have, however, demonstrated that ester prodrug versions of AI-2 are convenient sources of AI-2 because the esters can be easily purified on column chromatography and used directly in QS assays without prior deprotection of the esters.⁸⁵⁻⁸⁶ Presumably, esterases produced by bacteria hydrolyze the esters into the active compounds, obviating a need for ester unmasking. Therefore we proceeded to make the ester “pro-drug” versions of

compounds **3-15** to **3-20** as **3-34** to **3-39**. The propyl ester was chosen as we rationalized that perhaps the shorter methyl and ethyl esters would have volatility issues whereas the longer chains, greater than propyl, might be hydrolyzed slowly. This decision was just based on our intuition and not by any hard facts. Target compounds, **3-34** to **3-39** were synthesized using strategies shown in **Scheme 3-2**.



Scheme 3-1. Initial attempt to make dichloro AI-2 **3-17**.



Scheme 3-2. Synthesis of dihalogenated AI-2 analogs.

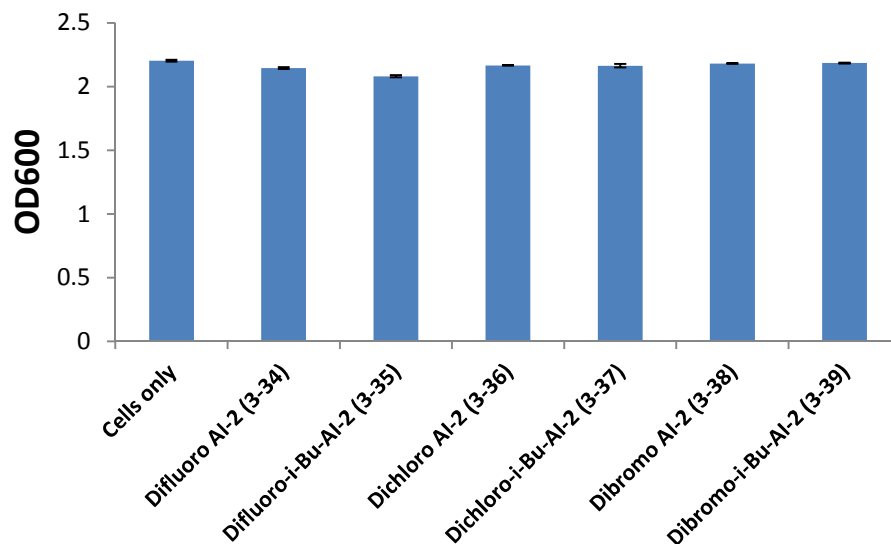


Figure 3-5. OD₆₀₀ value of *E. coli* LW7 (*luxS*⁻) after 24 hrs growth at different conditions: *E. coli* LW7 (*luxS*⁻) alone; and *E. coli* LW7 (*luxS*⁻) in the presence of 100 μ M of each analog, respectively.

With these molecules in hand, we investigated if they were non-toxic and could modulate quorum sensing in *E. coli*. Pleasingly, at 100 μ M concentration, all of the compounds were non-toxic towards *E. coli* (see **Figure 3-5**). Using the *E. coli* strain LW7 (*LuxS*⁻ and harboring the β -gal gene), we could use the β -galactosidase assay to evaluate our analogs.^{84c, d} The β -gal gene in LW7 is under the control of the LsrR repressor. At high concentration of P-AI-2, the ligand binds to LsrR to dissociate it from the LsrR promoter region and therefore permit the transcription of the genes under the control of the LsrR repressor.⁴⁰ We have previously reported that the size of the C1 alkyl group of AI-2 and analogs determines whether an analog would be an LsrR agonist or antagonist.^{84d} Recently a rationale for this observation was provided via the crystal structure of LsrR in complex with AI-2 or analogs.⁸¹ Based on the LsrR crystal structure analysis, we postulated that the C1 methyl dihalogen analogs would act as

agonists whereas the isobutyl dihalogen analogs would be antagonists, as long as the isosteric replacement of the geminal hydroxyl group with halogens does not adversely affect binding of the ligand to LsrR. Interestingly dibromo-AI-2 (**3-38**) and dichloro-AI-2 (**3-36**), but not difluoro-AI-2 (**3-34**), could induce β -gal transcription (analyzed via the β -galactosidase assay), see **Figure 3-6a**. In the absence of AI-2, the level of β -galactosidase is low, whereas when 20 μ M of AI-2 or dibromo-AI-2 (**3-38**) or dichloro-AI-2 (**3-36**) were added to LW7, the level of β -galactosidase increased (see activity assay in **Figure 3-6a**). The dibromo analog of AI-2 (**3-38**) was as potent as AI-2, the activity of the dichloro-AI-2 (**3-36**) was slightly lower than the native AI-2 molecule. In line with our expectation, none of the isobutyl dihalogen analogs were LsrR agonists, augmenting earlier observations that longer C1 chain AI-2 analogs are not agonists, but are rather antagonists.^{81, 83b, 84c, d}

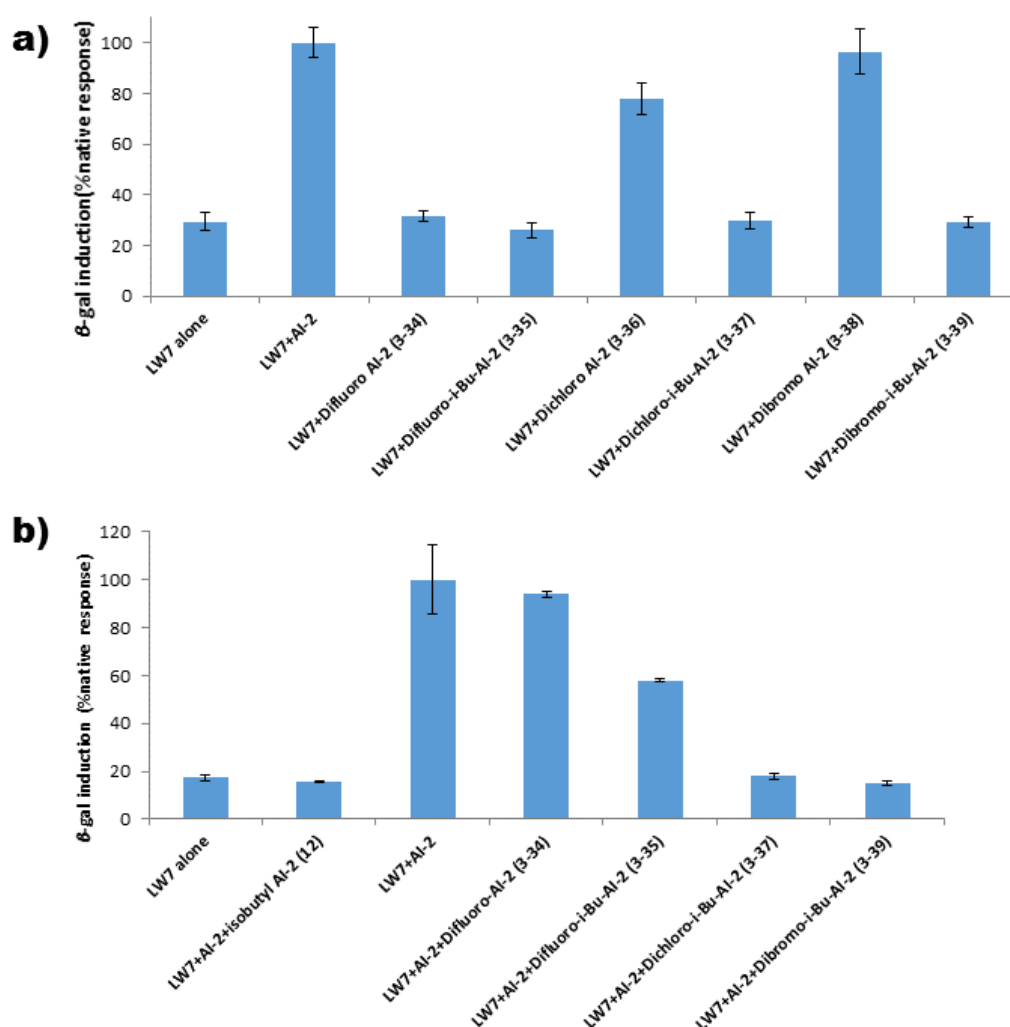


Figure 3-6. a) AI-2 dependent β -galactosidase production of *E. coli* LW7 (*luxS*⁻) in response to 20 μ M synthetic AI-2 or analogs. 100% native *E. coli* LW7 (*luxS*⁻) + AI-2 response = 167 Miller units. **b)** Analogs (20 μ M) inhibit native β -galactosidase production in *E. coli* LW7 (*luxS*⁻) in the presence of 20 μ M synthetic AI-2. 100% native *E. coli* LW7 (*luxS*⁻) + AI-2 response = 486 Miller units. (With the help of Yue Zheng, a graduate student from the Sintim group).

Isobutyl AI-2 (**3-14**) is a potent inhibitor of AI-2 signaling, via LsrR binding,^{81, 84c, d} and has been shown to inhibit *E. coli* biofilm formation, either alone or in combination with traditional antibiotics, such as gentamicin.¹¹⁶ In fact isobutyl AI-2 (**3-14**) has a higher affinity for LsrR than AI-2; the dissociation constant, *K*_d, of AI-2/LsrR

complex is 2.0 μM whereas isobutyl-AI-2/LsrR has a K_d of 0.5 μM . Since the dichloro and dibromo mimics of AI-2 (**3-36**, **3-38**) were potent LsrR agonists, we wondered if the isobutyl-dihalogenes would also be potent antagonists of LsrR. Interestingly both isobutyl dibromo and dichloro analogs of AI-2 were antagonists of LsrR (see **Figure 3-6b**). Whereas in the absence of these ligands 20 μM AI-2 could induce β -gal expression, when equimolar amounts of isobutyl dibromo (**3-39**) or dichloro AI-2 (**3-37**) were added, these could compete with AI-2 and prevent β -gal expression above the background, see **Figure 3-6b**. Here too the isobutyl difluoro analog (**3-35**) was not an effective antagonist.

Next, we examined the effects of our analogs on *E. coli* W3110 pCT6 (*luxS*⁺), which contains an *egfp* gene under LsrR control. Because W3110 pCT6 can make its own AI-2, in the absence of any AI-2 antagonist, about 90% of the population expressed the EGFP protein, see **Figure 3-7**. The addition of the dihalogenated isobutyl DPD analogs caused a reduction of the EGFP expression. In agreement with the β -gal assay (**Figure 3-7**), dibromo-iBu-AI-2 (**3-36**) was a better inhibitor than dichloro-iBu-AI-2 (**3-34**), which in turn was better than difluoro-iBu-AI-2 (**3-32**) (see **Figure 3-7**).

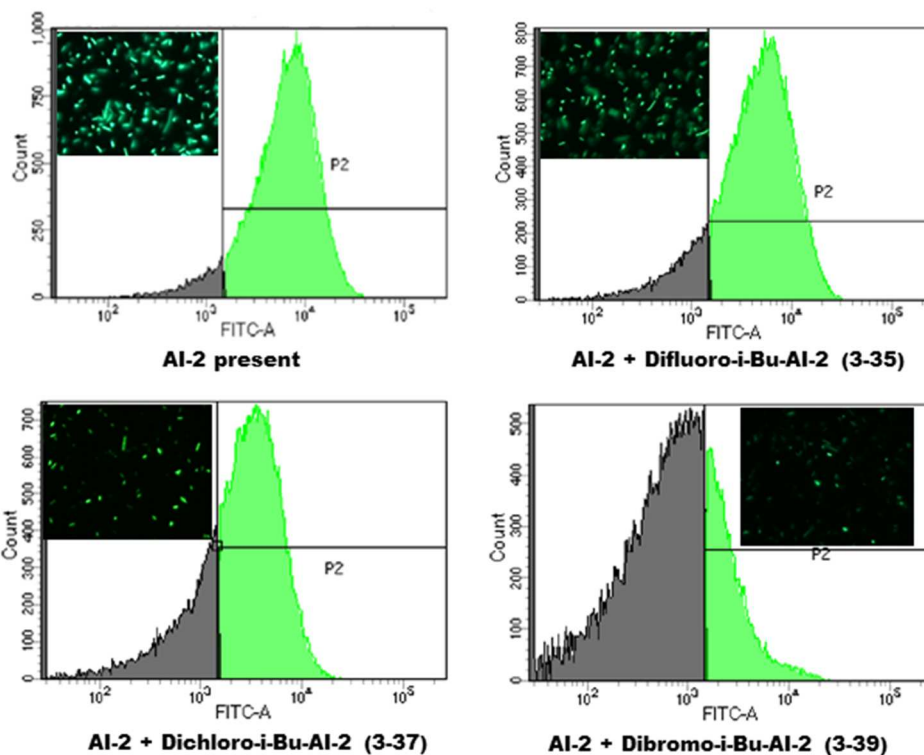


Figure 3-7. AI-2 dependent EGFP induction in *E. coli* W3110 pCT6(*luxS*⁺) in response to difluoro-*i*-Bu-AI-2 (**3-35**), dichloro-*i*-Bu-AI-2 (**3-37**) and dibromo-*i*-Bu-AI-2 (**3-39**) (FACS analysis with microscopic image). (Done by Jessica L. Terell, from the Bentley laboratory).

To explain our observations that the dibromo analog was a better mimic of hydrated AI-2 than the dichloro analog, which was also better than the difluoro analog, we compared the size (sterics) and electronics of the geminal dihydroxyl moiety with the various dihalogens in the cyclized and linear analog forms (see **Figures 3-8** and **Table 3-1**). The space-filling models of AI-2 and its halogenated analogs (**Figures 3-8**) revealed that the fluoro analog (**3-15**) was smaller in size compared with AI-2 DPD (**3-7**) while both the chloro and bromo analogs, (**3-17**) and (**3-19**), were bigger than AI-2 DPD (**3-7**) (see **Figures 3-8** and also **Table 3-1**).

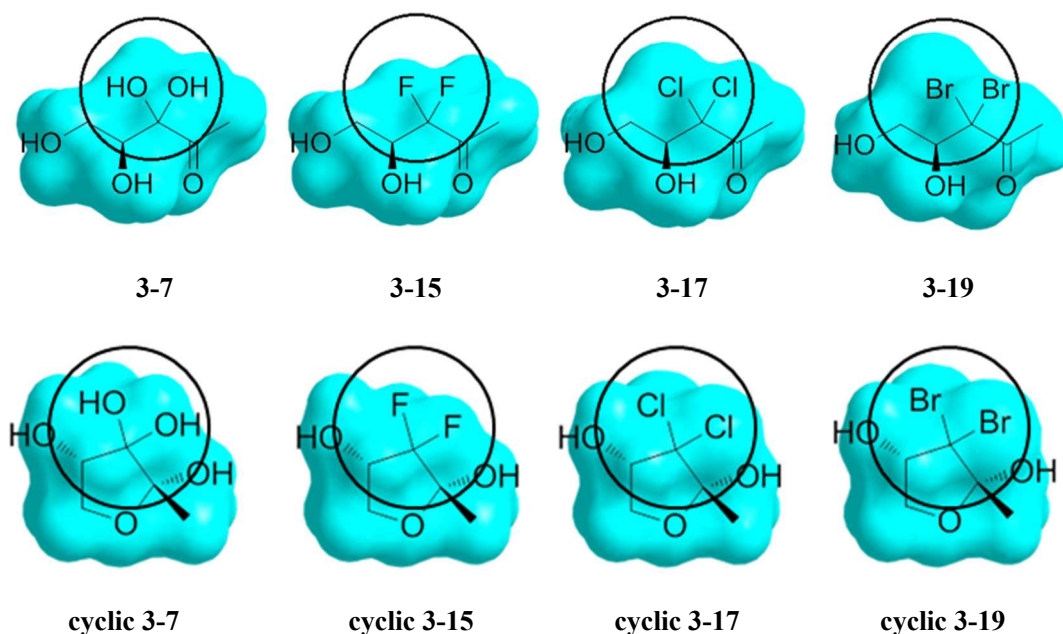


Figure 3-8. Structures of AI-2 and its halogenated analogs with varied shapes and sizes.

	X	Compd.	Mol. weight	Mol. volume/Å ³	C-X bond length/Å ²	Molecular dipole moment/D
	-OH	3-7	150.13	120.33	1.40	4.24
	-F	3-15	154.11	115.08	1.37	3.20
	-Cl	3-17	187.02	137.98	1.81	3.02
	-Br	3-19	275.92	149.46	2.00	2.97
	-OH	Cyclic 3-7	150.13	118.14	1.41	4.23
	-F	Cyclic 3-15	154.11	110.84	1.38	3.02
	-Cl	Cyclic 3-17	187.02	132.77	1.80	3.30
	-Br	Cyclic 3-19	275.92	144.87	1.96	3.12

Table 3-1. Comparison of properties of AI-2 and analogs.

Apart from size, electronics could also play an important role in ligand-receptor binding.

Electrostatic potential surfaces for AI-2 and analogs (**Figure 3-9**), in both linear and cyclic forms were calculated using Gaussian 09¹²¹ at B3LYP/6-31G(d) level with solvent effect (water, PCM model). For chloro- and bromo- analogs, in both linear and cyclized forms, there is a region of positive potential at the opposite end of the C-X

bond (on the halogen side). This positive region is called σ -hole, which is the basis of halogen bonding. So we speculate that chloro and bromo moieties in our analogs could function as electrophiles and partake in halogen bonding. Therefore even in the absence of hydroxyl groups, they could still interact with aspartic acid 243 in LsrR (see **Figure 3-9**). In the case of difluoro analogs, neither the size of fluoro moiety nor the electronics mimic the hydroxyl group well and hence the lack of activity (agonism or antagonism) seen with the difluoro substitution.

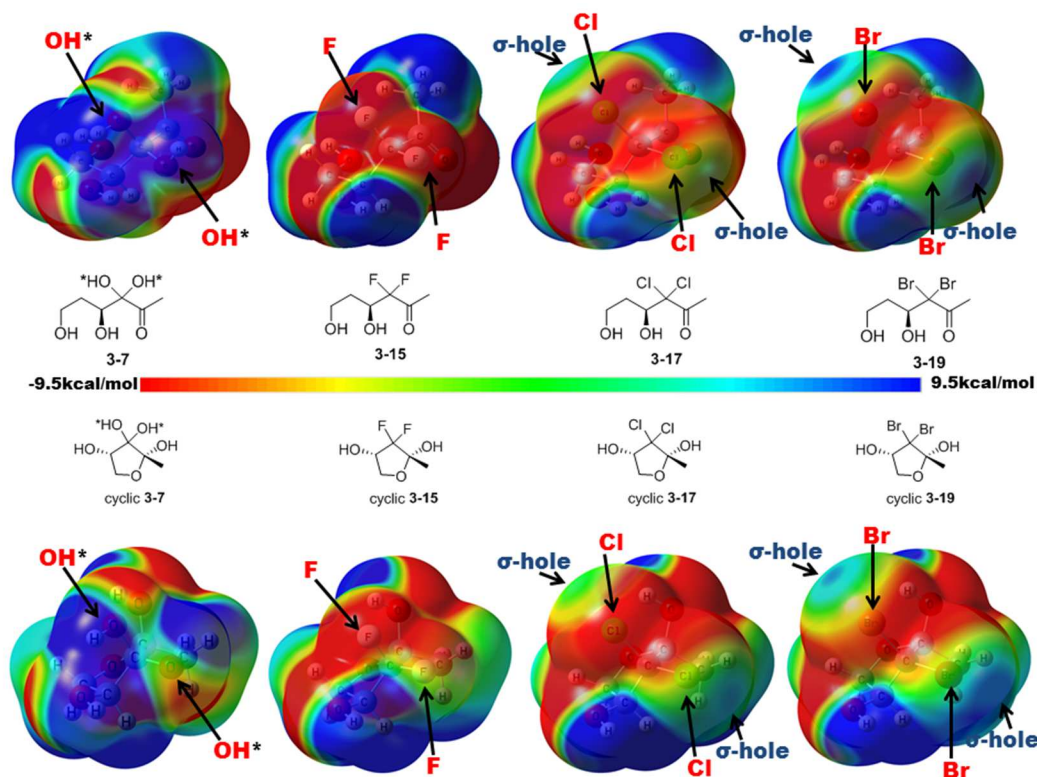


Figure 3-9. Molecular surface electrostatic potential of AI-2 and analogs in simplified models. Color ranges from -9.5 kcal/mol (red) to 9.5 kcal/mol (blue). Important atoms and σ -hole were labeled.

3.3 Conclusion.

In conclusion, we have designed and prepared a new generation of AI-2 analogs with dihalogen at C3 position. This set of analogs exhibited similar bioactivities with our earlier generation of analogs with modified C1 but intact C3 but has the added advantage that isomerization into a 1,3-diketo, which facilitates LsrF degradation, is not possible. This work demonstrates that geminal dihalogens, especially of higher halogens, are good mimics of hydrated moieties in biological ligands. It is expected that the substitution of geminal hydroxyl groups with dihalogen would afford molecules that could cross cell membranes more easily. Also for ligands whereby the hydrated form or keto form could facilitate degradation, such as in AI-2, isosteric replacement with dihalogens would provide more stable analogs.

3.4 Detailed experimental procedures and characterizations

Bioassay procedures

***β*-galactosidase assay:** Grew *E. coli* ZK126 (Wild-type strain derivative, W3110 *ΔlacU160-tna2*) and LW7 (ZK126 *ΔluxS*) with ampicillin overnight. Diluted the overnight culture 40 times and grew at 37 °C until OD₆₀₀ reached 0.8. Spin down the cells and resuspend the cell pellets in PBS. Made 500 μL aliquots, added the AI-2 analogs and grew the bacteria at 37 °C for 2 hours. Spin down the cells and resuspend the cell pellets in 500 μL Z-buffer. Use 250 μL of cell suspension for OD₆₀₀ measurement. The rest of cell suspension (250 μL) was mixed with 25 μL of CH₃Cl and

12.5 μ L of 0.1% SDS and incubated at room temperature for 5 min. After adding 50 μ L of ONPG (4 mg/mL in Z-buffer), samples were incubated at 28 °C for 40 min. 125 μ L of 1 M sodium carbonate solution was used to stop reaction. Centrifuged at 4 °C for 5 min and took 250 μ L supernatant for OD₄₂₀ and OD₅₅₀ measurement. Optical density was measured by Molecular Devices SpectraMax M5^e microplate reader. (With the help of Yue Zheng, a graduate student from the Sintim group).

β -galactosidase units was calculated using the following equation:

$$\beta\text{-galactosidase units} = 1000 \times (\text{OD}_{420} - (1.75 \times \text{OD}_{550})) / (0.25 \text{ (ml)} \times 40 \text{ (min)} \times \text{OD}_{600})$$

Flow cytometry assay: *E.coli* W3110 pCT6¹²² + pET200-EGFP-Lys¹²³ was cultured from colony in Luria-Bertani medium supplemented with ampicillin and kanamycin. At OD₆₀₀ 0.1, cultures were supplemented with 20 μ M of the AI-2 analog (or an equivalent volume of DMSO for negative controls) and incubated in triplicate for 6 h at 37 °C with shaking (250 rpm). The *E.coli* green fluorescence response was determined using fluorescence microscopy (Olympus BX60) and flow cytometric analysis. Samples were analyzed by flow cytometry (FACS CantoII, BD 394 Biosciences), using a 488 nm laser and 530/30 filter set with 50000 gated events analyzed per sample. (Done by Jessica L. Terell, from the Bentley laboratory).

Chemical synthesis procedures and characterization of new compounds

All reagents were obtained commercially unless otherwise noted. Reactions were performed using oven-dried glassware under an atmosphere of argon. Air- and

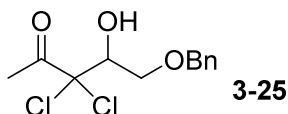
moisture-sensitive liquids and solutions were transferred via syringe or stainless steel cannula. Dry tetrahydrofuran (THF) and diethyl ether (Et₂O) were distilled over sodium prior to use and dry dichloromethane (DCM) was distilled over CaH₂ prior to use. Thin-layer chromatography (TLC) was performed on Merck Kieselgel 60 F254 plates. Visualization of the developed chromatogram was accomplished by UV light or by staining with KMnO₄ solution. Chromatographic purification of products was accomplished using flash column chromatography on silica gel (230 X 400 mesh) or GRACE Reveleris[®] X2 flash Chromatography system with Reveleris[®] flash cartridges (40 μM silica). Compounds purified by chromatography on silica gel were typically applied to the absorbent bed using the indicated solvents conditions with a minimum amount of added dichloromethane as needed for solubility. Solvents were removed from the reaction mixture or combined organic extracts by concentration under reduced pressure using an evaporator with bath at 30–40 °C. Elevated temperatures were obtained using thermostat-controlled silicone oil baths. Low temperatures were obtained by ice bath or by mixing dry-ice with organic solvents. NMR spectra were measured on Bruker AV-400, Bruker DRX-400 (¹H at 400 MHz, ¹³C at 100MHz), Bruker DRX-500 (¹H at 500 MHz, ¹³C at 125MHz) or Bruker AVIII-600 (¹H at 600 MHz, ¹³C at 150MHz). Data for ¹H -NMR spectra are reported as follows: chemical shift (ppm, relative to residual solvent peaks or indicated external standards; s = singlet, d = doublet, t = triplet, q = quartet, dd = doublet of doublets, td = triplet of doublets, m = multiplet), coupling constant (Hz), and integration. Data for ¹³C -NMR are reported in terms of chemical

shift (ppm) relative to residual solvent peak. Mass spectra (MS) and high resolution mass spectra (HRMS) were recorded by JEOL AccuTOF-CS (ESI positive, needle voltage 1800~2400 eV). Infrared spectra (IR) were recorded by a ThermoNicolet IR200 Spectrometer.

Initial attempt to make dichloro AI-2 **3-17**:

Refer to **Scheme 3-1**.

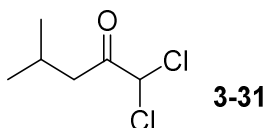
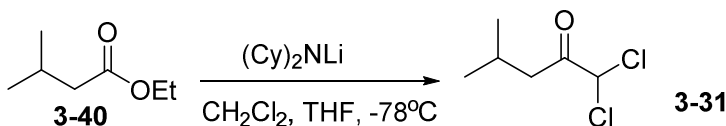
To a stirred suspension of *t*BuOK (6 mg, 0.1 equiv) in anhydrous THF was added 1,1-dichloro-2-propanone **3-23** (50 μ L, 0.50 mmol), followed by benzyloxyacetaldehyde **3-24** (70 μ L, 1.0 equiv) at -78 °C under argon. The reaction was allowed to warm up to room temperature gradually and stirred overnight. Then the reaction was quenched by saturated NH₄Cl (aq) carefully at 0 °C. The organic layer was separated and the aqueous layer was extracted with EtOAc three times. The combined organic phase was dried over MgSO₄. The product was purified by silica column chromatography (EtOAc: Hexanes = 1: 8, v/v) and **3-25** was obtained as 93 mg clear oil (67 % yield). To make dichloro AI-2 **3-17**, **3-25** (39 mg, 0.14 mmol) was dissolved in 2 mL methanol, which was suspended with Pd/C (5% on carbon, 29 mg, 10 mol%). The reaction flask was vacuumed and then charged by H₂ balloon. The reaction was stirred at room temperature overnight. Then Pd/C was filtered and the filtrate was evaporated at reduced pressure. However, the product **3-17** was volatile and left the flask empty. And then we turned into the ester-protected pro-drug strategy.



5-(benzyloxy)-3,3-dichloro-4-hydroxypentan-2-one (3-25):

3-25 was obtained as 93 mg clear oil (67 % yield). ^1H NMR (400 MHz, CDCl_3) δ ppm = 7.42-7.30 (5H, m), 4.65-4.58 (2H, m), 4.58-4.51 (1H, m), 3.98-3.90 (1H, m), 3.81-3.73 (1H, m), 3.23 (1H, d, $J = 5.2$ Hz), 2.52 (3H, s). ^{13}C NMR (100 MHz, CDCl_3) δ ppm = 196.4, 137.8, 128.9, 128.4, 128.2, 89.0, 75.4, 74.0, 70.4, 24.8. HRMS (ESI $^+$) m/z calcd. for $\text{C}_{12}\text{H}_{15}\text{Cl}_2\text{O}_3$ $[\text{M}+\text{H}]^+$ 277.0398, found 277.0422.

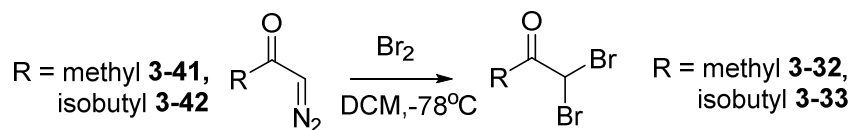
Synthesis of the starting materials for dihalogen AI-2 analogs:



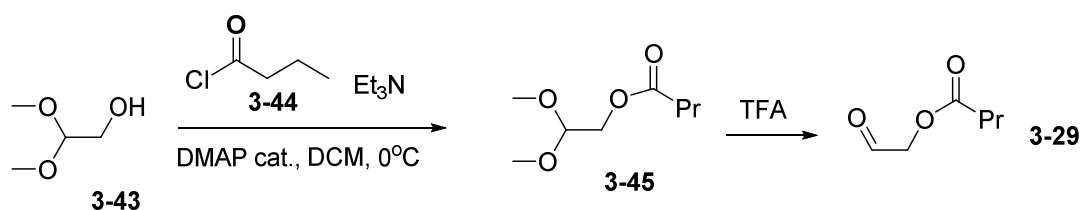
1,1-dichloro-4-methylpentan-2-one (3-31):

The synthesis was similar to the reference.¹²⁴ Generally, to a stirred solution of dichloromethane (10 mmol, 0.64 ml) and ethyl isovalerate **S3** (5 mmol, 0.75 ml) in anhydrous THF (10 ml), was added a solution of lithium dicyclohexylamide in 10 ml anhydrous THF over 10 min at -78°C under argon. The resulting mixture was stirred for another 20 min at -78°C and then carefully quenched with 6 M HCl (aq). The reaction was allowed to warm up slowly and then the white precipitate was filtered off. The filtrate was extracted with Et_2O (5ml x 3) and organic layer was dried with MgSO_4 . The solvent was carefully removed *in vacuo* to avoid the loss of volatile product **28**.

The product was obtained as 0.75 g slightly yellow liquid (89% yield) and used for the next step without purification.



The starting diazocarbonyls **S4** and **S5** were obtained using the same method reported by our group.⁸⁶ To a stirred solution of the diazocarbonyl (3 mmol) in anhydrous DCM (10 ml) was added a solution Br₂ (1.2 equiv, 0.18 ml) in in anhydrous DCM (5 ml) dropwise at -78 °C. The resulting solution was allowed to warm up to room temperature in 1 hr and then the reaction was quenched by saturated NaHSO₃ (aq). The organic layer was separated and dried with MgSO₄. The solvent was carefully removed *in vacuo* to avoid the loss of volatile product **29/30**. The yield was quantitative and if necessary, the product could be purified by a short column with hexanes.



The synthesis was similar to the reference.¹²⁵ Generally, To a solution of 2,2-dimethoxyethanol **3-43** (5 mmol, 0.51 ml), DMAP (catalytic) and dry Et₃N (1.1 equiv, 0.71 ml) in anhydrous DCM, was added butyryl chloride **3-44** (1 equiv, 0.50 ml) dropwise at 0 °C under argon. The reaction was allowed to warm up to room temperature and stirred overnight. The resulting solution was washed with saturated

NaHCO₃ (aq) and brine, then dried with MgSO₄. The solvent was removed at reduced pressure and the product **3-45** was obtained as clear oil at quantitative yield without further purification.

A well-stirred solution of **3-45** (5 mmol) in DCM (25 ml) was treated with TFA (9.75 equiv, 3.8 ml) and water (10 equiv, 0.9 ml) at room temperature. After stirring for 5 hr, the solution was evaporated and the crude product was purified by flash silica chromatography (EtOAc: Hexanes = 1: 2, v/v). The product **3-29** was obtained as clear thick oil (560 mg, 86% yield).

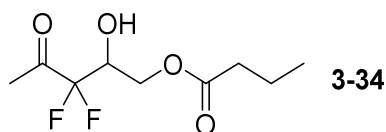
Synthesis of difluoro AI-2 analogs:

Refer to **Scheme 3-2**.

The synthesis was similar to the reference.¹²⁶ Generally, a solution of corresponding Grignard reagent (2M in Et₂O, 30 mmol) was slowly added a solution of chlorodifluoroacetic acid **3-26** (10 mmol, 0.84 ml) in anhydrous diethyl ether at -20 °C under argon. The resulting mixture was kept stirring for another 12 hr. Then the reaction mixture was hydrolyzed with 6M HCl (aq) below 0 °C and stirred for 1 hr at room temperature. The resulting mixture was extracted with diethyl ether (10 ml x 3) and the combined organic layer was washed with saturated NaHCO₃ (aq) and brine, then dried with MgSO₄ and finally concentrated in mild vacuum to avoid the loss of volatile product **3-27/3-28**. Products were obtained in high yield without further purification.

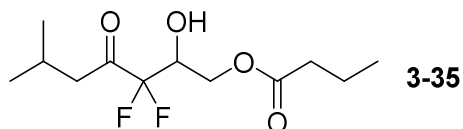
Acid-activated Zn powder (3 equiv, 149 mg) and CuI (0.1 equiv, 8 mg) were suspended

in anhydrous THF and stirred for 0.5 hr at room temperature under argon. To the resulting mixture was added a solution of corresponding chlorodifluoromethyl ketone **3-27/3-28** (100 mg, 0.76 mmol) and **3-29** in anhydrous THF. The mixture was refluxed for 4 hr and then cooled down to room temperature. The reaction mixture was then filtered with Celite and the filtrate was concentrated under vacuum. The products of difluoro AI-2 analogs **3-34/3-35** were purified by flash silica chromatography (EtOAc: Hexanes = 1: 6, v/v).



3,3-difluoro-2-hydroxy-4-oxopentyl butyrate (3-34):

3-34 was obtained as 60 mg clear oil (35 % yield). ^1H NMR (500 MHz, CDCl_3) δ ppm = 4.45-4.26 (3H, m), 3.00-2.92 (1H, m), 2.45-2.40 (3H, m), 2.37 (2H, t, $J = 7.4$ Hz), 1.74-1.65 (2H, m), 0.99 (3H, t, $J = 7.4$ Hz). ^{13}C NMR (125 MHz, CDCl_3) δ ppm = 198.8 (t, $J = 31.2$ Hz), 174.0, 114.4 (t, $J = 253.8$ Hz), 69.9 (m), 62.7, 35.8, 25.2, 18.2, 13.5. ^{19}F NMR (376 MHz, CDCl_3) δ ppm = -113.54 (1F, dd, $J = 279.2, 6.4$ Hz), -123.21 (1F, dd, $J = 280.7, 15.6$ Hz). HRMS (ESI $^+$) m/z calcd. for $\text{C}_9\text{H}_{15}\text{F}_2\text{O}_4$ $[\text{M}+\text{H}]^+$ 225.0938, found 225.0923.



3,3-difluoro-2-hydroxy-6-methyl-4-oxoheptyl butyrate (3-35):

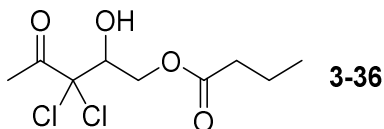
3-35 was obtained as 93 mg clear oil (67 % yield). ^1H NMR (400 MHz, CD_2Cl_2) δ ppm

= 4.41-4.26 (3H, m), 3.14-3.02 (1H, m), 2.64 (2H, d, $J = 6.7$ Hz), 2.36 (2H, t, $J = 7.4$ Hz), 2.27-2.16 (1H, m), 1.74-1.60 (2H, m), 1.02-0.90 (9H, m). ^{13}C NMR (125 MHz, CD_2Cl_2) δ ppm = 200.6 (t, $J = 27.5$ Hz), 173.8, 114.7 (t, $J = 255.0$ Hz), 69.8 (t, $J = 27.5$ Hz), 62.6, 46.2, 35.7, 23.4, 22.0, 18.2, 13.2. ^{19}F NMR (376 MHz, CD_2Cl_2) δ ppm = -114.30 (1F, dd, $J = 276.3, 6.3$ Hz), -124.34 (1F, dd, $J = 275.5, 17.7$ Hz). HRMS (ESI $^+$) m/z calcd. for $\text{C}_{12}\text{H}_{24}\text{F}_2\text{NO}_4$ $[\text{M}+\text{NH}_4]^+$ 284.1673, found 284.1690.

Synthesis of dichloro and dibromo AI-2 analogs:

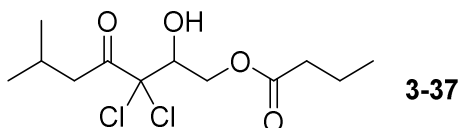
Refer to **Scheme 3-2**.

Generally, to a stirred suspension of *t*BuOK (0.1 equiv) in anhydrous THF was added a solution of corresponding dihalogen ketone (1 equiv) and **3-29** (1 equiv) in anhydrous THF at -78°C under argon. The reaction was allowed to warm up to room temperature gradually and stirred overnight. Then the reaction was quenched by saturated NH_4Cl (aq) carefully at 0°C . The organic layer was separated and the aqueous layer was extracted with EtOAc three times. The combined organic phase was dried over MgSO_4 . The product was purified by silica column chromatography (EtOAc: Hexanes = 1: 6, v/v)



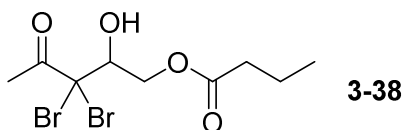
3,3-dichloro-2-hydroxy-4-oxopentyl butyrate (3-36):

3-36 was obtained as 51 mg clear oil (64% yield). ^1H NMR (400 MHz, CDCl_3) δ ppm = 4.63-4.52 (2H, m), 4.47-4.35 (1H, m), 3.23 (1H, s, br), 2.57 (3H, s), 2.37 (2H, t, J = 7.4 Hz), 1.74-1.65 (2H, m), 0.98 (3H, t, J = 7.4 Hz). ^{13}C NMR (100 MHz, CDCl_3) δ ppm = 196.7, 174.2, 87.4, 74.7, 64.7, 36.4, 24.2, 18.7, 14.0. HRMS (ESI^+) m/z calcd. for $\text{C}_9\text{H}_{15}\text{Cl}_2\text{O}_4$ $[\text{M}+\text{H}]^+$ 257.0347, found 257.0340.



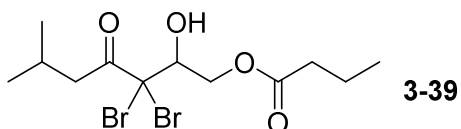
3,3-dichloro-2-hydroxy-6-methyl-4-oxoheptyl butyrate (3-37):

3-37 was obtained as 74 mg clear oil (61% yield). ^1H NMR (400 MHz, CDCl_3) δ ppm = 4.62-4.51 (2H, m), 4.44-4.34 (1H, m), 3.22 (1H, s, br), 2.87-2.73 (2H, m), 2.36 (2H, t, J = 7.4 Hz), 2.29-2.18 (1H, m), 1.75-1.61 (2H, m), 1.03-0.86 (9H, m). ^{13}C NMR (100 MHz, CDCl_3) δ ppm = 198.6, 174.2, 87.6, 74.7, 64.8, 45.0, 36.4, 25.0, 22.7, 22.5, 18.7, 14.0. HRMS (ESI^+) m/z calcd. for $\text{C}_{12}\text{H}_{21}\text{Cl}_2\text{O}_4$ $[\text{M}+\text{H}]^+$ 299.0817, found 299.0821.



3,3-dibromo-2-hydroxy-4-oxopentyl butyrate (3-38):

3-38 was obtained as 74 mg clear oil (61% yield). ^1H NMR (400 MHz, CDCl_3) δ ppm = 4.75-4.65 (1H, m), 4.48-4.36 (2H, m), 3.37 (1H, s, br), 2.72 (3H, s), 2.38 (2H, t, J = 7.4 Hz), 1.77-1.62 (2H, m), 0.98 (3H, t, J = 7.4 Hz). ^{13}C NMR (100 MHz, CDCl_3) δ ppm = 196.9, 174.2, 75.0, 69.4, 66.5, 36.4, 24.8, 18.8, 14.1. HRMS (ESI^+) m/z calcd. for $\text{C}_9\text{H}_{15}\text{Br}_2\text{O}_4$ $[\text{M}+\text{H}]^+$ 346.9317, found 346.9340.

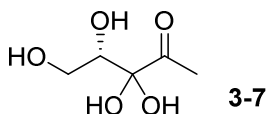


3,3-dibromo-2-hydroxy-6-methyl-4-oxoheptyl butyrate (3-39):

3-39 was obtained as 53 mg clear oil (40% yield). ^1H NMR (400 MHz, CDCl_3) δ ppm = 4.73-4.64 (1H, m), 4.50-4.34 (2H, m), 3.38 (1H, s, br), 3.05-2.92 (2H, m), 2.37 (2H, d, $J = 7.4$ Hz), 2.32-2.18 (1H, m), 1.76-1.62 (2H, m), 1.04-0.90 (9H, m). ^{13}C NMR (100 MHz, CDCl_3) δ ppm = 198.7, 174.2, 75.0, 70.1, 66.6, 45.5, 36.4, 25.4, 22.7, 22.5, 18.8, 14.1. HRMS (ESI $^+$) m/z calcd. for $\text{C}_{12}\text{H}_{21}\text{Br}_2\text{O}_4$ $[\text{M}+\text{H}]^+$ 388.9786, found 388.9804.

Gaussian calculation results

All the structures interested were optimized at B3LYP/6-31g(d) level using Gaussian 09.¹²¹ A polarizable continuum model (PCM) was used as the SCRF method when solvation effect (water) is considered.



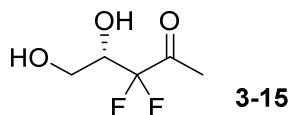
Total energy of the optimized structure: -572.6433216 a.u.

Number of imaginary frequencies: 0

Cartesian Coordinates:

Center Number	Atomic Number	Atomic Type	Coordinates (Angstroms)		
			X	Y	Z
1	6	0	-1.203529	1.564230	0.149776
2	6	0	-1.161643	0.160716	-0.438110
3	6	0	-0.005068	-0.722572	0.100486
4	6	0	1.400010	-0.177156	-0.262557

5	8	0	-0.096917	-0.865156	1.492751
6	8	0	-0.219802	-1.970875	-0.552828
7	6	0	2.294892	0.311235	0.848482
8	8	0	-0.041320	2.259358	-0.289077
9	8	0	-2.382792	-0.468146	-0.058650
10	8	0	1.740320	-0.195874	-1.431677
11	1	0	-2.123157	2.055491	-0.196962
12	1	0	-1.245344	1.495284	1.244615
13	1	0	-1.060350	0.218349	-1.529707
14	1	0	-1.045966	-1.005460	1.677626
15	1	0	0.303079	-2.638782	-0.077017
16	1	0	2.501349	-0.504452	1.550804
17	1	0	3.230649	0.681825	0.424713
18	1	0	1.796520	1.103835	1.413455
19	1	0	0.028204	3.076979	0.227259
20	1	0	-2.328862	-1.376244	-0.407391



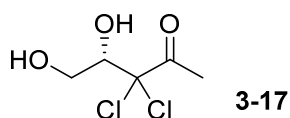
Total energy of the optimized structure: -620.6888831 a.u.

Number of imaginary frequencies: 0

Cartesian Coordinates:

Center Number	Atomic Number	Atomic Type	Coordinates (Angstroms)		
			X	Y	Z
1	6	0	-1.346482	1.469234	0.095975
2	6	0	-1.207153	0.049106	-0.441618
3	6	0	0.023638	-0.658602	0.150399
4	6	0	1.391942	-0.129531	-0.339161
5	9	0	-0.029149	-0.629865	1.522739
6	9	0	-0.037706	-1.989216	-0.213513
7	6	0	2.366908	0.362356	0.695577
8	8	0	-0.146697	2.167660	-0.211813
9	8	0	-2.386246	-0.644003	-0.087201
10	8	0	1.626179	-0.191043	-1.531376
11	1	0	-2.223879	1.935318	-0.374371
12	1	0	-1.524820	1.417874	1.178452
13	1	0	-1.056847	0.076518	-1.531676

14	1	0	1.914263	1.163519	1.286625
15	1	0	2.619911	-0.451594	1.386549
16	1	0	3.271817	0.721816	0.201636
17	1	0	-0.097665	2.971629	0.353566
18	1	0	-2.420082	-1.479647	-0.607731

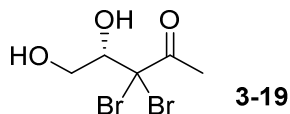


Total energy of the optimized structure: -1341.3842177 a.u.

Number of imaginary frequencies: 0

Cartesian Coordinates:

Center Number	Atomic Number	Atomic Type	Coordinates (Angstroms)		
			X	Y	Z
1	6	0	-1.509572	-1.629098	-0.132275
2	6	0	-0.118003	-1.222030	-0.619205
3	6	0	0.373100	0.105392	0.035867
4	6	0	-0.433153	1.338889	-0.497858
5	17	0	0.372099	-0.031032	1.838856
6	17	0	2.102776	0.386759	-0.498432
7	6	0	-1.008332	2.336402	0.469335
8	8	0	-2.378142	-0.509965	-0.252873
9	8	0	0.722786	-2.314220	-0.335751
10	8	0	-0.518052	1.447105	-1.703506
11	1	0	-1.846287	-2.472145	-0.749944
12	1	0	-1.430706	-1.975577	0.904948
13	1	0	-0.153612	-1.000555	-1.692768
14	1	0	-0.218851	2.767995	1.094143
15	1	0	-1.502809	3.125154	-0.100107
16	1	0	-1.725323	1.847404	1.133977
17	1	0	-3.166894	-0.681044	0.284235
18	1	0	1.534642	-2.219282	-0.859828

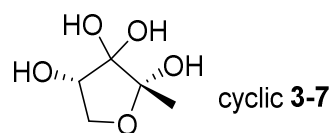


Total energy of the optimized structure: -5564.4100094 a.u.

Number of imaginary frequencies: 0

Cartesian Coordinates:

Center Number	Atomic Number	Atomic Type	Coordinates (Angstroms)		
			X	Y	Z
1	6	0	2.035562	0.054599	1.542411
2	6	0	0.517330	0.237038	1.489021
3	6	0	-0.032182	0.180165	0.036869
4	6	0	0.366362	1.432359	-0.801828
5	35	0	0.431872	-1.537737	-0.806352
6	35	0	-2.029613	0.251211	0.152736
7	6	0	0.966670	1.261472	-2.170320
8	8	0	2.631874	0.978000	0.641148
9	8	0	-0.017420	-0.768165	2.315697
10	8	0	0.134985	2.515756	-0.303900
11	1	0	2.357583	0.230312	2.577443
12	1	0	2.273233	-0.982722	1.279610
13	1	0	0.257100	1.242230	1.845845
14	1	0	0.278583	0.714053	-2.823663
15	1	0	1.168374	2.249333	-2.587656
16	1	0	1.890857	0.680882	-2.109611
17	1	0	3.550870	0.705224	0.496017
18	1	0	-0.973648	-0.609445	2.398097



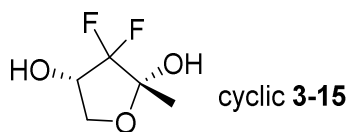
Total energy of the optimized structure: -572.6508389 a.u.

Number of imaginary frequencies: 0

Cartesian Coordinates:

Center Number	Atomic Number	Atomic Type	Coordinates (Angstroms)		
			X	Y	Z

1	6	0	-1.252736	0.371585	-0.564494
2	6	0	-0.714961	1.682871	-0.003230
3	8	0	0.705692	1.554326	-0.077756
4	6	0	1.117464	0.174041	0.050210
5	6	0	-0.226147	-0.638777	-0.017305
6	8	0	-2.560420	0.112147	-0.068078
7	8	0	1.785650	-0.036243	1.264458
8	6	0	2.101118	-0.113585	-1.072897
9	8	0	-0.203990	-1.773715	-0.844579
10	8	0	-0.577499	-0.975958	1.306682
11	1	0	-1.230942	0.366245	-1.659131
12	1	0	-1.010663	2.560262	-0.583638
13	1	0	-1.059673	1.810764	1.033441
14	1	0	-2.964132	-0.570731	-0.629002
15	1	0	1.088633	-0.182992	1.931715
16	1	0	1.633528	0.040827	-2.048096
17	1	0	2.951701	0.568445	-0.977535
18	1	0	2.467919	-1.141848	-1.014211
19	1	0	0.333833	-2.449665	-0.397246
20	1	0	-1.554114	-0.902570	1.344185



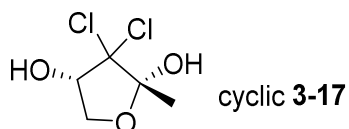
Total energy of the optimized structure: -620.6812635 a.u.

Number of imaginary frequencies: 0

Cartesian Coordinates:

Center Number	Atomic Number	Atomic Type	Coordinates (Angstroms)		
			X	Y	Z
1	6	0	-1.285222	0.335658	-0.523979
2	6	0	-0.782180	1.644092	0.083722
3	8	0	0.649086	1.559890	0.017300
4	6	0	1.105689	0.195288	0.022409
5	6	0	-0.216395	-0.626655	-0.000121
6	8	0	-2.597773	0.057114	-0.099300
7	8	0	1.870682	-0.079134	1.160378

8	6	0	1.996579	-0.033362	-1.188501
9	1	0	-1.201798	0.368128	-1.618249
10	1	0	-1.098773	2.529391	-0.471318
11	1	0	-1.132097	1.726127	1.121967
12	1	0	-2.940565	-0.678589	-0.631885
13	1	0	1.266996	-0.132304	1.921281
14	1	0	1.450810	0.159310	-2.115469
15	1	0	2.843559	0.656151	-1.131192
16	1	0	2.371617	-1.059597	-1.199857
17	9	0	-0.532877	-0.992168	1.290122
18	9	0	-0.116738	-1.781355	-0.719396



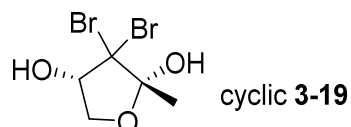
Total energy of the optimized structure: -1341.3884811 a.u.

Number of imaginary frequencies: 0

Cartesian Coordinates:

Center Number	Atomic Number	Atomic Type	Coordinates (Angstroms)		
			X	Y	Z
1	6	0	-0.876672	0.827794	-0.849972
2	6	0	-0.115227	2.048189	-0.315637
3	8	0	1.141722	1.570078	0.190377
4	6	0	1.274091	0.147442	0.055444
5	6	0	-0.233817	-0.308332	-0.021676
6	8	0	-2.256952	1.016500	-0.705973
7	8	0	1.977587	-0.350235	1.140766
8	6	0	2.091922	-0.199740	-1.186894
9	17	0	-0.479660	-1.932688	-0.758034
10	17	0	-0.945463	-0.325625	1.649712
11	1	0	-0.612550	0.638083	-1.897452
12	1	0	0.060976	2.793811	-1.096290
13	1	0	-0.684341	2.508196	0.499462
14	1	0	-2.717074	0.357745	-1.251672
15	1	0	1.516526	-0.067664	1.950986
16	1	0	1.594563	0.123510	-2.104211

17	1	0	3.045741	0.328031	-1.104158
18	1	0	2.282618	-1.273252	-1.244144



Total energy of the optimized structure: -5564.4136272 a.u.

Number of imaginary frequencies: 0

Cartesian Coordinates:

Center Number	Atomic Number	Atomic Type	Coordinates (Angstroms)		
			X	Y	Z

1	6	0	0.496505	0.159023	1.583279
2	6	0	1.903534	0.715166	1.330244
3	8	0	1.832091	1.475733	0.113114
4	6	0	0.534509	1.395912	-0.507270
5	6	0	-0.048209	0.092521	0.145407
6	8	0	0.567144	-1.046699	2.292806
7	8	0	0.683035	1.347516	-1.883845
8	6	0	-0.271944	2.658254	-0.205234
9	35	0	-1.998131	-0.066186	0.082109
10	35	0	0.724995	-1.495230	-0.761059
11	1	0	-0.116393	0.894783	2.119889
12	1	0	2.244833	1.358840	2.145731
13	1	0	2.607678	-0.114842	1.205327
14	1	0	-0.333929	-1.295045	2.559715
15	1	0	1.178054	0.535680	-2.102740
16	1	0	-0.435908	2.786110	0.867357
17	1	0	0.307893	3.509424	-0.572105
18	1	0	-1.236974	2.636935	-0.715091

Chapter 4. 3-Aminooxazolidinone head group-based AHL analogs that function as quorum sensing agonists in Gram-negative bacteria

4.1 Introduction

The old view that bacteria live in solitary mode has now been replaced with a community-based bacterial lifestyle, whereby most bacteria live on surfaces as part of polymicrobial biofilms¹²⁷ and communicate with neighbors using diffusible molecules. Bacteria also communicate via contact, using surface associated receptors^{113b} or connecting nanotubes.¹²⁸ Even in the planktonic state, bacteria can still communicate with self and non-self neighboring cells and respond to population density via response to small molecule autoinducers secreted by other bacteria.^{19a} The cell-to-cell communication between bacteria, called quorum sensing (QS), regulates diverse phenotypes, including biofilm formation, competence, bioluminescence, virulence factors production, antibiotic synthesis.¹²⁹ Additionally both plant and animal hosts respond to bacterial signaling molecules and some QS molecules have been shown promote apoptosis or programmed cell death in diverse eukaryotic cell types.¹³⁰

In the last decade many small molecules that modulate quorum sensing have been developed.^{9, 88, 131} These QS modulators have been either agonists or antagonists and have the potential to be used in diverse applications ranging from inhibition of bacterial toxin production and biofilm formation (QS antagonists)¹³² to manipulation of bacterial behavior and synthetic biology applications (both agonists and antagonists)¹³³ to the inhibition of cancer (by 3-oxo-C12 HSL **4-1** of *Pseudomonas*

aeruginosa).¹³⁴ Thus far acylhomoserine lactone (AHL)-based QS modulators have been the most rigorously pursued by many groups. The majority of these compounds have targeted LasR from *P. aeruginosa*.⁹⁻¹⁵

Most of the AHL analogs developed to date have kept the acylhomoserine lactone headgroup and modified the acyl chain. A few lactone head group modifications have also been reported but often, modification of the head group usually lead to dramatic reduction of activity.^{90b} Unfortunately γ -lactones are not chemically stable and can hydrolyze in mild acidic or basic environments.¹³⁵ Additionally bacterial, plant or animal lactonases¹³⁶ and acylases¹³⁷ have been shown to readily inactivate AHLs so there is clearly a need for an AHL head group that is resistant to hydrolysis and at the same time maintains the high QS modulatory activity seen with homoserine lactones.

We docked several lactone mimics into the active site of *P. aeruginosa* LasR and found that oxazolidinone-based AHL analogs had similar conformation in the binding site of LasR as the native 3-oxo-C12-HSL **4-1**. The docking results were surprising to us because many reports have documented the importance of the chirality at the C3 position for AHL autoinducers in activating QS-mediated processes.^{92b, 131b, 138} In this report we show that these 3-aminooxazolidinone analogs that lack C3 chirality still bind to LuxR-type receptors and are potent in binding to LasR as the native 3-oxo-C12 HSL **4-1**. As an added advantage, the 3-aminooxazolidinone head group is more resistant to hydrolysis than AHLs and are therefore good replacements for the lactone head group in AHL-based QS modulators. These analogs (**Figure 4-1**)

can be made from inexpensive materials in a few steps and are drug-like (examples of oxazolidinone drugs are linezolid¹³⁹ and rivaroxaban¹⁴⁰).

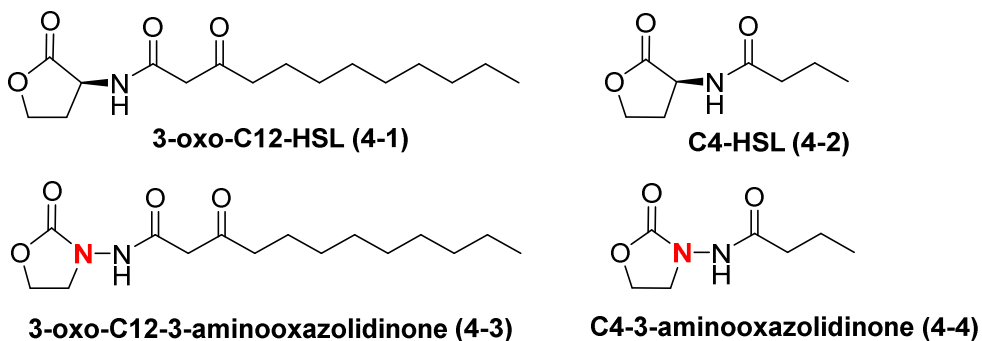
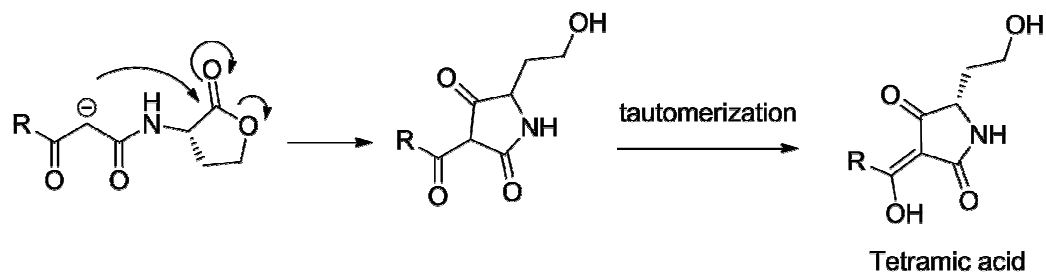


Figure 4-1. Structures of oxazolidin AHL analogs compared with natural AI-1.

4.2 Results and Discussion

3-oxo-HSLs are known to degrade under weakly basic conditions and tautomerize to a tetramic acid derivative via a mechanism shown in **Scheme 4-1**.¹³⁵ To demonstrate that our 3-aminooxazolidinone-based analogs are superior to natural AHLs in terms of chemical stability, we monitored the degradation 3-oxo-C12-HSL **4-1** and 3-oxo-C12-3-aminooxazolidinone **4-3**, at pH = 8.0 by monitoring UV absorption at 278 nm, which is an absorption maxima for tetramic acid, as a function of time (**Figure 4-2**). Whereas the UV absorption for the 3-oxo-C12-HSL **4-1** incubation increased over time, that of the analog **4-3** remained stable over 3 h. TLC analysis also revealed that analog **4-3** remained intact after 3 h after incubation in Tris buffer (pH = 8.0), see **Figure 4-3**. We therefore concluded that 3-aminooxazolidinone analog **4-3** is more stable than 3-oxo-C12-HSL **4-1** towards basic hydrolysis.



Scheme 4-1. Degradation of AHL under basic condition.

Recently Raines revealed that the conformation of free AHLs is different from when complexed to LasR. In the free state, the lone pairs of the amide carbonyl forms a favorable interaction with the π^* of the lactone carbonyl.¹⁴¹ This n to π^* interaction (worth about 0.64 kcal/mol), is disrupted upon binding to LasR. Interestingly the substitution of the C3 in 3-oxo-C12-HSL **4-1** with N3 (aminooxazolidinone-based analogs) did not abrogate the n to π^* interaction in the free state (see **Figure 4-4**). Also the C3 to N3 substitution did not drastically change the surface charge potentials of the head group moieties (see compare compounds C2-HSL **4-5** and C2-3-aminooxazolidinone **4-6** in **Figure 4-4**), implying that our analogs would be able to partake in charge-charge interactions in the 3-oxo-C12-HSL **4-1** binding site.

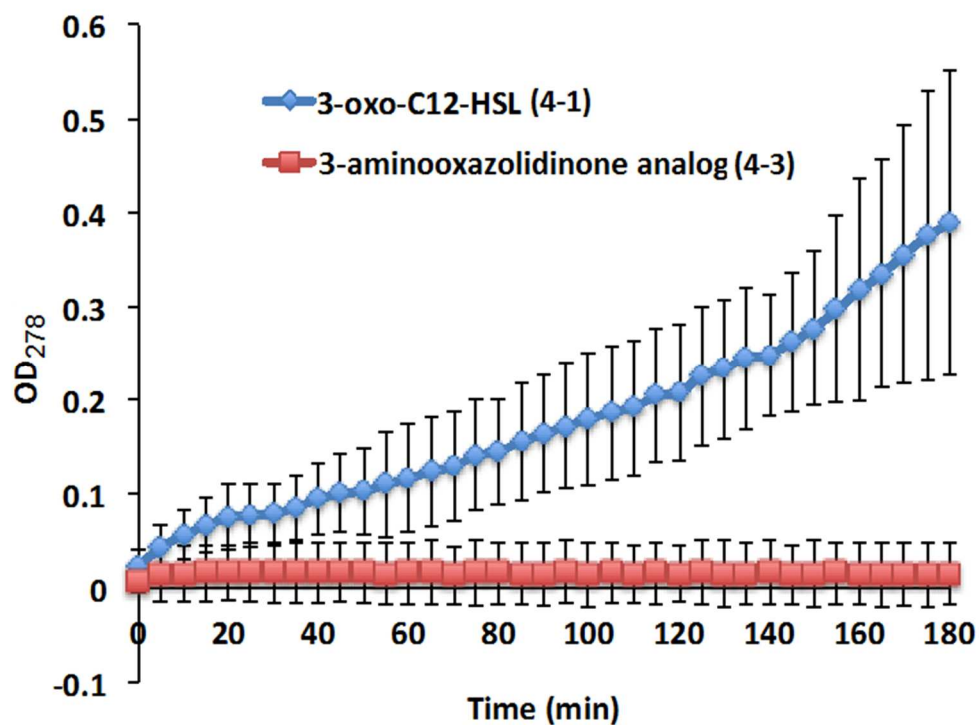


Figure 4-2. Stability studies of 3-oxo-C12-HSL **4-1** and 3-oxo-C12-3-aminooxazolidinone **4-3**. (Done by Yue Zheng, a graduate student in the Sintim group).

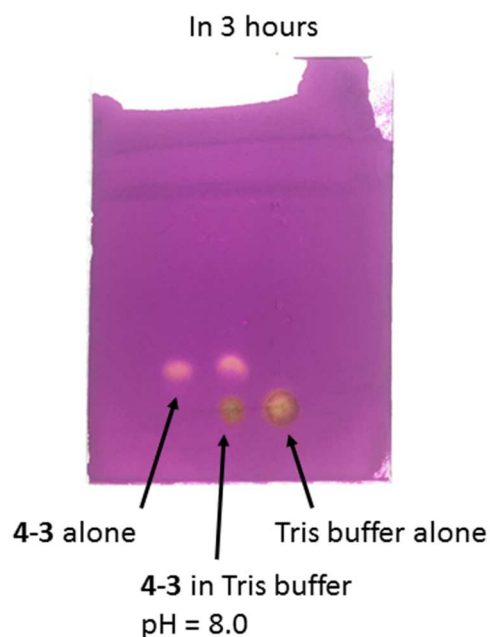


Figure 4-3. Stability studies of 3-oxo-C12-3-aminooxazolidinone **4-3** monitored by TLC (stained with KMnO_4 solution).

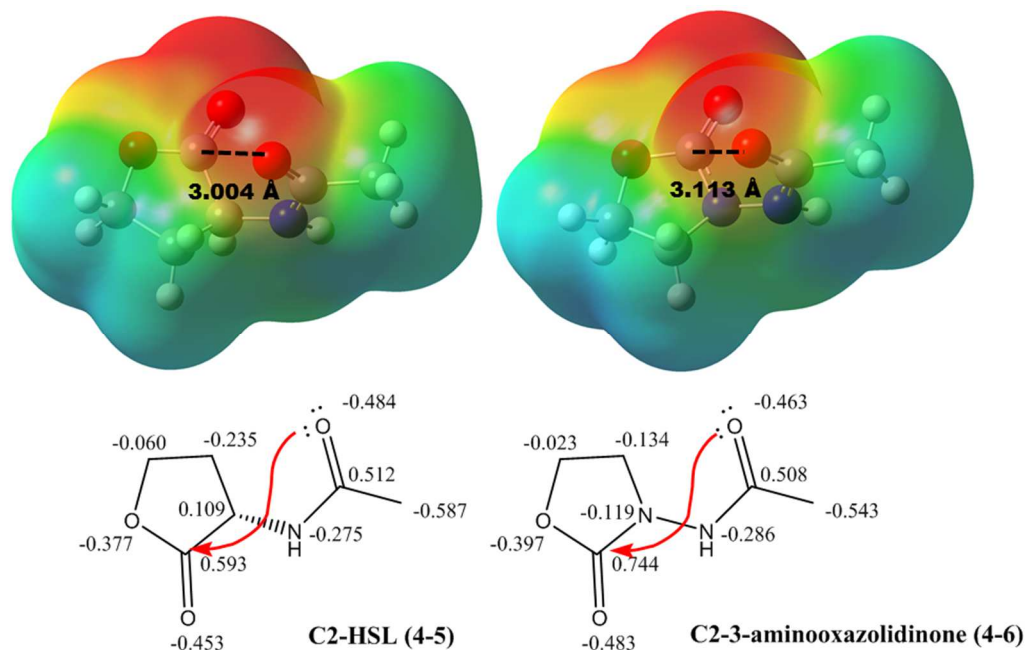


Figure 4-4. Surface charge potential on simplified models of AHL and oxazolidinone based mimic. $n \rightarrow \pi^*$ interactions from one lone pair (n) of the acyl carbonyl group oxygen to the empty π^* on the carbon of carbonyl group in the lactone ring and the distances are highlighted. Computational level: B3LYP/6-311+G(d,2p).¹²¹

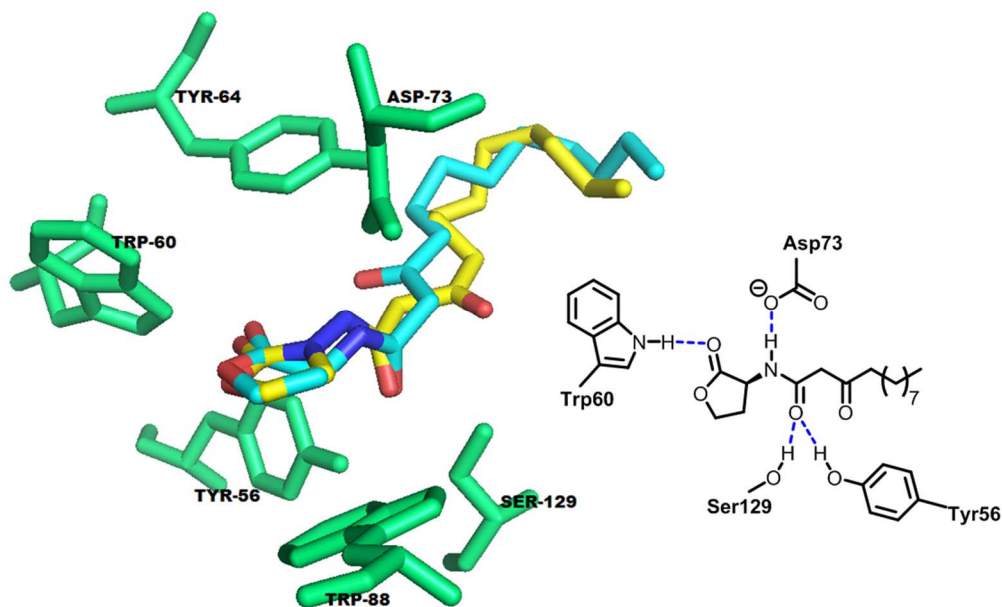


Figure 4-5. The binding domain (green) in crystal structure of LasR (PDB code: 2UV0) with native 3-oxo-C12-HSL 4-1 (cyan) and re-docked analog 4-3 (yellow).

In most LuxR-type proteins reported to date, Trp60 is highly conserved.¹⁴² Both

Suga and Blackwell have shown that this residue determines whether a ligand acts as an agonist or antagonist.¹⁴³ Ligands that exhibit unfavorable interactions with Trp60 have antagonistic profiles. Recently Blackwell also revealed that the interactions between a ligand and Tyr56 and Ser129 in LasR are also important in determining whether a ligand acts as an antagonist or agonist since these residues bond to the carbonyl of the 3-oxo-C12-HSL **4-1** ligand to position the lactone head group towards Tyr 60, which is a key residue.^{143a, 144} Docking experiments¹⁴⁵ revealed that the docked pose of 3-oxo-C12-HSL **4-1** and 3-aminooxazolidinone analog **4-3** are similar, with the exception of the orientation of the 3-oxo group, see **Figure 4-5**. Importantly, the carbonyl head group of both the native ligand and the 3-aminooxazolidinone analog **4-3** are similarly oriented towards the key Trp60 residue, hinting that 3-aminooxazolidinone analog **4-3** would also act as an agonist.

To test whether 3-aminooxazolidinone analog **4-3** would function similarly as native 3-oxo-C12-HSL **4-1**, as predicted by the docking experiment (see **Figure 4-5**), we used bacterial reporter strain *E. coli* pSB1075 (*lasRI*::*luxCDABE*) to test for agonsim. In the presence of native 3-oxo-C12-HSL **4-1** (10 nM), this bacterial strain produced bioluminescence as expected, see **Figure 4-6**. Similarly, 3-aminooxazolidinone analog **4-3** (10 nM), could also induce bioluminescence in *E. coli* pSB1075 and the bioluminescence intensities induced by both the native 3-oxo-C12-HSL **4-1** and 3-oxo-C12-3-aminooxazolidinone **4-3** were remarkably similar (**Figure 4-6**).

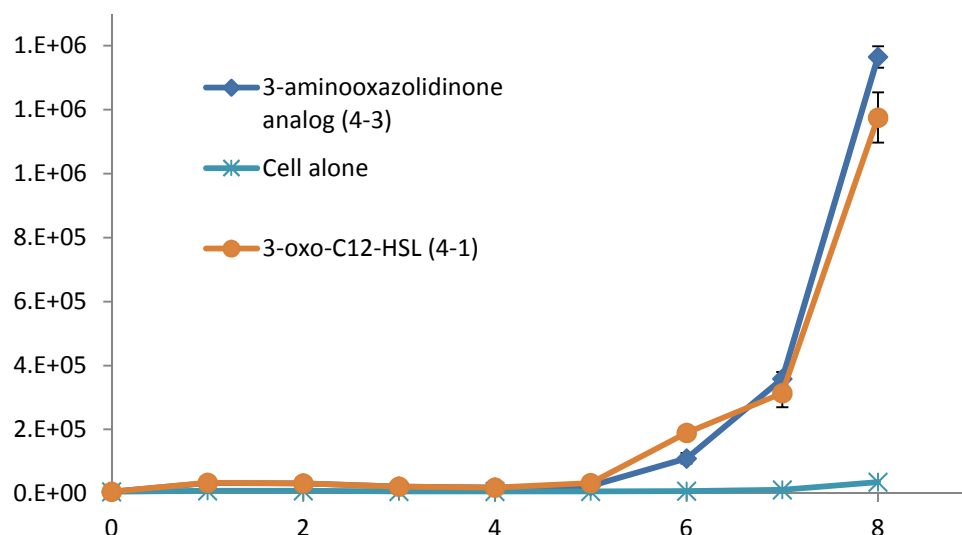


Figure 4-6. Bioluminescence production induced by native 3-oxo-C12-HSL **4-1** (10 nM orange) and 3-oxo-C12-3-aminooxazolidinone **4-3** (10 nM, blue) in *E. coli* pSB1075. (With the help of Yue Zheng, a graduate student in the Sintim group).

Next, we investigated if other LuxR-type proteins would also respond to oxazolidinone analogs. *Chromobacterium violaceum* CV026 is a biosensor strain that does not produce its own AI-1 but can respond to C4 to C8 AHL molecules, via binding to its LuxR type QS system CviR, to produce violacein.¹⁴⁶ However, long chain AHLs such as 3-oxo-C12-HSL can inhibit the C4-C8 AHL-induced production of violacein.¹⁴⁶ Addition of 20 μ M of C4-HSL **4-2** to agar or liquid culture incubated with CV026 led to the production of a violet pigment (**Figure 4-7a** and **4-8**). C4-3-aminooxazolidinone **4-4** was also able to induce the purple colonies, but unlike LasR, CviR preferred the native C4 HSL **4-2** to C4-3-aminooxazolidinone **4-4** as a higher concentration of analog **4-4** (200 μ M, compare **Figure 4-7b** with **Figure 4-7a** that used 20 μ M of C4-HSL **4-2**) was needed to give the same degree of pigmentation.

3-oxo-C12-HSL **4-1** can inhibit the C4-HSL **4-2** induced violacein production

in CV026 in both agar and liquid cultures, see **Figures 4-7c** and **4-8**. The 3-oxo-C12-3-aminooxazolidinone **4-3**, could also inhibit C4-HSL **4-2** induced violacein production in CV026, but here too the concentration of 3-aminooxazolidinone analog **4-3** needed to inhibit the activity of 20 mM C4-HSL **4-2** was higher than the natural 3-oxo-C12-HSL **4-1** ligand (see **Figures 4-7d** and **Figure 4-8**).

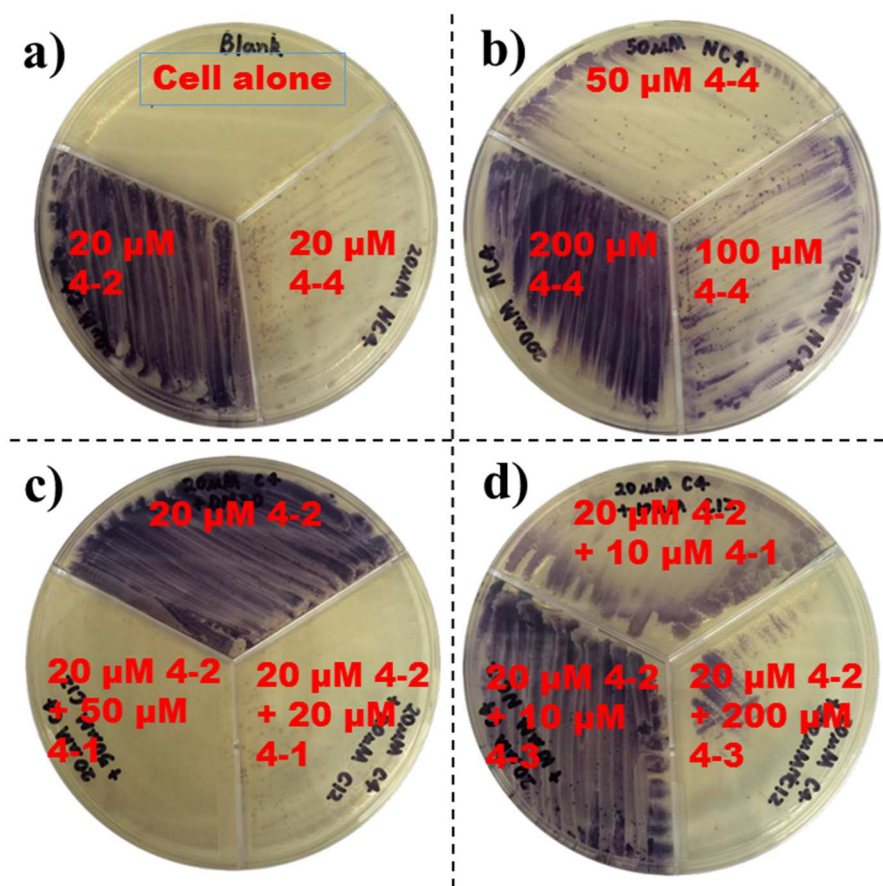


Figure 4-7. *Chromobacterium violaceum* CV026 agar assay. **a)** and **b)**: cultured with different concentrations of C4-HSL **4-2** and analog **4-4**. **c)** and **d)**: cultured with different concentrations of 3-oxo-C12-HSL **4-1** and analog **4-3** in presence of C4-HSL **4-2**. (Done by Yue Zheng, a graduate student of the Sintim group).

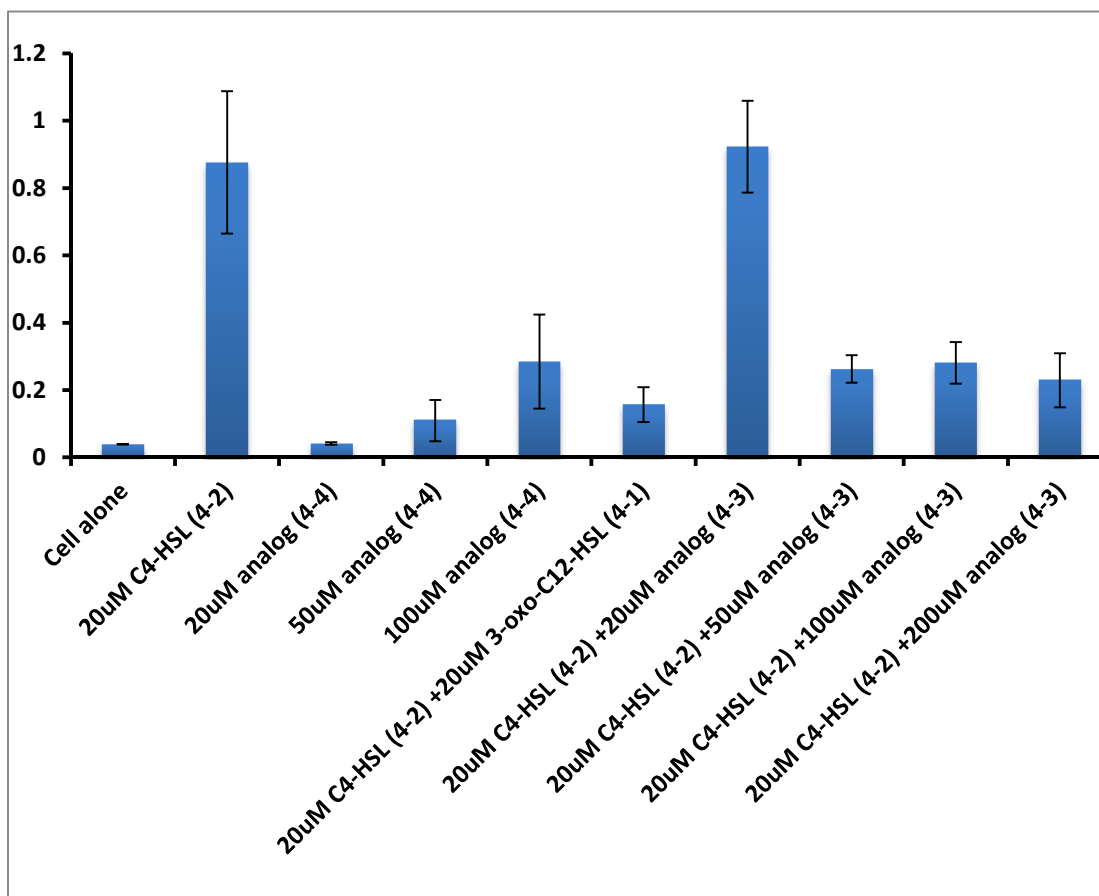


Figure 4-8. *Chromobacterium violaceum* CV026 liquid broth assay with various additives. (Done by Yue Zheng, a graduate student in the Sintim group)

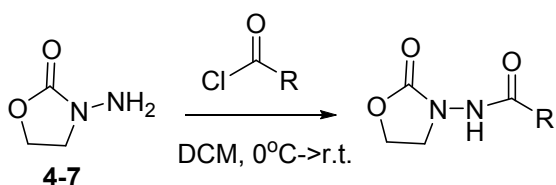
4.3 Conclusion.

In the past decade intensive efforts have been dedicated to the discovery of QS agonists and inhibitors. QS autoinducers have been shown to activate the immune system and hence these molecules and more stable analogs thereof have the potential to be used in cancer immunotherapy.¹³⁴ Hence hydrolytically stable 3-oxo-C12-HSL analog **4-3** described in this manuscript could have anticancer properties and future works along this line are planned. AI-1-based agonists also have the potential to be used in synthetic biology applications whereby genetic circuits that are regulated by engineered LuxR-type proteins could be regulated by these molecules.¹⁴⁷ In this regard,

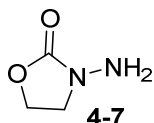
agonists described in this paper, which are more stable towards chemical degradation than the natural autoinducer, could become useful in these applications. LasR receptors could accommodate the C3 to N3 substitution better than CviR protein. LasR is key to the production of various virulence factors during *P. aeruginosa* infection and future work will focus on making side chain variants of the oxazolidinone analogs and test for activity against *P. aeruginosa*.

4.4 Detailed experimental procedures and characterizations

General procedures for preparation of oxazolidin analogs:

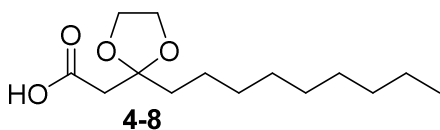


Scheme 4-2. Synthesis of oxazolidin analogs.

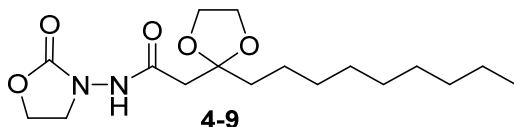


The starting material **4-7** is commercially available. It is however expensive but can be prepared on gram scale as follows: To a mixture of 2-hydroxyethylhydrazine (2.3g, 30 mmol) and dimethyl carbonate (4.0 mL, 48 mmol) was added a solution of NaOH (0.1g, 2.5 mmol) in 0.5 mL methanol. The resulting mixture was heated and stirred at 70 °C for 3 h. Then the reaction was cooled down to room temperature and the unreacted dimethyl carbonate was removed *in vacuo*. The residue was purified by silica column chromatography (methanol: dichloromethane = 1: 30, v/v) to afford **4-7** as a white solid

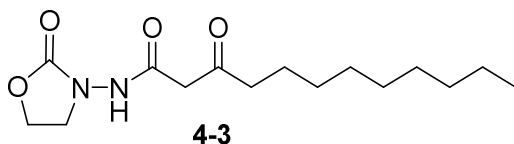
(2.01 g, 65%).



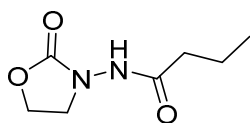
Compound **4-2** was synthesized according to literature procedure.¹⁴⁸



To a solution of **4-8** (50 mg, 0.19 mmol) in anhydrous dichloromethane was added oxalyl chloride (40 μ L, 2.3 equiv) at room temperature. The mixture was allowed to stir for 5 h. Then the reaction was concentrated to remove solvent and excess oxalyl chloride. The residue was re-subjected to dry dichloromethane and the resulting solution was added slowly to a solution of **4-7** (39 mg, 2 equiv) in dry dichloromethane at 0 °C. The mixture was allowed to slowly warm up to room temperature and stirred overnight. Then the reaction was concentrated under vacuum, and the residue was purified by silica column chromatography (methanol: dichloromethane = 1: 40, *v/v*) to afford **4-9** as a white solid (59 mg, 90% yield). ¹H NMR (CDCl₃, 400 MHz) δ 8.39 (s, 1H), 4.41 (t, *J* = 7.8 Hz, 2H), 4.11-4.02 (m, 2H), 4.02-3.93 (m, 2H), 3.81 (t, *J* = 7.8 Hz, 2H), 2.65 (s, 2H), 1.78-1.67 (m, 2H), 1.44-1.32 (m, 2H), 1.32-1.18 (m, 12H), 0.87 (t, *J* = 6.8 Hz, 3H); ¹³C NMR (CDCl₃, 100 MHz) δ 168.8, 157.8, 109.8, 65.6, 62.3, 46.3, 43.5, 38.0, 32.3, 30.1, 29.9, 29.7, 24.0, 23.1, 14.5; HRMS (ESI-TOF) *m/z* calcd. for C₁₇H₃₁N₂O₅ [M+1]⁺ 343.2233, found 343.2199.



Compound **4-9** (55 mg, 0.16 mmol) was dissolved in trifluoroacetic acid (0.64 ml) and water (0.16 ml). The mixture was stirred at room temperature overnight. Then the reaction was quenched by saturated NaHCO_3 (aq) until the solution turned neutral. Dichloromethane was used to extract the product three times and the organic phase was dried with anhydrous MgSO_4 . The product was purified by silica column chromatography (methanol: dichloromethane = 1: 40, v/v) and afforded **4-3** as a white solid (34 mg, 71% yield). ^1H NMR (CDCl_3 , 400 MHz) δ 9.08 (s, 1H), 4.44 (t, J = 7.8 Hz, 2H), 3.84 (t, J = 7.8 Hz, 2H), 3.52 (s, 2H), 2.56 (t, J = 7.4 Hz, 2H), 1.64-1.52 (m, 2H), 1.35-1.18 (m, 12H), 0.88 (t, J = 6.8 Hz, 3H); ^{13}C NMR (CDCl_3 , 100 MHz) δ 205.8, 165.9, 158.0, 62.5, 48.0, 46.4, 44.1, 32.2, 29.8, 29.6, 29.4, 23.1, 14.5; HRMS (ESI-TOF) m/z calcd. for $\text{C}_{15}\text{H}_{27}\text{N}_2\text{O}_4$ $[\text{M}+1]^+$ 299.1971, found 299.1967.



C4-3-aminooxazolidinone (4-4)

To a solution of **4-7** (102 mg, 1 mmol, 2 equiv) in anhydrous dichloromethane was added butyryl chloride (50 μL , 0.5 mmol, 1 equiv) at 0°C . The mixture was allowed to warm up to room temperature slowly and stir for 3 h. Then the reaction was concentrated under vacuum, and the residue was purified by silica column chromatography (methanol: dichloromethane = 1: 30, v/v) and afforded **4-4** as 34 mg

pale yellow oil (40% yield). ^1H NMR (CDCl_3 , 400 MHz) δ 8.49 (brs, 1H), 4.45 (t, J = 8.1 Hz, 2H), 3.84 (t, J = 8.1 Hz, 2H), 2.23 (t, J = 7.4 Hz, 2H), 1.78-1.61 (m, 2H), 0.98 (t, J = 7.4 Hz, 3H); ^{13}C NMR (CDCl_3 , 100 MHz) δ 172.9, 158.5, 62.5, 46.4, 36.0, 19.0, 14.0; HRMS (ESI-TOF) m/z calcd. for $\text{C}_7\text{H}_{13}\text{N}_2\text{O}_3$ $[\text{M}+1]^+$ 173.0926, found 173.0903.

Docking calculations:

Docking calculations were performed using Autodock Vina 1.1.1.^{145a} A large grid box, which is enough to encompass the ligand in the binding pocket was chosen. The exhaustiveness value was set as 32 in the Autodock calculations and the rest of the parameters were used as default. The ligand PDB files were prepared with ChemDraw. Autodock Tools 1.5.4 was used to convert the PDB files into PDBPT files for the Autodock vina calculations. The top-ranked conformation poses were selected for analysis. Results were visualized using PyMOL viewer version 1.3.^{145b}

Stability studies:

Stability of 3-oxo-C12-HSL **4-1** and 3-oxo-C12-3-aminooxazolidinone **4-3** towards basic pH was determined via UV monitoring.^{109, 135} Briefly, the decomposition of AI-1 or analog (1 mM) in 180 mM Tris-HCl, pH 8.0 at 25 °C was monitored by following absorbance changes at 278 nm, using Jasco V-630 Spectrophotometer for 3 hours. (Done by Yue Zheng, a graduate student in the Sintim group).

Stability of 3-oxo-C12-3-aminooxazolidinone **4-3** towards basic pH was determined

via TLC, as well (Figure S1). 10 mM of analog **4-3** in methanol was mixed with equivolume of 250 mM Tris-HCl buffer (pH = 8.0) and left at 25 °C for 3 hours. The mixture along with analog **4-3** stock solution and Tris-HCl buffer were spotted on TLC plate and developed using eluent (methanol: dichloromethane = 1: 40, v/v). After developing, the TLC plate was air dried and stained by KMnO₄ solution.

Bioluminescence assay:

E. coli JM109 (pSB1075) (containing luxRI::luxCDABE, bioluminescent reporter,) was cultured at 37 °C overnight and diluted 10 times with fresh medium. After culture at 37 °C for 7 hours, OD₆₀₀ was measured and diluted to OD₆₀₀=0.01. Cell culture was grown in 37 °C for another hour and diluted to OD₆₀₀=0.005. Different concentrations of AI-1 and analogs were added to cells and incubated at 37 °C with shaking for 8 hours. Bioluminescence was measured with a Nichols Institute Diagnostics luminometer.

***C. violaceum* CV026 AHL reporter assay:**

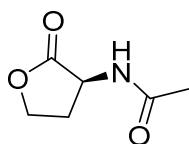
Agar plate assay:¹⁴⁹ Different concentration of AI-1 and analogs were added into LB agar. *C. violaceum* CV026 was stretched onto the agar plates. Plates were incubated at 37 °C for one day and 25 °C for another 2 days.

Extraction and quantification of violacein:¹⁵⁰ *C. violaceum* CV026 overnight culture was diluted to OD₆₀₀=0.1 and mixed with AI-1 or analog. After incubation at 27 °C for 60 hours, 1 ml of bacteria culture was centrifuged at 14000 rpm for 5 min. Supernatant was removed and pellet was resuspended in 1 ml DMSO. Cells were removed by centrifugation and OD₅₈₅ was measured by Molecular devices SpectraMax M5^e

microplate reader. (Done by Yue Zheng, a graduate student in the Sintim group).

Gaussian calculations:

All the structures interested were optimized at B3LYP/6-311+G(d,2p) level using Gaussian 09.¹²¹



C2-HSL (4-5)

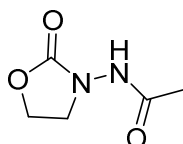
Total energy of the optimized structure: -530.6919083 a.u.

Number of imaginary frequencies: 0

Cartesian Coordinates:

Center Number	Atomic Number	Atomic Type	Coordinates (Angstroms)		
			X	Y	Z
1	8	0	-2.207400	0.597804	0.417294
2	6	0	-2.488988	-0.789922	0.126249
3	6	0	-1.135221	-1.405660	-0.243829
4	7	0	-0.426173	-0.199802	-0.663400
5	6	0	-0.986195	0.933748	-0.067118
6	8	0	-0.509517	2.030586	-0.019531
7	7	0	0.938859	-0.227980	-0.868638
8	6	0	1.806973	-0.233053	0.212484
9	6	0	3.253739	0.026629	-0.139456
10	8	0	1.418354	-0.456282	1.338508
11	1	0	-2.938874	-1.233962	1.011189
12	1	0	-3.197045	-0.822955	-0.703787
13	1	0	-1.215010	-2.123624	-1.060265
14	1	0	-0.641145	-1.869584	0.612245
15	1	0	1.241964	0.170495	-1.744742
16	1	0	3.463705	-0.079523	-1.204685

17	1	0	3.501542	1.045191	0.167576
18	1	0	3.882720	-0.658875	0.426597



C2-3-aminooxazolidinone (4-6)

Total energy of the optimized structure: -514.6702856 a.u.

Number of imaginary frequencies: 0

Cartesian Coordinates:

Center Number	Atomic Number	Atomic Type	Coordinates (Angstroms)		
			X	Y	Z
1	8	0	2.134690	0.578829	-0.515899
2	6	0	2.415670	-0.823569	-0.282464
3	6	0	1.119685	-1.442440	0.254461
4	6	0	0.421095	-0.234184	0.887613
5	6	0	1.001203	0.962826	0.109672
6	8	0	0.575851	2.079839	0.082757
7	7	0	-1.024813	-0.253123	0.923912
8	6	0	-1.777717	-0.220358	-0.223210
9	6	0	-3.262048	0.005887	-0.029387
10	8	0	-1.277448	-0.368928	-1.324122
11	1	0	2.740697	-1.248342	-1.229975
12	1	0	3.237967	-0.880390	0.434742
13	1	0	1.312689	-2.244081	0.967066
14	1	0	0.511857	-1.825909	-0.561280
15	1	0	0.760761	-0.105998	1.919653
16	1	0	-1.465837	0.048584	1.777201

17	1	0	-3.594605	-0.155548	0.997147
18	1	0	-3.492810	1.034358	-0.316175
19	1	0	-3.809104	-0.657712	-0.697768

Chapter 5. Conclusions.

5.1 AI-2 mediated quorum sensing inhibitors.

In this dissertation, we have shown that small molecules that are based on natural QS autoinducers can be used to modulate quorum sensing. Others^{83b, 84a, 87, 107a, 108, 117} and us^{83a, 84c, d} have proven that minor chemical changes (**Figure 6-1**) on the ubiquitous universal bacterial signaling molecule AI-2 can impact the agonist or antagonistic profile of the analog.

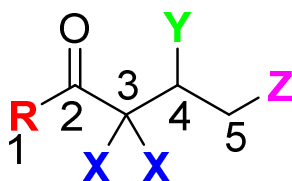


Figure 5-1. Chemical modification sites on AI-2.

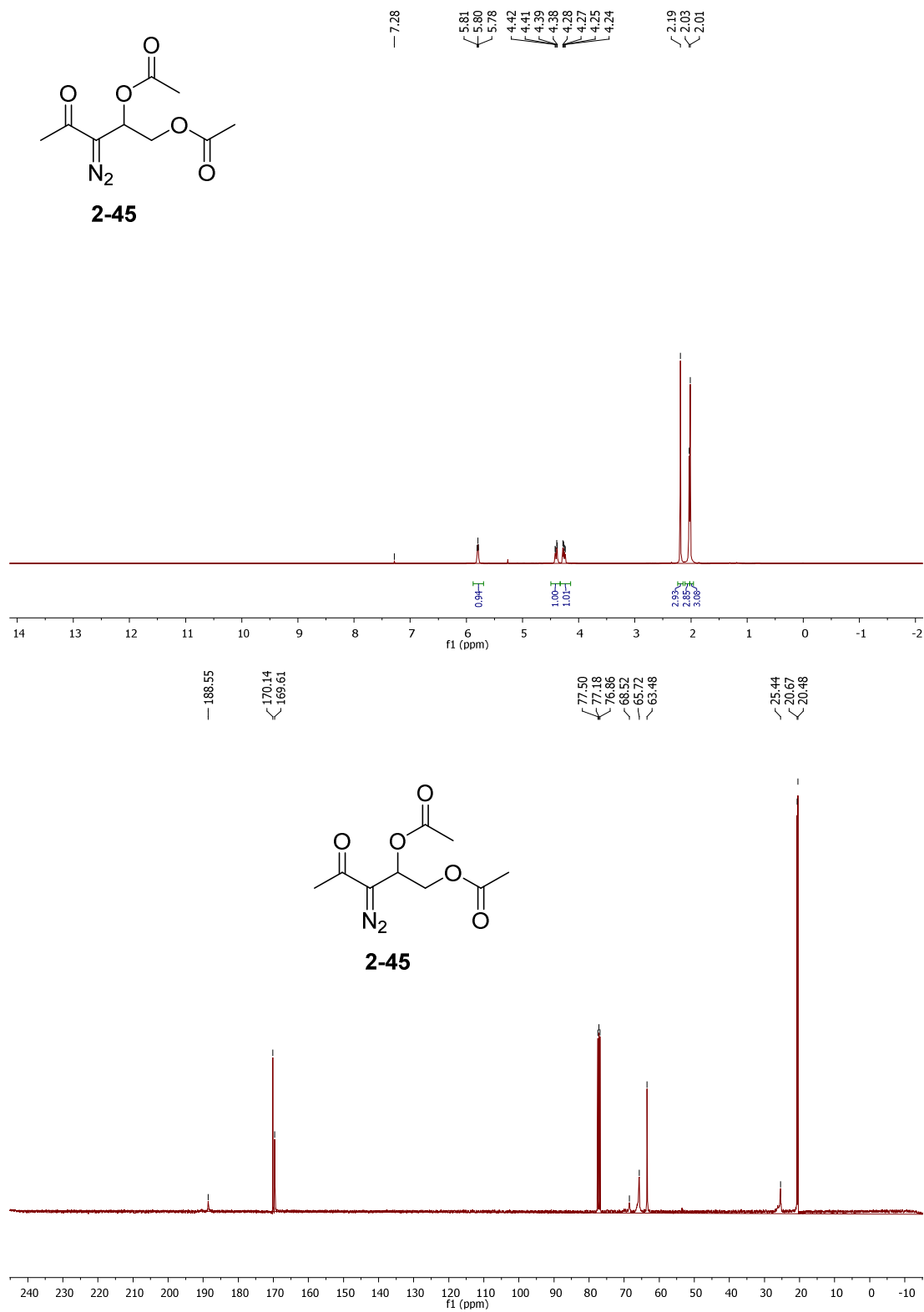
Thus far, AI-2 analogs with different alkyl groups on C1 position, including linear, branched and cyclic alkyl chains as well as aromatic rings have been made and tested for QS activity. In the majority of cases, C1 alkyl analogs of AI-2 were antagonists.^{83, 84c, d} We have replaced the 3,3'-hydroxyl groups with germinal halogens at C3 position and shown that these are active QS modulators (agonists or antagonists, depending on the nature of C1 substituent). C5 alkyl analogs of AI-2 have also been reported and these compounds exhibit agonistic behavior to some extent depending on the nature of the substituent.⁸⁷ The group of Gardiner, et al. replaced the C4 hydroxyl group of AI-2 and the C4-fluoro analog exhibited antagonist activity.¹¹⁷ Stable analogs of AI-2, which can be readily purified on column chromatography, have also been

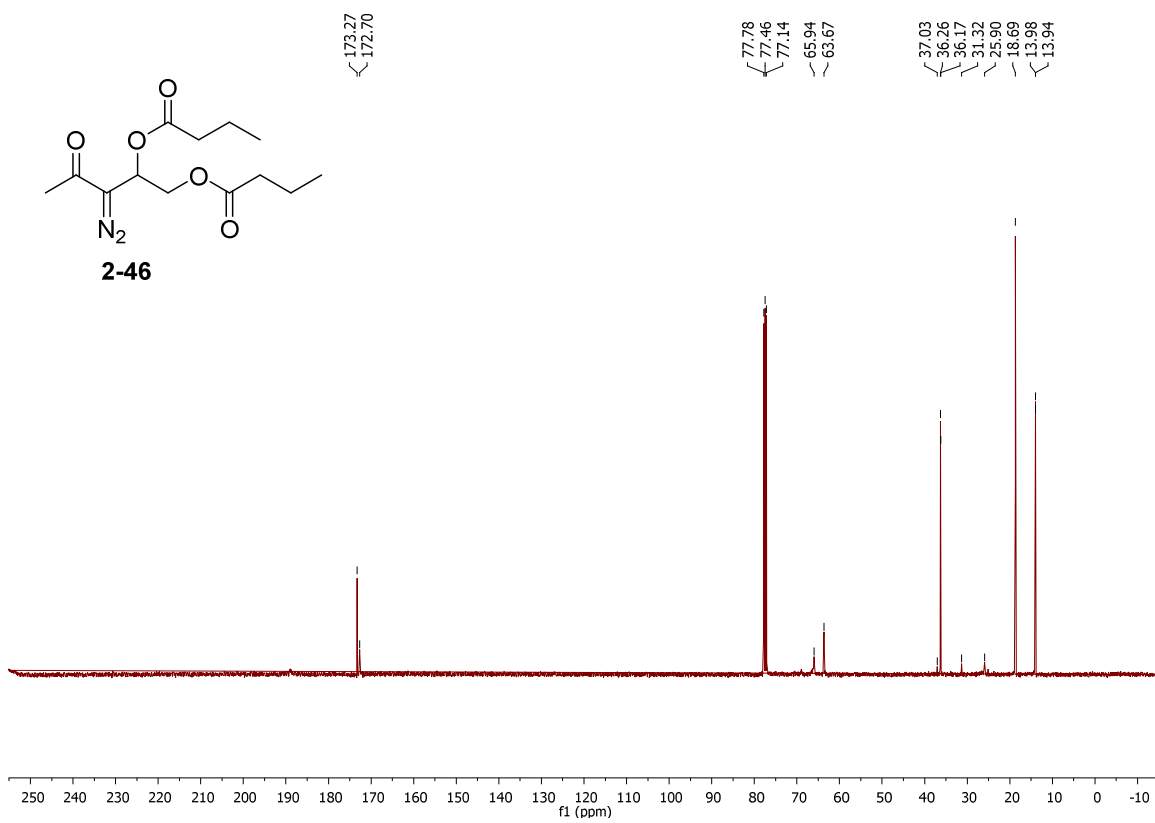
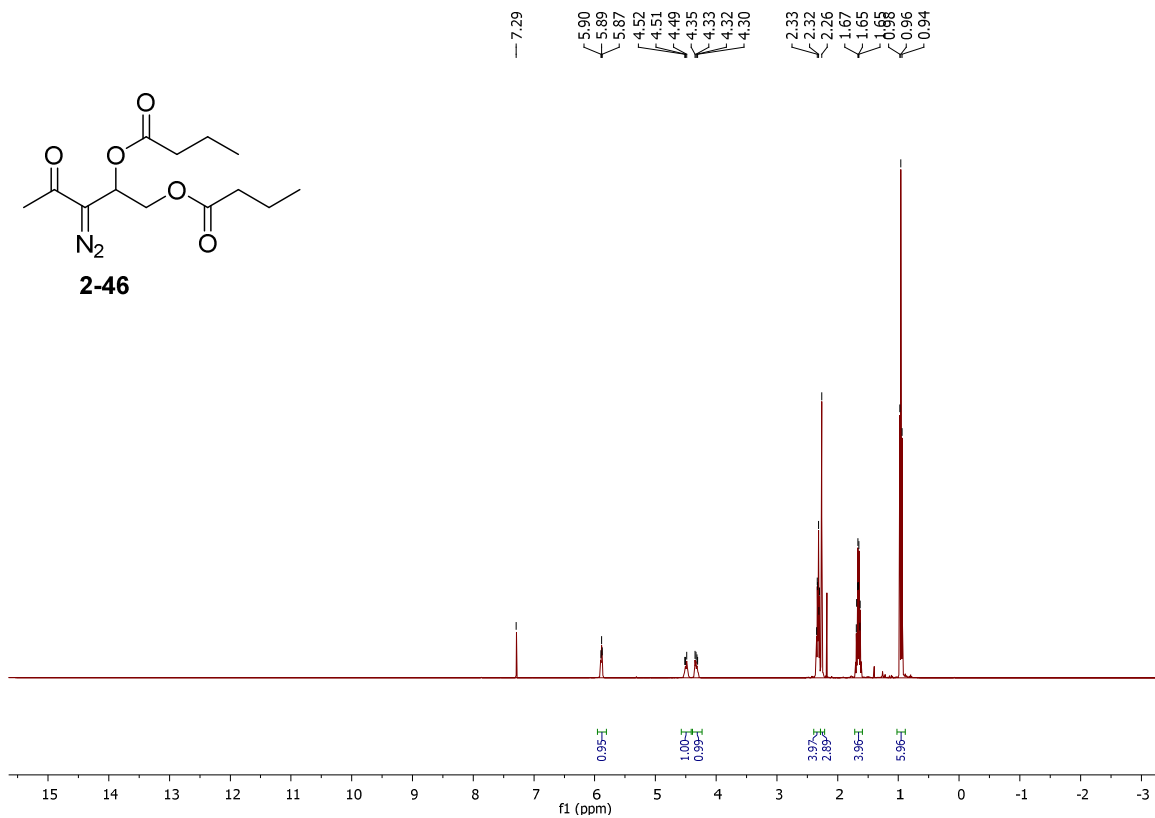
reported by others and us. These stable analogs are ester protected compounds (hydroxyl groups at C4 and C5 were protected) can be deprotected in vivo by cellular esterases to yield the active compounds.^{85-86, 107a} Janda has also reported carbocyclic analogs of AI-2 but these analogs were not potent QS modulators.¹¹⁰ The majority of AI-2 analogs reported to date have been tested on only *V. harveyi* or *E. coli/Salmonella*. However AI-2 signaling has been observed in many bacteria (see Table X). In future these compounds could be investigated for their QS modulation in other bacteria that respond to AI-2.

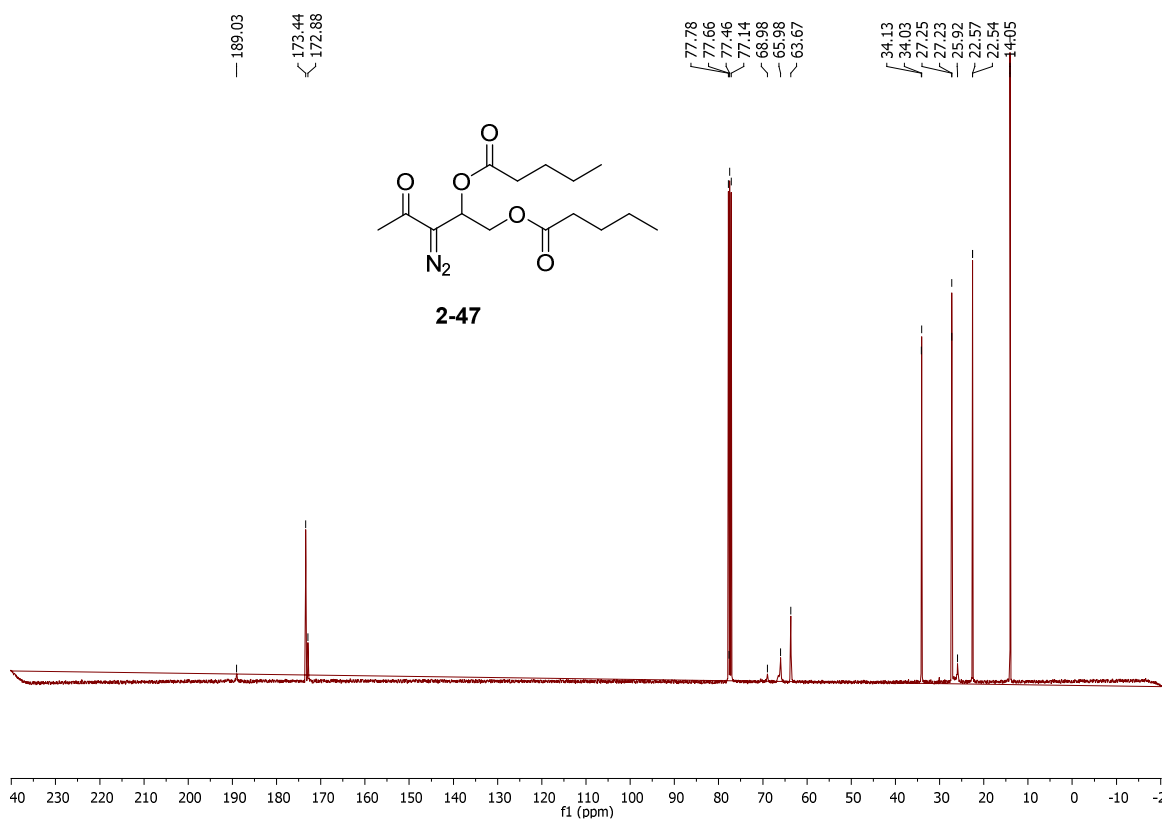
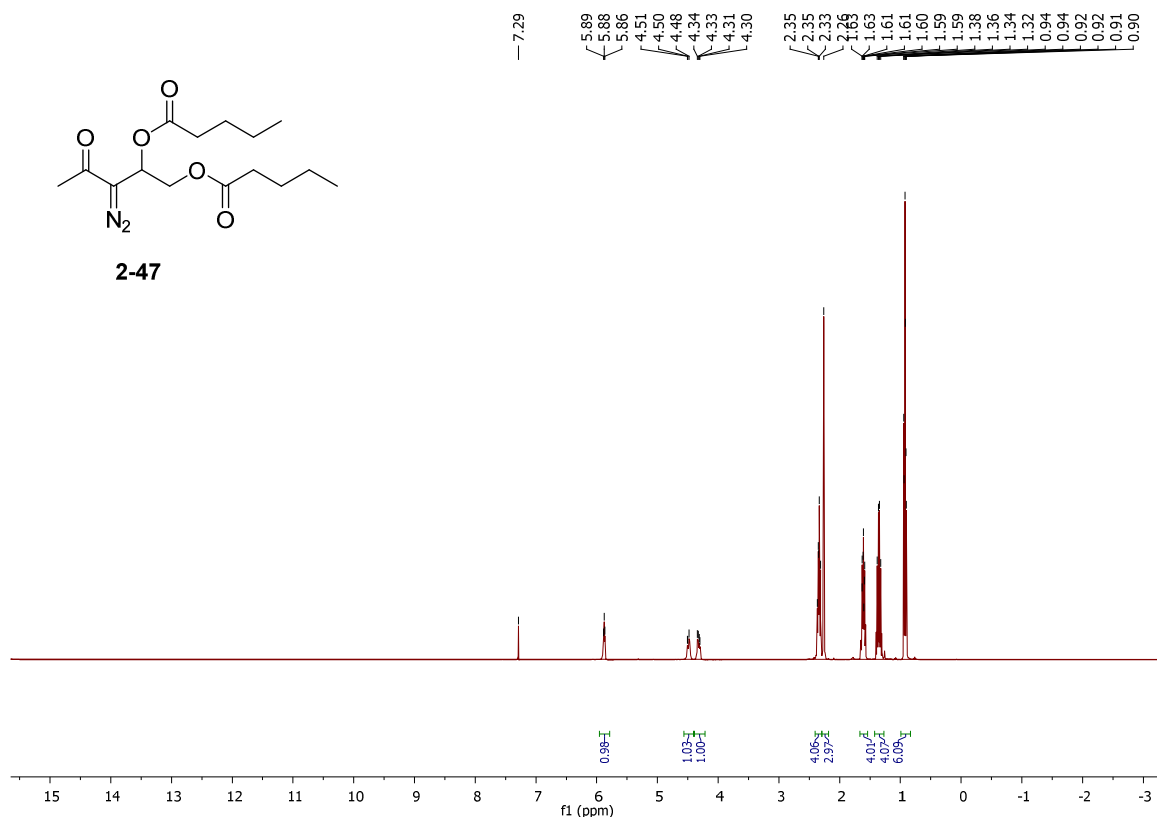
5.2 AI-1 mediated quorum sensing inhibitors.

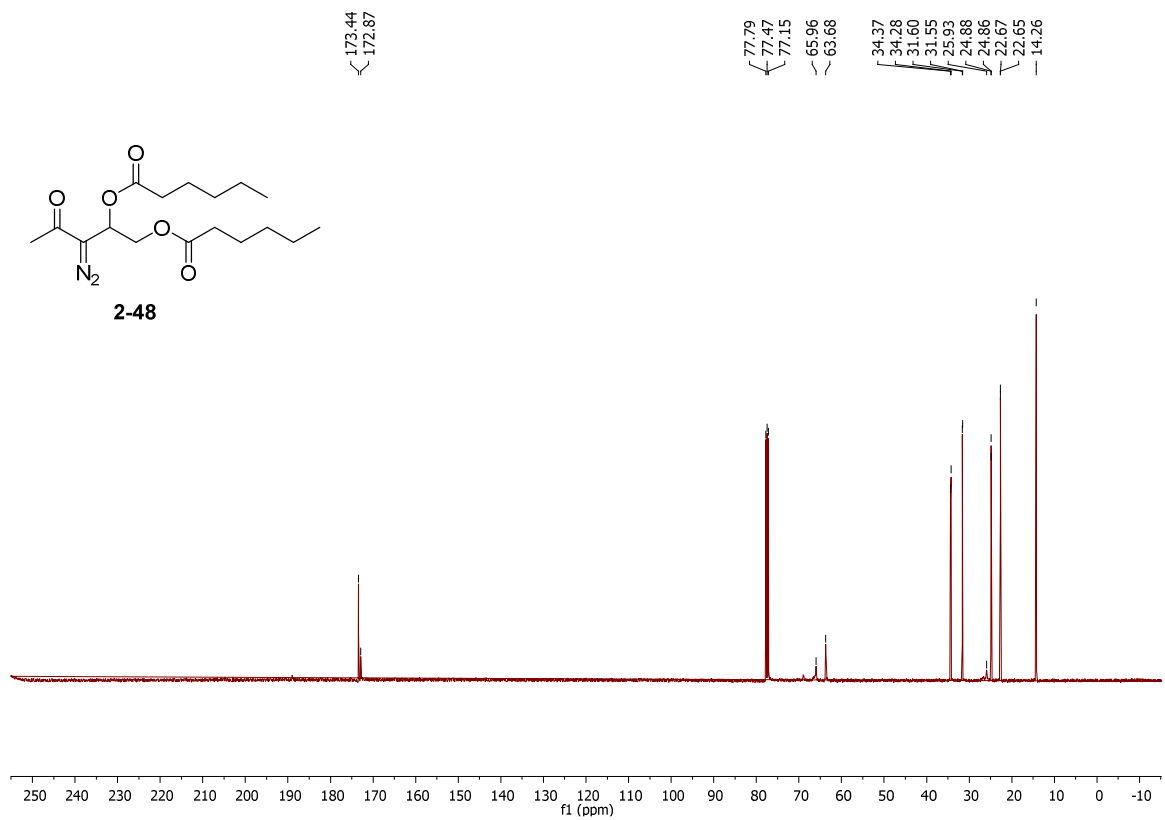
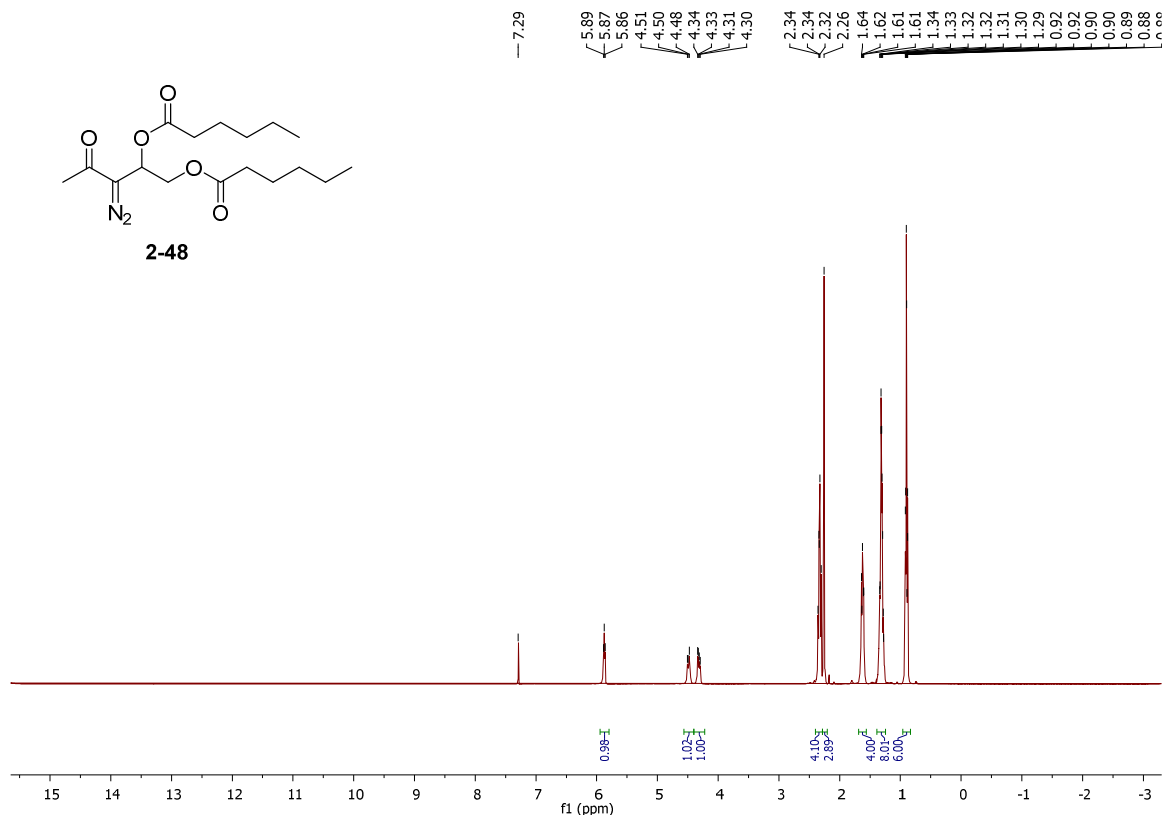
AI-1 in Gram-negative bacteria regulates many processes and analogs thereof have been intensively studied in the past three decades and most of them were based on *N*-acyl homoserine lactone (AHL) head group. In this dissertation, we presented a very promising head group, 3-aminooxazolidinone, which has remained largely unexplored. We proved that this head group was superior to the native AHL in terms of chemical stability and also retained similar activities as the native one. Hence it is a good platform/structure to develop drug-like QS inhibitors. Future work in the Sintim group will focus on the synthesis of 3-aminooxazolidinone libraries to discover new QS antagonists that interrupt AI-1 signaling in Gram negative bacteria, such as *P. aeruginosa*.

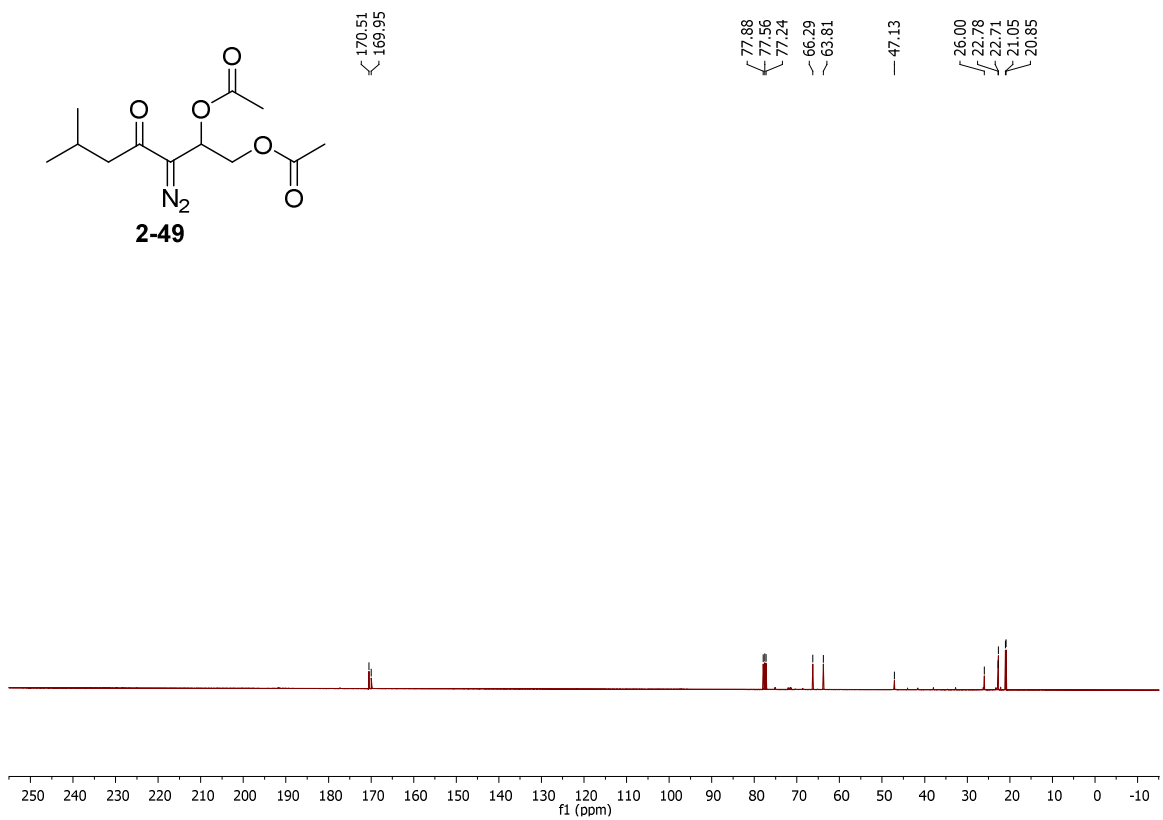
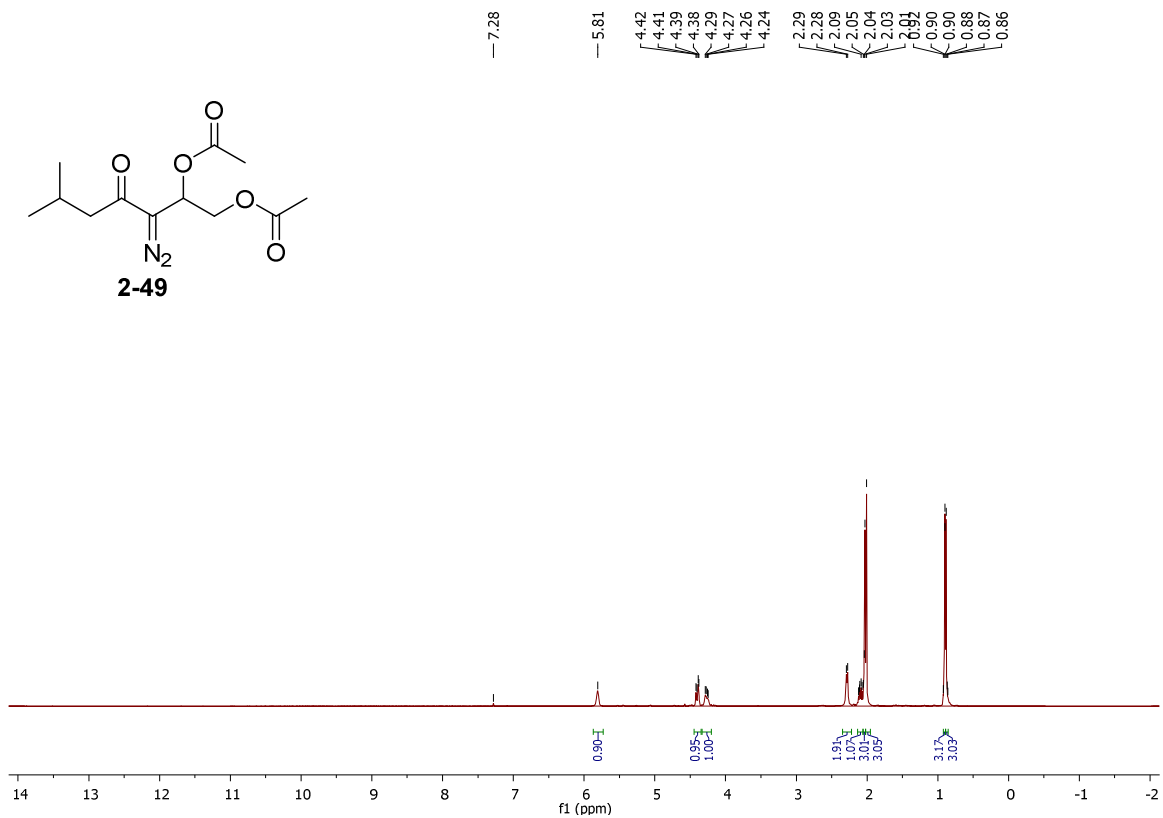
Appendix. NMR spectra

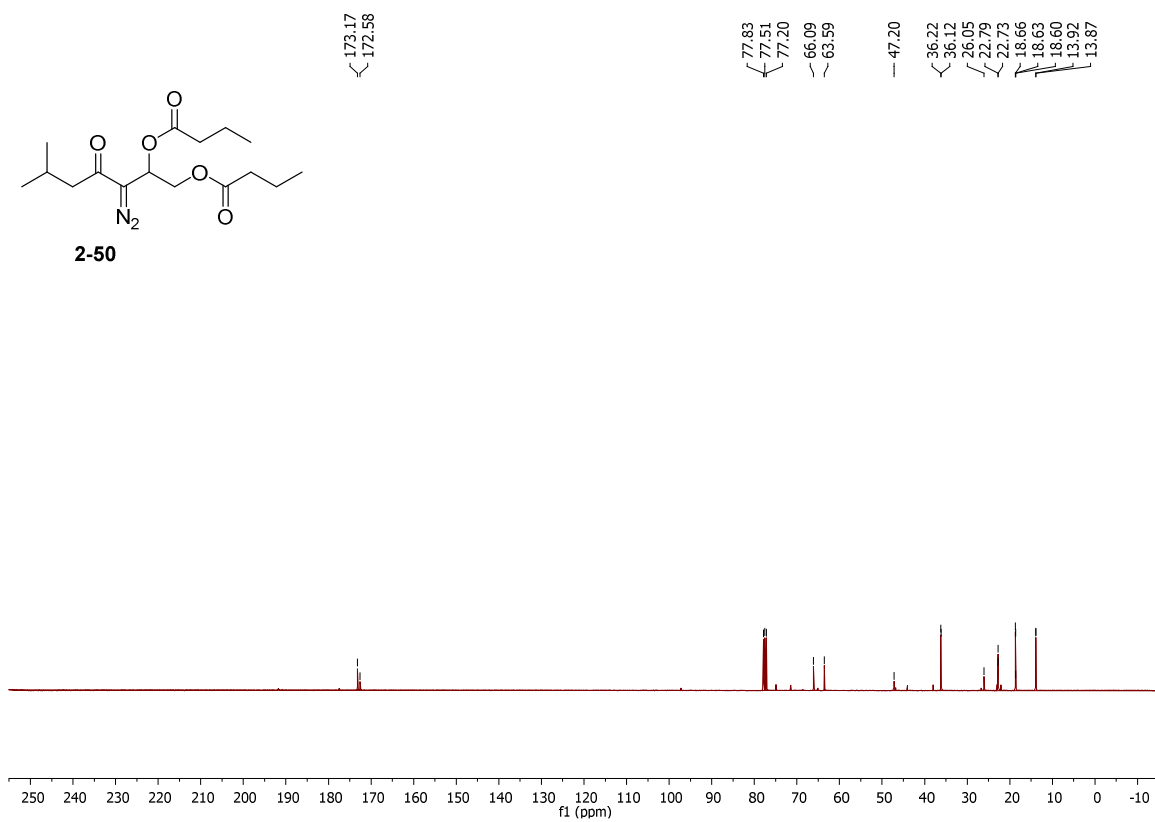
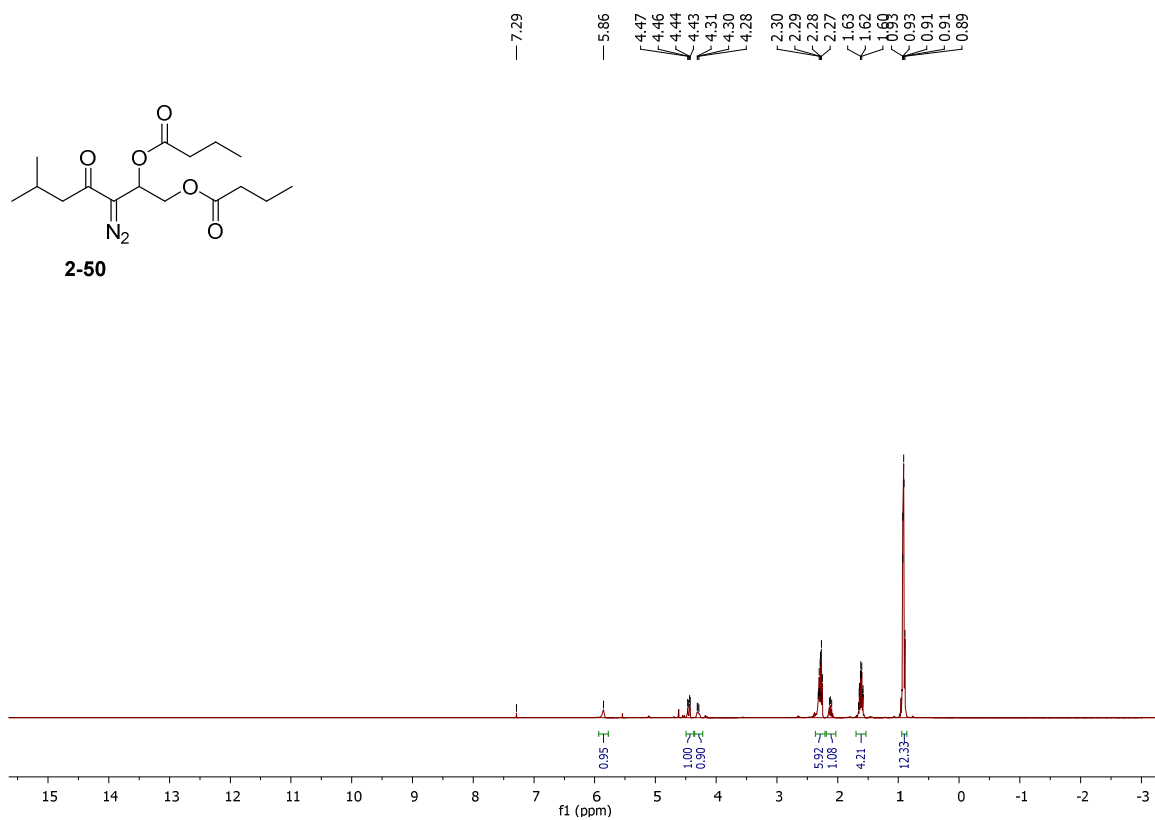


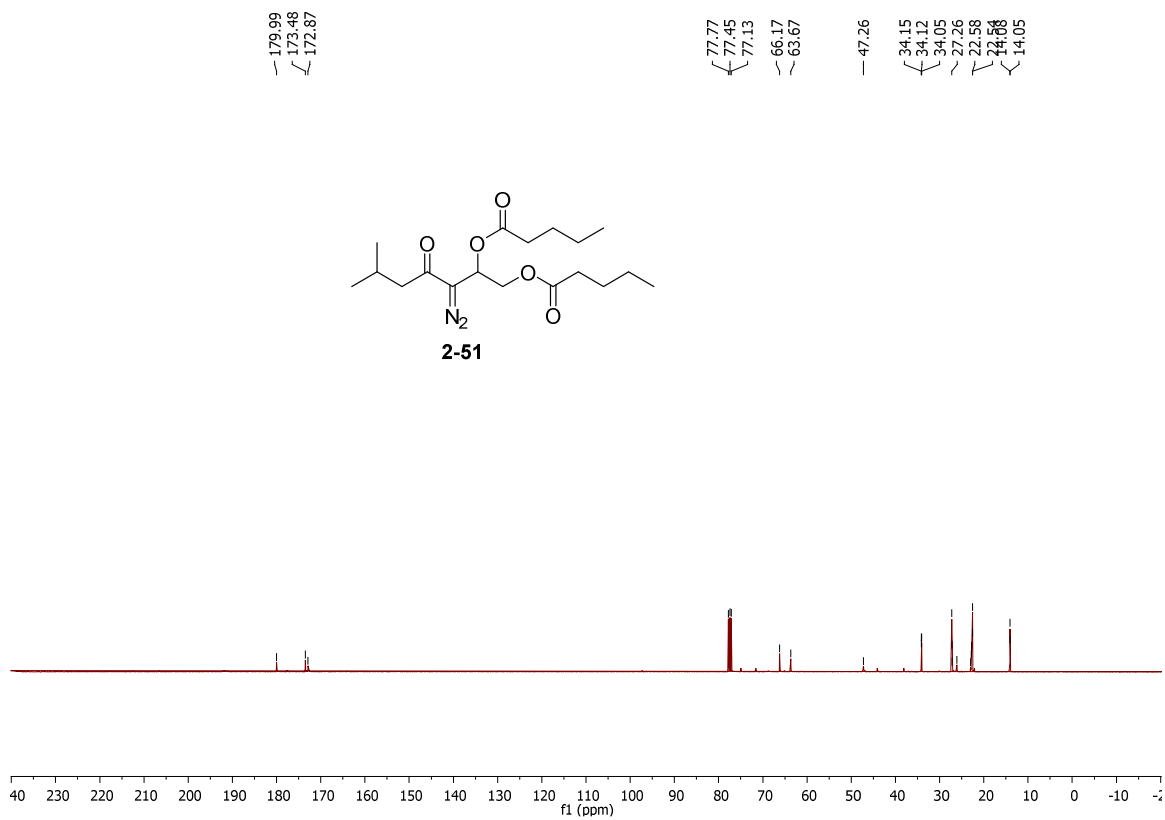
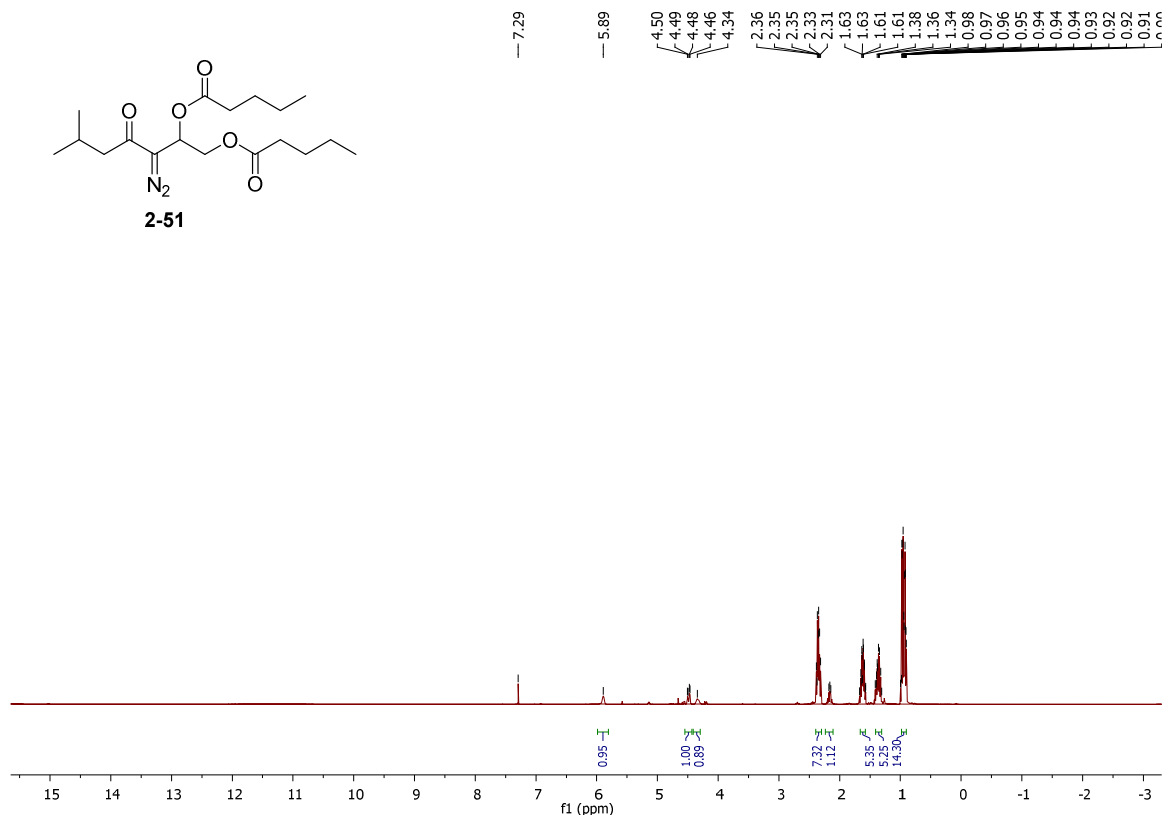


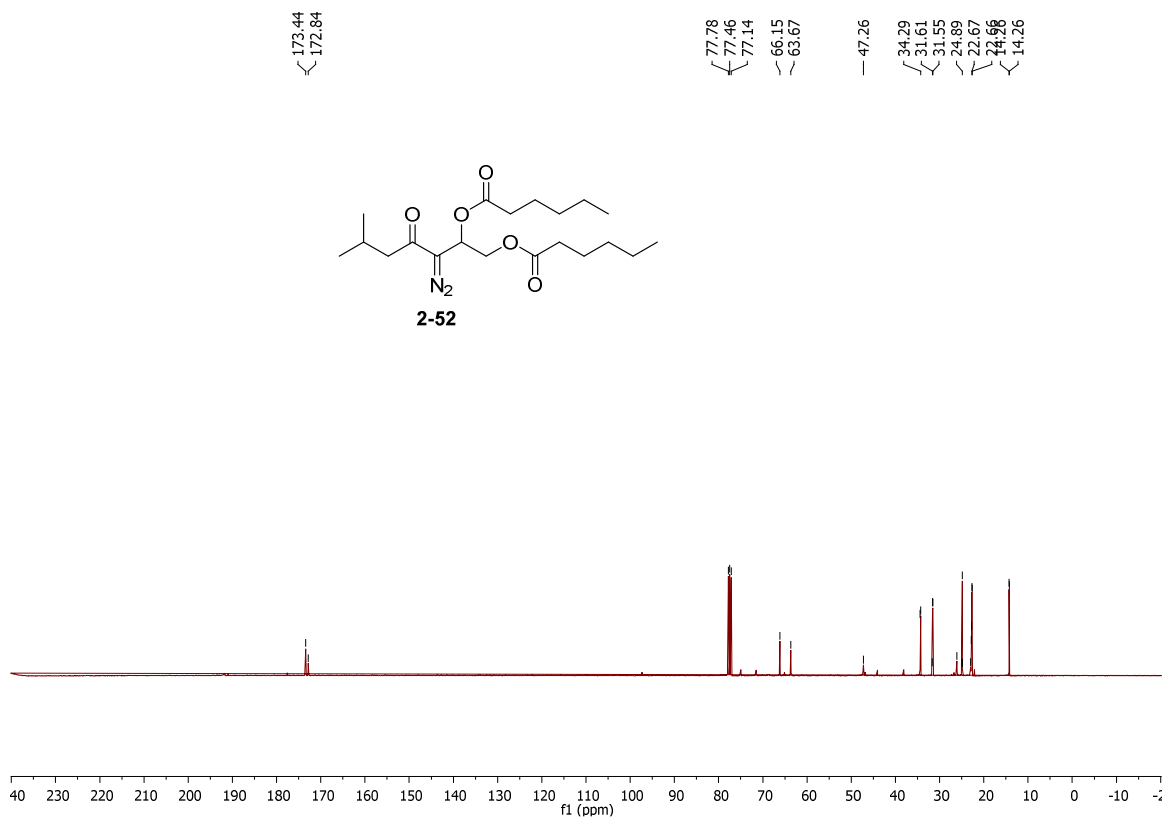
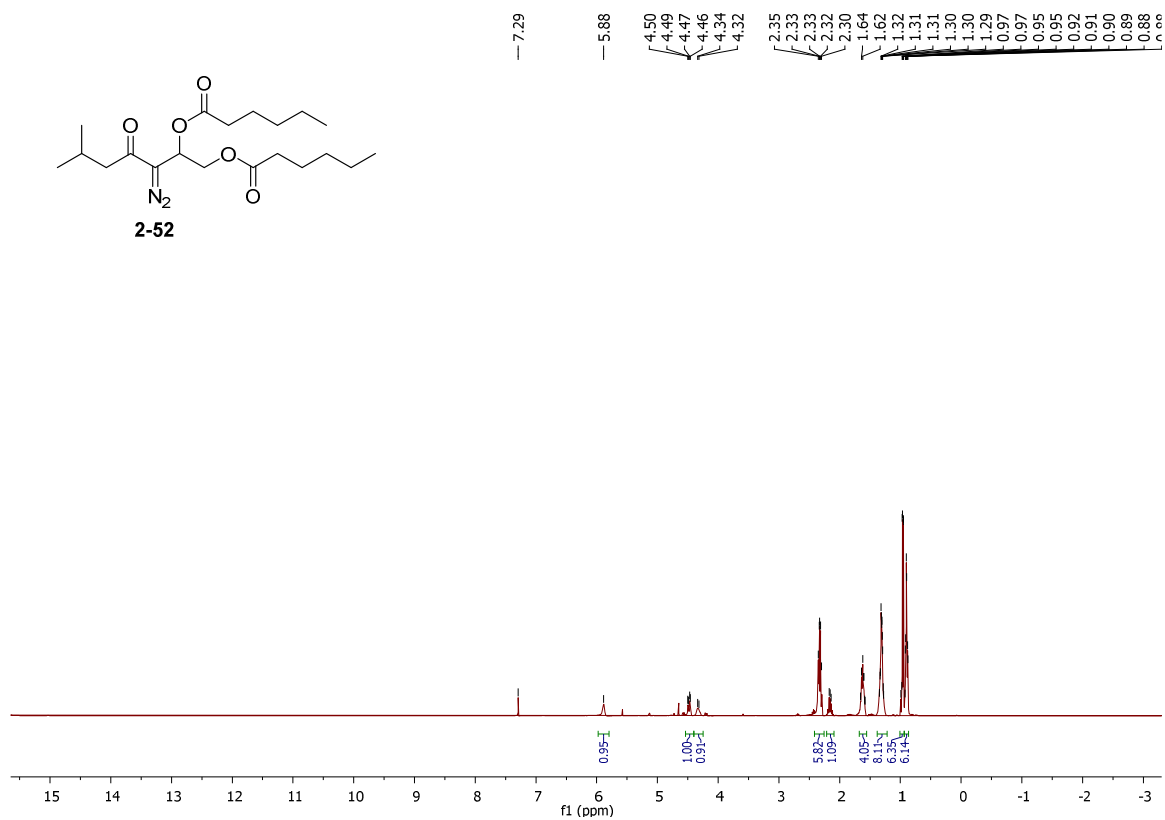


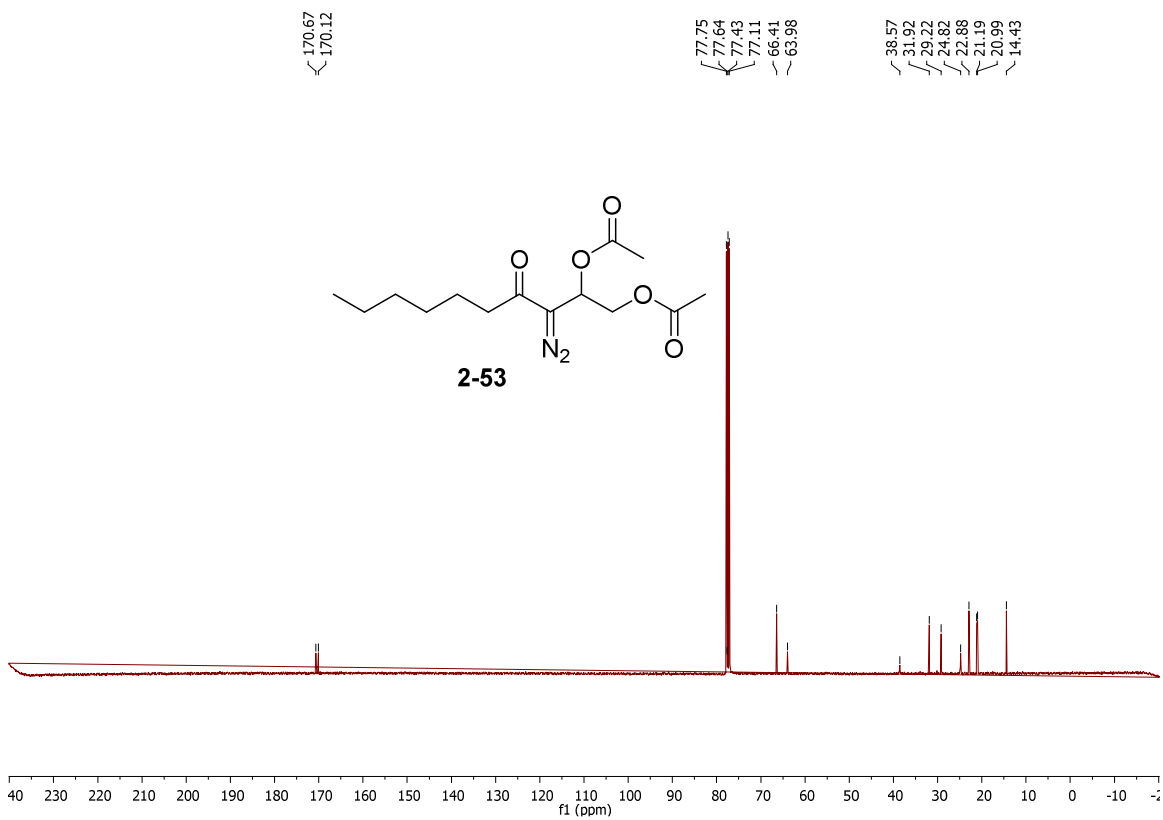
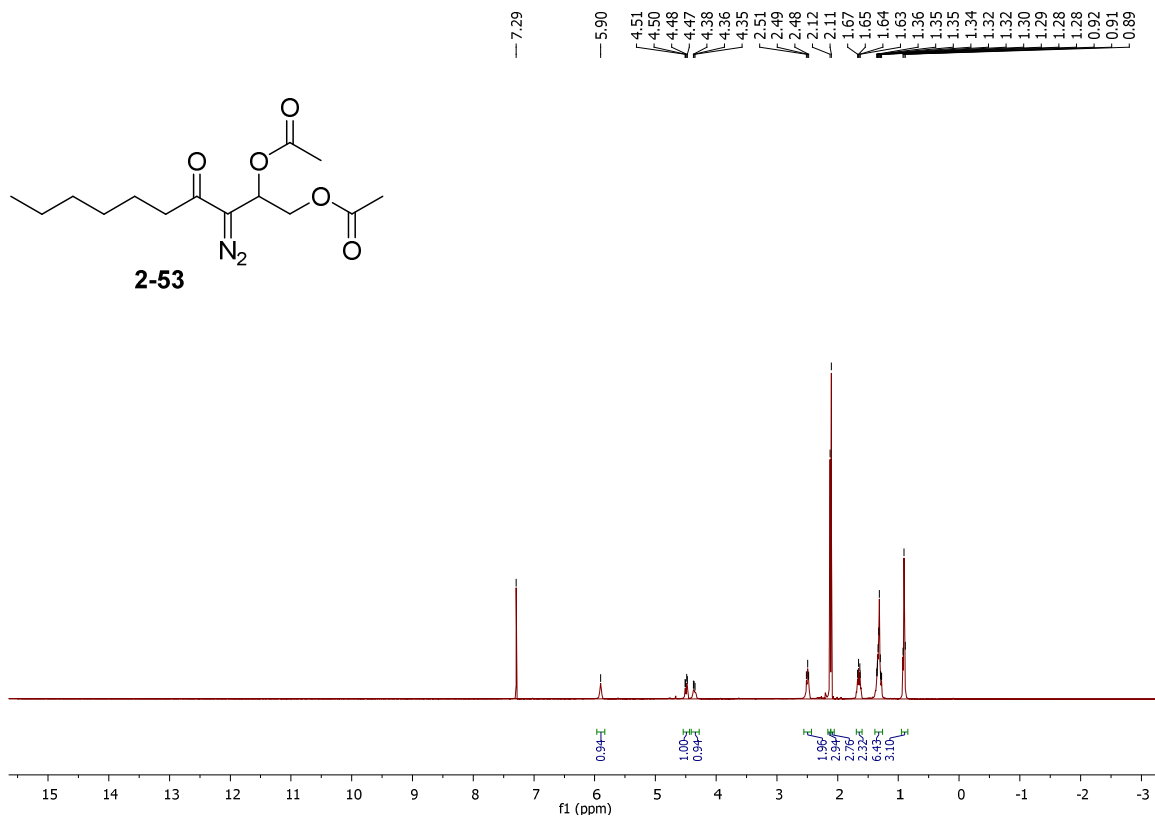


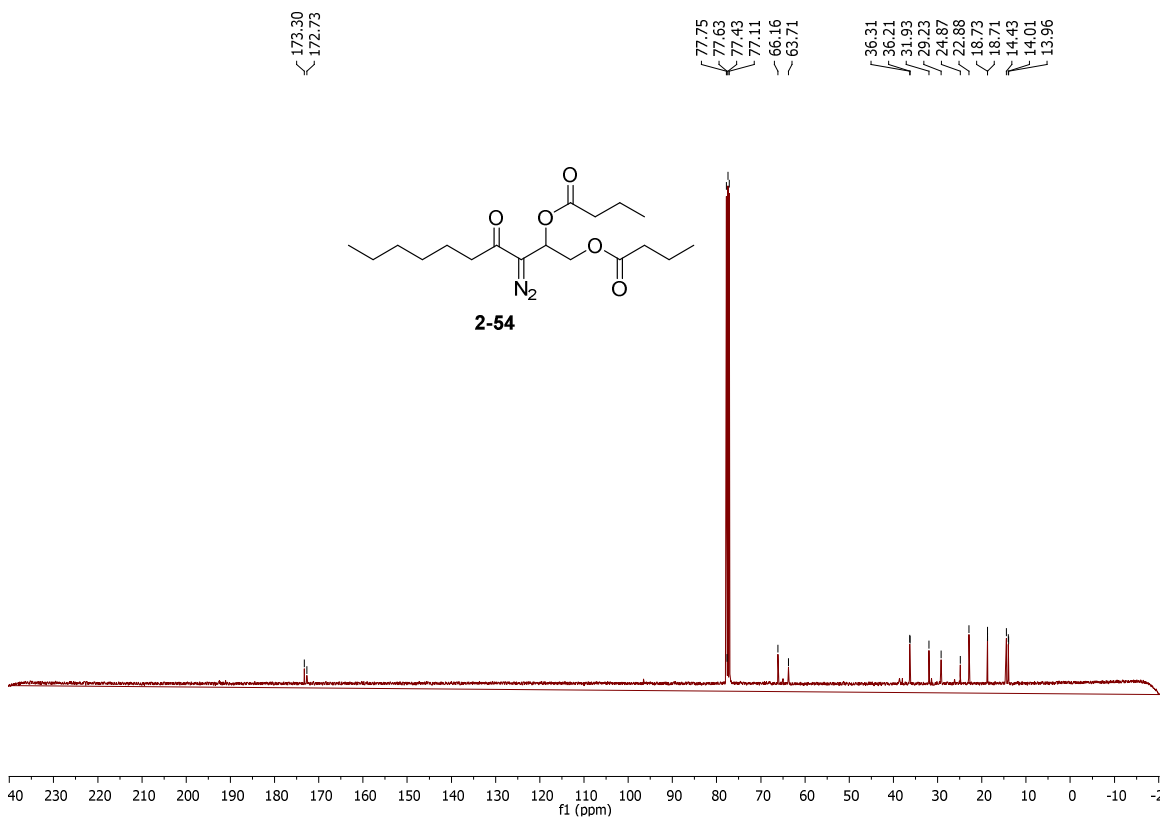
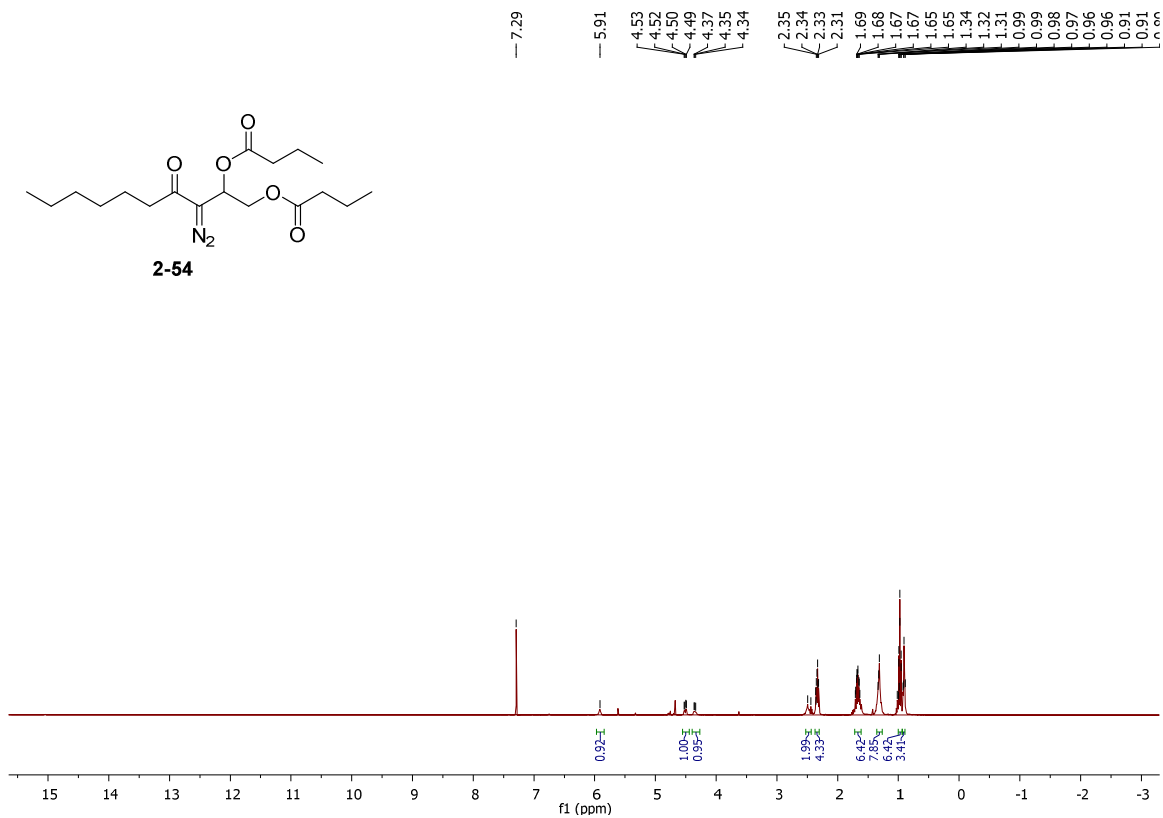


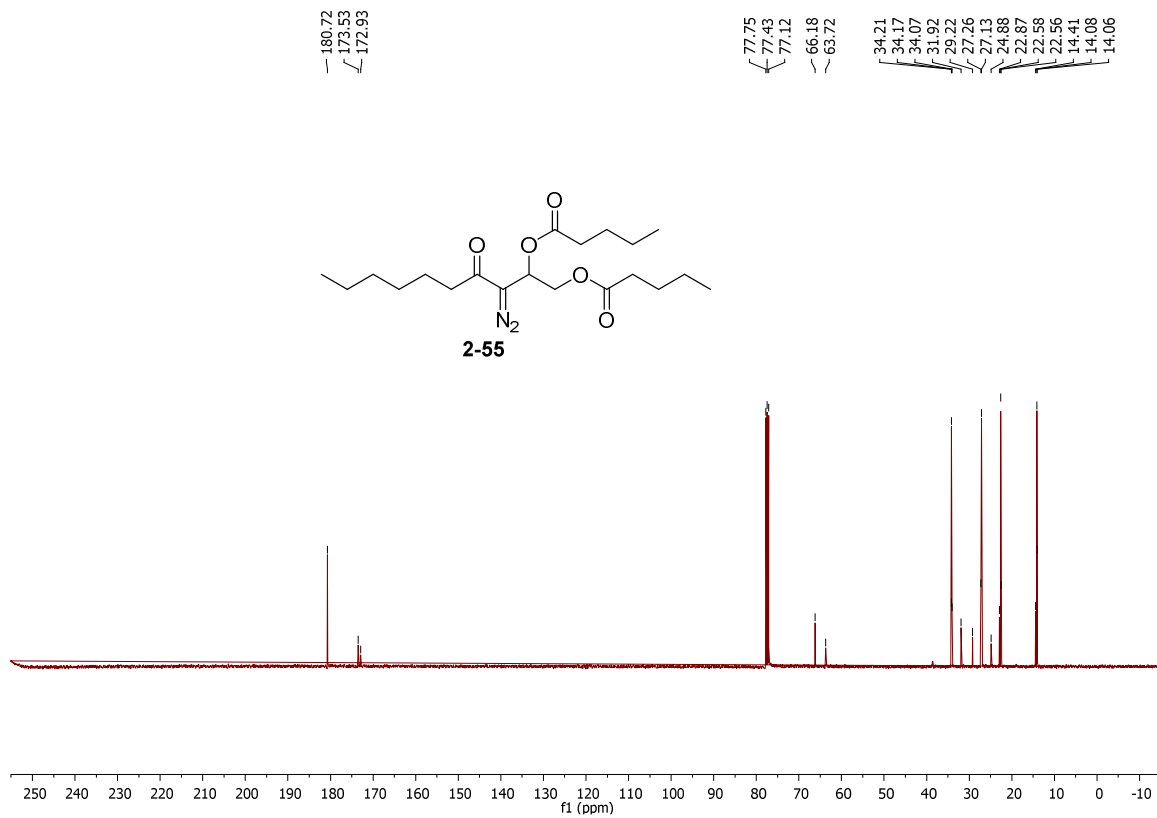
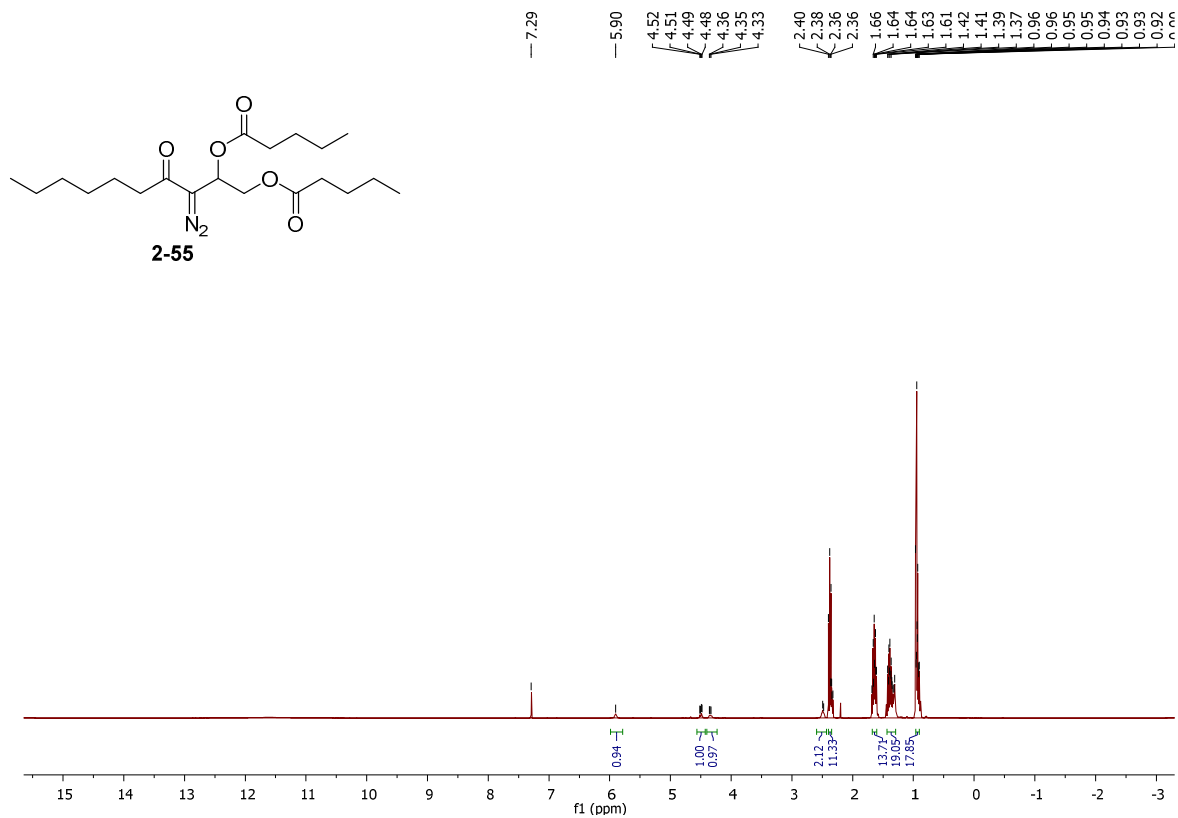


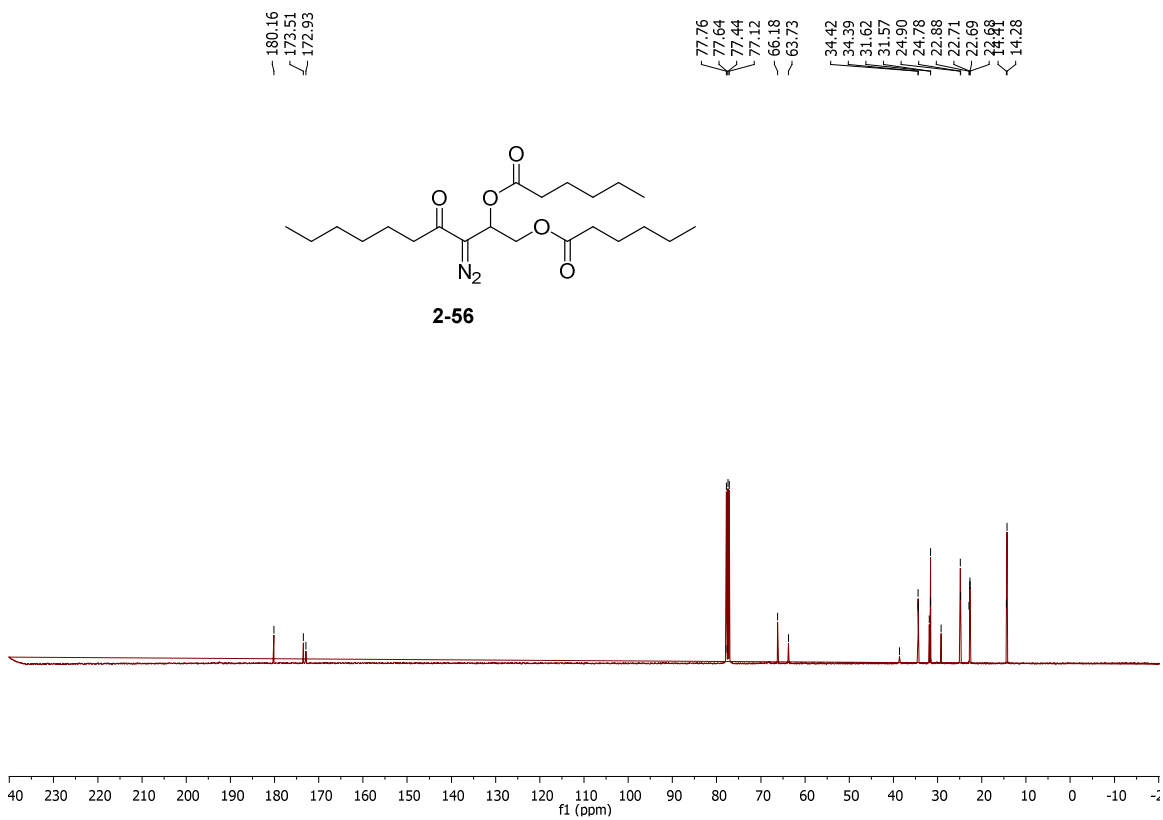
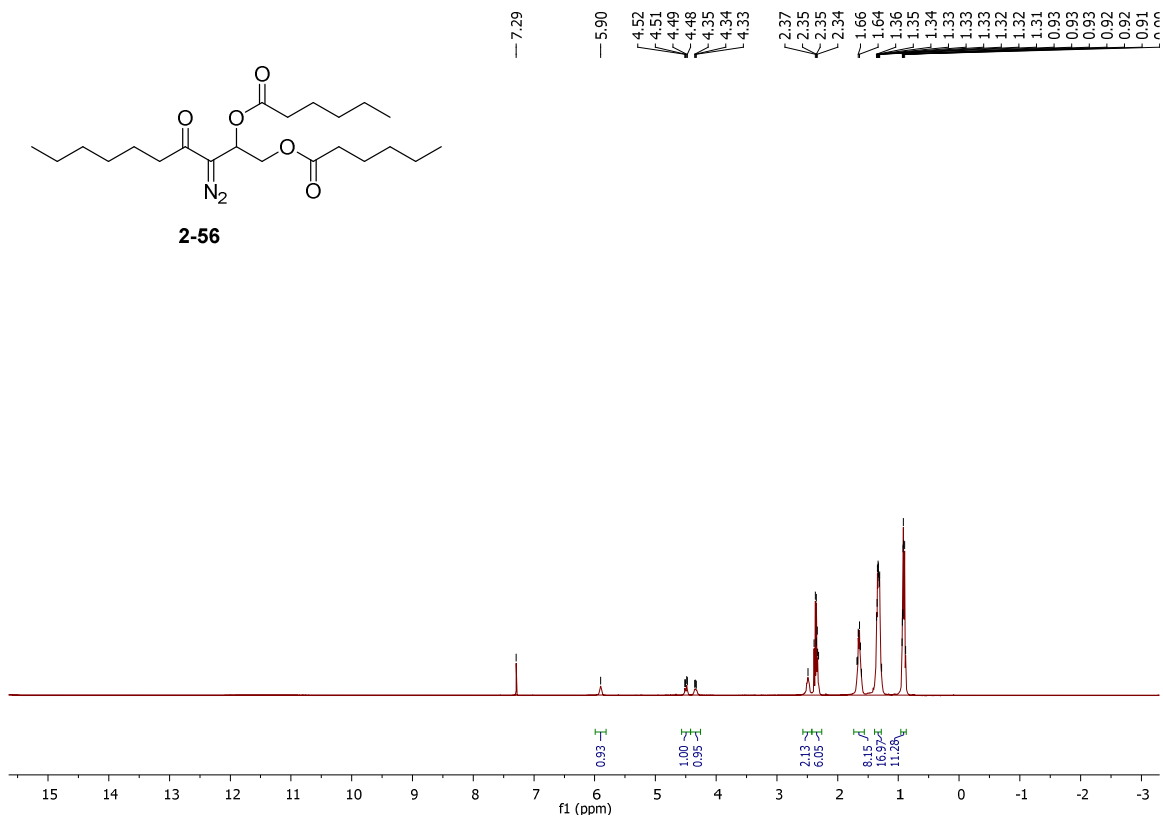


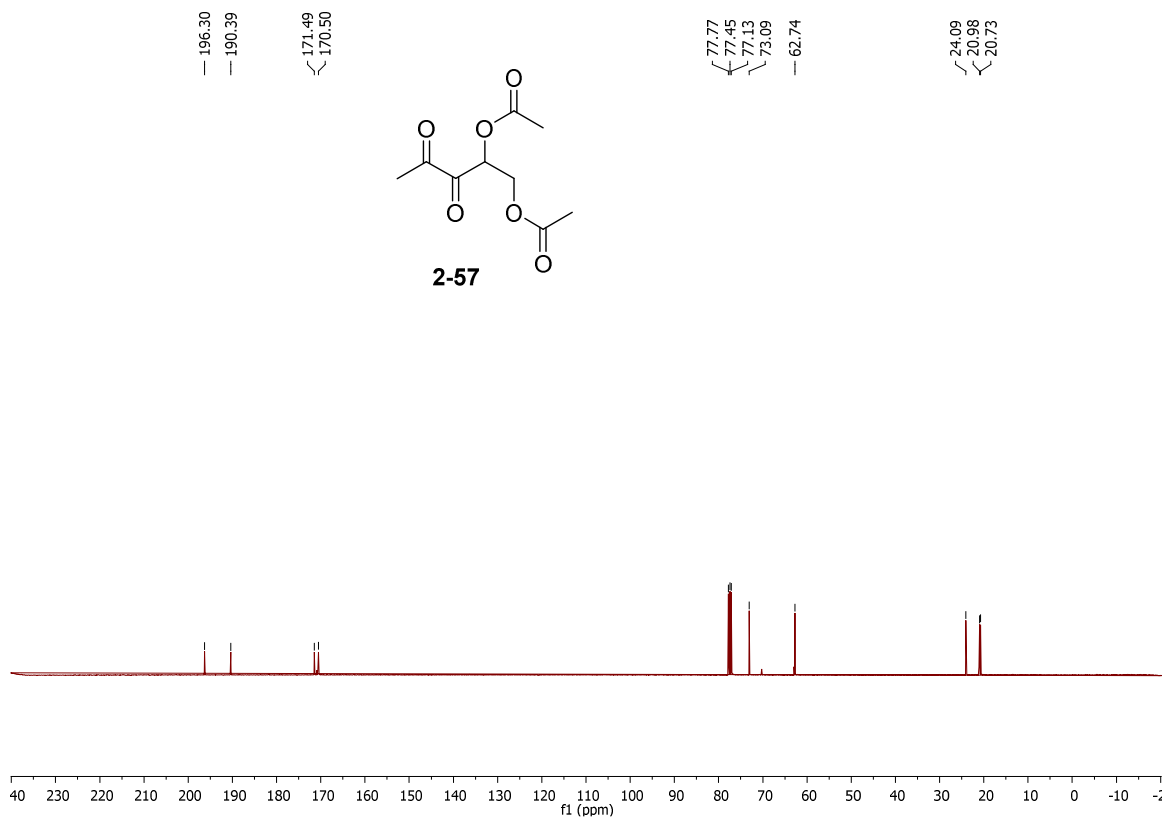
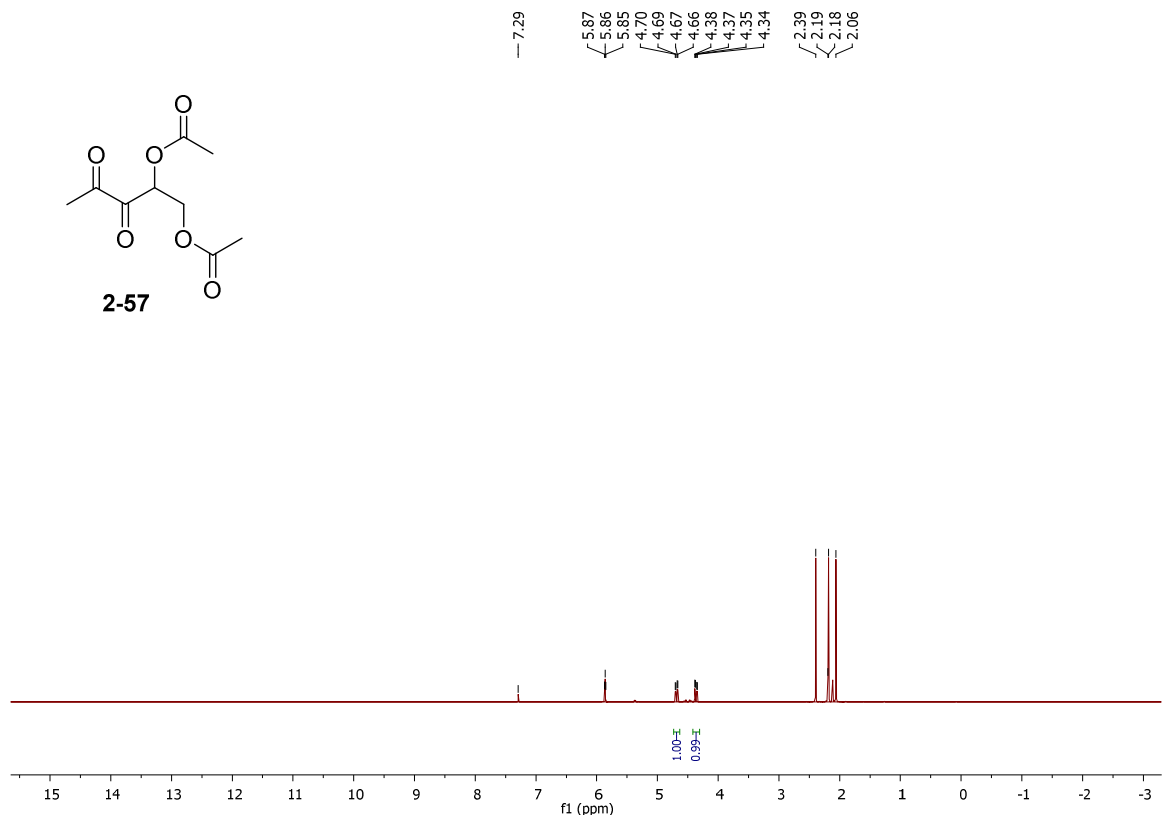


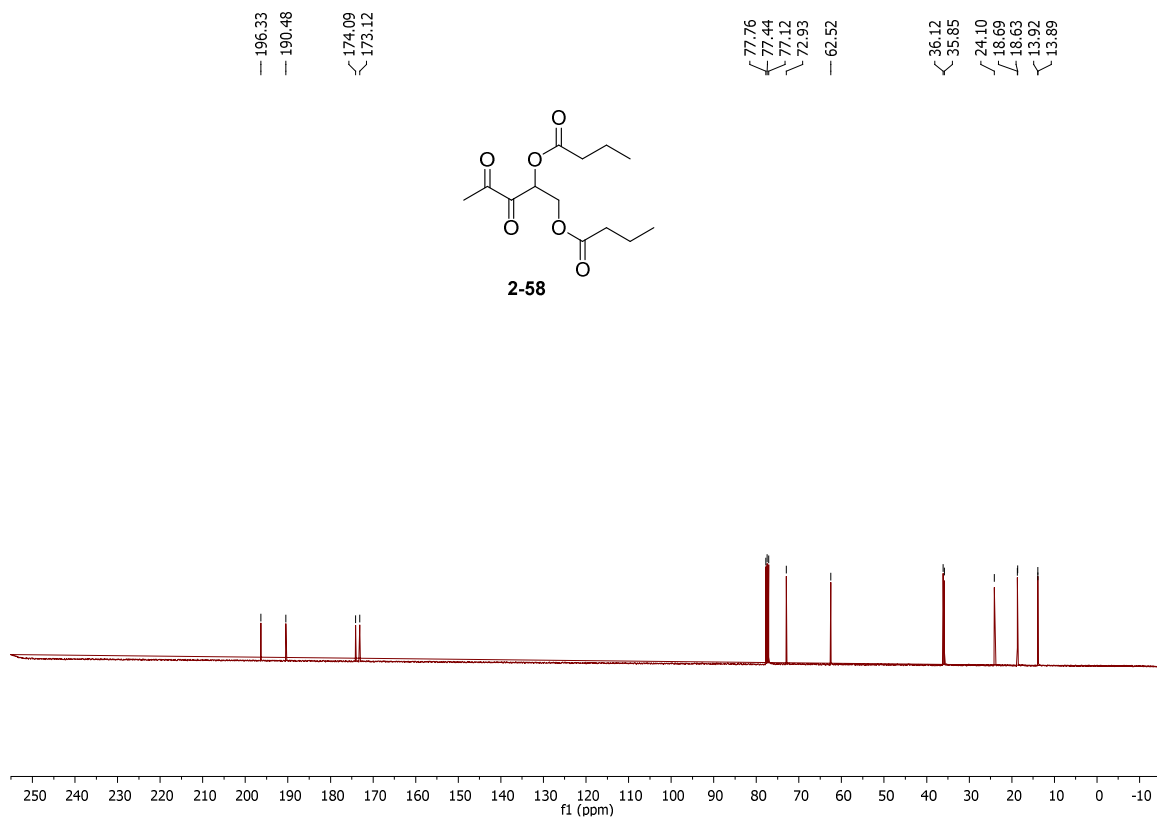
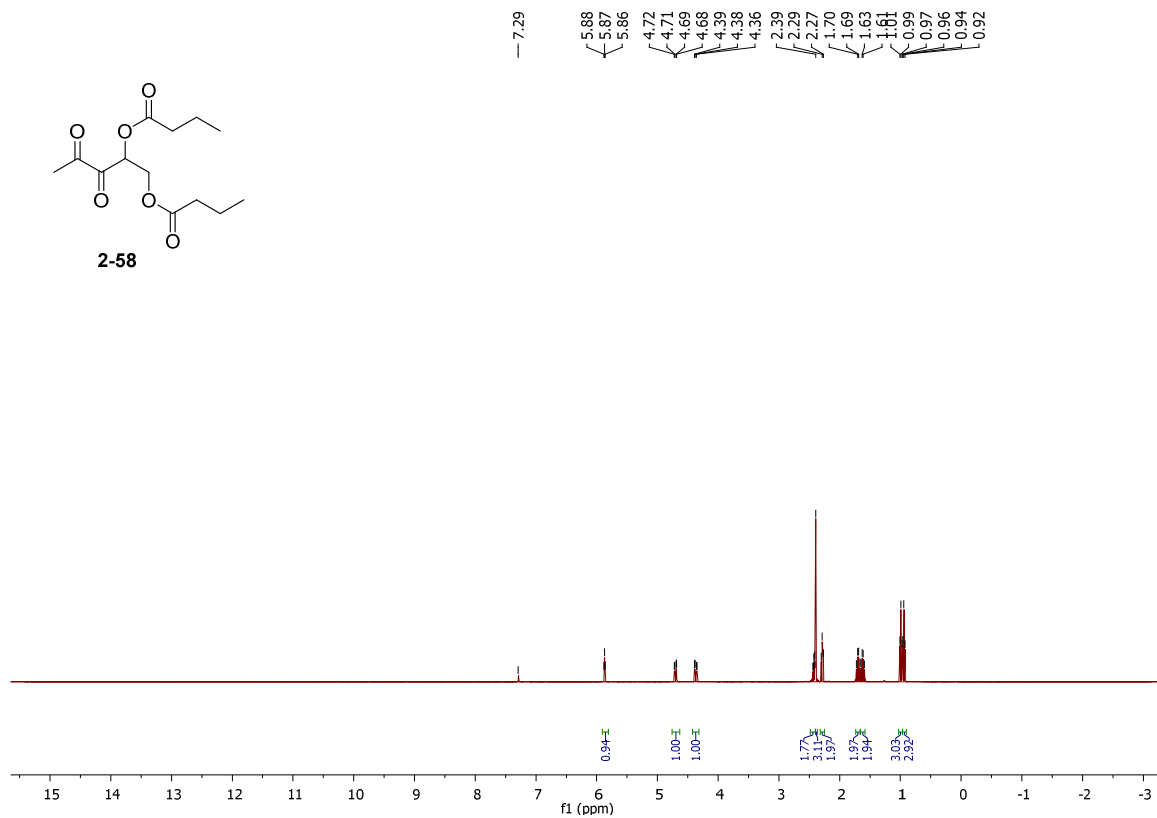


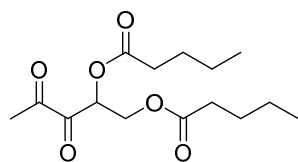




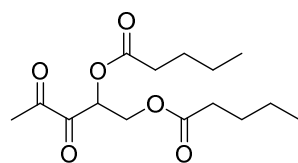
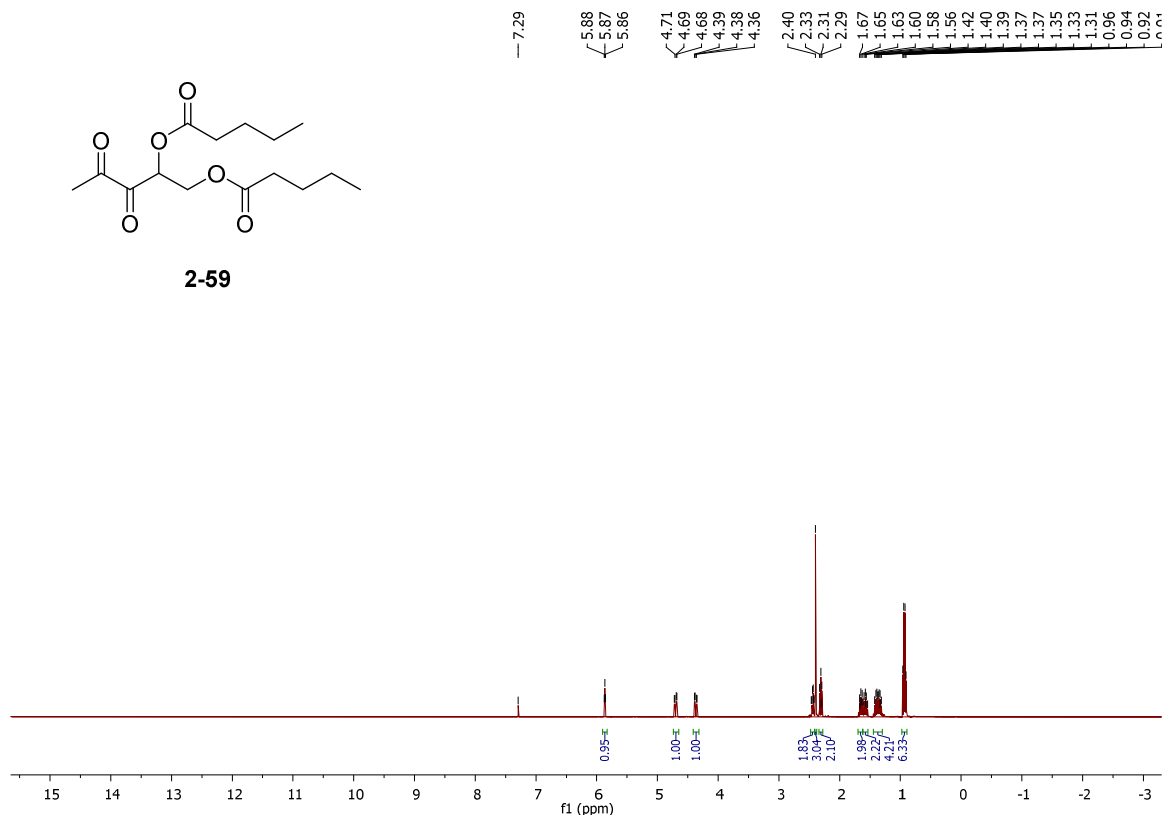




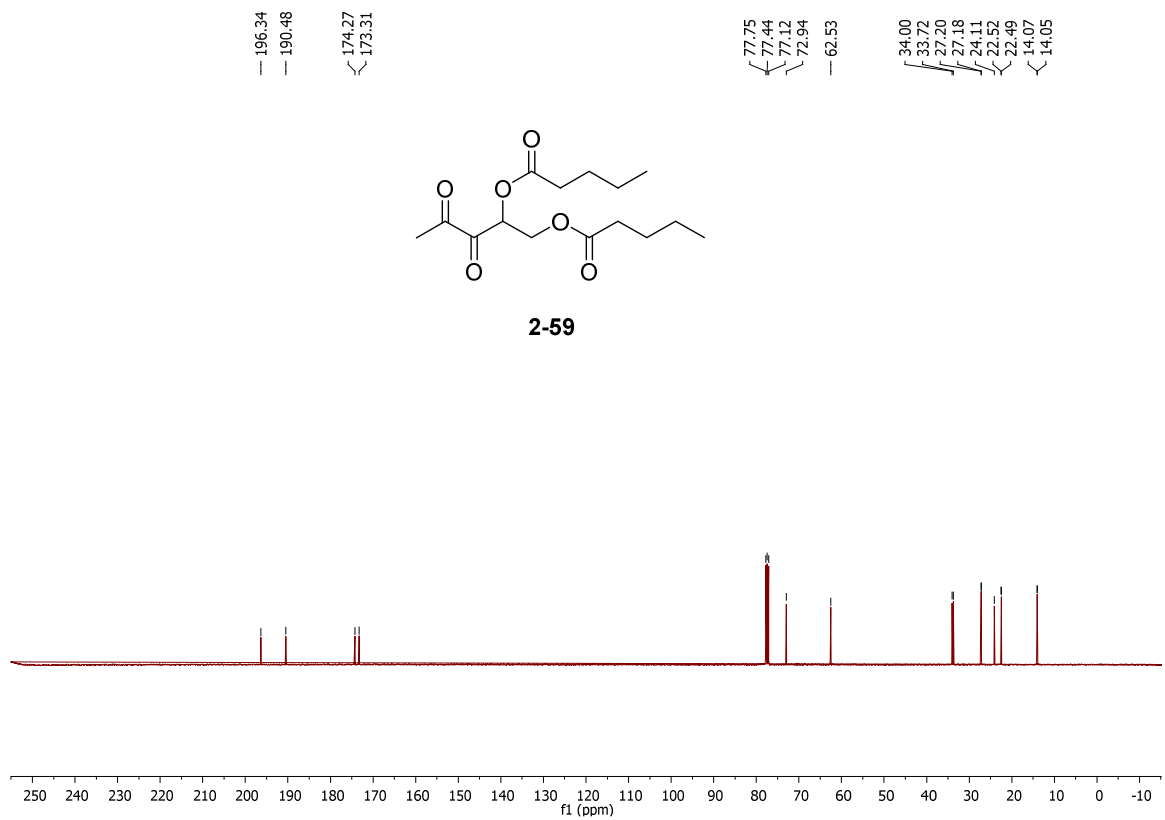


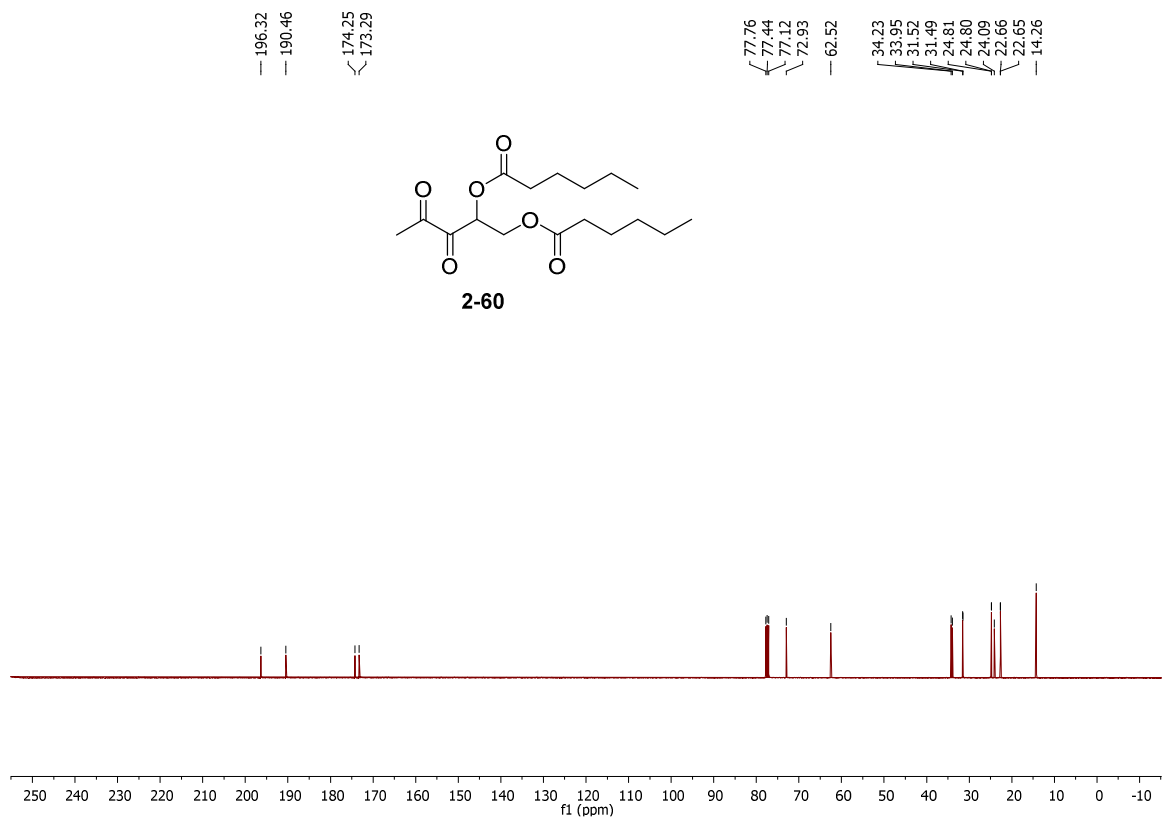
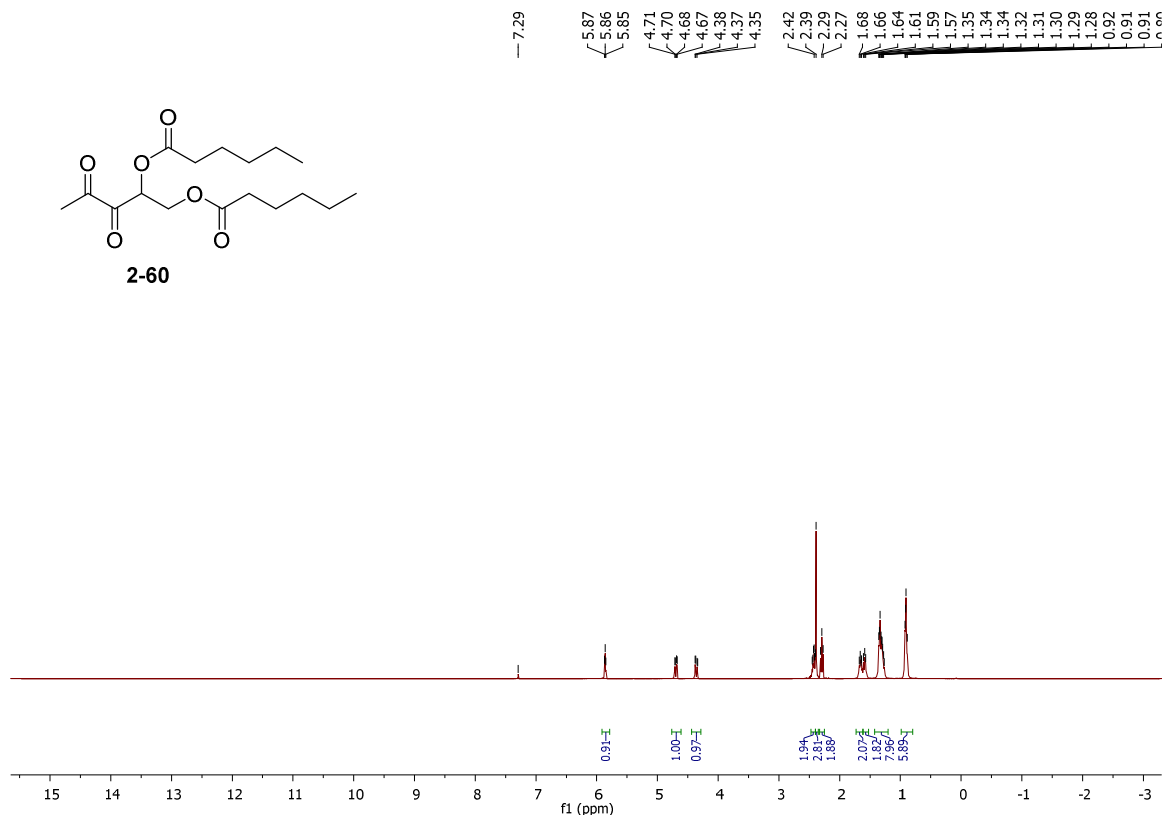


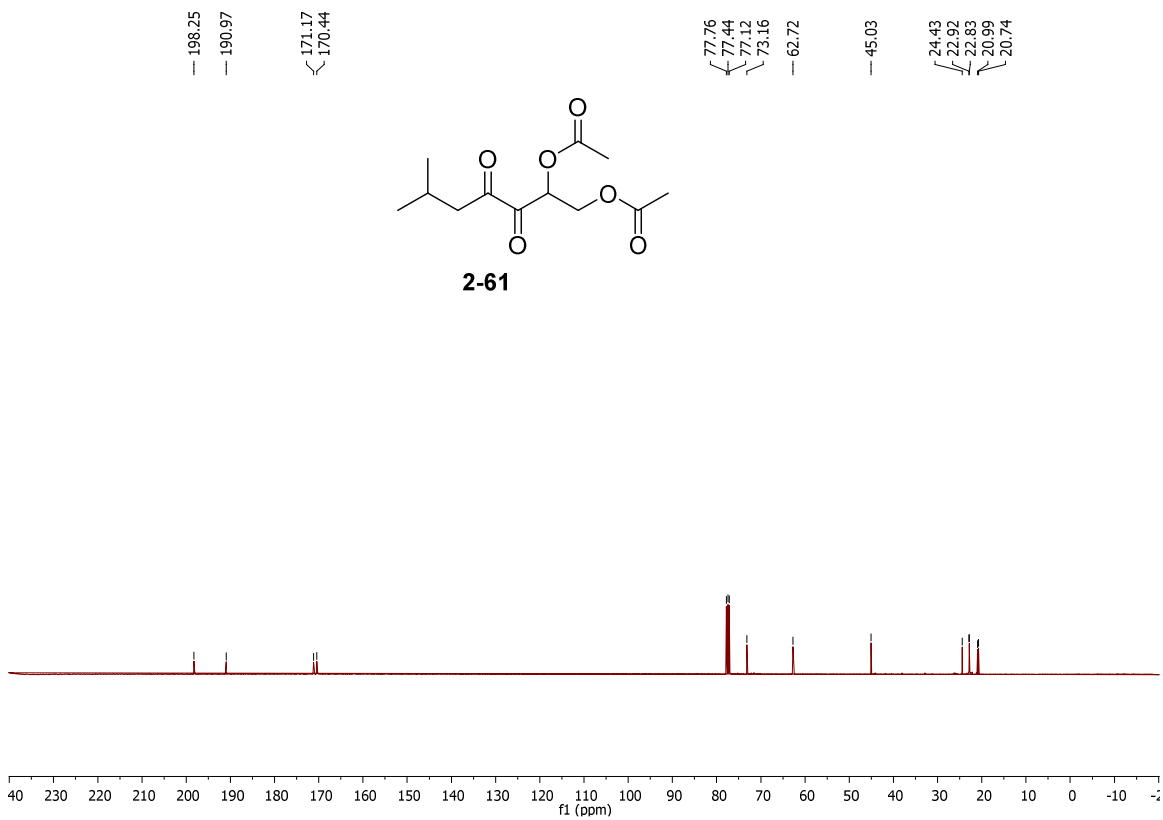
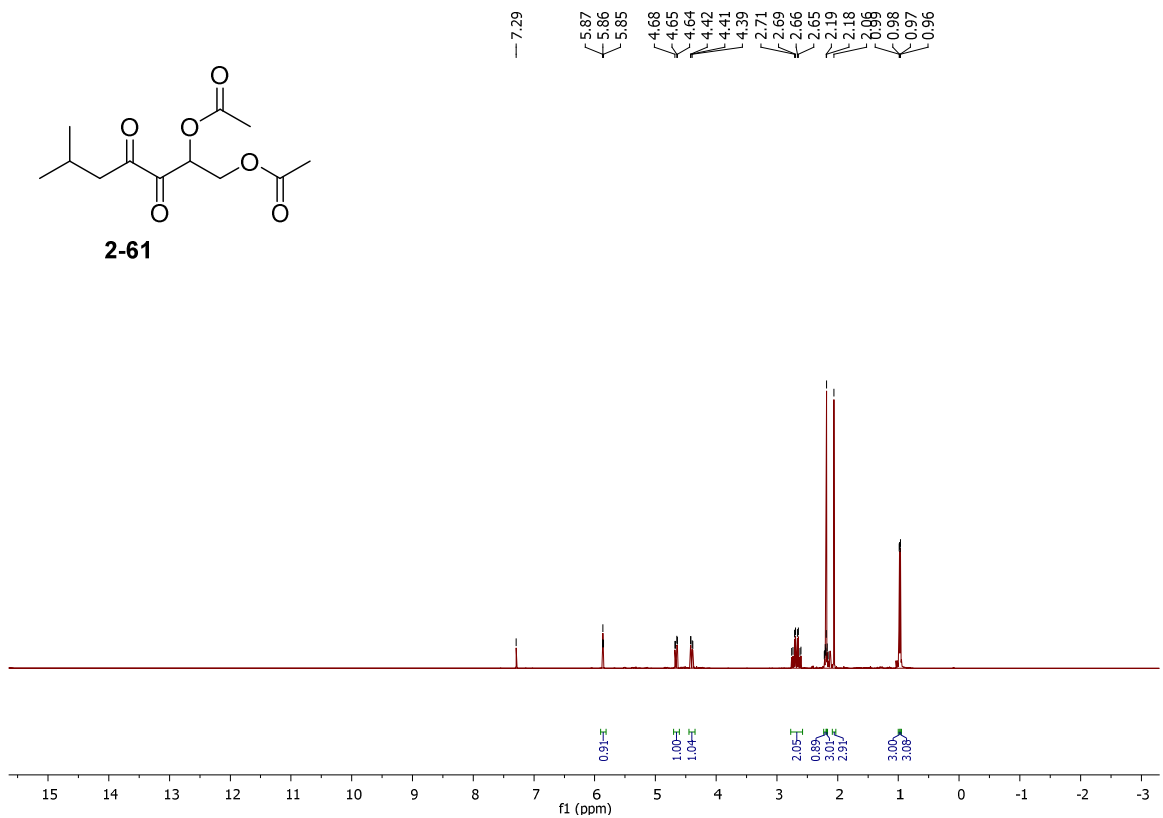
2-59

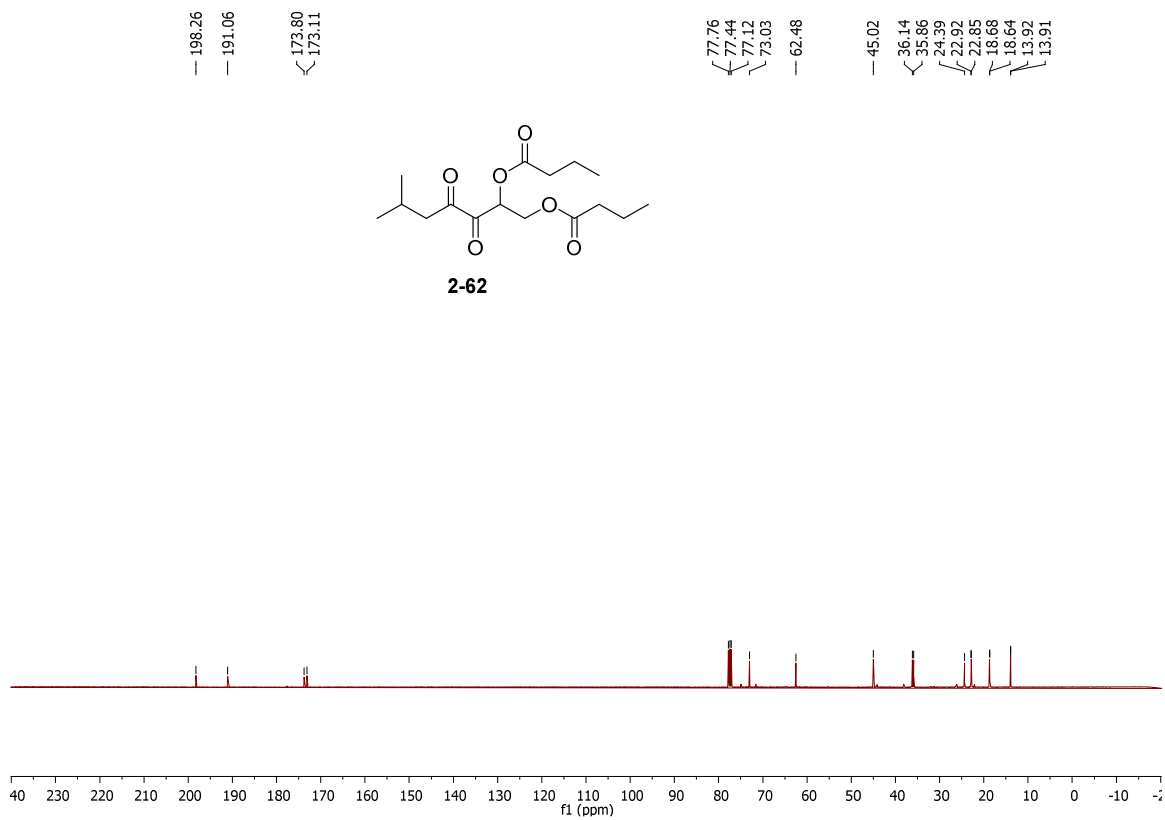
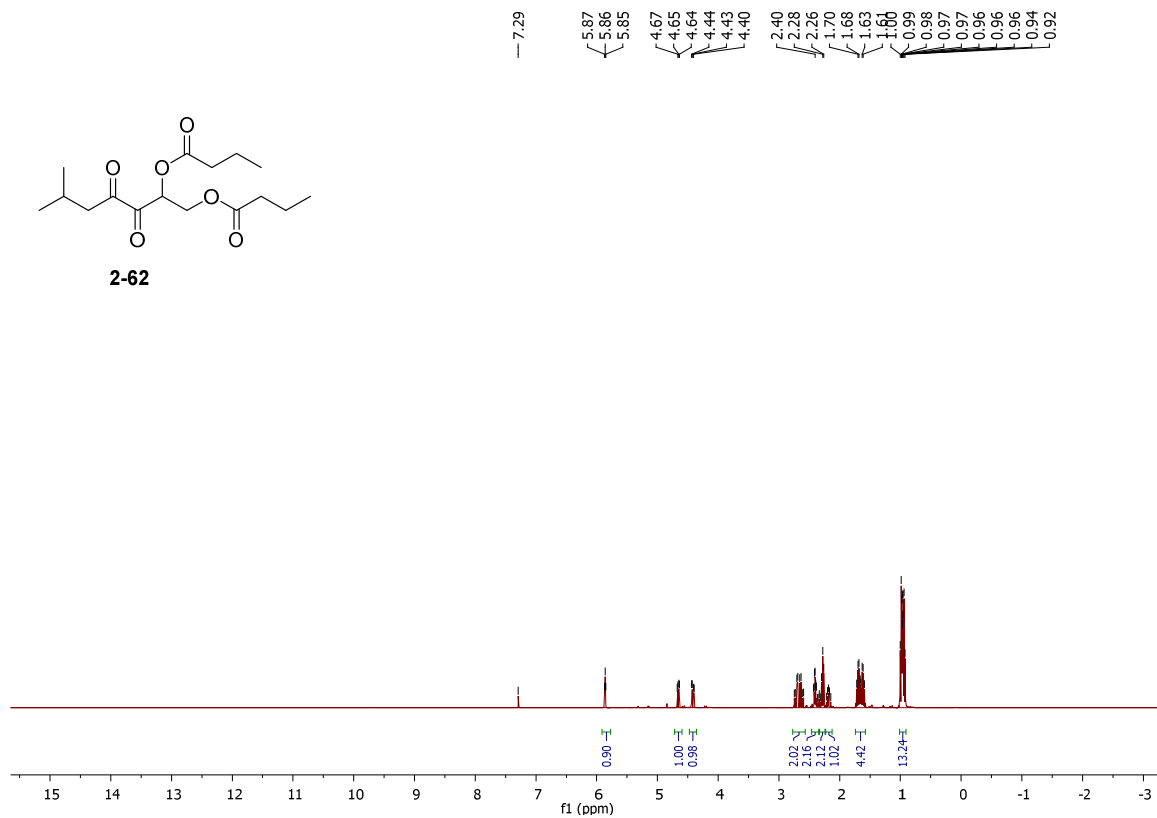


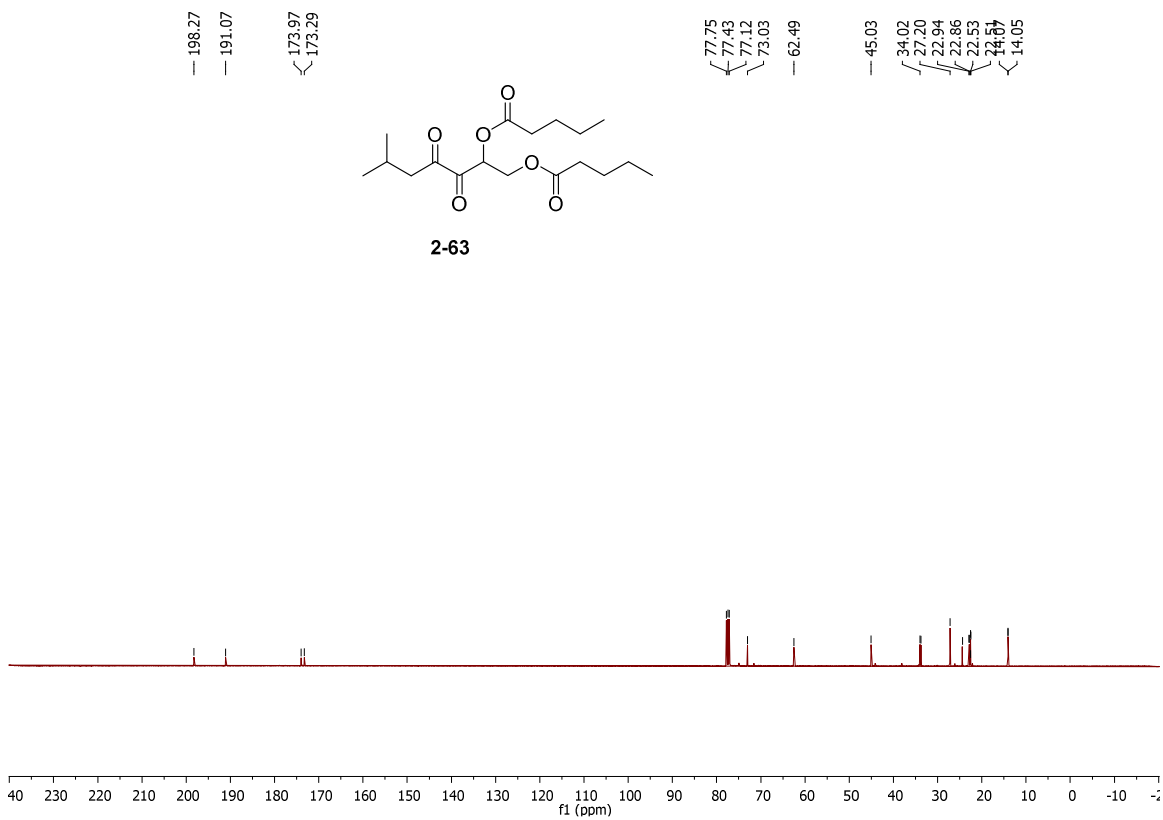
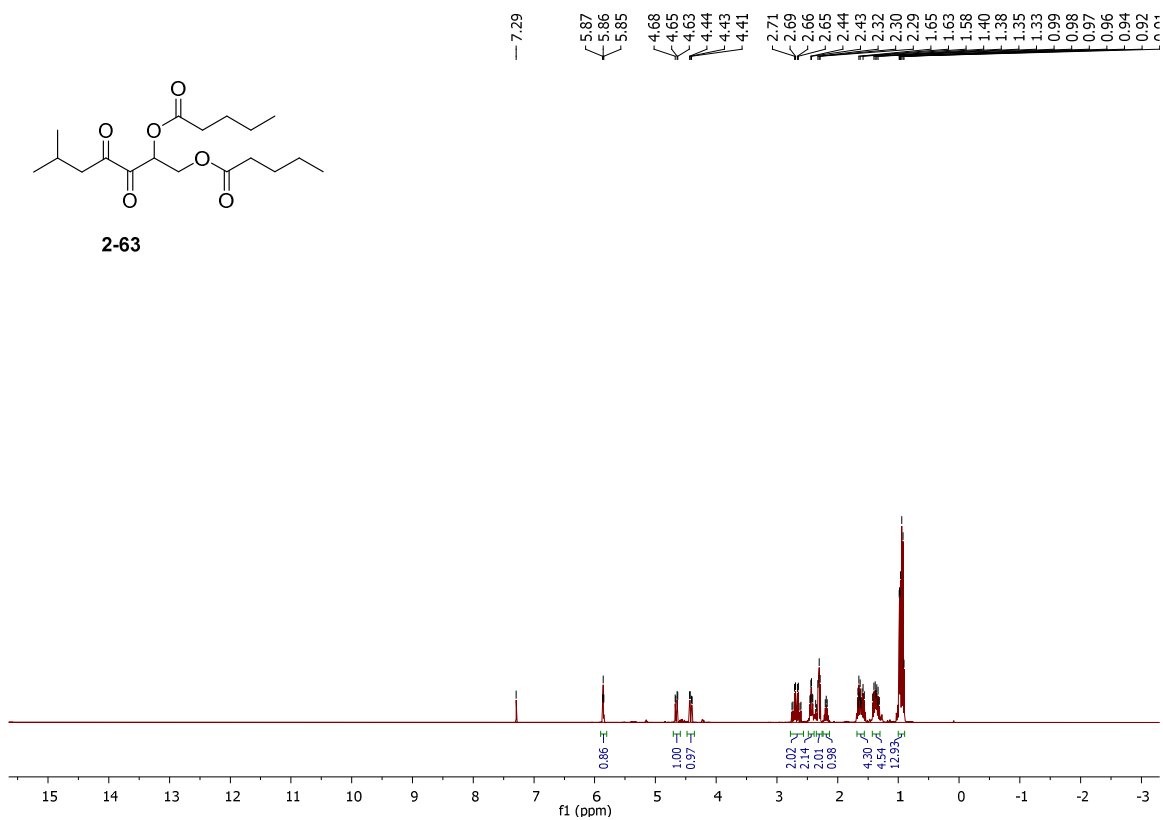
2-59

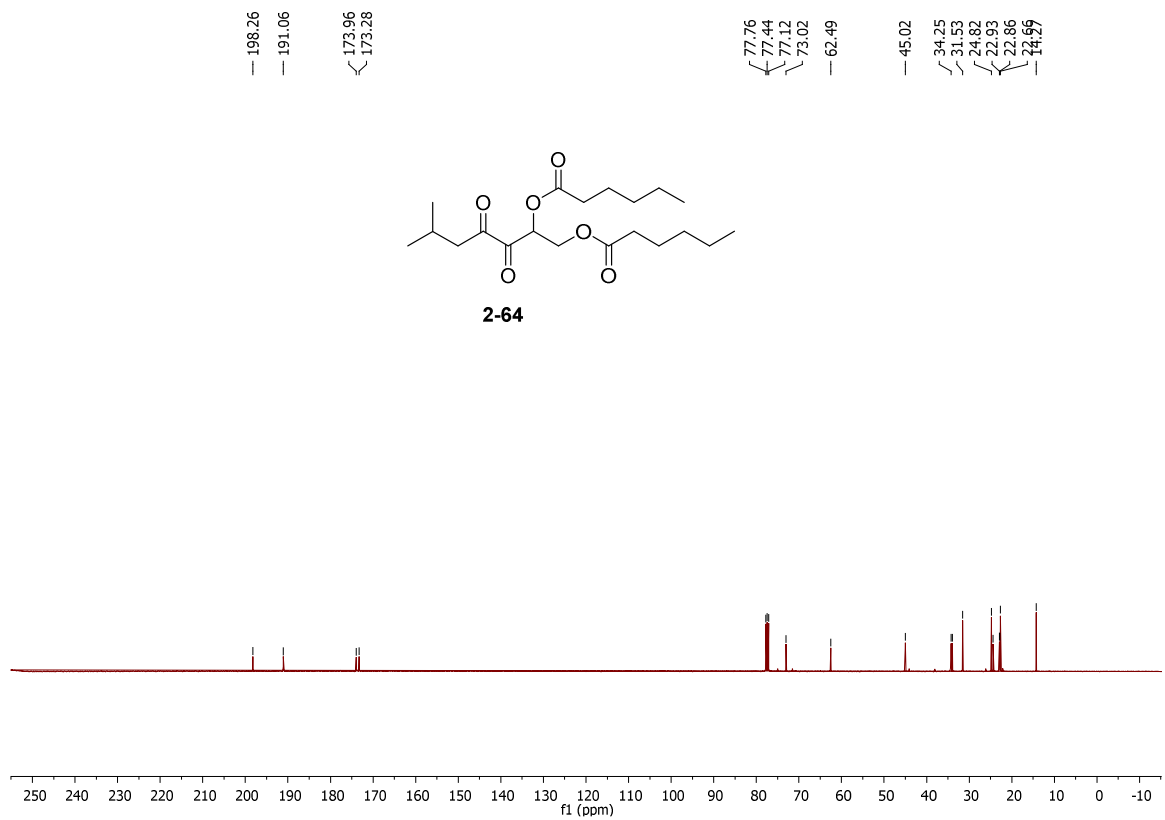
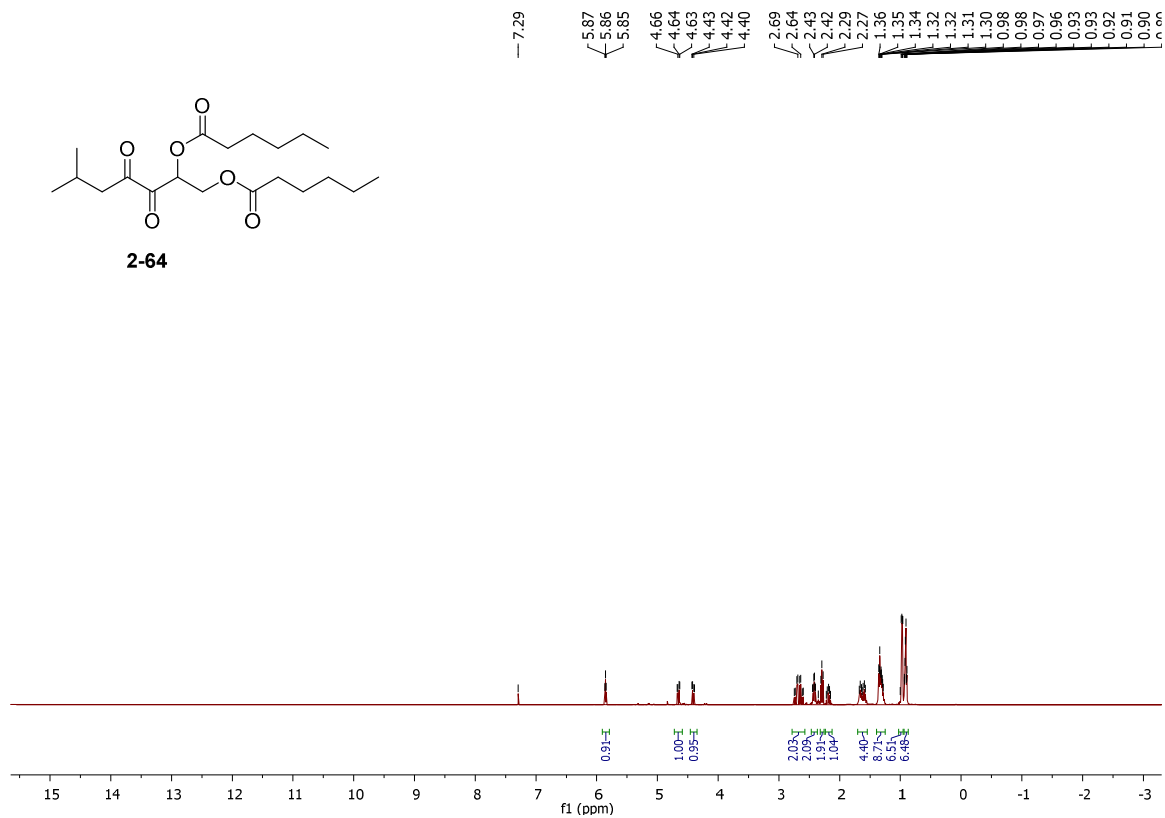


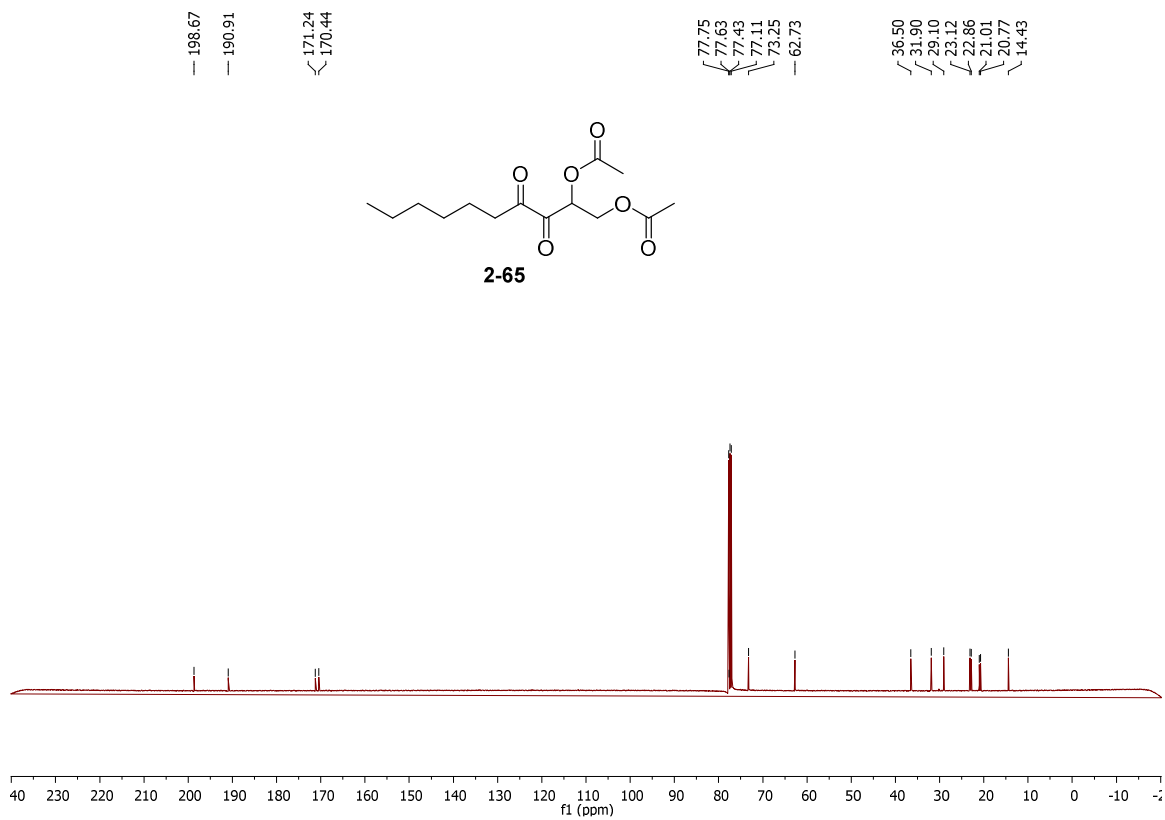
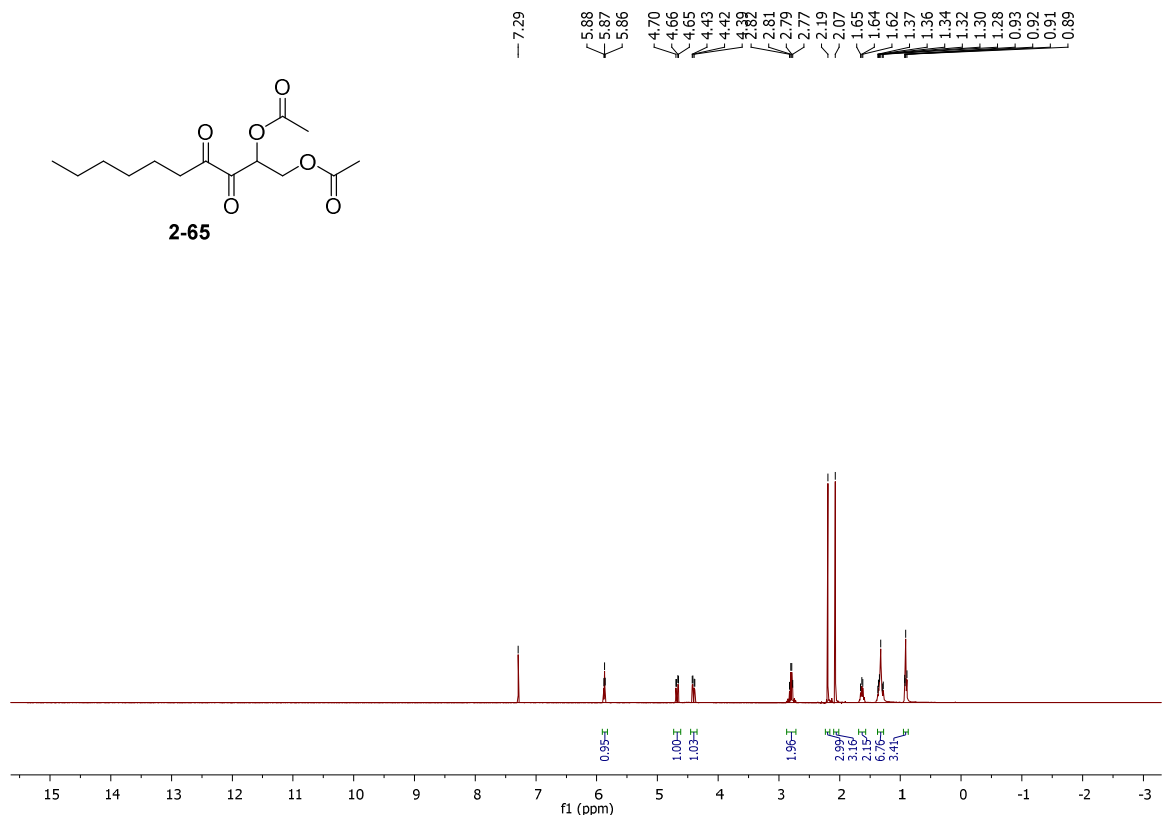


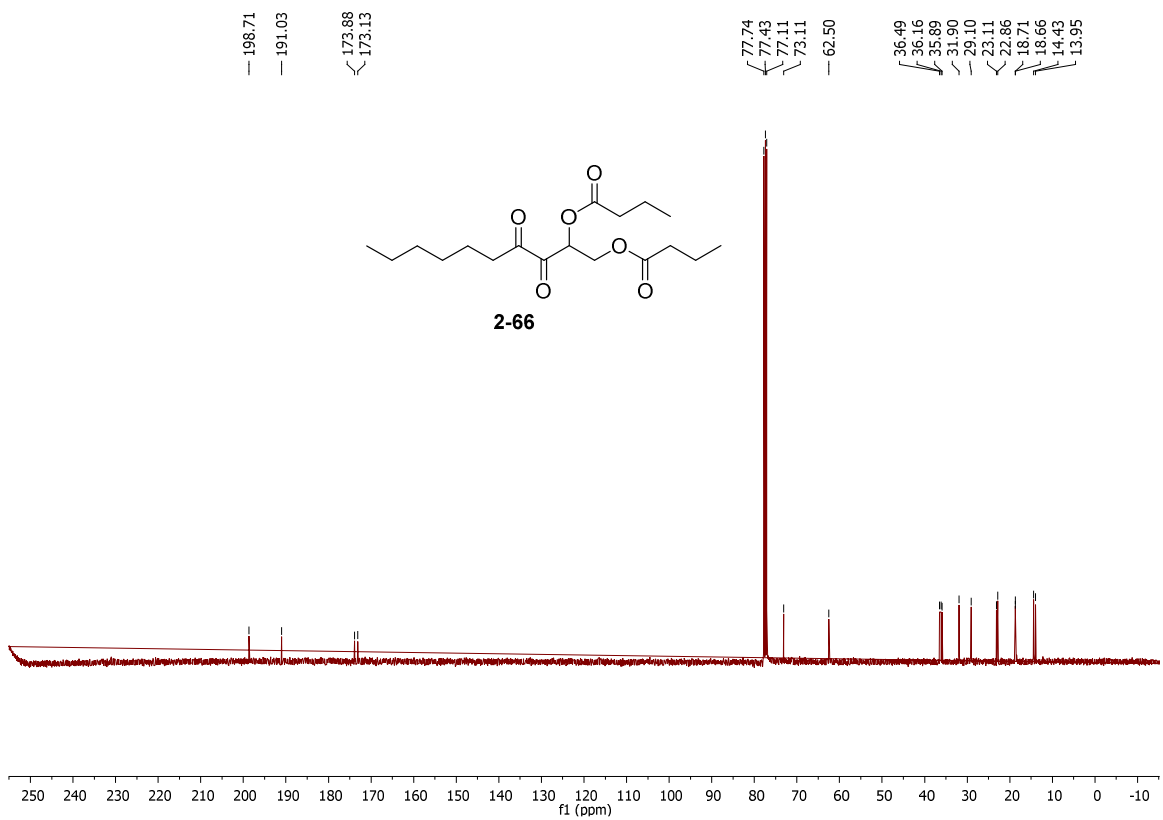
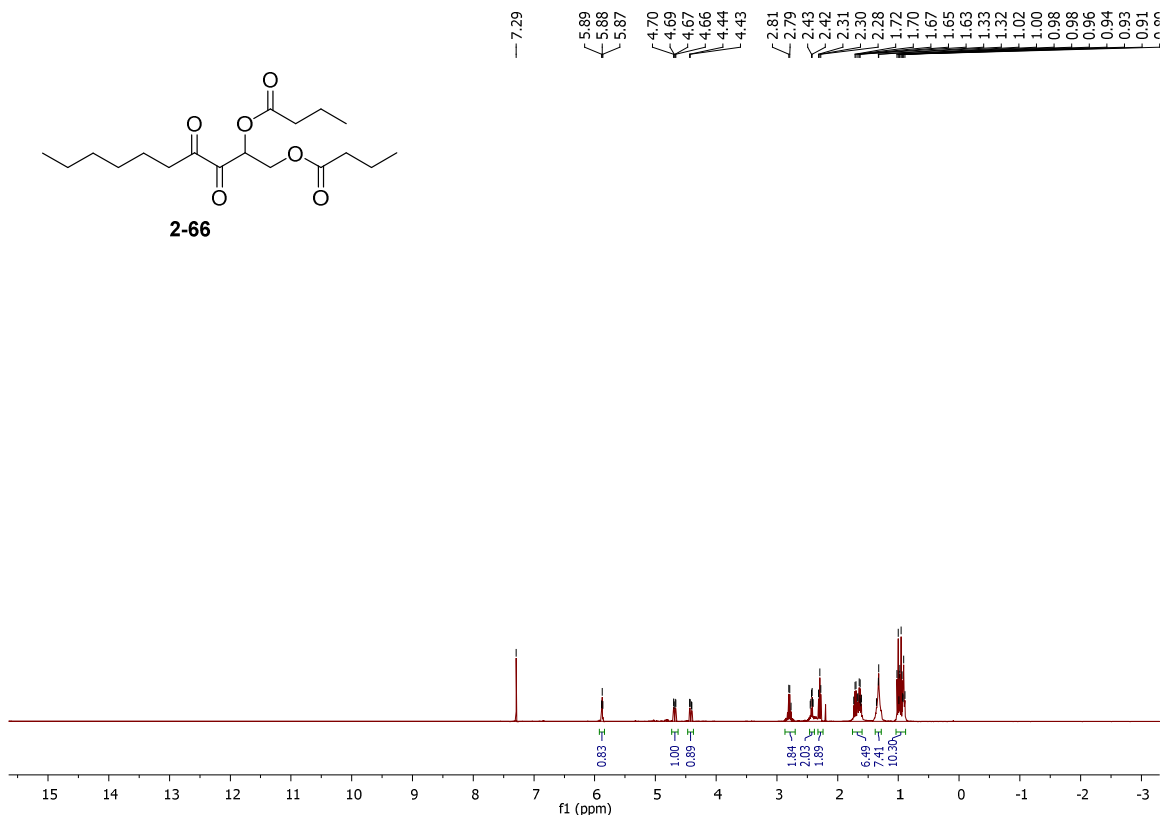


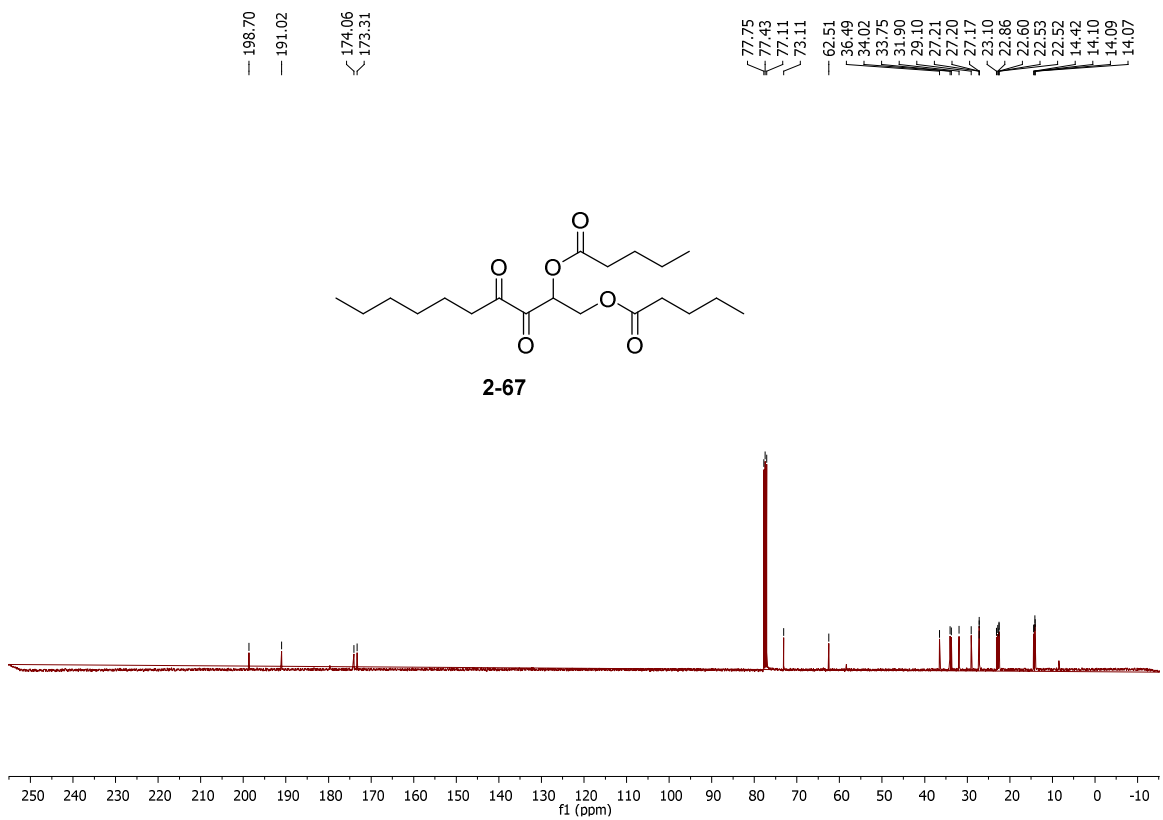
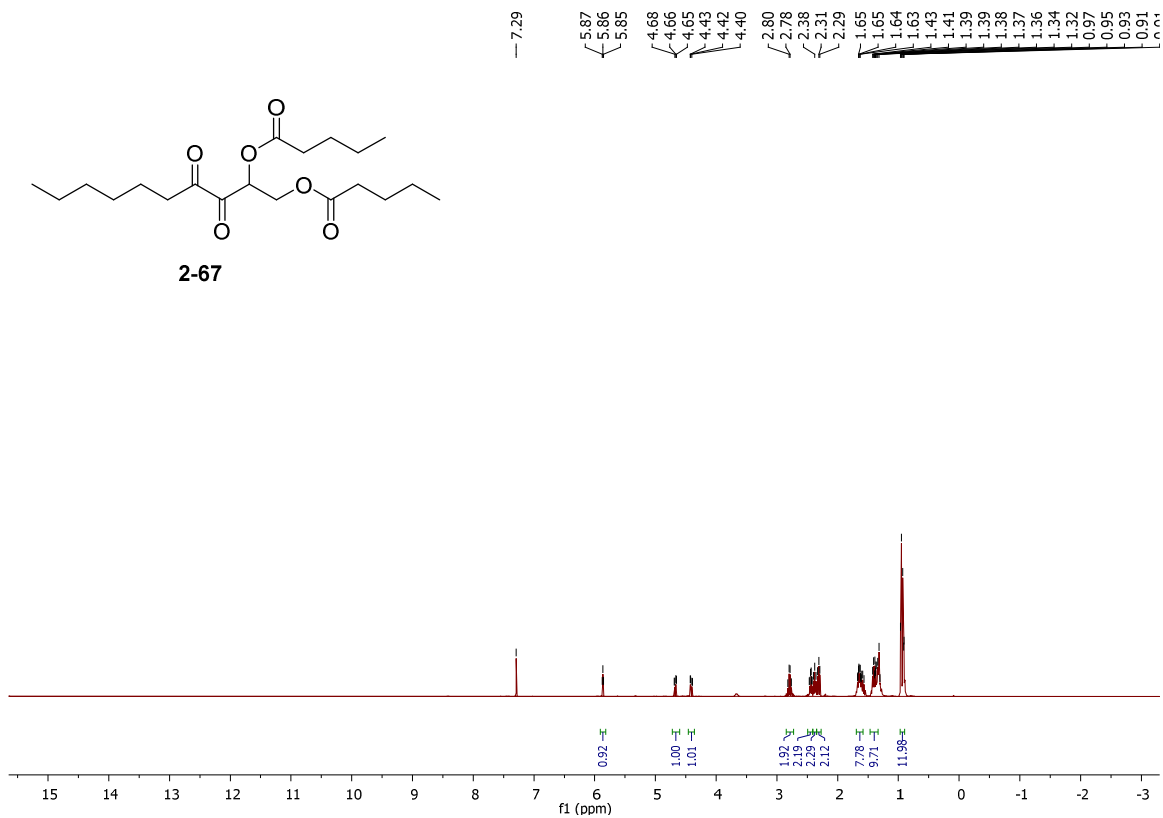


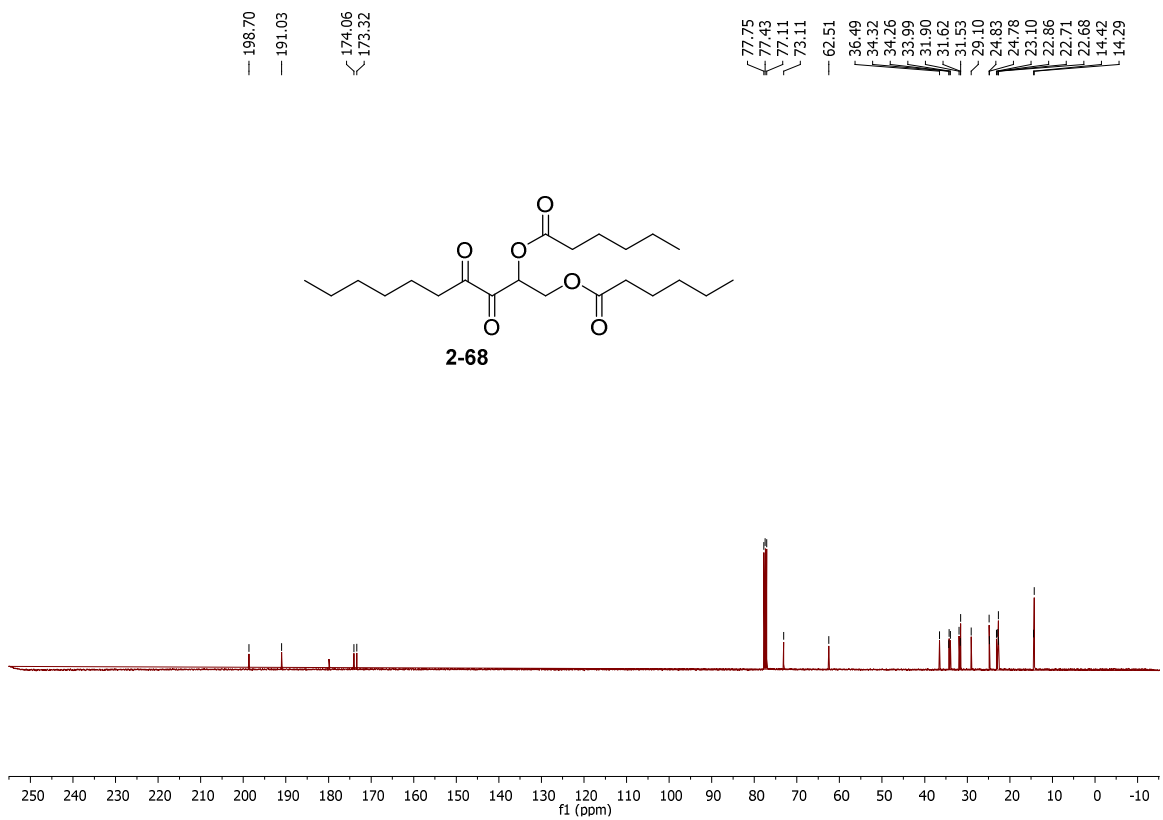
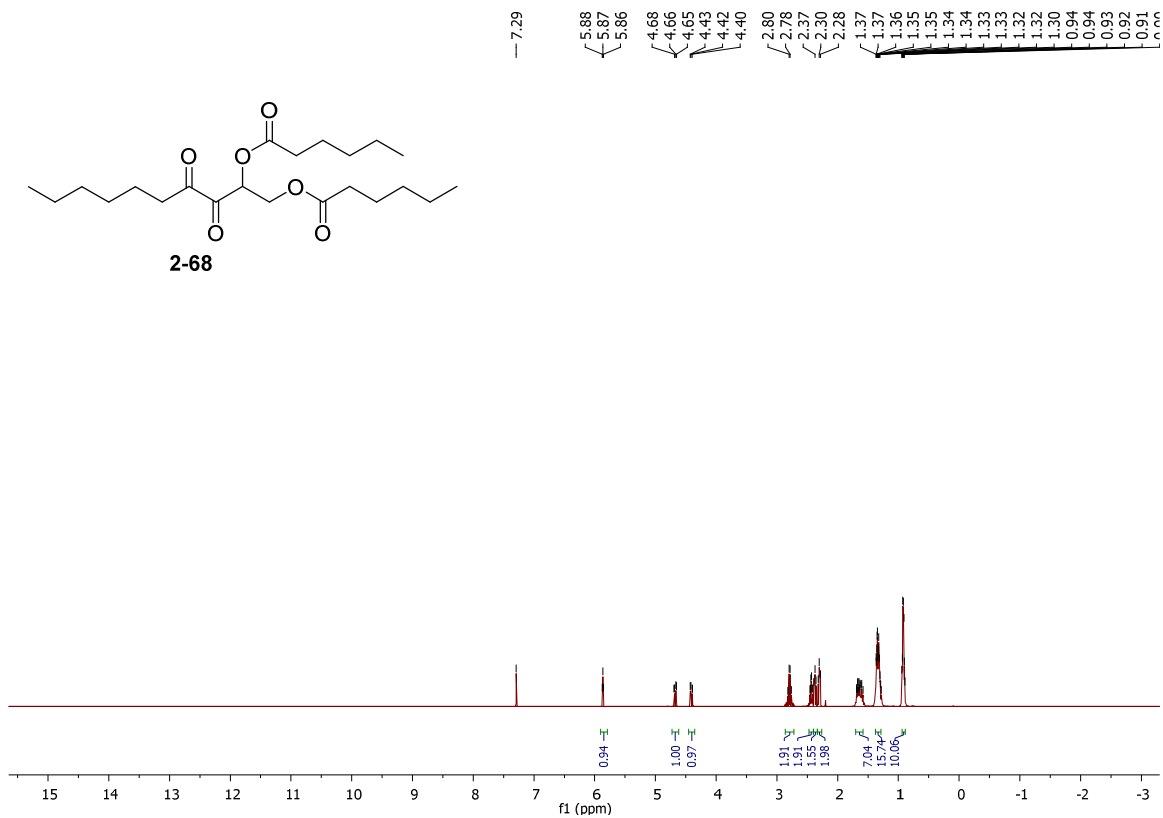


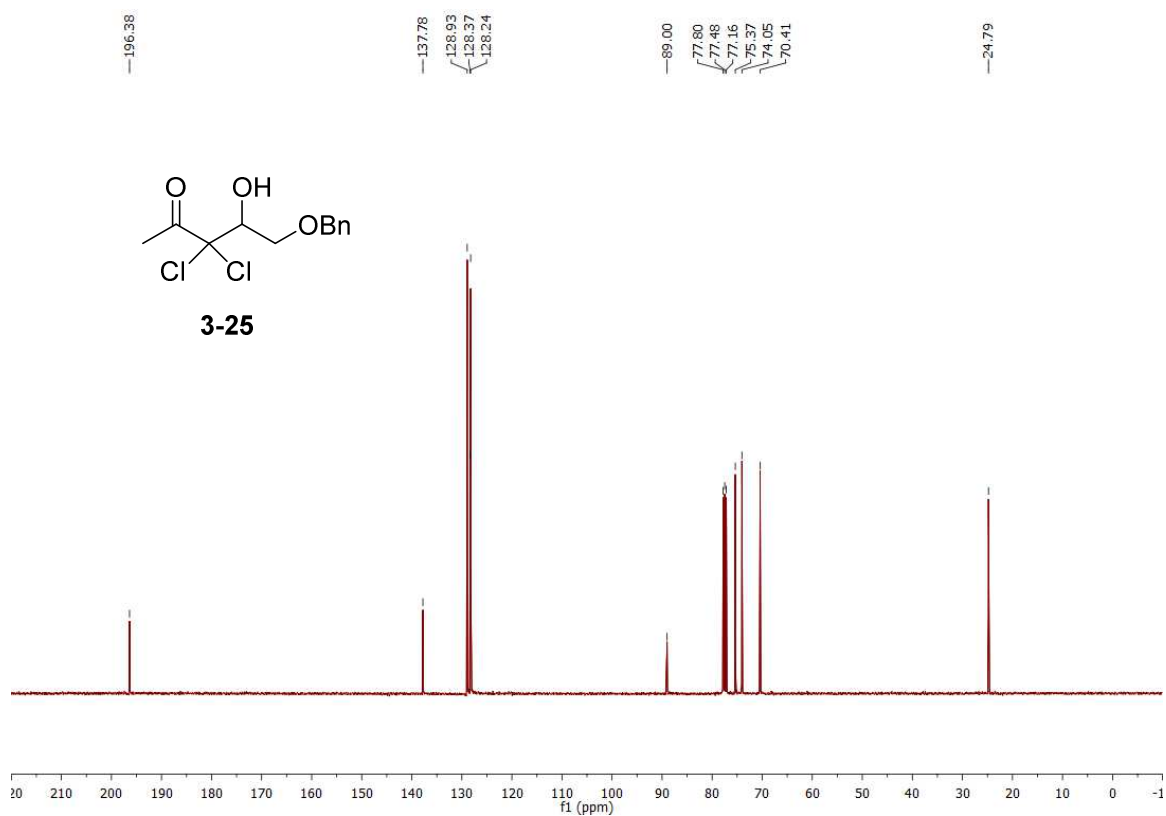
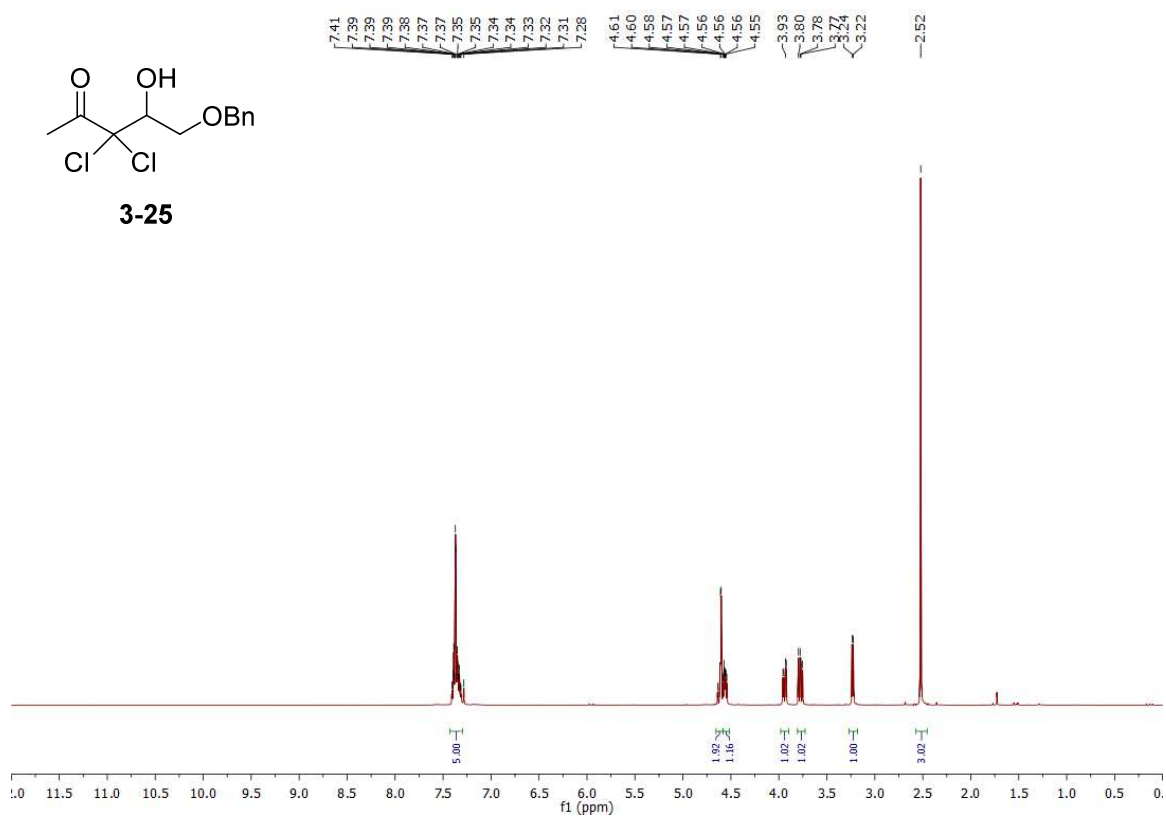


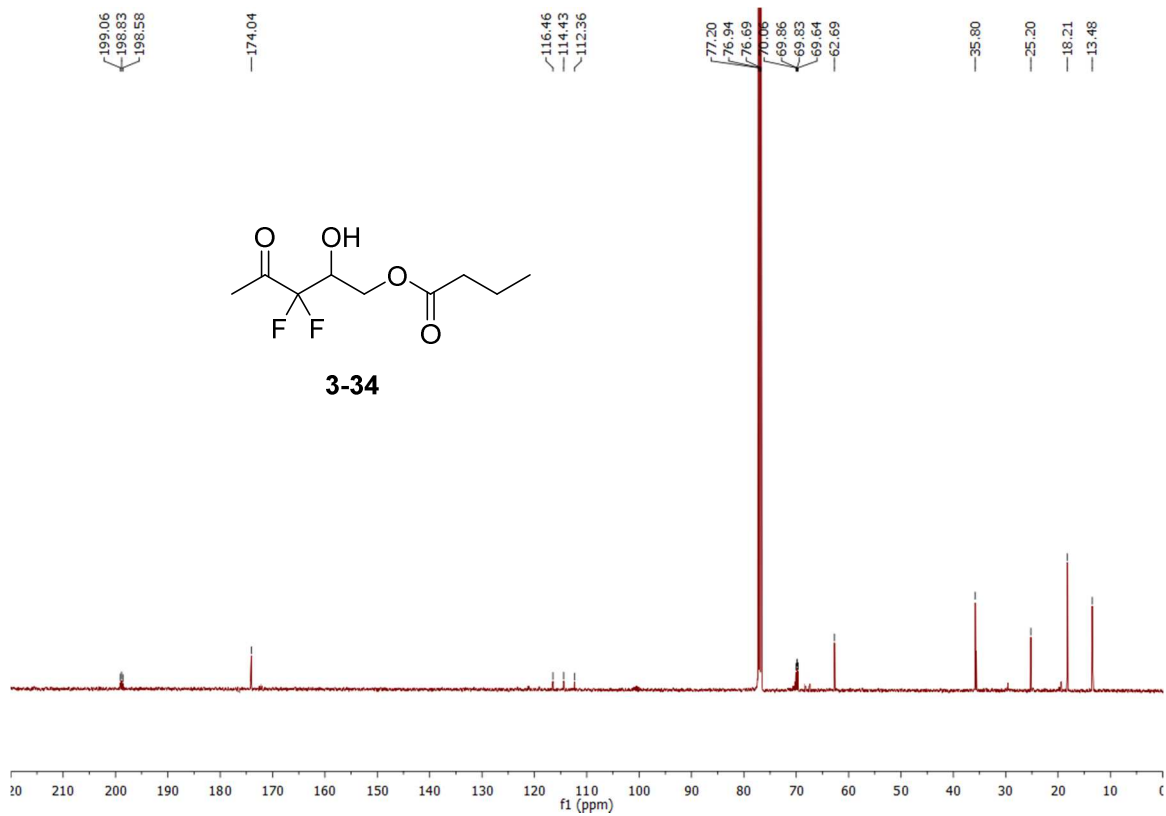
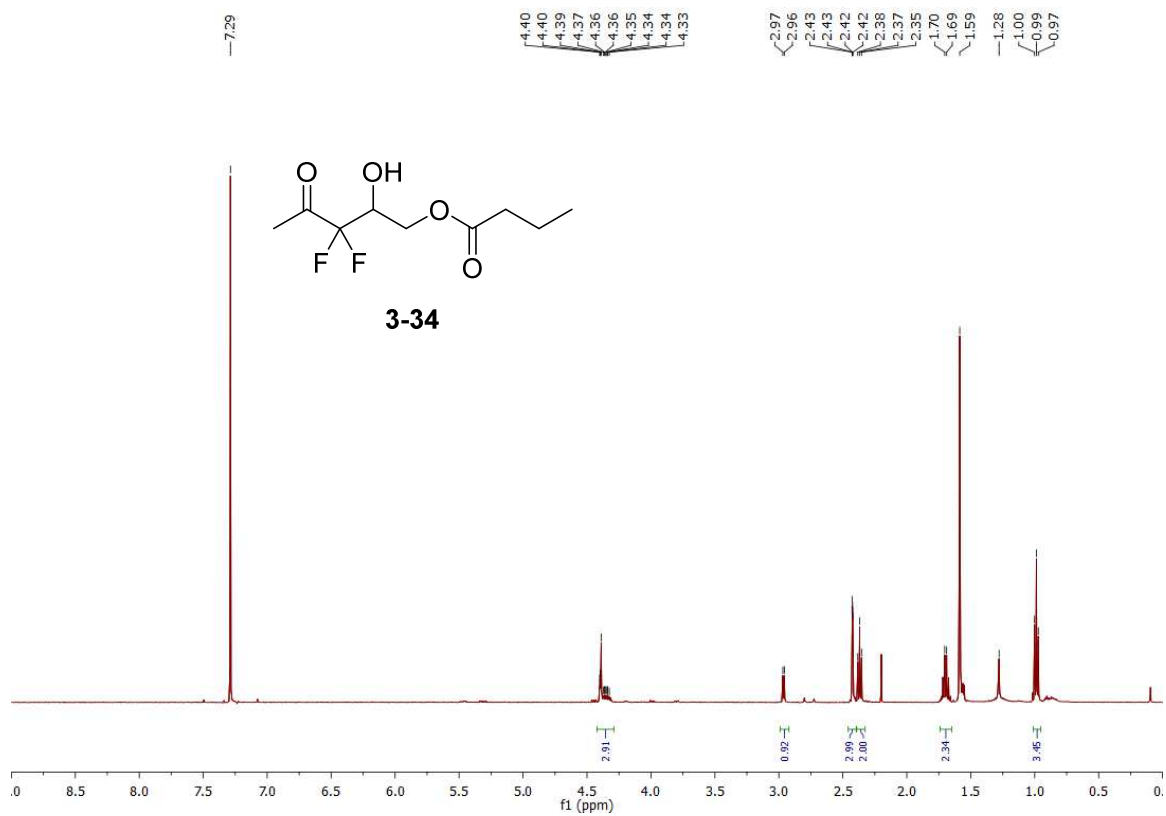


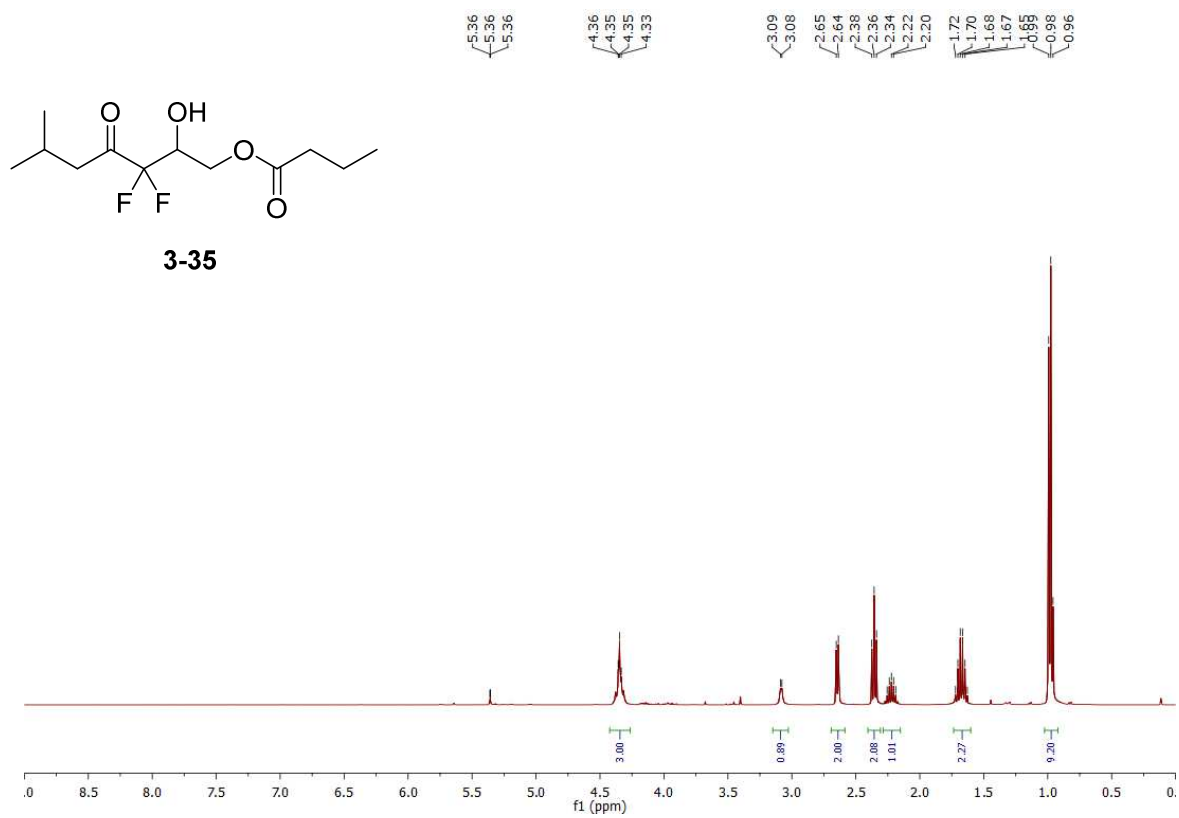
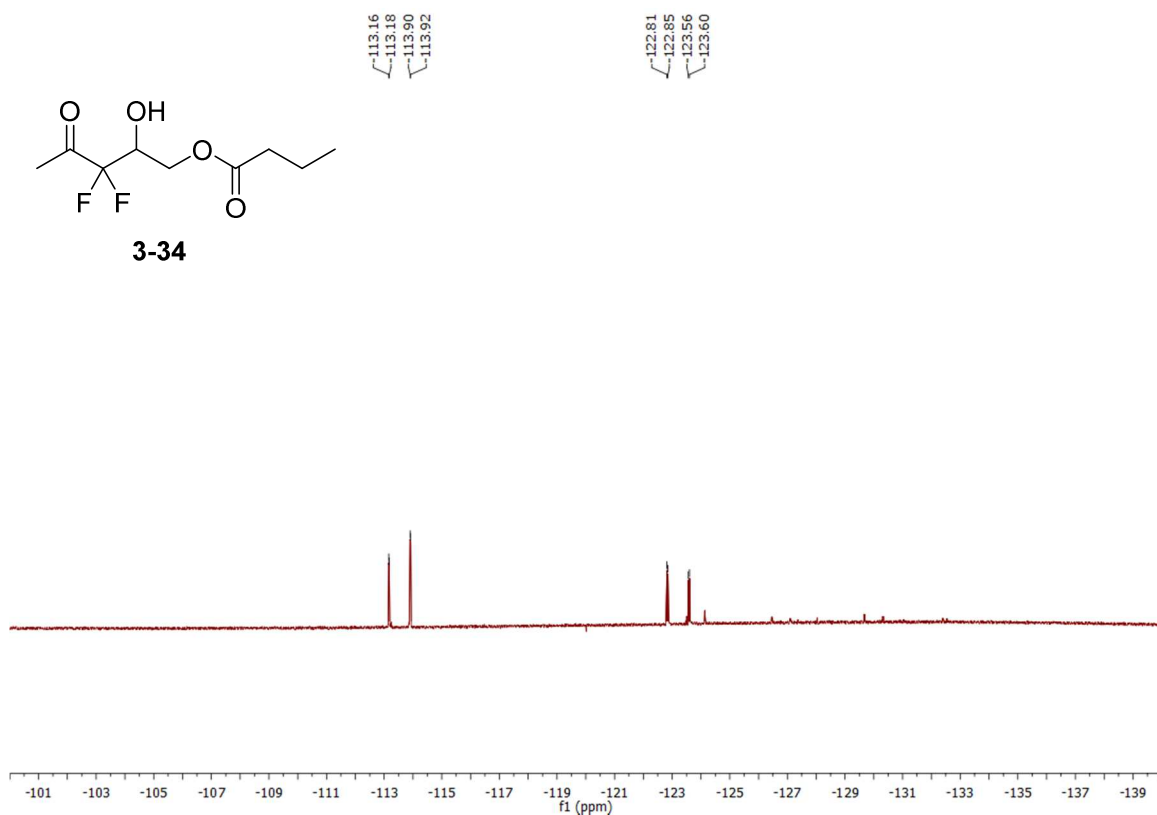


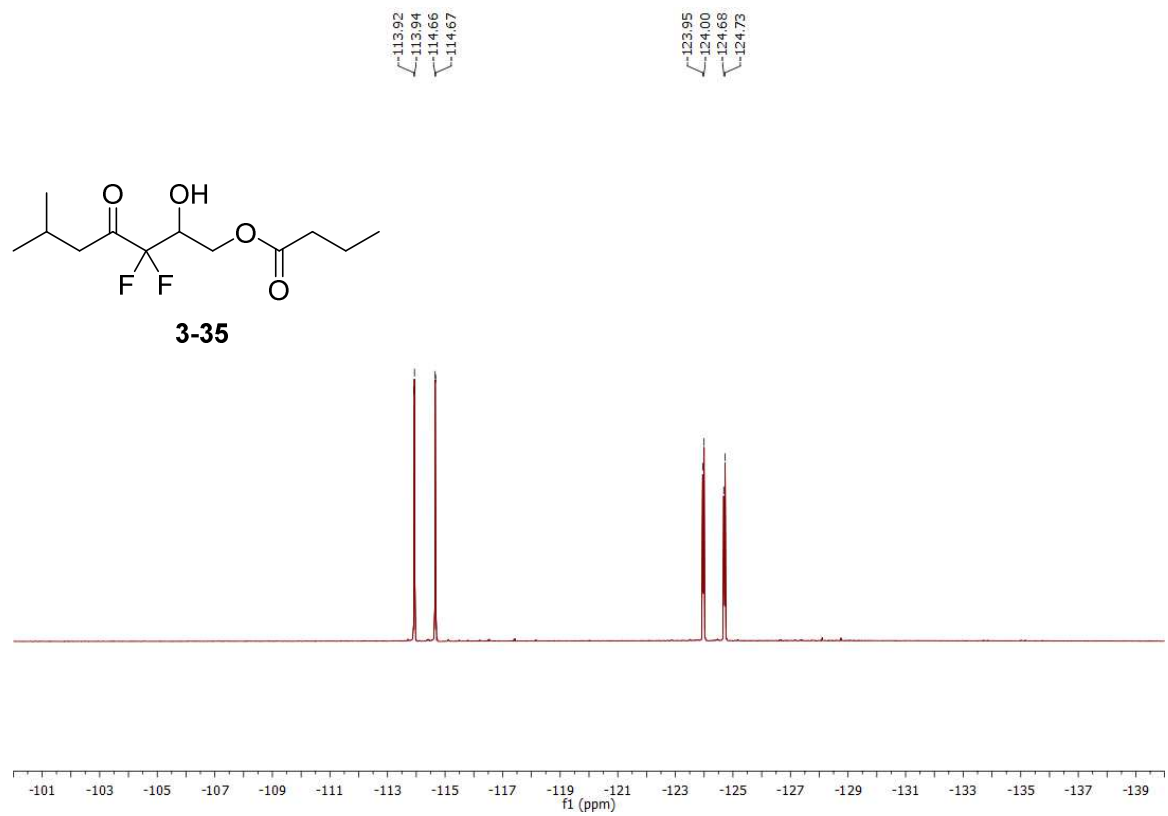
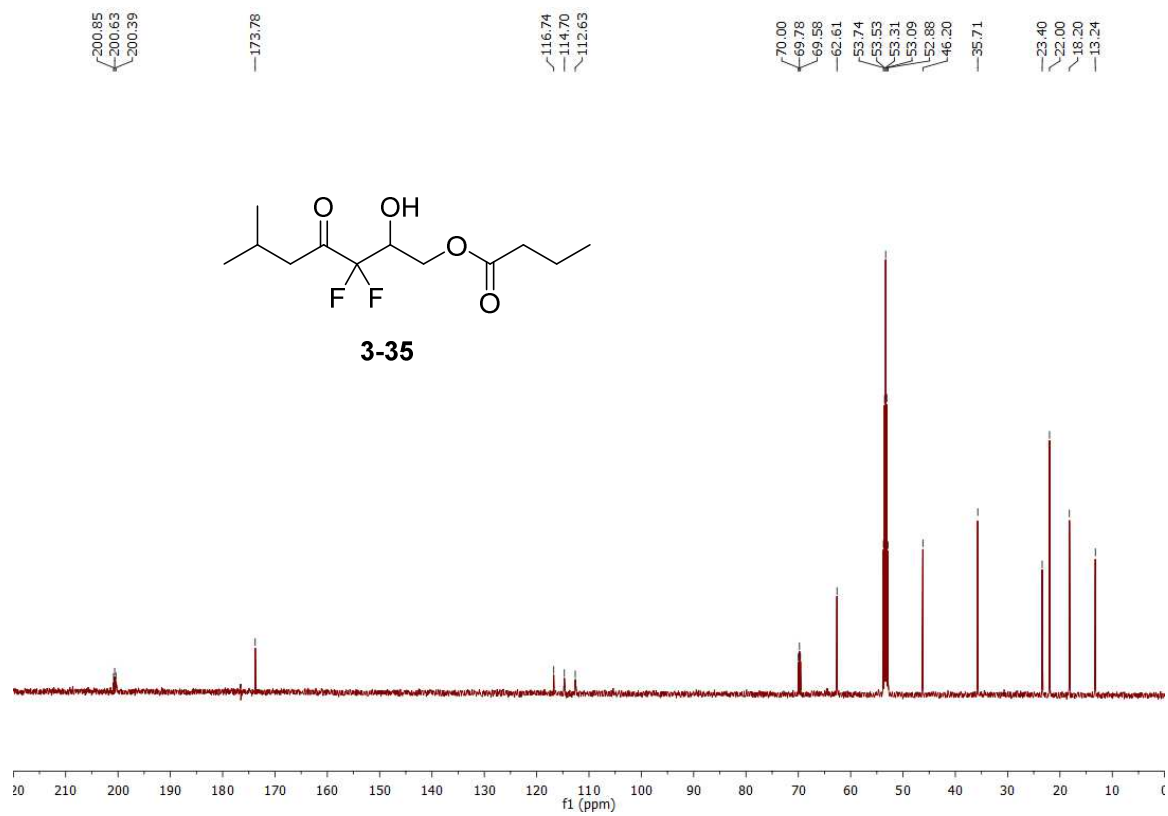


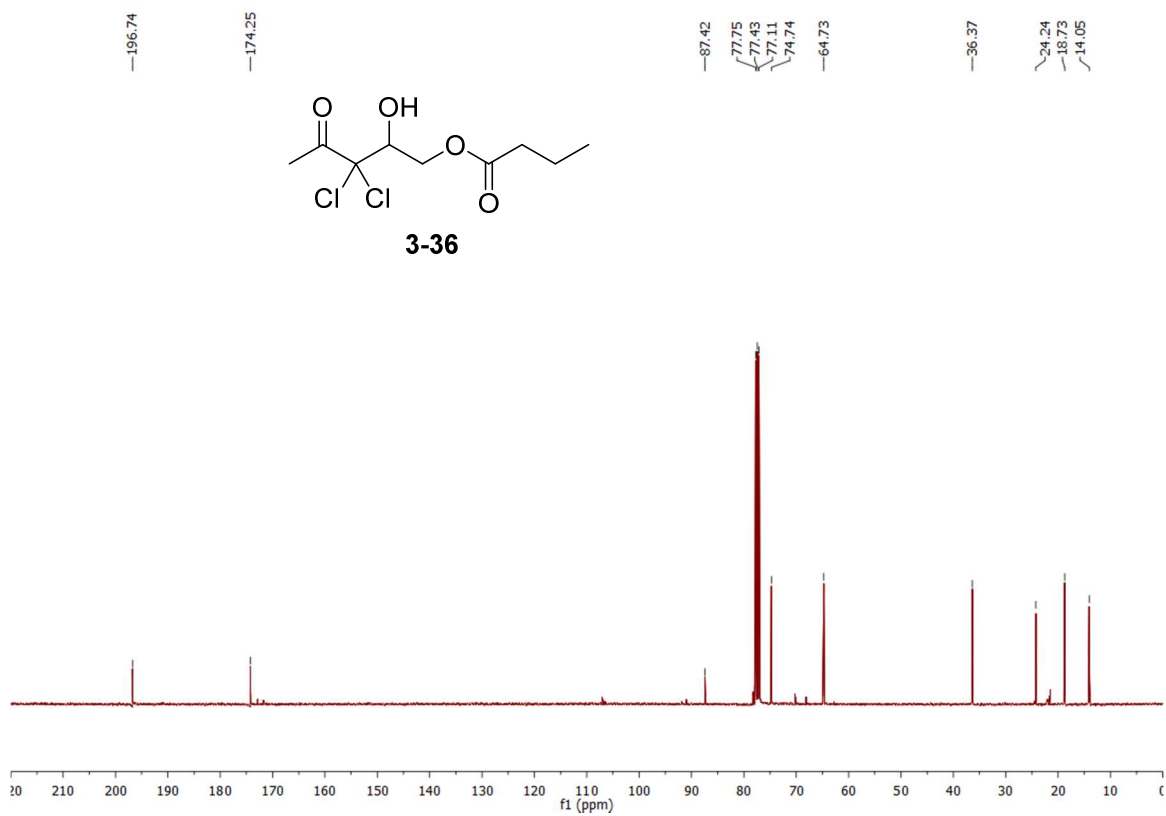
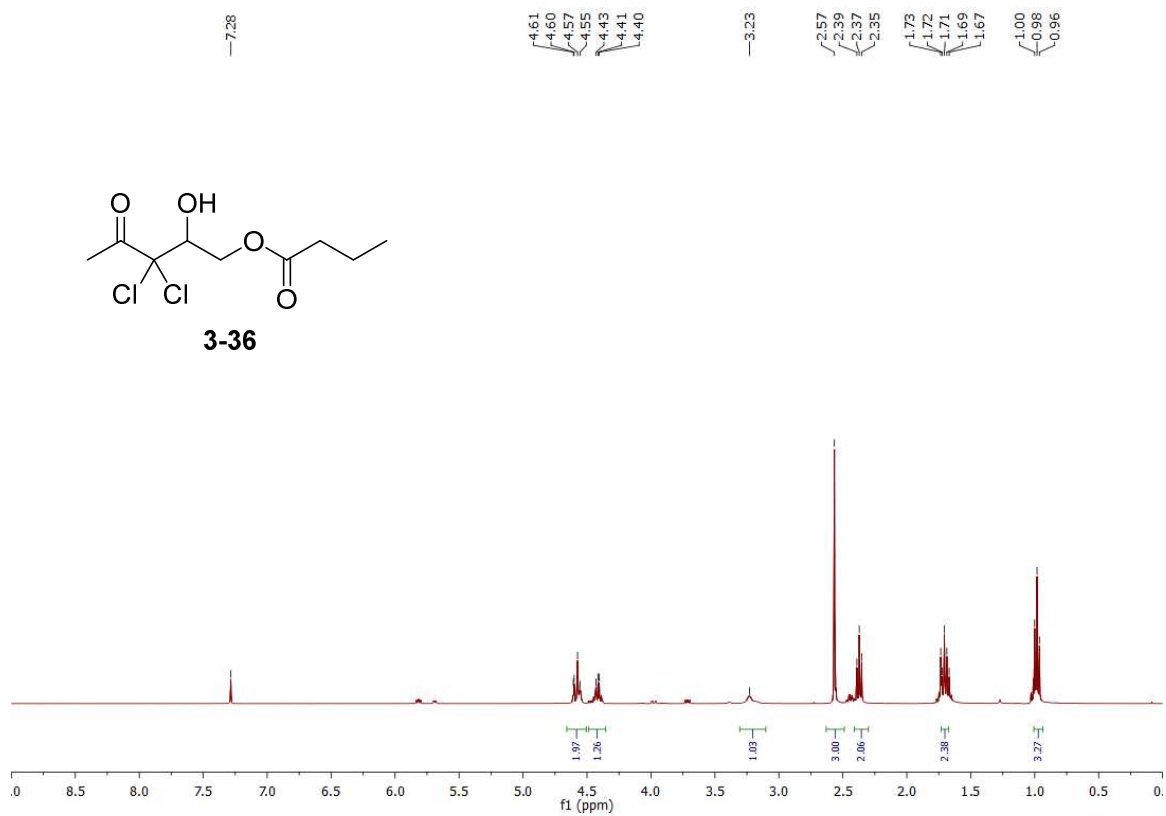


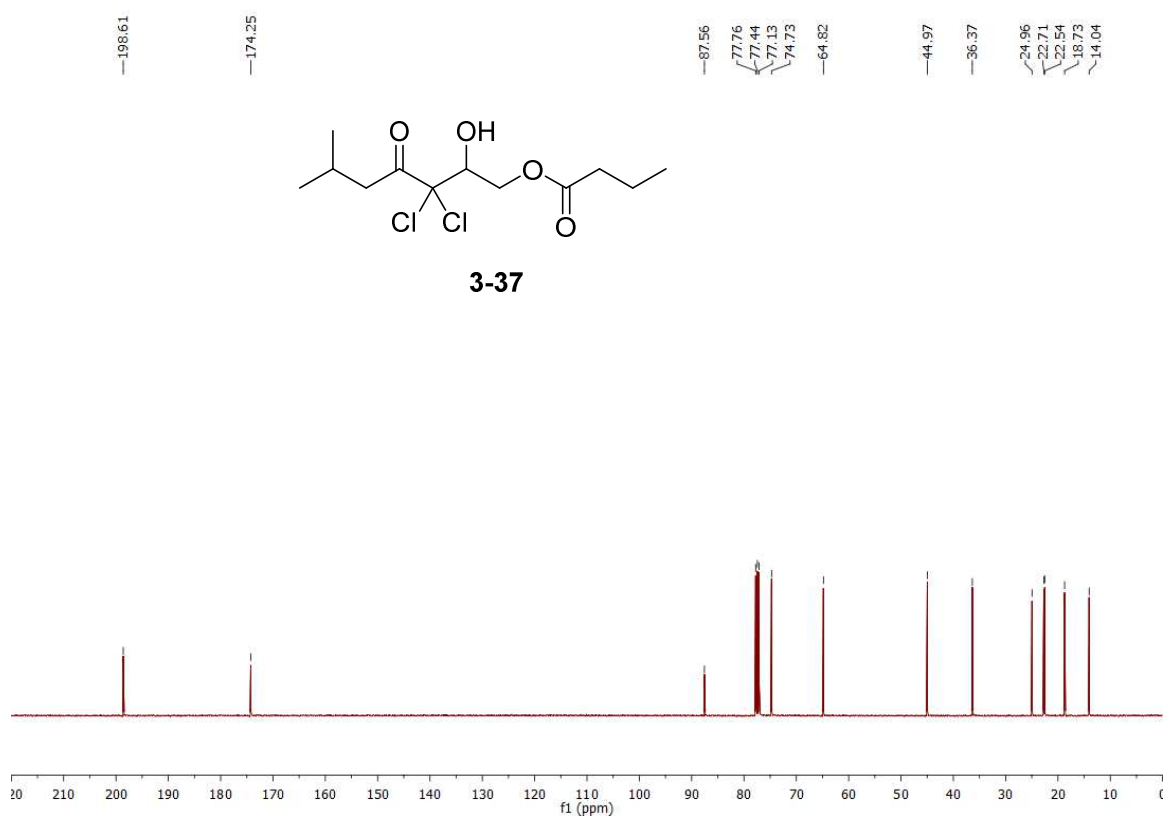
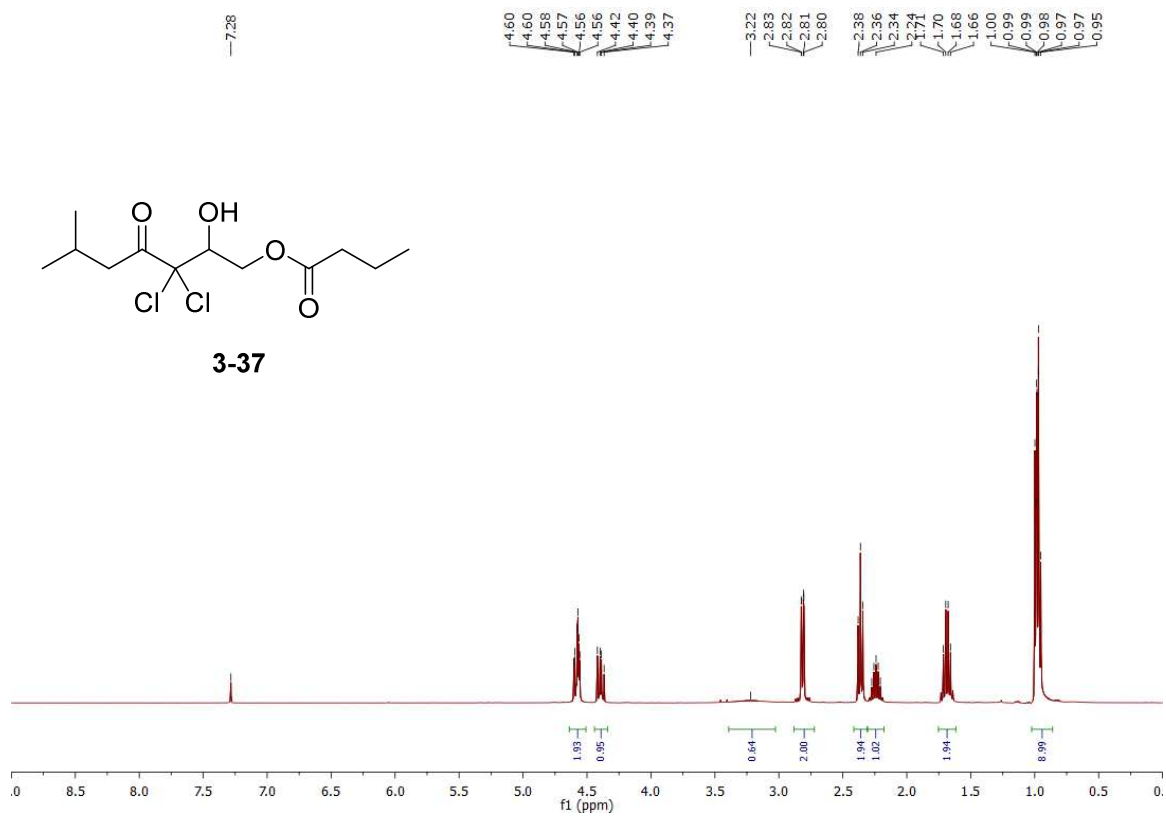


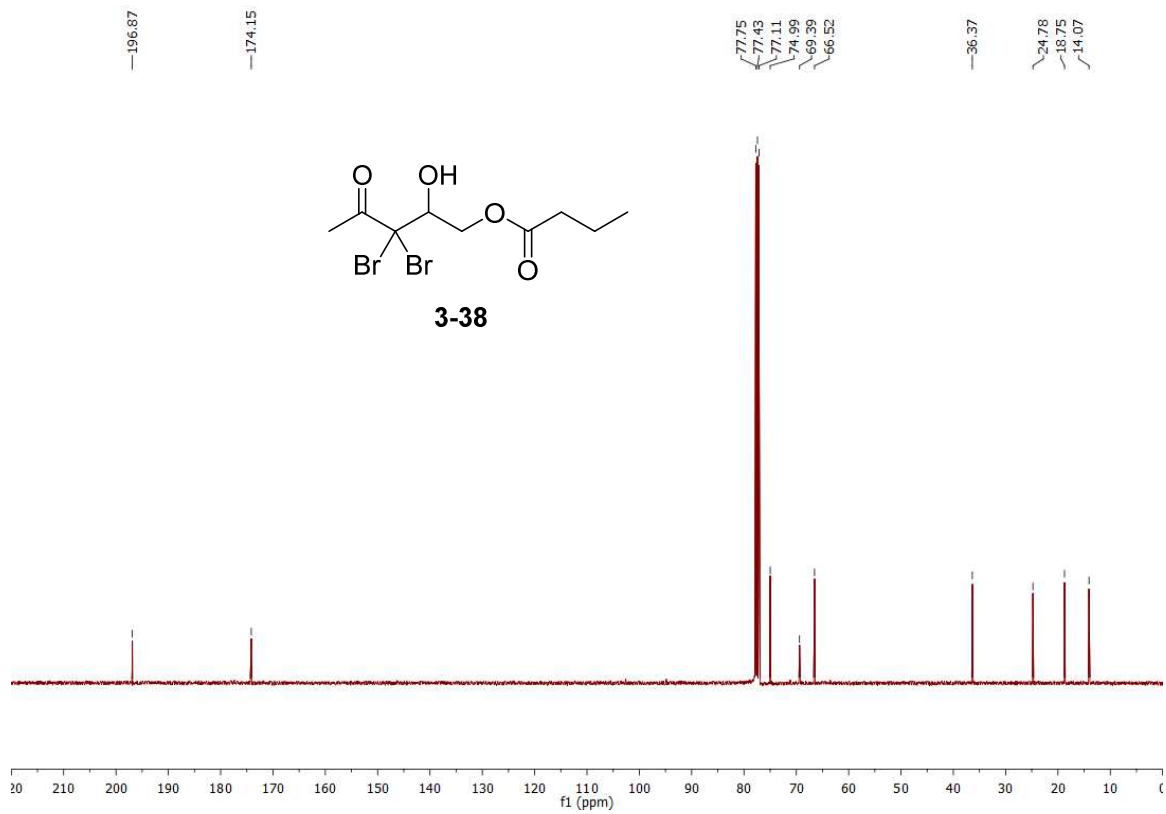
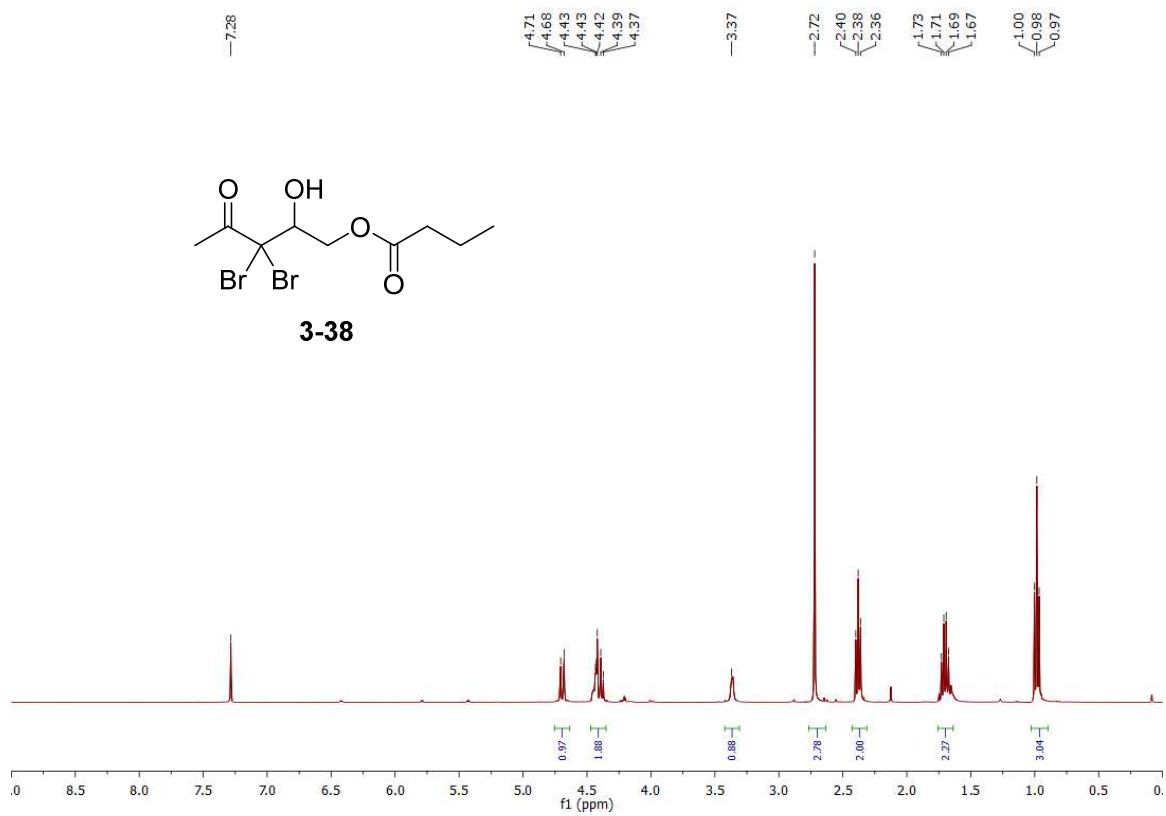


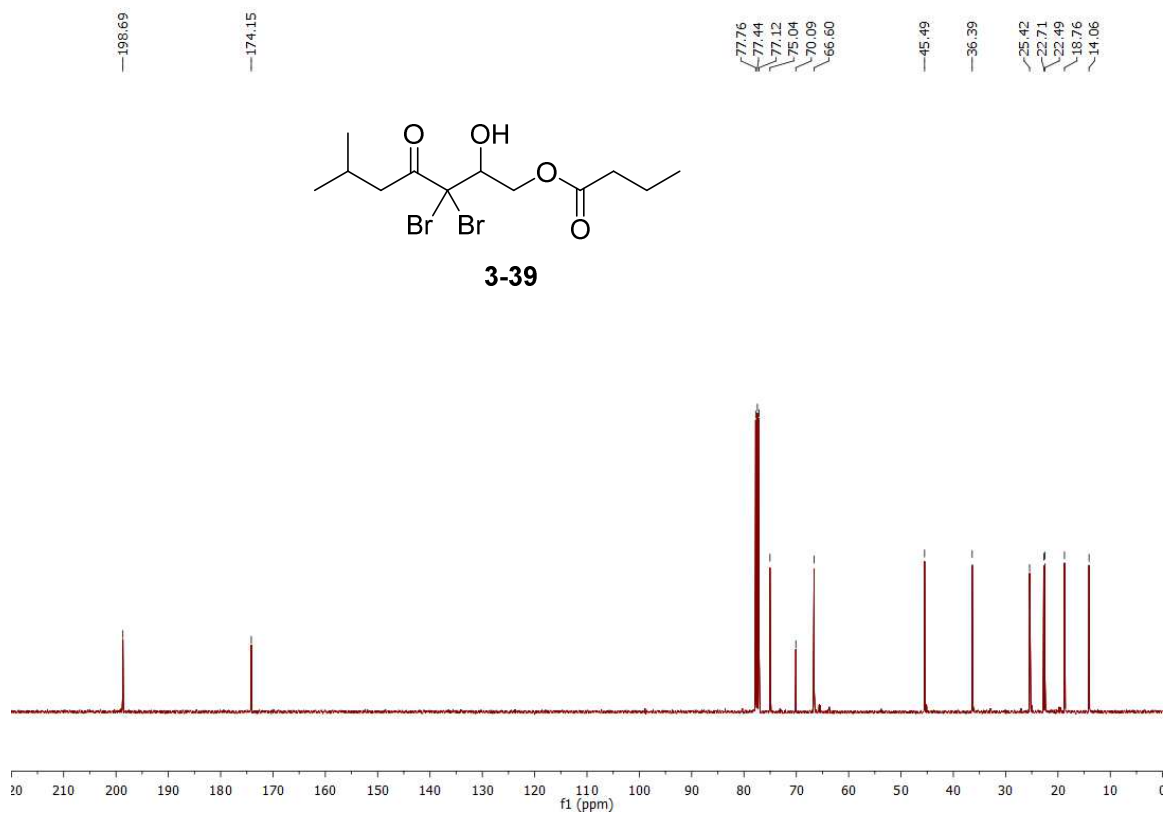
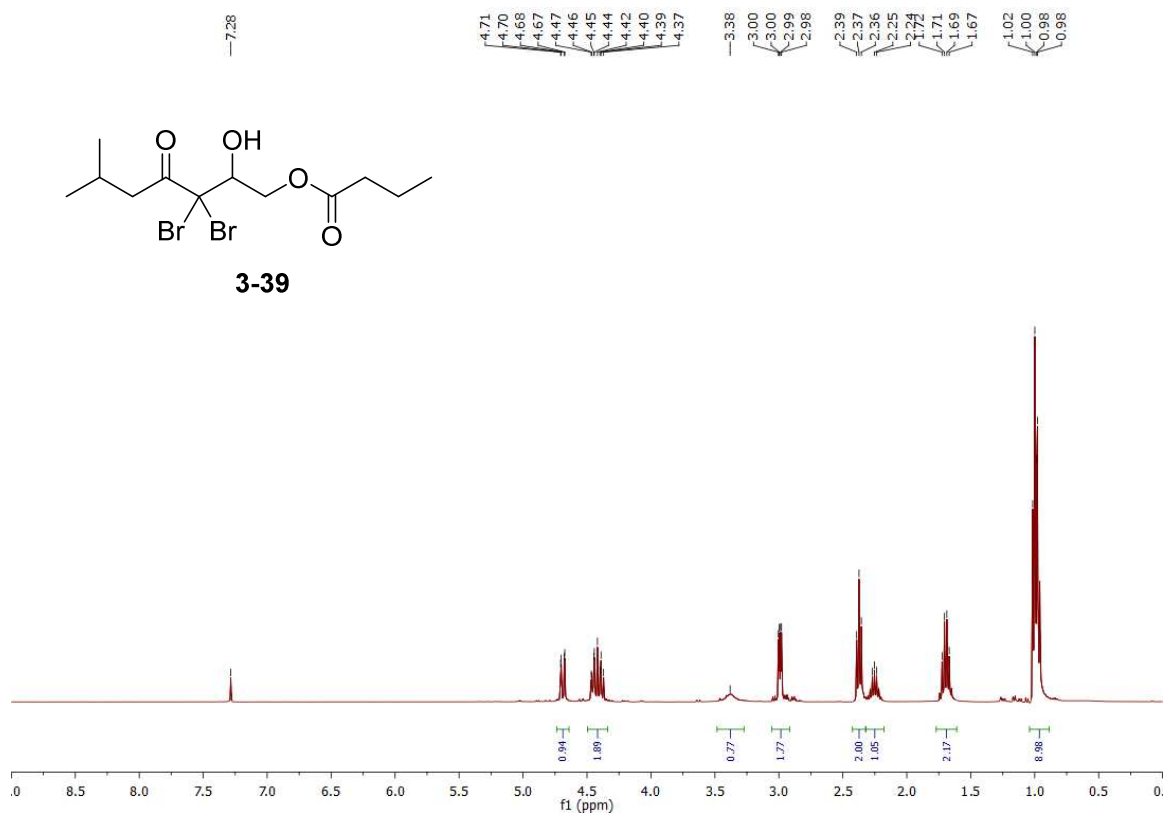


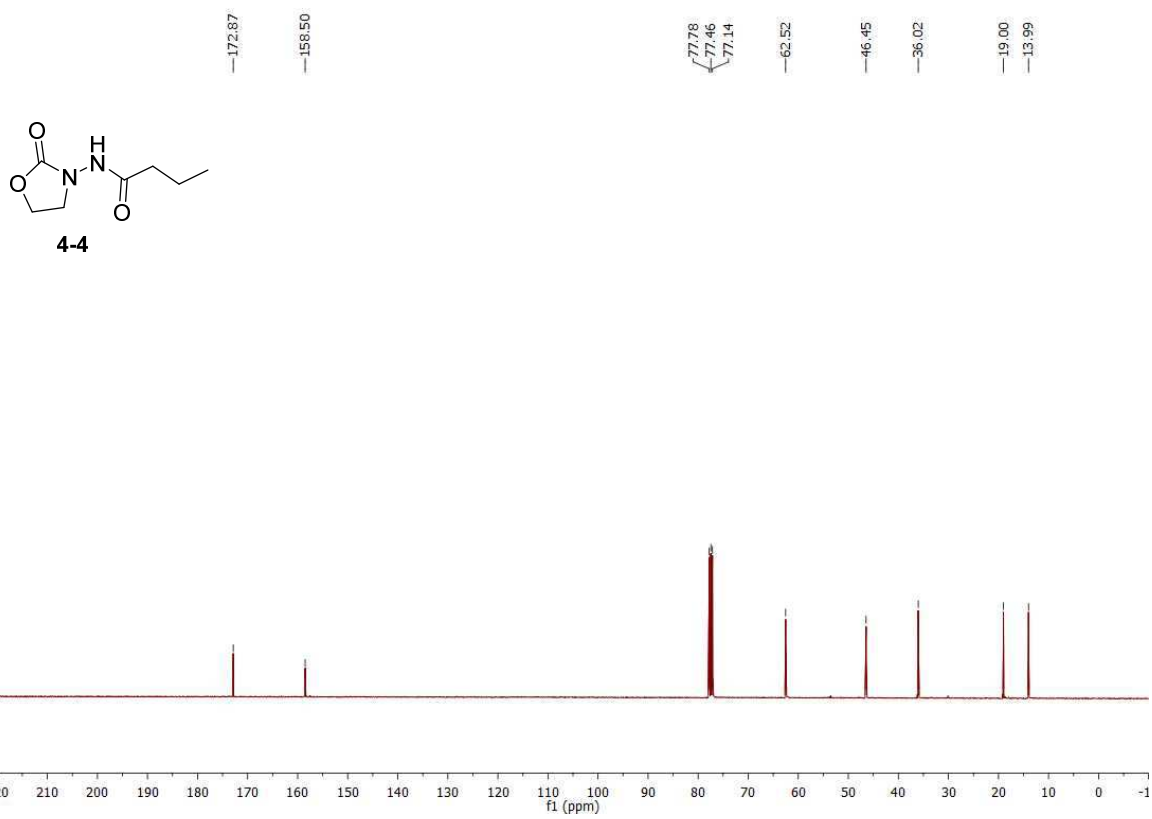
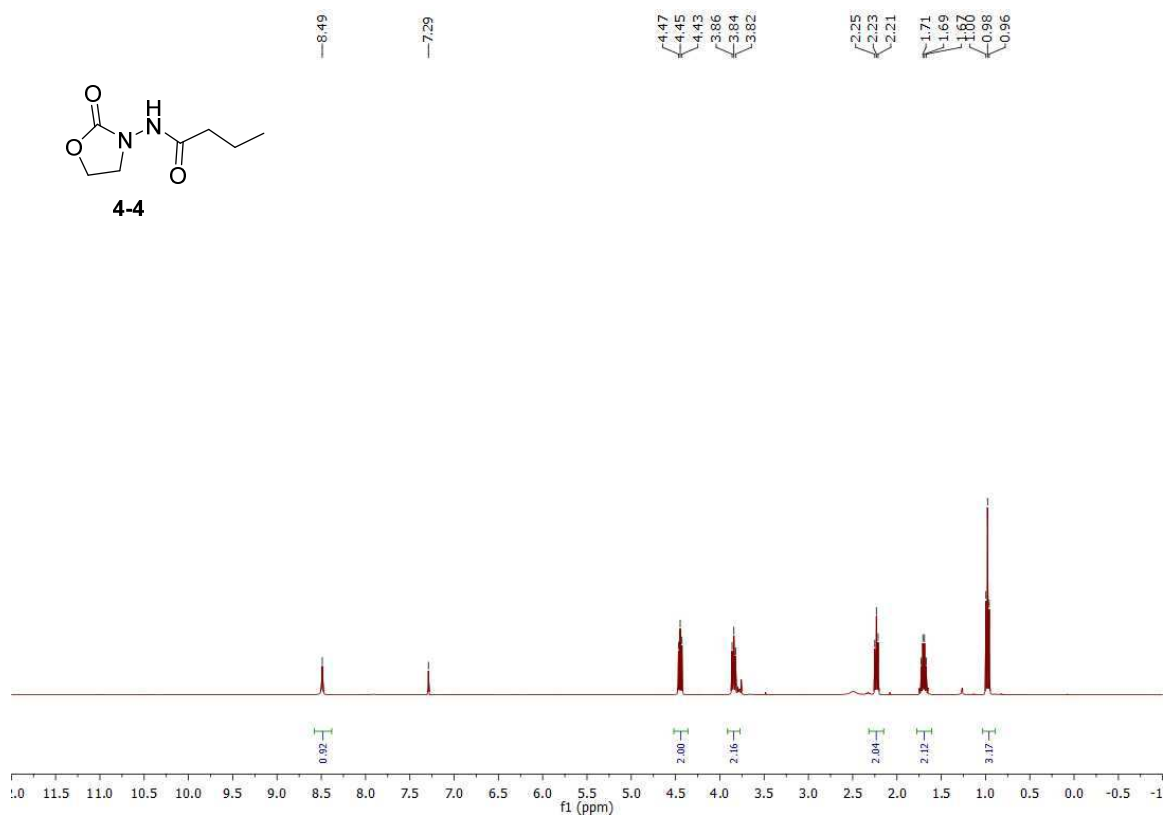
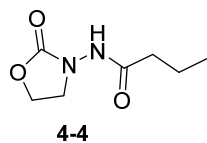


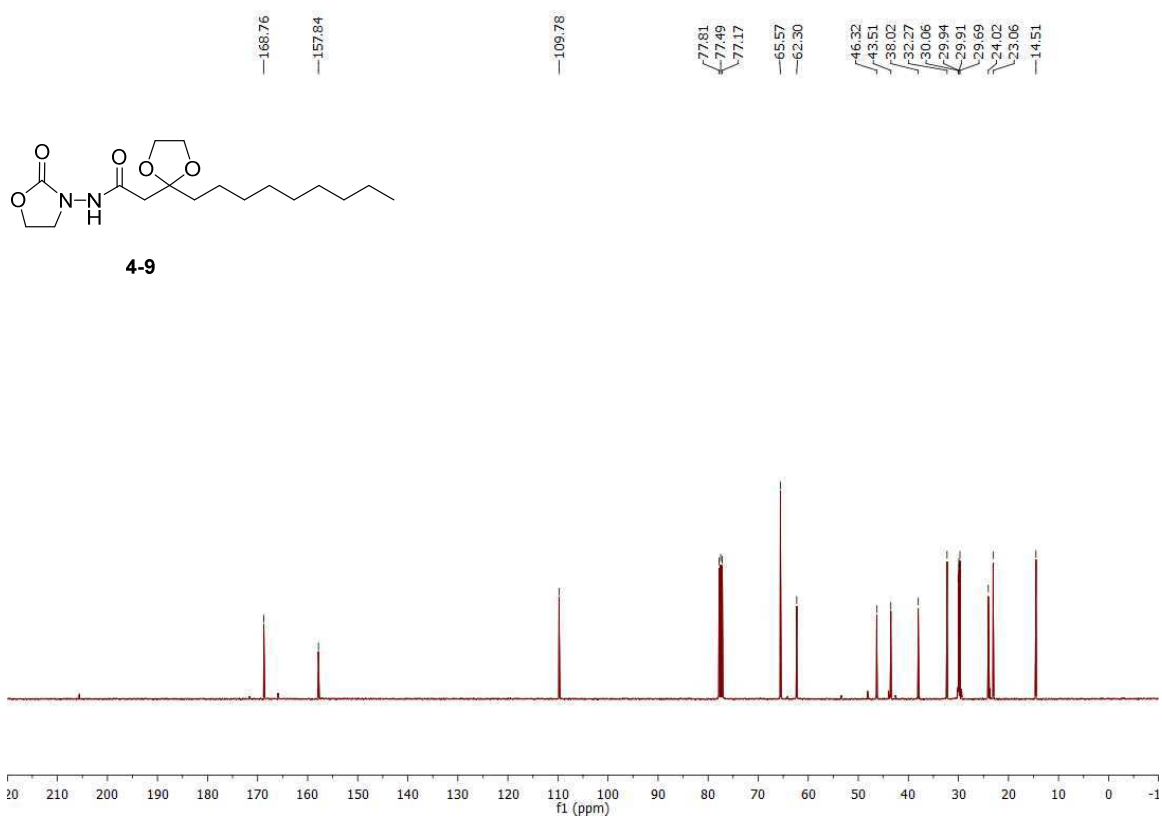
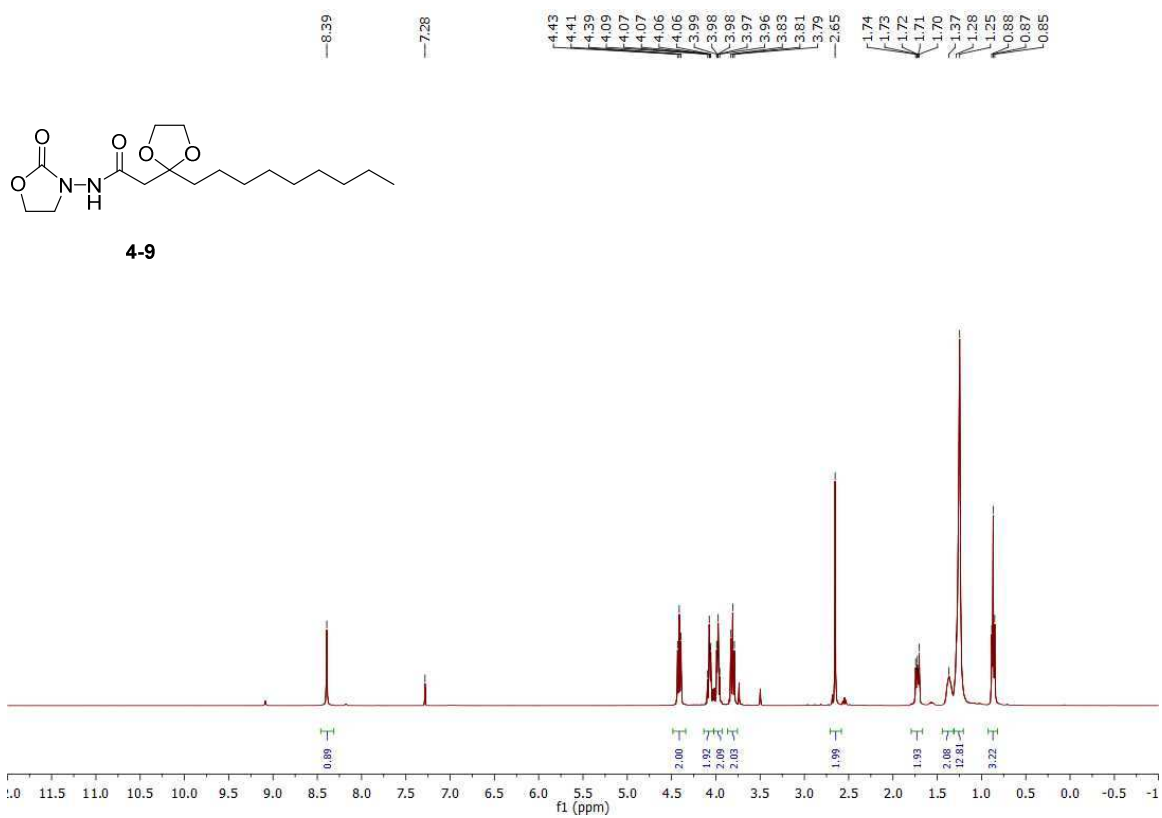


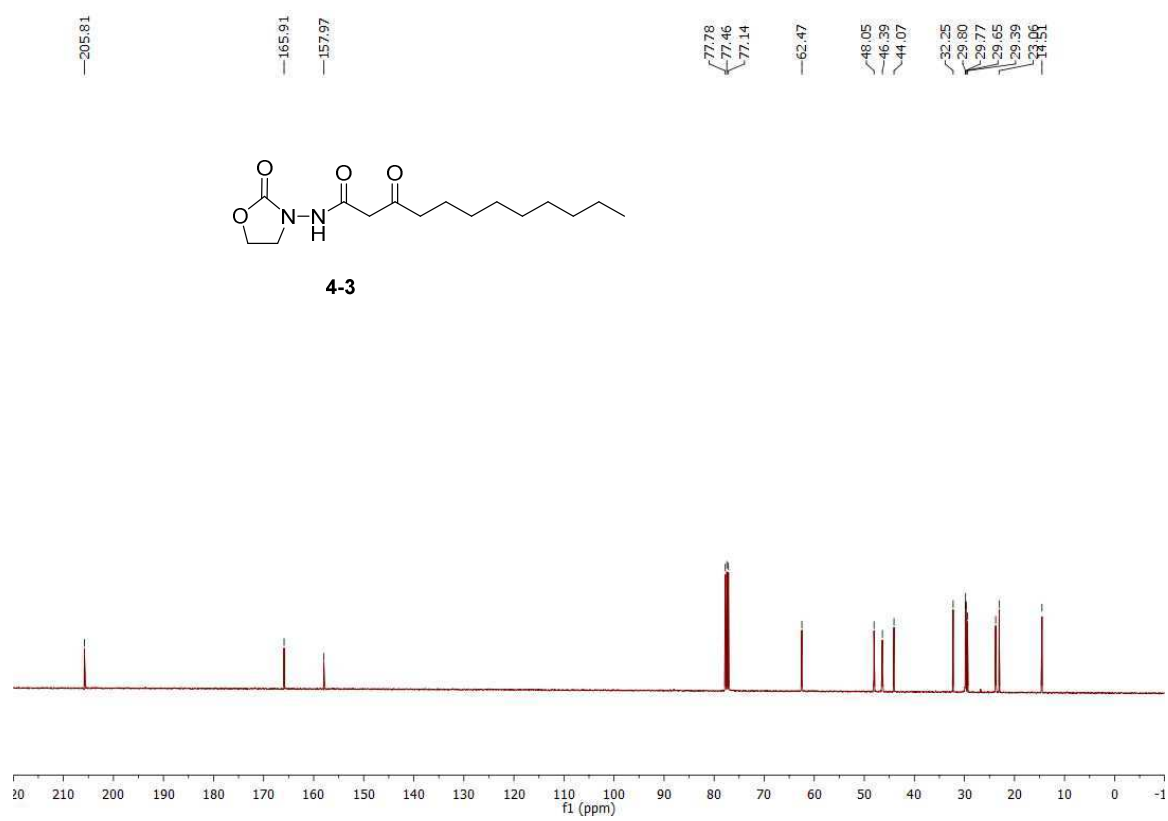
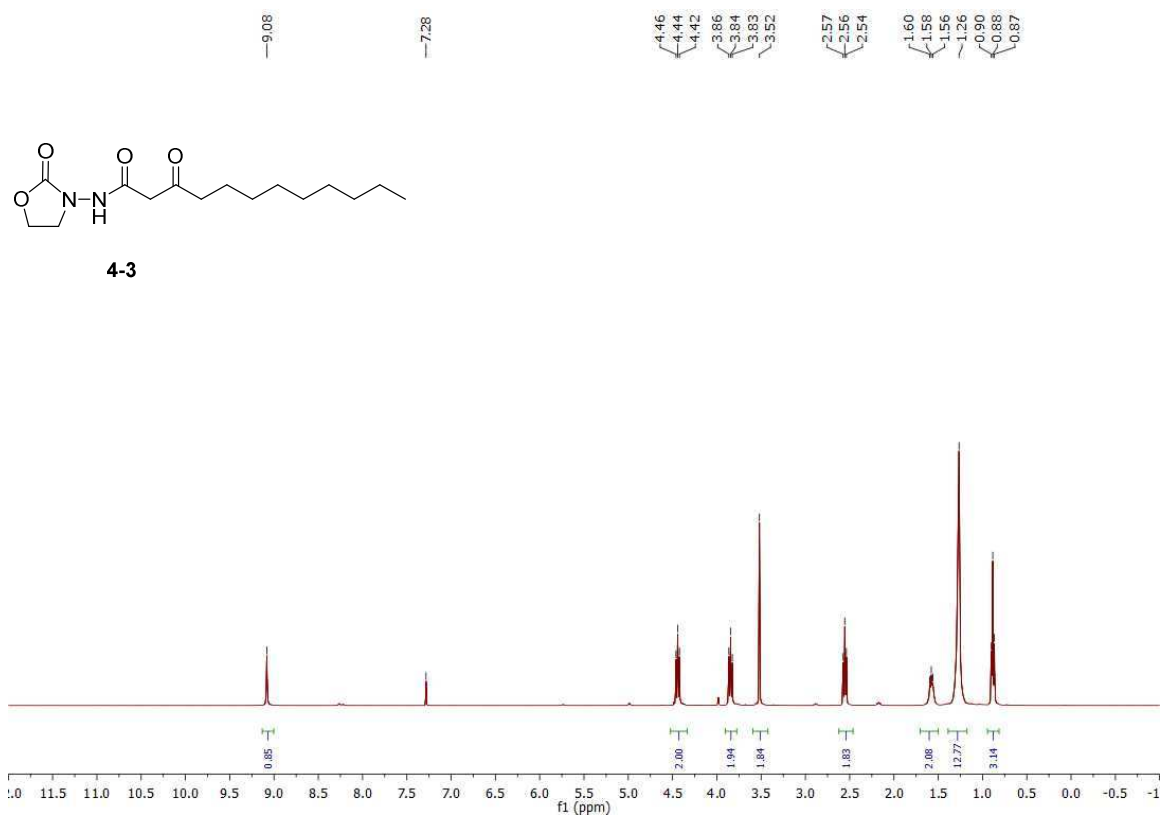












References

1. (a) Palumbi, S. R., Humans as the world's greatest evolutionary force. *Science* **2001**, 293 (5536), 1786-90; (b) Clatworthy, A. E.; Pierson, E.; Hung, D. T., Targeting virulence: a new paradigm for antimicrobial therapy. *Nat Chem Biol* **2007**, 3 (9), 541-8; (c) Walsh, C. T.; Wencewicz, T. A., Prospects for new antibiotics: a molecule-centered perspective. *J Antibiot (Tokyo)* **2014**, 67 (1), 7-22.
2. Kluytmans, J.; van Belkum, A.; Verbrugh, H., Nasal carriage of *Staphylococcus aureus*: epidemiology, underlying mechanisms, and associated risks. *Clin Microbiol Rev* **1997**, 10 (3), 505-20.
3. Fischbach, M. A.; Walsh, C. T., Antibiotics for emerging pathogens. *Science* **2009**, 325 (5944), 1089-93.
4. Clardy, J.; Fischbach, M. A.; Walsh, C. T., New antibiotics from bacterial natural products. *Nat Biotechnol* **2006**, 24 (12), 1541-50.
5. D'Costa, V. M.; King, C. E.; Kalan, L.; Morar, M.; Sung, W. W.; Schwarz, C.; Froese, D.; Zazula, G.; Calmels, F.; Debruyne, R.; Golding, G. B.; Poinar, H. N.; Wright, G. D., Antibiotic resistance is ancient. *Nature* **2011**, 477 (7365), 457-61.
6. (a) Lyon, B. R.; Skurray, R., Antimicrobial resistance of *Staphylococcus aureus*: genetic basis. *Microbiol Rev* **1987**, 51 (1), 88-134; (b) Davies, J.; Davies, D., Origins and evolution of antibiotic resistance. *Microbiol Mol Biol Rev* **2010**, 74 (3), 417-33.
7. D'Costa, V. M.; McGrann, K. M.; Hughes, D. W.; Wright, G. D., Sampling the antibiotic resistome. *Science* **2006**, 311 (5759), 374-7.
8. Gorbach, S. L., Antimicrobial use in animal feed--time to stop. *N Engl J Med* **2001**, 345 (16), 1202-3.
9. Sintim, H. O.; Smith, J. A. I.; Wang, J.; Nakayama, S.; Yan, L., Paradigm shift in discovering next-generation anti-infective agents: targeting quorum sensing, c-di-GMP signaling and biofilm formation in bacteria with small molecules. *Future Medicinal Chemistry* **2010**, 2 (6), 1005-1035.
10. Appelbaum, P. C., 2012 and beyond: potential for the start of a second pre-antibiotic era? *J Antimicrob Chemother* **2012**, 67 (9), 2062-8.
11. Walsh, C., *Antibiotics: actions, origins, resistance*. ASM Press: Washington, DC, 2003.
12. America, I. D. S. o., The 10 x '20 Initiative: pursuing a global commitment to develop 10 new antibacterial drugs by 2020. *Clin Infect Dis* **2010**, 50 (8), 1081-3.
13. WHO, Antimicrobial resistance: global report on surveillance **2014**.
14. Guo, M.; Gamby, S.; Zheng, Y.; Sintim, H. O., Small molecule inhibitors of AI-2 signaling in bacteria: state-of-the-art and future perspectives for anti-quorum sensing agents. *Int J Mol Sci* **2013**, 14 (9), 17694-728.
15. Hoiby, N.; Bjarnsholt, T.; Givskov, M.; Molin, S.; Ciofu, O., Antibiotic resistance of bacterial biofilms. *Int J Antimicrob Agents* **2010**, 35 (4), 322-32.

16. (a) Bassler, B. L., How bacteria talk to each other: regulation of gene expression by quorum sensing. *Curr Opin Microbiol* **1999**, 2 (6), 582-7; (b) Fuqua, W. C.; Winans, S. C.; Greenberg, E. P., Quorum sensing in bacteria: the LuxR-LuxI family of cell density-responsive transcriptional regulators. *J Bacteriol* **1994**, 176 (2), 269-75; (c) Antunes, L. C.; Ferreira, R. B.; Buckner, M. M.; Finlay, B. B., Quorum sensing in bacterial virulence. *Microbiology* **2010**, 156 (Pt 8), 2271-82.
17. Tomasz, A., Control of the competent state in *Pneumococcus* by a hormone-like cell product: an example for a new type of regulatory mechanism in bacteria. *Nature* **1965**, 208 (5006), 155-9.
18. Lazazzera, B. A.; Grossman, A. D., The ins and outs of peptide signaling. *Trends Microbiol* **1998**, 6 (7), 288-94.
19. (a) Nealson, K. H.; Platt, T.; Hastings, J. W., Cellular control of the synthesis and activity of the bacterial luminescent system. *J Bacteriol* **1970**, 104 (1), 313-22; (b) Nealson, K. H., Autoinduction of bacterial luciferase. Occurrence, mechanism and significance. *Arch Microbiol* **1977**, 112 (1), 73-9.
20. Henke, J. M.; Bassler, B. L., Quorum sensing regulates type III secretion in *Vibrio harveyi* and *Vibrio parahaemolyticus*. *J Bacteriol* **2004**, 186 (12), 3794-805.
21. Eberhard, A.; Burlingame, A. L.; Eberhard, C.; Kenyon, G. L.; Nealson, K. H.; Oppenheimer, N. J., Structural identification of autoinducer of *Photobacterium fischeri* luciferase. *Biochemistry* **1981**, 20 (9), 2444-9.
22. Magnuson, R.; Solomon, J.; Grossman, A. D., Biochemical and genetic characterization of a competence pheromone from *B. subtilis*. *Cell* **1994**, 77 (2), 207-16.
23. Chen, X.; Schauder, S.; Potier, N.; Van Dorsselaer, A.; Pelczer, I.; Bassler, B. L.; Hughson, F. M., Structural identification of a bacterial quorum-sensing signal containing boron. *Nature* **2002**, 415 (6871), 545-9.
24. Pesci, E. C.; Milbank, J. B.; Pearson, J. P.; McKnight, S.; Kende, A. S.; Greenberg, E. P.; Iglewski, B. H., Quinolone signaling in the cell-to-cell communication system of *Pseudomonas aeruginosa*. *Proc Natl Acad Sci U S A* **1999**, 96 (20), 11229-34.
25. (a) Takano, E., Gamma-butyrolactones: *Streptomyces* signalling molecules regulating antibiotic production and differentiation. *Curr Opin Microbiol* **2006**, 9 (3), 287-94; (b) Khokhlov, A. S.; Tovarova, II; Borisova, L. N.; Pliner, S. A.; Shevchenko, L. N.; Kornitskaia, E.; Ivkina, N. S.; Rapoport, I. A., [The A-factor, responsible for streptomycin biosynthesis by mutant strains of *Actinomyces streptomycini*]. *Dokl Akad Nauk SSSR* **1967**, 177 (1), 232-5.
26. (a) Miller, M. B.; Skorupski, K.; Lenz, D. H.; Taylor, R. K.; Bassler, B. L., Parallel quorum sensing systems converge to regulate virulence in *Vibrio cholerae*. *Cell* **2002**, 110 (3), 303-14; (b) Higgins, D. A.; Pomianek, M. E.; Kraml, C. M.; Taylor, R. K.; Semmelhack, M. F.; Bassler, B. L., The major *Vibrio cholerae* autoinducer and its role in virulence factor production. *Nature* **2007**, 450 (7171), 883-6.
27. Barber, C. E.; Tang, J. L.; Feng, J. X.; Pan, M. Q.; Wilson, T. J.; Slater, H.; Dow,

- J. M.; Williams, P.; Daniels, M. J., A novel regulatory system required for pathogenicity of *Xanthomonas campestris* is mediated by a small diffusible signal molecule. *Mol Microbiol* **1997**, *24* (3), 555-66.
28. Kesarwani, M.; Hazan, R.; He, J.; Que, Y. A.; Apidianakis, Y.; Lesic, B.; Xiao, G.; Dekimpe, V.; Milot, S.; Deziel, E.; Lepine, F.; Rahme, L. G., A quorum sensing regulated small volatile molecule reduces acute virulence and promotes chronic infection phenotypes. *PLoS Pathog* **2011**, *7* (8), e1002192.
29. Holden, M. T.; Ram Chhabra, S.; de Nys, R.; Stead, P.; Bainton, N. J.; Hill, P. J.; Manefield, M.; Kumar, N.; Labatte, M.; England, D.; Rice, S.; Givskov, M.; Salmond, G. P.; Stewart, G. S.; Bycroft, B. W.; Kjelleberg, S.; Williams, P., Quorum-sensing cross talk: isolation and chemical characterization of cyclic dipeptides from *Pseudomonas aeruginosa* and other gram-negative bacteria. *Mol Microbiol* **1999**, *33* (6), 1254-66.
30. Lee, J.; Wu, J.; Deng, Y.; Wang, J.; Wang, C.; Chang, C.; Dong, Y.; Williams, P.; Zhang, L. H., A cell-cell communication signal integrates quorum sensing and stress response. *Nat Chem Biol* **2013**, *9* (5), 339-43.
31. Havarstein, L. S.; Coomaraswamy, G.; Morrison, D. A., An unmodified heptadecapeptide pheromone induces competence for genetic transformation in *Streptococcus pneumoniae*. *Proc Natl Acad Sci U S A* **1995**, *92* (24), 11140-4.
32. Ng, W. L.; Bassler, B. L., Bacterial quorum-sensing network architectures. *Annu Rev Genet* **2009**, *43*, 197-222.
33. Waters, C. M.; Bassler, B. L., The *Vibrio harveyi* quorum-sensing system uses shared regulatory components to discriminate between multiple autoinducers. *Genes Dev* **2006**, *20* (19), 2754-67.
34. Bassler, B. L.; Greenberg, E. P.; Stevens, A. M., Cross-species induction of luminescence in the quorum-sensing bacterium *Vibrio harveyi*. *J Bacteriol* **1997**, *179* (12), 4043-5.
35. Henke, J. M.; Bassler, B. L., Three parallel quorum-sensing systems regulate gene expression in *Vibrio harveyi*. *J Bacteriol* **2004**, *186* (20), 6902-14.
36. Schauder, S.; Bassler, B. L., The languages of bacteria. *Genes Dev* **2001**, *15* (12), 1468-80.
37. Neiditch, M. B.; Federle, M. J.; Pompeani, A. J.; Kelly, R. C.; Swem, D. L.; Jeffrey, P. D.; Bassler, B. L.; Hughson, F. M., Ligand-induced asymmetry in histidine sensor kinase complex regulates quorum sensing. *Cell* **2006**, *126* (6), 1095-108.
38. Lenz, D. H.; Mok, K. C.; Lilley, B. N.; Kulkarni, R. V.; Wingreen, N. S.; Bassler, B. L., The small RNA chaperone Hfq and multiple small RNAs control quorum sensing in *Vibrio harveyi* and *Vibrio cholerae*. *Cell* **2004**, *118* (1), 69-82.
39. Miller, S. T.; Xavier, K. B.; Campagna, S. R.; Taga, M. E.; Semmelhack, M. F.; Bassler, B. L.; Hughson, F. M., *Salmonella typhimurium* recognizes a chemically distinct form of the bacterial quorum-sensing signal AI-2. *Mol Cell* **2004**, *15* (5), 677-87.
40. Taga, M. E.; Miller, S. T.; Bassler, B. L., Lsr-mediated transport and processing of

- AI-2 in *Salmonella typhimurium*. *Mol Microbiol* **2003**, *50* (4), 1411-27.
41. Marques, J. C.; Oh, I. K.; Ly, D. C.; Lamosa, P.; Ventura, M. R.; Miller, S. T.; Xavier, K. B., LsrF, a coenzyme A-dependent thiolase, catalyzes the terminal step in processing the quorum sensing signal autoinducer-2. *Proc Natl Acad Sci U S A* **2014**, *111* (39), 14235-40.
 42. (a) Li, J.; Attila, C.; Wang, L.; Wood, T. K.; Valdes, J. J.; Bentley, W. E., Quorum sensing in *Escherichia coli* is signaled by AI-2/LsrR: effects on small RNA and biofilm architecture. *J Bacteriol* **2007**, *189* (16), 6011-20; (b) Wang, L.; Li, J.; March, J. C.; Valdes, J. J.; Bentley, W. E., luxS-dependent gene regulation in *Escherichia coli* K-12 revealed by genomic expression profiling. *J Bacteriol* **2005**, *187* (24), 8350-60; (c) Gonzalez Barrios, A. F.; Zuo, R.; Hashimoto, Y.; Yang, L.; Bentley, W. E.; Wood, T. K., Autoinducer 2 controls biofilm formation in *Escherichia coli* through a novel motility quorum-sensing regulator (MqsR, B3022). *J Bacteriol* **2006**, *188* (1), 305-16.
 43. Ahmer, B. M., Cell-to-cell signalling in *Escherichia coli* and *Salmonella enterica*. *Mol Microbiol* **2004**, *52* (4), 933-45.
 44. Zhou, X.; Meng, X.; Sun, B., An EAL domain protein and cyclic AMP contribute to the interaction between the two quorum sensing systems in *Escherichia coli*. *Cell Res* **2008**, *18* (9), 937-48.
 45. James, D.; Shao, H.; Lamont, R. J.; Demuth, D. R., The *Actinobacillus actinomycetemcomitans* ribose binding protein RbsB interacts with cognate and heterologous autoinducer 2 signals. *Infect Immun* **2006**, *74* (7), 4021-9.
 46. Shao, H.; Lamont, R. J.; Demuth, D. R., Autoinducer 2 is required for biofilm growth of *Aggregatibacter (Actinobacillus) actinomycetemcomitans*. *Infect Immun* **2007**, *75* (9), 4211-8.
 47. Li, L.; Sun, L.; Song, Y.; Wu, X.; Zhou, X.; Liu, Z.; Zhou, R., Screening of *Actinobacillus pleuropneumoniae* LuxS inhibitors. *Curr Microbiol* **2013**, *67* (5), 564-71.
 48. Bozue, J.; Powell, B. S.; Cote, C. K.; Moody, K. L.; Gelhaus, H. C.; Vietri, N. J.; Rozak, D. A., Disrupting the luxS quorum sensing gene does not significantly affect *Bacillus anthracis* virulence in mice or guinea pigs. *Virulence* **2012**, *3* (6), 504-9.
 49. Auger, S.; Krin, E.; Aymerich, S.; Gohar, M., Autoinducer 2 affects biofilm formation by *Bacillus cereus*. *Appl Environ Microbiol* **2006**, *72* (1), 937-41.
 50. Lombardia, E.; Rovetto, A. J.; Arabolaza, A. L.; Grau, R. R., A LuxS-dependent cell-to-cell language regulates social behavior and development in *Bacillus subtilis*. *J Bacteriol* **2006**, *188* (12), 4442-52.
 51. Babb, K.; von Lackum, K.; Wattier, R. L.; Riley, S. P.; Stevenson, B., Synthesis of autoinducer 2 by the lyme disease spirochete, *Borrelia burgdorferi*. *J Bacteriol* **2005**, *187* (9), 3079-87.
 52. Castillo, S.; Heredia, N.; Garcia, S., 2(5H)-Furanone, epigallocatechin gallate, and a citric-based disinfectant disturb quorum-sensing activity and reduce motility and biofilm formation of *Campylobacter jejuni*. *Folia Microbiol (Praha)* **2014**, in press.

53. (a) Carter, G. P.; Purdy, D.; Williams, P.; Minton, N. P., Quorum sensing in *Clostridium difficile*: analysis of a luxS-type signalling system. *J Med Microbiol* **2005**, *54* (Pt 2), 119-27; (b) Lee, A. S.; Song, K. P., LuxS/autoinducer-2 quorum sensing molecule regulates transcriptional virulence gene expression in *Clostridium difficile*. *Biochem Biophys Res Commun* **2005**, *335* (3), 659-66.
54. Bansal, T.; Jesudhasan, P.; Pillai, S.; Wood, T. K.; Jayaraman, A., Temporal regulation of enterohemorrhagic *Escherichia coli* virulence mediated by autoinducer-2. *Appl Microbiol Biotechnol* **2008**, *78* (5), 811-9.
55. (a) Wood, T. K., Insights on *Escherichia coli* biofilm formation and inhibition from whole-transcriptome profiling. *Environ Microbiol* **2009**, *11* (1), 1-15; (b) Hegde, M.; Englert, D. L.; Schrock, S.; Cohn, W. B.; Vogt, C.; Wood, T. K.; Manson, M. D.; Jayaraman, A., Chemotaxis to the quorum-sensing signal AI-2 requires the Tsr chemoreceptor and the periplasmic LsrB AI-2-binding protein. *J Bacteriol* **2010**, *193* (3), 768-73; (c) Niu, C.; Robbins, C. M.; Pittman, K. J.; Osborn, J. L.; Stubblefield, B. A.; Simmons, R. B.; Gilbert, E. S., LuxS influences *Escherichia coli* biofilm formation through autoinducer-2-dependent and autoinducer-2-independent modalities. *FEMS Microbiol Ecol* **2013**, *83* (3), 778-91.
56. Shao, C.; Shang, W.; Yang, Z.; Sun, Z.; Li, Y.; Guo, J.; Wang, X.; Zou, D.; Wang, S.; Lei, H.; Cui, Q.; Yin, Z.; Li, X.; Wei, X.; Liu, W.; He, X.; Jiang, Z.; Du, S.; Liao, X.; Huang, L.; Wang, Y.; Yuan, J., LuxS-dependent AI-2 regulates versatile functions in *Enterococcus faecalis* V583. *J Proteome Res* **2012**, *11* (9), 4465-75.
57. Armbruster, C. E.; Pang, B.; Murrah, K.; Juneau, R. A.; Perez, A. C.; Weimer, K. E.; Swords, W. E., RbsB (NTHI_0632) mediates quorum signal uptake in nontypeable *Haemophilus influenzae* strain 86-028NP. *Mol Microbiol* **2011**, *82* (4), 836-50.
58. Rader, B. A.; Wreden, C.; Hicks, K. G.; Sweeney, E. G.; Ottemann, K. M.; Guillemin, K., *Helicobacter pylori* perceives the quorum-sensing molecule AI-2 as a chemorepellent via the chemoreceptor TlpB. *Microbiology* **2011**, *157* (Pt 9), 2445-55.
59. (a) Balestrino, D.; Haagensen, J. A.; Rich, C.; Forestier, C., Characterization of type 2 quorum sensing in *Klebsiella pneumoniae* and relationship with biofilm formation. *J Bacteriol* **2005**, *187* (8), 2870-80; (b) De Araujo, C.; Balestrino, D.; Roth, L.; Charbonnel, N.; Forestier, C., Quorum sensing affects biofilm formation through lipopolysaccharide synthesis in *Klebsiella pneumoniae*. *Res Microbiol* **2010**, *161* (7), 595-603.
60. Sela, S.; Frank, S.; Belausov, E.; Pinto, R., A Mutation in the luxS gene influences *Listeria monocytogenes* biofilm formation. *Appl Environ Microbiol* **2006**, *72* (8), 5653-8.
61. Armbruster, C. E.; Hong, W.; Pang, B.; Weimer, K. E.; Juneau, R. A.; Turner, J.; Swords, W. E., Indirect pathogenicity of *Haemophilus influenzae* and *Moraxella catarrhalis* in polymicrobial otitis media occurs via interspecies quorum signaling. *MBio* **2010**, *1* (3).
62. Geier, H.; Mostowy, S.; Cangelosi, G. A.; Behr, M. A.; Ford, T. E., Autoinducer-2

triggers the oxidative stress response in *Mycobacterium avium*, leading to biofilm formation. *Appl Environ Microbiol* **2008**, 74 (6), 1798-804.

63. Winzer, K.; Sun, Y. H.; Green, A.; Delory, M.; Blackley, D.; Hardie, K. R.; Baldwin, T. J.; Tang, C. M., Role of *Neisseria meningitidis* luxS in cell-to-cell signaling and bacteremic infection. *Infect Immun* **2002**, 70 (4), 2245-8.

64. Burgess, N. A.; Kirke, D. F.; Williams, P.; Winzer, K.; Hardie, K. R.; Meyers, N. L.; Aduse-Opoku, J.; Curtis, M. A.; Camara, M., LuxS-dependent quorum sensing in *Porphyromonas gingivalis* modulates protease and haemagglutinin activities but is not essential for virulence. *Microbiology* **2002**, 148 (Pt 3), 763-72.

65. Duan, K.; Dammel, C.; Stein, J.; Rabin, H.; Surette, M. G., Modulation of *Pseudomonas aeruginosa* gene expression by host microflora through interspecies communication. *Mol Microbiol* **2003**, 50 (5), 1477-91.

66. (a) Jesudhasan, P. R.; Cepeda, M. L.; Widmer, K.; Dowd, S. E.; Soni, K. A.; Hume, M. E.; Zhu, J.; Pillai, S. D., Transcriptome analysis of genes controlled by luxS/autoinducer-2 in *Salmonella enterica* serovar Typhimurium. *Foodborne Pathog Dis* **2009**, 7 (4), 399-410; (b) Choi, J.; Shin, D.; Kim, M.; Park, J.; Lim, S.; Ryu, S., LsrR-mediated quorum sensing controls invasiveness of *Salmonella typhimurium* by regulating SPI-1 and flagella genes. *PLoS One* **2012**, 7 (5), e37059.

67. Pereira, C. S.; McAuley, J. R.; Taga, M. E.; Xavier, K. B.; Miller, S. T., *Sinorhizobium meliloti*, a bacterium lacking the autoinducer-2 (AI-2) synthase, responds to AI-2 supplied by other bacteria. *Mol Microbiol* **2008**, 70 (5), 1223-35.

68. Zhu, S.; Wu, H.; Zeng, M.; Zunying, L.; Zhao, Y.; Dong, S., Regulation of Spoilage-Related Activities of *Shewanella putrefaciens* and *Shewanella baltica* by an Autoinducer-2 Analogue, (Z)-5-(Bromomethylene)furan-2(5H)-One. *Journal of Food Processing and Preservation* **2014**, in press.

69. Zhao, L.; Xue, T.; Shang, F.; Sun, H.; Sun, B., *Staphylococcus aureus* AI-2 quorum sensing associates with the KdpDE two-component system to regulate capsular polysaccharide synthesis and virulence. *Infect Immun* **2010**, 78 (8), 3506-15.

70. Li, M.; Villaruz, A. E.; Vadyvaloo, V.; Sturdevant, D. E.; Otto, M., AI-2-dependent gene regulation in *Staphylococcus epidermidis*. *BMC Microbiol* **2008**, 8, 4.

71. Ahmed, N. A.; Petersen, F. C.; Scheie, A. A., AI-2 quorum sensing affects antibiotic susceptibility in *Streptococcus anginosus*. *J Antimicrob Chemother* **2007**, 60 (1), 49-53.

72. Ahmed, N. A.; Petersen, F. C.; Scheie, A. A., AI-2/LuxS is involved in increased biofilm formation by *Streptococcus intermedius* in the presence of antibiotics. *Antimicrob Agents Chemother* **2009**, 53 (10), 4258-63.

73. (a) Cuadra-Saenz, G.; Rao, D. L.; Underwood, A. J.; Belapure, S. A.; Campagna, S. R.; Sun, Z.; Tammariello, S.; Rickard, A. H., Autoinducer-2 influences interactions amongst pioneer colonizing streptococci in oral biofilms. *Microbiology* **2012**, 158 (Pt 7), 1783-95; (b) McNab, R.; Ford, S. K.; El-Sabaeny, A.; Barbieri, B.; Cook, G. S.; Lamont, R. J., LuxS-based signaling in *Streptococcus gordonii*: autoinducer 2 controls

- carbohydrate metabolism and biofilm formation with *Porphyromonas gingivalis*. *J Bacteriol* **2003**, *185* (1), 274-84.
74. Sztajer, H.; Lemme, A.; Vilchez, R.; Schulz, S.; Geffers, R.; Yip, C. Y.; Levesque, C. M.; Cvitkovitch, D. G.; Wagner-Dobler, I., Autoinducer-2-regulated genes in *Streptococcus mutans* UA159 and global metabolic effect of the luxS mutation. *J Bacteriol* **2008**, *190* (1), 401-15.
75. Vidal, J. E.; Howery, K. E.; Ludewick, H. P.; Nava, P.; Klugman, K. P., Quorum-sensing systems LuxS/autoinducer 2 and Com regulate *Streptococcus pneumoniae* biofilms in a bioreactor with living cultures of human respiratory cells. *Infect Immun* **2013**, *81* (4), 1341-53.
76. Antonova, E. S.; Hammer, B. K., Quorum-sensing autoinducer molecules produced by members of a multispecies biofilm promote horizontal gene transfer to *Vibrio cholerae*. *FEMS Microbiol Lett* **2011**, *322* (1), 68-76.
77. Bassler, B. L.; Wright, M.; Silverman, M. R., Multiple signalling systems controlling expression of luminescence in *Vibrio harveyi*: sequence and function of genes encoding a second sensory pathway. *Mol Microbiol* **1994**, *13* (2), 273-86.
78. Verma, S. C.; Miyashiro, T., Quorum sensing in the squid-Vibrio symbiosis. *Int J Mol Sci* **2013**, *14* (8), 16386-401.
79. Kim, S. Y.; Lee, S. E.; Kim, Y. R.; Kim, C. M.; Ryu, P. Y.; Choy, H. E.; Chung, S. S.; Rhee, J. H., Regulation of *Vibrio vulnificus* virulence by the LuxS quorum-sensing system. *Mol Microbiol* **2003**, *48* (6), 1647-64.
80. Kavanaugh, J. S.; Gakhar, L.; Horswill, A. R., The structure of LsrB from *Yersinia pestis* complexed with autoinducer-2. *Acta Crystallogr Sect F Struct Biol Cryst Commun* **2011**, *67* (Pt 12), 1501-5.
81. Ha, J. H.; Eo, Y.; Grishaev, A.; Guo, M.; Smith, J. A.; Sintim, H. O.; Kim, E. H.; Cheong, H. K.; Bentley, W. E.; Ryu, K. S., Crystal structures of the LsrR proteins complexed with phospho-AI-2 and two signal-interrupting analogues reveal distinct mechanisms for ligand recognition. *J Am Chem Soc* **2013**, *135* (41), 15526-35.
82. Lowery, C. A.; McKenzie, K. M.; Qi, L.; Meijler, M. M.; Janda, K. D., Quorum sensing in *Vibrio harveyi*: probing the specificity of the LuxP binding site. *Bioorg Med Chem Lett* **2005**, *15* (9), 2395-8.
83. (a) Smith, J. A.; Wang, J.; Nguyen-Mau, S. M.; Lee, V.; Sintim, H. O., Biological screening of a diverse set of AI-2 analogues in *Vibrio harveyi* suggests that receptors which are involved in synergistic agonism of AI-2 and analogues are promiscuous. *Chem Commun (Camb)* **2009**, (45), 7033-5; (b) Lowery, C. A.; Park, J.; Kaufmann, G. F.; Janda, K. D., An unexpected switch in the modulation of AI-2-based quorum sensing discovered through synthetic 4,5-dihydroxy-2,3-pentanedione analogues. *J Am Chem Soc* **2008**, *130* (29), 9200-1.
84. (a) Tsuchikama, K.; Lowery, C. A.; Janda, K. D., Probing autoinducer-2 based quorum sensing: the biological consequences of molecules unable to traverse equilibrium states. *J Org Chem* **2011**, *76* (17), 6981-9; (b) Roy, V.; Meyer, M. T.; Smith,

- J. A.; Gamby, S.; Sintim, H. O.; Ghodssi, R.; Bentley, W. E., AI-2 analogs and antibiotics: a synergistic approach to reduce bacterial biofilms. *Appl Microbiol Biotechnol* **2013**, *97* (6), 2627-38; (c) Gamby, S.; Roy, V.; Guo, M.; Smith, J. A.; Wang, J.; Stewart, J. E.; Wang, X.; Bentley, W. E.; Sintim, H. O., Altering the communication networks of multispecies microbial systems using a diverse toolbox of AI-2 analogues. *ACS Chem Biol* **2012**, *7* (6), 1023-30; (d) Roy, V.; Smith, J. A.; Wang, J.; Stewart, J. E.; Bentley, W. E.; Sintim, H. O., Synthetic analogs tailor native AI-2 signaling across bacterial species. *J Am Chem Soc* **2010**, *132* (32), 11141-50.
85. Frezza, M.; Soulere, L.; Balestrino, D.; Gohar, M.; Deshayes, C.; Queneau, Y.; Forestier, C.; Doutheau, A., Ac2-DPD, the bis-(O)-acetylated derivative of 4,5-dihydroxy-2,3-pentanedione (DPD) is a convenient stable precursor of bacterial quorum sensing autoinducer AI-2. *Bioorg Med Chem Lett* **2007**, *17* (5), 1428-31.
86. Guo, M.; Gamby, S.; Nakayama, S.; Smith, J.; Sintim, H. O., A pro-drug approach for selective modulation of AI-2-mediated bacterial cell-to-cell communication. *Sensors (Basel)* **2012**, *12* (3), 3762-72.
87. Rui, F.; Marques, J. C.; Miller, S. T.; Maycock, C. D.; Xavier, K. B.; Ventura, M. R., Stereochemical diversity of AI-2 analogs modulates quorum sensing in *Vibrio harveyi* and *Escherichia coli*. *Bioorg Med Chem* **2012**, *20* (1), 249-56.
88. Galloway, W. R.; Hodgkinson, J. T.; Bowden, S. D.; Welch, M.; Spring, D. R., Quorum sensing in Gram-negative bacteria: small-molecule modulation of AHL and AI-2 quorum sensing pathways. *Chem Rev* **2011**, *111* (1), 28-67.
89. Zhu, P.; Li, M., Recent progresses on AI-2 bacterial quorum sensing inhibitors. *Curr Med Chem* **2012**, *19* (2), 174-86.
90. (a) Eberhard, A.; Widrig, C. A.; McBath, P.; Schineller, J. B., Analogs of the autoinducer of bioluminescence in *Vibrio fischeri*. *Arch Microbiol* **1986**, *146* (1), 35-40; (b) Schaefer, A. L.; Hanzelka, B. L.; Eberhard, A.; Greenberg, E. P., Quorum sensing in *Vibrio fischeri*: probing autoinducer-LuxR interactions with autoinducer analogs. *J Bacteriol* **1996**, *178* (10), 2897-901.
91. More, M. I.; Finger, L. D.; Stryker, J. L.; Fuqua, C.; Eberhard, A.; Winans, S. C., Enzymatic synthesis of a quorum-sensing autoinducer through use of defined substrates. *Science* **1996**, *272* (5268), 1655-8.
92. (a) Ishida, T.; Ikeda, T.; Takiguchi, N.; Kuroda, A.; Ohtake, H.; Kato, J., Inhibition of quorum sensing in *Pseudomonas aeruginosa* by N-acyl cyclopentylamides. *Appl Environ Microbiol* **2007**, *73* (10), 3183-8; (b) Ikeda, T.; Kajiyama, K.; Kita, T.; Takiguchi, N.; Kuroda, A.; Kato, J.; Ohtake, H., The Synthesis of Optically Pure Enantiomers of N-Acyl-homoserine Lactone Autoinducers and Their Analogues. *Chemistry Letters* **2001**, *30* (4), 314-315.
93. O'Loughlin, C. T.; Miller, L. C.; Siryaporn, A.; Drescher, K.; Semmelhack, M. F.; Bassler, B. L., A quorum-sensing inhibitor blocks *Pseudomonas aeruginosa* virulence and biofilm formation. *Proc Natl Acad Sci U S A* **2013**, *110* (44), 17981-6.
94. (a) Geske, G. D.; Wezeman, R. J.; Siegel, A. P.; Blackwell, H. E., Small molecule

- inhibitors of bacterial quorum sensing and biofilm formation. *J Am Chem Soc* **2005**, *127* (37), 12762-3; (b) Reverchon, S.; Chantegrel, B.; Deshayes, C.; Doutheau, A.; Cotte-Pattat, N., New synthetic analogues of N-acyl homoserine lactones as agonists or antagonists of transcriptional regulators involved in bacterial quorum sensing. *Bioorg Med Chem Lett* **2002**, *12* (8), 1153-7; (c) Geske, G. D.; O'Neill, J. C.; Blackwell, H. E., N-phenylacetanoyl-L-homoserine lactones can strongly antagonize or superagonize quorum sensing in *Vibrio fischeri*. *ACS Chem Biol* **2007**, *2* (5), 315-9.
95. Smith, K. M.; Bu, Y.; Suga, H., Induction and inhibition of *Pseudomonas aeruginosa* quorum sensing by synthetic autoinducer analogs. *Chem Biol* **2003**, *10* (1), 81-9.
96. Smith, K. M.; Bu, Y.; Suga, H., Library screening for synthetic agonists and antagonists of a *Pseudomonas aeruginosa* autoinducer. *Chem Biol* **2003**, *10* (6), 563-71.
97. Passador, L.; Tucker, K. D.; Guertin, K. R.; Journet, M. P.; Kende, A. S.; Iglewski, B. H., Functional analysis of the *Pseudomonas aeruginosa* autoinducer PAI. *J Bacteriol* **1996**, *178* (20), 5995-6000.
98. Kline, T.; Bowman, J.; Iglewski, B. H.; de Kievit, T.; Kakai, Y.; Passador, L., Novel synthetic analogs of the *Pseudomonas* autoinducer. *Bioorg Med Chem Lett* **1999**, *9* (24), 3447-52.
99. Castang, S.; Chantegrel, B.; Deshayes, C.; Dolmazon, R.; Gouet, P.; Haser, R.; Reverchon, S.; Nasser, W.; Hugouvieux-Cotte-Pattat, N.; Doutheau, A., N-Sulfonyl homoserine lactones as antagonists of bacterial quorum sensing. *Bioorg Med Chem Lett* **2004**, *14* (20), 5145-9.
100. Olsen, J. A.; Severinsen, R.; Rasmussen, T. B.; Hentzer, M.; Givskov, M.; Nielsen, J., Synthesis of new 3- and 4-substituted analogues of acyl homoserine lactone quorum sensing autoinducers. *Bioorg Med Chem Lett* **2002**, *12* (3), 325-8.
101. Frezza, M.; Castang, S.; Estephane, J.; Soulere, L.; Deshayes, C.; Chantegrel, B.; Nasser, W.; Queneau, Y.; Reverchon, S.; Doutheau, A., Synthesis and biological evaluation of homoserine lactone derived ureas as antagonists of bacterial quorum sensing. *Bioorg Med Chem* **2006**, *14* (14), 4781-91.
102. Amara, N.; Mashiach, R.; Amar, D.; Krief, P.; Spieser, S. A.; Bottomley, M. J.; Aharoni, A.; Meijler, M. M., Covalent inhibition of bacterial quorum sensing. *J Am Chem Soc* **2009**, *131* (30), 10610-9.
103. Boukraa, M.; Sabbah, M.; Soulere, L.; El Efrat, M. L.; Queneau, Y.; Doutheau, A., AHL-dependent quorum sensing inhibition: synthesis and biological evaluation of alpha-(N-alkyl-carboxamide)-gamma-butyrolactones and alpha-(N-alkyl-sulfonamide)-gamma-butyrolactones. *Bioorg Med Chem Lett* **2011**, *21* (22), 6876-9.
104. Lee, L. Y.; Hupfield, T.; Nicholson, R. L.; Hodgkinson, J. T.; Su, X.; Thomas, G. L.; Salmond, G. P.; Welch, M.; Spring, D. R., 2-Methoxycyclopentyl analogues of a *Pseudomonas aeruginosa* quorum sensing modulator. *Mol Biosyst* **2008**, *4* (6), 505-7.
105. Frezza, M.; Soulere, L.; Reverchon, S.; Guilian, N.; Jerez, C.; Queneau, Y.;

- Doutheau, A., Synthetic homoserine lactone-derived sulfonylureas as inhibitors of *Vibrio fischeri* quorum sensing regulator. *Bioorg Med Chem* **2008**, *16* (7), 3550-6.
106. Pace, V.; Verniest, G.; Sinisterra, J. V.; Alcantara, A. R.; De Kimpe, N., Improved Arndt-Eistert synthesis of alpha-diazoketones requiring minimal diazomethane in the presence of calcium oxide as acid scavenger. *J Org Chem* **2010**, *75* (16), 5760-3.
107. (a) Tsuchikama, K.; Zhu, J.; Lowery, C. A.; Kaufmann, G. F.; Janda, K. D., C4-alkoxy-HPD: a potent class of synthetic modulators surpassing nature in AI-2 quorum sensing. *J Am Chem Soc* **2012**, *134* (33), 13562-4; (b) Semmelhack, M. F.; Campagna, S. R.; Federle, M. J.; Bassler, B. L., An expeditious synthesis of DPD and boron binding studies. *Org Lett* **2005**, *7* (4), 569-72; (c) De Keersmaecker, S. C.; Varszegi, C.; van Boxel, N.; Habel, L. W.; Metzger, K.; Daniels, R.; Marchal, K.; De Vos, D.; Vanderleyden, J., Chemical synthesis of (S)-4,5-dihydroxy-2,3-pentanedione, a bacterial signal molecule precursor, and validation of its activity in *Salmonella typhimurium*. *J Biol Chem* **2005**, *280* (20), 19563-8; (d) Frezza, M.; Soulère, L.; Queneau, Y.; Doutheau, A., A Baylis–Hillman/ozonolysis route towards (\pm) 4,5-dihydroxy-2,3-pentanedione (DPD) and analogues. *Tetrahedron Letters* **2005**, *46* (38), 6495-6498; (e) Kadirvel, M.; Stimpson, W. T.; Moumene-Afifi, S.; Arsic, B.; Glynn, N.; Halliday, N.; Williams, P.; Gilbert, P.; McBain, A. J.; Freeman, S.; Gardiner, J. M., Synthesis and bioluminescence-inducing properties of autoinducer (S)-4,5-dihydroxypentane-2,3-dione and its enantiomer. *Bioorg Med Chem Lett* **2010**, *20* (8), 2625-8; (f) Ascenso, O. S.; Marques, J. C.; Santos, A. R.; Xavier, K. B.; Ventura, M. R.; Maycock, C. D., An efficient synthesis of the precursor of AI-2, the signalling molecule for inter-species quorum sensing. *Bioorg Med Chem* **2011**, *19* (3), 1236-41.
108. Meijler, M. M.; Hom, L. G.; Kaufmann, G. F.; McKenzie, K. M.; Sun, C.; Moss, J. A.; Matsushita, M.; Janda, K. D., Synthesis and biological validation of a ubiquitous quorum-sensing molecule. *Angew Chem Int Ed Engl* **2004**, *43* (16), 2106-8.
109. Kamaraju, K.; Smith, J.; Wang, J.; Roy, V.; Sintim, H. O.; Bentley, W. E.; Sukharev, S., Effects on membrane lateral pressure suggest permeation mechanisms for bacterial quorum signaling molecules. *Biochemistry* **2011**, *50* (32), 6983-93.
110. Tavender, T. J.; Halliday, N. M.; Hardie, K. R.; Winzer, K., LuxS-independent formation of AI-2 from ribulose-5-phosphate. *BMC Microbiol* **2008**, *8*, 98.
111. Xavier, K. B.; Miller, S. T.; Lu, W.; Kim, J. H.; Rabinowitz, J.; Pelczar, I.; Semmelhack, M. F.; Bassler, B. L., Phosphorylation and processing of the quorum-sensing molecule autoinducer-2 in enteric bacteria. *ACS Chem Biol* **2007**, *2* (2), 128-36.
112. (a) Ren, D.; Sims, J. J.; Wood, T. K., Inhibition of biofilm formation and swarming of *Escherichia coli* by (5Z)-4-bromo-5-(bromomethylene)-3-butyl-2(5H)-furanone. *Environ Microbiol* **2001**, *3* (11), 731-6; (b) Niu, C.; Afre, S.; Gilbert, E. S., Subinhibitory concentrations of cinnamaldehyde interfere with quorum sensing. *Lett Appl Microbiol* **2006**, *43* (5), 489-94; (c) Ni, N.; Choudhary, G.; Li, M.; Wang, B.,

- Pyrogallol and its analogs can antagonize bacterial quorum sensing in *Vibrio harveyi*. *Bioorganic & Medicinal Chemistry Letters* **2008**, *18* (5), 1567-1572; (d) Peng, H.; Cheng, Y.; Ni, N.; Li, M.; Choudhary, G.; Chou, H. T.; Lu, C. D.; Tai, P. C.; Wang, B., Synthesis and evaluation of new antagonists of bacterial quorum sensing in *Vibrio harveyi*. *ChemMedChem* **2009**, *4* (9), 1457-68; (e) Ni, N.; Choudhary, G.; Peng, H.; Li, M.; Chou, H. T.; Lu, C. D.; Gilbert, E. S.; Wang, B., Inhibition of quorum sensing in *Vibrio harveyi* by boronic acids. *Chem Biol Drug Des* **2009**, *74* (1), 51-6.
- 113.(a) Niu, C.; Robbins, C. M.; Pittman, K. J.; Osborn, J. L.; Stubblefield, B. A.; Simmons, R. B.; Gilbert, E. S., LuxS influences *Escherichia coli* biofilm formation through autoinducer-2-dependent and autoinducer-2-independent modalities. *FEMS Microbiology Ecology* **2013**, *83* (3), 778-791; (b) Rickard, A. H.; Palmer, R. J., Jr.; Blehert, D. S.; Campagna, S. R.; Semmelhack, M. F.; Eglund, P. G.; Bassler, B. L.; Kolenbrander, P. E., Autoinducer 2: a concentration-dependent signal for mutualistic bacterial biofilm growth. *Mol Microbiol* **2006**, *60* (6), 1446-56; (c) Kolenbrander, P. E.; Palmer, R. J., Jr.; Periasamy, S.; Jakubovics, N. S., Oral multispecies biofilm development and the key role of cell-cell distance. *Nat Rev Microbiol* **2010**, *8* (7), 471-80.
- 114.Yu, J.; Madsen, M. L.; Carruthers, M. D.; Phillips, G. J.; Kavanaugh, J. S.; Boyd, J. M.; Horswill, A. R.; Minion, F. C., Analysis of autoinducer-2 quorum sensing in *Yersinia pestis*. *Infect Immun* **2013**, *81* (11), 4053-62.
- 115.Winzer, K.; Hardie, K. R.; Burgess, N.; Doherty, N.; Kirke, D.; Holden, M. T.; Linfoth, R.; Cornell, K. A.; Taylor, A. J.; Hill, P. J.; Williams, P., LuxS: its role in central metabolism and the in vitro synthesis of 4-hydroxy-5-methyl-3(2H)-furanone. *Microbiology* **2002**, *148* (Pt 4), 909-22.
- 116.Roy, V.; Meyer, M. T.; Smith, J. A.; Gamby, S.; Sintim, H. O.; Ghodssi, R.; Bentley, W. E., AI-2 analogs and antibiotics: a synergistic approach to reduce bacterial biofilms. *Appl Microbiol Biotechnol* **2012**, *97* (6), 2627-38.
- 117.Kadirvel, M.; Fanimarvasti, F.; Forbes, S.; McBain, A.; Gardiner, J. M.; Brown, G. D.; Freeman, S., Inhibition of quorum sensing and biofilm formation in *Vibrio harveyi* by 4-fluoro-DPD; a novel potent inhibitor of signalling. *Chem Commun (Camb)* **2014**, *50* (39), 5000-2.
- 118.(a) Metrangolo, P.; Resnati, G., Halogen bonding: a paradigm in supramolecular chemistry. *Chemistry* **2001**, *7* (12), 2511-9; (b) Auffinger, P.; Hays, F. A.; Westhof, E.; Ho, P. S., Halogen bonds in biological molecules. *Proc Natl Acad Sci U S A* **2004**, *101* (48), 16789-94.
- 119.Kool, E. T.; Sintim, H. O., The difluorotoluene debate--a decade later. *Chem Commun (Camb)* **2006**, (35), 3665-75.
120. Riley, K. E.; Rezac, J.; Hobza, P., Competition between halogen, dihalogen and hydrogen bonds in bromo- and iodomethanol dimers. *J Mol Model* **2013**, *19* (7), 2879-83.
121. Frisch, M. J.; Trucks, G. W.; Schlegel, H. B.; Scuseria, G. E.; Robb, M. A.;

- Cheeseman, J. R.; Scalmani, G.; Barone, V.; Mennucci, B.; Petersson, G. A.; Nakatsuji, H.; Caricato, M.; Li, X.; Hratchian, H. P.; Izmaylov, A. F.; Bloino, J.; Zheng, G.; Sonnenberg, J. L.; Hada, M.; Ehara, M.; Toyota, K.; Fukuda, R.; Hasegawa, J.; Ishida, M.; Nakajima, T.; Honda, Y.; Kitao, O.; Nakai, H.; Vreven, T.; Montgomery Jr., J. A.; Peralta, J. E.; Ogliaro, F.; Bearpark, M. J.; Heyd, J.; Brothers, E. N.; Kudin, K. N.; Staroverov, V. N.; Kobayashi, R.; Normand, J.; Raghavachari, K.; Rendell, A. P.; Burant, J. C.; Iyengar, S. S.; Tomasi, J.; Cossi, M.; Rega, N.; Millam, N. J.; Klene, M.; Knox, J. E.; Cross, J. B.; Bakken, V.; Adamo, C.; Jaramillo, J.; Gomperts, R.; Stratmann, R. E.; Yazyev, O.; Austin, A. J.; Cammi, R.; Pomelli, C.; Ochterski, J. W.; Martin, R. L.; Morokuma, K.; Zakrzewski, V. G.; Voth, G. A.; Salvador, P.; Dannenberg, J. J.; Dapprich, S.; Daniels, A. D.; Farkas, Ö.; Foresman, J. B.; Ortiz, J. V.; Cioslowski, J.; Fox, D. J. *Gaussian 09*, Gaussian, Inc.: Wallingford, CT, USA, 2009.
122. Tsao, C. Y.; Hooshangi, S.; Wu, H. C.; Valdes, J. J.; Bentley, W. E., Autonomous induction of recombinant proteins by minimally rewiring native quorum sensing regulon of *E. coli*. *Metab Eng* **2010**, *12* (3), 291-7.
123. Liu, Y.; Terrell, J. L.; Tsao, C.-Y.; Wu, H.-C.; Javvaji, V.; Kim, E.; Cheng, Y.; Wang, Y.; Ulijn, R. V.; Raghavan, S. R.; Rubloff, G. W.; Bentley, W. E.; Payne, G. F., Biofabricating Multifunctional Soft Matter with Enzymes and Stimuli-Responsive Materials. *Advanced Functional Materials* **2012**, *22* (14), 3004-3012.
124. Barluenga, J.; Llavona, L.; Concellon, J. M.; Yus, M., A simple and unambiguous synthesis of α,α - and α,α' -dihalogeno ketones. *Journal of the Chemical Society, Perkin Transactions 1* **1991**, (2), 297-300.
125. Painter, G. R. R. B. L., Chapel Hill, NC, 27514, US), Liotta, Dennis C. (251 Montrose Drive, McDonough, GA, 30253, US), Almond, Merrick (1034 West Sterlington Place, Apex, NC, 27502, US), Cleary, Darryl (4610 Falconbridge Road, Chapel Hill, NC, 27514, US), Soria, Jose (2502 Pangborn Circle, Decatur, GA, 30033, US), Sznajdman, Marcos Luis (5222 Greyfield Boulevard, Durham, NC, 27713, US) METHOD OF MANUFACTURE OF 1,3-OXATHIOLANE NUCLEOSIDES. 2000.
126. Kuroboshi, M.; Ishihara, T., An Efficient and General Method for the Reformatsky-Type Reaction of Chlorodifluoromethyl Ketones with Carbonyl Compounds Giving α,α -Difluoro- β -hydroxy Ketones. *Bulletin of the Chemical Society of Japan* **1990**, *63* (2), 428-437.
127. Hall-Stoodley, L.; Costerton, J. W.; Stoodley, P., Bacterial biofilms: from the natural environment to infectious diseases. *Nat Rev Microbiol* **2004**, *2* (2), 95-108.
128. Dubey, G. P.; Ben-Yehuda, S., Intercellular nanotubes mediate bacterial communication. *Cell* **2011**, *144* (4), 590-600.
129. Waters, C. M.; Bassler, B. L., Quorum sensing: cell-to-cell communication in bacteria. *Annu Rev Cell Dev Biol* **2005**, *21*, 319-46.
130. (a) Usher, L. R.; Lawson, R. A.; Geary, I.; Taylor, C. J.; Bingle, C. D.; Taylor, G. W.; Whyte, M. K., Induction of neutrophil apoptosis by the *Pseudomonas aeruginosa* exotoxin pyocyanin: a potential mechanism of persistent infection. *J Immunol* **2002**,

168 (4), 1861-8; (b) Kaufman, M. R.; Jia, J.; Zeng, L.; Ha, U.; Chow, M.; Jin, S., *Pseudomonas aeruginosa* mediated apoptosis requires the ADP-ribosylating activity of *exoS*. *Microbiology* **2000**, *146* (Pt 10), 2531-41; (c) Jacobi, C. A.; Schiffner, F.; Henkel, M.; Waibel, M.; Stork, B.; Daubrawa, M.; Eberl, L.; Gregor, M.; Wesselborg, S., Effects of bacterial N-acyl homoserine lactones on human Jurkat T lymphocytes-OddHL induces apoptosis via the mitochondrial pathway. *Int J Med Microbiol* **2009**, *299* (7), 509-19; (d) Li, H.; Wang, L.; Ye, L.; Mao, Y.; Xie, X.; Xia, C.; Chen, J.; Lu, Z.; Song, J., Influence of *Pseudomonas aeruginosa* quorum sensing signal molecule N-(3-oxododecanoyl) homoserine lactone on mast cells. *Med Microbiol Immunol* **2009**, *198* (2), 113-21.

131. (a) Lowery, C. A.; Dickerson, T. J.; Janda, K. D., Interspecies and interkingdom communication mediated by bacterial quorum sensing. *Chem Soc Rev* **2008**, *37* (7), 1337-46; (b) Geske, G. D.; O'Neill, J. C.; Blackwell, H. E., Expanding dialogues: from natural autoinducers to non-natural analogues that modulate quorum sensing in Gram-negative bacteria. *Chem Soc Rev* **2008**, *37* (7), 1432-47.

132. (a) Givskov, M.; de Nys, R.; Manefield, M.; Gram, L.; Maximilien, R.; Eberl, L.; Molin, S.; Steinberg, P. D.; Kjelleberg, S., Eukaryotic interference with homoserine lactone-mediated prokaryotic signalling. *J Bacteriol* **1996**, *178* (22), 6618-22; (b) Hentzer, M.; Wu, H.; Andersen, J. B.; Riedel, K.; Rasmussen, T. B.; Bagge, N.; Kumar, N.; Schembri, M. A.; Song, Z.; Kristoffersen, P.; Manefield, M.; Costerton, J. W.; Molin, S.; Eberl, L.; Steinberg, P.; Kjelleberg, S.; Hoiby, N.; Givskov, M., Attenuation of *Pseudomonas aeruginosa* virulence by quorum sensing inhibitors. *EMBO J* **2003**, *22* (15), 3803-15; (c) Hjelmgaard, T.; Persson, T.; Rasmussen, T. B.; Givskov, M.; Nielsen, J., Synthesis of furanone-based natural product analogues with quorum sensing antagonist activity. *Bioorg Med Chem* **2003**, *11* (15), 3261-71; (d) Kwan, J. C.; Meickle, T.; Ladwa, D.; Teplitski, M.; Paul, V.; Luesch, H., Lyngbyoic acid, a "tagged" fatty acid from a marine cyanobacterium, disrupts quorum sensing in *Pseudomonas aeruginosa*. *Mol Biosyst* **2011**, *7* (4), 1205-16; (e) Geske, G. D.; O'Neill, J. C.; Miller, D. M.; Mattmann, M. E.; Blackwell, H. E., Modulation of bacterial quorum sensing with synthetic ligands: systematic evaluation of N-acylated homoserine lactones in multiple species and new insights into their mechanisms of action. *J Am Chem Soc* **2007**, *129* (44), 13613-25.

133. (a) Adams, B. L.; Carter, K. K.; Guo, M.; Wu, H. C.; Tsao, C. Y.; Sintim, H. O.; Valdes, J. J.; Bentley, W. E., Evolved Quorum sensing regulator, LsrR, for altered switching functions. *ACS Synth Biol* **2013**, *3* (4), 210-9; (b) Hong, S. H.; Hegde, M.; Kim, J.; Wang, X.; Jayaraman, A.; Wood, T. K., Synthetic quorum-sensing circuit to control consortial biofilm formation and dispersal in a microfluidic device. *Nat Commun* **2012**, *3*, 613; (c) Shong, J.; Collins, C. H., Engineering the *esaR* promoter for tunable quorum sensing- dependent gene expression. *ACS Synth Biol* **2013**, *2* (10), 568-75.

134. Kravchenko, V.; Garner, A. L.; Mathison, J.; Seit-Nebi, A.; Yu, J.; Gileva, I.

- P.; Ulevitch, R.; Janda, K. D., Facilitating cytokine-mediated cancer cell death by proteobacterial N-acylhomoserine lactones. *ACS Chem Biol* **2013**, *8* (6), 1117-20.
135. Kaufmann, G. F.; Sartorio, R.; Lee, S. H.; Rogers, C. J.; Meijler, M. M.; Moss, J. A.; Clapham, B.; Brogan, A. P.; Dickerson, T. J.; Janda, K. D., Revisiting quorum sensing: Discovery of additional chemical and biological functions for 3-oxo-N-acylhomoserine lactones. *Proc Natl Acad Sci U S A* **2005**, *102* (2), 309-14.
136. (a) Dong, Y. H.; Gusti, A. R.; Zhang, Q.; Xu, J. L.; Zhang, L. H., Identification of quorum-quenching N-acyl homoserine lactonases from *Bacillus* species. *Appl Environ Microbiol* **2002**, *68* (4), 1754-9; (b) Draganov, D. I.; Teiber, J. F.; Speelman, A.; Osawa, Y.; Sunahara, R.; La Du, B. N., Human paraoxonases (PON1, PON2, and PON3) are lactonases with overlapping and distinct substrate specificities. *J Lipid Res* **2005**, *46* (6), 1239-47; (c) Dong, Y. H.; Zhang, L. H., Quorum sensing and quorum-quenching enzymes. *J Microbiol* **2005**, *43 Spec No*, 101-9; (d) Teplitski, M.; Mathesius, U.; Rumbaugh, K. P., Perception and degradation of N-acyl homoserine lactone quorum sensing signals by mammalian and plant cells. *Chem Rev* **2011**, *111* (1), 100-16.
137. (a) Leadbetter, J. R.; Greenberg, E. P., Metabolism of acyl-homoserine lactone quorum-sensing signals by *Variovorax paradoxus*. *J Bacteriol* **2000**, *182* (24), 6921-6; (b) Morohoshi, T.; Nakazawa, S.; Ebata, A.; Kato, N.; Ikeda, T., Identification and characterization of N-acylhomoserine lactone-acylase from the fish intestinal *Shewanella* sp. strain MIB015. *Biosci Biotechnol Biochem* **2008**, *72* (7), 1887-93; (c) Huang, J. J.; Han, J. I.; Zhang, L. H.; Leadbetter, J. R., Utilization of acyl-homoserine lactone quorum signals for growth by a soil pseudomonad and *Pseudomonas aeruginosa* PAO1. *Appl Environ Microbiol* **2003**, *69* (10), 5941-9; (d) Romero, M.; Diggle, S. P.; Heeb, S.; Camara, M.; Otero, A., Quorum quenching activity in *Anabaena* sp. PCC 7120: identification of AiiC, a novel AHL-acylase. *FEMS Microbiol Lett* **2008**, *280* (1), 73-80.
138. Geske, G. D.; O'Neill, J. C.; Miller, D. M.; Wezeman, R. J.; Mattmann, M. E.; Lin, Q.; Blackwell, H. E., Comparative analyses of N-acylated homoserine lactones reveal unique structural features that dictate their ability to activate or inhibit quorum sensing. *Chembiochem* **2008**, *9* (3), 389-400.
139. Brickner, S. J., Oxazolidinone antibacterial agents. *Current Pharmaceutical Design* **1996**, *2* (2), 175-194.
140. Roehrig, S.; Straub, A.; Pohlmann, J.; Lampe, T.; Pernerstorfer, J.; Schlemmer, K. H.; Reinemer, P.; Perzborn, E., Discovery of the novel antithrombotic agent 5-chloro-N-({(5S)-2-oxo-3-[4-(3-oxomorpholin-4-yl)phenyl]-1,3-oxazolidin-5-yl}methyl)thiophene-2-carboxamide (BAY 59-7939): an oral, direct factor Xa inhibitor. *J Med Chem* **2005**, *48* (19), 5900-8.
141. Newberry, R. W.; Raines, R. T., A key n \rightarrow pi* Interaction in N-acyl homoserine lactones. *ACS Chem Biol* **2014**, *9* (4), 880-3.
142. (a) Zhang, R. G.; Pappas, K. M.; Brace, J. L.; Miller, P. C.; Oulmassov, T.;

- Molyneaux, J. M.; Anderson, J. C.; Bashkin, J. K.; Winans, S. C.; Joachimiak, A., Structure of a bacterial quorum-sensing transcription factor complexed with pheromone and DNA. *Nature* **2002**, *417* (6892), 971-4; (b) Lintz, M. J.; Oinuma, K.; Wysoczynski, C. L.; Greenberg, E. P.; Churchill, M. E., Crystal structure of QscR, a *Pseudomonas aeruginosa* quorum sensing signal receptor. *Proc Natl Acad Sci U S A* **2011**, *108* (38), 15763-8; (c) Bottomley, M. J.; Muraglia, E.; Bazzo, R.; Carfi, A., Molecular insights into quorum sensing in the human pathogen *Pseudomonas aeruginosa* from the structure of the virulence regulator LasR bound to its autoinducer. *J Biol Chem* **2007**, *282* (18), 13592-600; (d) Chen, G.; Swem, L. R.; Swem, D. L.; Stauff, D. L.; O'Loughlin, C. T.; Jeffrey, P. D.; Bassler, B. L.; Hughson, F. M., A strategy for antagonizing quorum sensing. *Mol Cell* **2011**, *42* (2), 199-209; (e) Zou, Y.; Nair, S. K., Molecular basis for the recognition of structurally distinct autoinducer mimics by the *Pseudomonas aeruginosa* LasR quorum-sensing signaling receptor. *Chem Biol* **2009**, *16* (9), 961-70; (f) Vannini, A.; Volpari, C.; Gargioli, C.; Muraglia, E.; Cortese, R.; De Francesco, R.; Neddermann, P.; Marco, S. D., The crystal structure of the quorum sensing protein TraR bound to its autoinducer and target DNA. *EMBO J* **2002**, *21* (17), 4393-401.
143. (a) Gerdt, J. P.; McInnis, C. E.; Schell, T. L.; Rossi, F. M.; Blackwell, H. E., Mutational Analysis of the Quorum-Sensing Receptor LasR Reveals Interactions that Govern Activation and Inhibition by Nonlactone Ligands. *Chem Biol* **2014**; (b) Jog, G. J.; Igarashi, J.; Suga, H., Stereoisomers of *P. aeruginosa* autoinducer analog to probe the regulator binding site. *Chem Biol* **2006**, *13* (2), 123-8.
144. Zheng, Y.; Sintim, Herman O., Molecular Insights into How Ligands Activate or Inactivate LasR. *Chemistry & Biology* **2014**, *21* (10), 1261-1263.
145. (a) Trott, O.; Olson, A. J., AutoDock Vina: Improving the speed and accuracy of docking with a new scoring function, efficient optimization, and multithreading. *Journal of Computational Chemistry* **2010**, *31* (2), 455-461; (b) Schrodinger, LLC, The PyMOL Molecular Graphics System, Version 1.3r1. 2010; (c) Ahumado, M.; Drosos, J. C.; Vivas-Reyes, R., Application of molecular docking and ONIOM methods for the description of interactions between anti-quorum sensing active (AHL) analogues and the *Pseudomonas aeruginosa* LasR binding site. *Mol Biosyst* **2014**, *10* (5), 1162-71.
146. McClean, K. H.; Winson, M. K.; Fish, L.; Taylor, A.; Chhabra, S. R.; Camara, M.; Daykin, M.; Lamb, J. H.; Swift, S.; Bycroft, B. W.; Stewart, G. S.; Williams, P., Quorum sensing and *Chromobacterium violaceum*: exploitation of violacein production and inhibition for the detection of N-acylhomoserine lactones. *Microbiology* **1997**, *143* (Pt 12), 3703-11.
147. (a) Collins, C. H.; Leadbetter, J. R.; Arnold, F. H., Dual selection enhances the signaling specificity of a variant of the quorum-sensing transcriptional activator LuxR. *Nat Biotechnol* **2006**, *24* (6), 708-12; (b) Koch, B.; Liljefors, T.; Persson, T.; Nielsen, J.; Kjelleberg, S.; Givskov, M., The LuxR receptor: the sites of interaction with quorum-sensing signals and inhibitors. *Microbiology* **2005**, *151* (Pt 11), 3589-602.

148. Hodgkinson, J. T.; Galloway, W. R. J. D.; Casoli, M.; Keane, H.; Su, X.; Salmond, G. P. C.; Welch, M.; Spring, D. R., Robust routes for the synthesis of N-acylated-L-homoserine lactone (AHL) quorum sensing molecules with high levels of enantiomeric purity. *Tetrahedron Letters* **2011**, 52 (26), 3291-3294.
149. Anbazhagan, D.; Mansor, M.; Yan, G. O.; Md Yusof, M. Y.; Hassan, H.; Sekaran, S. D., Detection of quorum sensing signal molecules and identification of an autoinducer synthase gene among biofilm forming clinical isolates of *Acinetobacter* spp. *PLoS One* **2012**, 7 (7), e36696.
150. Zhu, H.; He, C. C.; Chu, Q. H., Inhibition of quorum sensing in *Chromobacterium violaceum* by pigments extracted from *Auricularia auricular*. *Lett Appl Microbiol* **2011**, 52 (3), 269-74.